Copolymers at the
Solid-Liquid Interface

C.M. Wijmans

COPOLYMERS AT THE SOLID-LIQUID INTERFACE

(1)

Het feit dat in de kolloïdchemie de verhouding tussen theorie en experiment kan variëren van zeer op elkaar betrokken tot bijna geheel naast elkaar staand, is kenmerkend voor de positie die de kolloïdchemie inneemt tussen de traditionele natuurkunde en scheikunde in.

(2)

De middelbare laagdikte van polymeer geadsorbeerd op een gekromd oppervlak kan bij toenemende kromming van dit oppervlak toenemen, terwijl tegelijkertijd de hydrodynamische laagdikte afneemt.

Dit proefschrift, hoofdstuk 4

(3)

Het is niet nodig om, zoals Milner doet, een polydispersiteitsargument te gebruiken om kwantitatieve overeenstemming te vinden tussen de experimenteel gevonden interactie tussen twee polymeerborstels en de theoretische voorspelling daarvan.

S.T. Milner, *Europhys. Lett.*, **1988**, 7, 695; dit proefschrift hoofdstuk 5

(4)

Depletievlokking van een sol door niet-adsorberend polymeer kan voorkomen worden door dit polymeer in zeer lage dichtheden op de soldeeltjes te verankeren.

Dit proefschrift, hoofdstuk 5

(5)

Voor het verkrijgen van een zo hoog mogelijke kolloïdchemische *performance* dient men multiblok-copolymeren te gebruiken.

Dit proefschrift, hoofdstuk 6

(6)

Het is bedroevend dat campagnes om het imago van "De Chemie" te verbeteren niet verder komen dan het éénzijdig opsommen van verworvenheden die aan de chemische technologie te danken zijn. Zowel het creatieve karakter van de scheikunde als zijn maatschappelijke rol worden hierdoor tekort gedaan.

(7)

Niet de ontwikkeling van de twintigste eeuwse "nieuwe fysica" betekende, zoals Capra beweert, het einde van het mechanistische wereldbeeld, maar de al rond 1700 in brede kring geaccepteerde gravitatietheorie van Newton, die de definitieve mathematisering van de natuurkunde inluidde.

F. Capra, *The Turning Point* (Toronto, 1982)

(8)

De wederzijdse relatie tussen techniek en fundamentele natuurwetenschap is een ten onrechte door techniekfilosofen verwaarloosd onderwerp.

Zie bijv. H. Achterhuis (red.), De maat van de techniek (Baarn, 1992)

(9)

Volgens de definitie die de IUPAC geeft van een polymer is een eiwit geen polymer.

IUPAC, *Pure Appl. Chem.* **1974**, 40, 479.

(10)

Van Dale zou naast het overgankelijke gebruik van het werkwoord adsorberen ook het onovergankelijke gebruik van dit woord dienen te vermelden.

Van Dale, *Groot Woordenboek der Nederlands Taal*, 12de druk, 1993

(11)

Wetenschap is wetenschap als er "Wetenschap" op staat.

(12)

Alles is chemie, maar chemie is niet alles.

(13)

De kolloïdchemie is ouder dan Mozes.

vgl. F.A.M. Leermakers (1989) proefschrift LUW, stelling 10.

(14)

Het streven naar hogere efficiëntie in het (universitair) onderwijs heeft in de praktijk vaak tot gevolg dat het doel van dit onderwijs verwordt tot examentraining.

(15)

Ook in stedelijke gebieden zou, ter bevordering van het welzijn van plant, dier èn mens, de aanleg en instandhouding van een Ecologische Hoofdstructuur nagestreefd moeten worden. De stadsontwikkeling in Amsterdam van de afgelopen jaren kan daarbij niet als voorbeeld dienen.

(16)

Zestig jaar geleden constateerde Baas Becking: "de meest krasse vervreemding van de natuurwetenschap, waaraan een groot gedeelte van de Nederlandsche intellectueelen lijden, bijv. vele van onze leiders, die over het algemeen uit rechtsgeleerde kringen komen, doet hen vreemd staan tegenover de rol die deze wetenschap in een moderne maatschappij vervult." Hedentendage heeft deze constatering haar actualiteit helaas nog niet verloren.

Vakblad voor Biologen, **14** (1932-1933) 151

(17)

Het is verbazingwekkend hoeveel aandacht er tijdens practica aan de Landbouwuniversiteit aan veiligheid besteed wordt, gezien de desinteresse voor gezondheid en veiligheid van studenten en personeel die spreekt uit het beleid van deze universiteit ten aanzien van roken in haar gebouwen.

(18)

De huidige, ongewenste praktijk dat een parlementslid in Nederland niet aan *de kiezer* maar aan *de partij* verantwoording schuldig is, kan alleen doorbroken worden worden door het invoeren van een kiesstelsel zoals het Britse districtenstelsel, waarbij kandidaten direct gekozen worden.

(19)

Met name in trein, tram en bus zou het lezen van dagbladen aanzienlijk vergemakkelijkt worden, indien de artikelen die op de voorpagina van deze bladen beginnen in hun geheel op deze pagina worden afgedrukt, dan wel op de achterpagina vervolgd worden.

Stellingen
behorende bij het proefschrift
"Copolymers at the Solid-Liquid Interface"
van C.M. Wijmans, Landbouwuniversiteit
Wageningen, 13 april 1994.

To my parents

Voorwoord

Een goed gebruik in ere houdend begin ik dit proefschrift met enige woorden van dank aan diegenen zonder wie dit proefschrift niet zijn uiteindelijke vorm had verkregen. De eerste die ik wil noemen is Jan Scheutjens. De uitwerking van de meeste onderwerpen die in dit proefschrift beschreven worden heeft hij door zijn vroegtijdig overlijden helaas niet meegemaakt. Toch kan hij met recht de initiator van dit onderzoek worden genoemd. Ik kijk met veel plezier terug op het schrijven van hoofdstuk één, wat samen met Jan gebeurde. Ik heb toen van hem kunnen leren om noch met de inhoud noch met de presentatie van het geschrevene te snel tevreden te zijn. Ik hoop dat de later geschreven hoofdstukken zijn goedkeuring hadden kunnen verkrijgen.

In 1990 Jan brought me into contact with Katya Zhulina. This was certainly not the least important act of his with respect to my thesis research. When we first met we could not have imagined how fruitful our co-operation would be. Chapters one, three, and five are the direct results of our collaboration, but also throughout the other chapters I benefited greatly from discussions with Katya: spasibo!

Het afgelopen jaar heb ik veel profijt gehad van de aanwezigheid van Frans Leermakers. Hoewel de grote lijnen van het proefschrift al vast stonden bij zijn komst naar de vakgroep, heb ik vooral in hoofdstukken twee en zes goed gebruik kunnen maken van nieuwe ideeën die Frans aanbracht. Het enthousiasme en de snelheid waarmee hij de concept-hoofdstukken becommentarieerde waren zeer stimulerend.

Ik ben mijn promotor, Gerard Fleer, zeer erkentelijk voor de grote vrijheid die hij me liet bij het uitkiezen van van de precieze onderzoeksonderwerpen en de uitwerking daarvan. Tijdens de laatste maanden was hij nauw bij het schrijfwerk betrokken. Na "Het Boek" is zo het volgende boekje uit de polymeerclub voortgekomen. Het gedetailleerde commentaar dat Gerard steeds leverde heeft de presentatie van de onderzoeksresultaten op veel plaatsen zeer verduidelijkt. Mocht de lezer nog op onnauwkeurigheden of onduidelijkheden stuiten dan ligt de oorzaak daarvan zeker niet bij mijn promotor.

Hoewel iets minder direct van invloed op het proefschrift, was ook de samenwerking met de andere leden van de theoriegroep (Rafel Israëls, Cas Meijer, Klaas Besseling, Katinka van der Linden en Peter Barneveld) heel plezierig. Voor het oplossen van probleempjes en discussies over eigen of andermans onderzoek was altijd de ruimte. De "twee-weken weddenschap" met Rafel was een goede aansporing om het werk niet al tè lang te laten uitlopen. Met kamergenoot Klaas had

ik leuke en leerzame gesprekken. Van met name Peters continue inspanningen om de informaticainfrastructuur goed te laten functioneren, heb ik veel profijt gehad.

Gedurende een groot deel van mijn tijd heb ik in de personen van mijn kamergenotes Riet van de Steeg en Nynke Hoogeveen het experimentele polymeeronderzoek van nabij kunnen gadeslaan (dat was voordat de management-gestuurde werkkamertoebedelingspolitiek werd ingevoerd). Ook het brede wetenschappelijke aandachtsterrein van de rest van de vakgroep om me heen leverde een welkome verruiming van mijn aandachtsblik buiten het "gereken aan ketenmoleculen".

Chris Wijmans
Januari 1994

CONTENTS

Introduction

Already in the third millennium BC, an advanced civilization existed in Egypt. For a great deal this civilization was based upon an important development that had greatly influenced early information technology: the invention of ink. Carbon black particles were mixed with solutions of naturally occurring biopolymers, such as casein (from milk), albumin (from egg white), and gum arabic (from the *Acacia* tree). In the language of modern colloid science, the result was a sterically stabilized colloidal dispersion.[1-3] This is an example of the application of polymers in colloid technology, many centuries before anyone had yet coined the words "colloid" or "polymer". In our present society this same phenomenon of steric stabilization is widely applied in the manufacturing of a whole variety of industrial products, including (still!) inks and paints. The technological importance of steric stabilization forms a major impetus for fundamental scientific research into the behaviour of polymer molecules near interfaces, including the present thesis.

The first scientific investigation of the effect of polymer adsorption was probably performed by Faraday in the middle of the 19th century.[4] He prepared gold sols by reducing solutions of gold chloride. Faraday was especially interested in the optical properties of the gold sols and from these properties he deduced that the gold was dispersed as small particles throughout the solution. He further found that the addition of small traces of electrolyte leads to an irreversible coagulation of the gold. However, when the sol had first been treated with gelatine, Faraday found that it became protected against coagulation by the electrolyte. For the modern student of colloid science these experimental results sound very familiar.

A lyophobic sol, like Faraday's gold sol, is a thermodynamically unstable system. The van der Waals forces cause the particles to attract each other and coagulate. These sols can, however, be stabilized electrostatically. The sol particles carry a charge on their surfaces and are surrounded by a diffuse layer of ions with a counter-charge. When two of such diffuse layers start to overlap they repel each other, which may stabilize the system against flocculation. The equilibrium physics of the interaction between two charged sol particles has been understood for about half a century and is described by the DLVO theory (named after the four scientists - Derjaguin, Verwey, Landau, and Overbeek - who were largely responsible for its development).[5,6] The protective action of the polymer gelatine is called steric stabilization. There exists no theory which can describe such steric stabilization in the same handsome manner as the DLVO theory describes electrostatic

stabilization. Nevertheless, much effort has been put into understanding what happens to a polymer molecule when it adsorbs at a solid-liquid interface, and much is nowadays known. This thesis is but one bead on a long necklace of theoretical and experimental studies to investigate this subject. In the subsequent chapters we shall consider various systems where copolymers are adsorbed at solid-liquid interfaces, and try to gain more insight into the characteristics of these systems, using statistical thermodynamic arguments. But first we will briefly explain what a (co-)polymer is.

Polymers

The literal meaning of the word *polymer* is a molecule consisting of many (from the Greek, πολυ) monomeric units (μερος). The official definition given by the IUPAC[7] is "a substance composed of molecules characterized by the multiple repetition of one or more species of atoms or groups of atoms (constitutional units) linked to each other in amounts sufficient to provide a set of properties that do not vary markedly with the addition or removal of one or a few of the constitutional units." Probably the simplest example of a polymer is polythene (PET):

$$-CH_2-CH_2-CH_2-CH_2-CH_2- \qquad \text{or} \qquad -(CH_2-CH_2-)_N$$
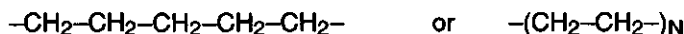
which is formed by the polymerization of ethene. The degree of polymerization N, which can be as large as 10^5, gives the number of monomers in one polymer molecule, and is called the chain length. Polythene has been known for about half a century, and is used in many applications. We only mention one historically interesting application, which is its contribution to the successful development of many branches of radar during World War II.[8] This was based upon the unrivalled dielectric properties of polythene. We give two more examples of polymers which are nowadays produced in gigantic quantities all over the world:

polystyrene (PS): $\qquad -[CH_2-CH(C_6H_5)-]_N$

and

polyvinyl chloride (PVC): $\qquad -(CH_2-CHCl-)_N$

In these three examples, the polymer molecules are built up from one type of constitutional unit, or monomer: ethene, styrene, and vinyl chloride, respectively. They are therefore called homopolymers. Polymers built up from more than one type

2

of monomer are called copolymers. A copolymer of two monomer units A and B has very different properties from those of an A or B homopolymer. Synthetic copolymers are produced to improve certain properties, or even as the only means to gain a new property. Copolymers that are produced industrially are nearly always random copolymers. The different monomer units form an irregular sequence in a random copolymer molecule. Copolymers also exist where the monomer units of one type are grouped together in one or more blocks. These are called block copolymers. In general, the chemical synthesis of block copolymers requires more effort than that of random copolymers. Block copolymers are very interesting molecules, as they can exhibit very special characteristics. Most of this thesis is concerned with block copolymers. Further on in this introduction we will consider block copolymers in a little more detail. First we will finish this short general overview of polymers.

The above might give rise to the impression that polymers are in general synthetic molecules. This is certainly not true. There are many examples of biopolymers. For example, the carbohydrate polymers: cellulose, which is the chief structural material of the plant and vegetable world; starch, the energy reserve in plants; and glycogen, the energy reserve in animals. Proteins, the building stones of all living species, are a special type of copolymer. (Strictly speaking, proteins do not obey the IUPAC definition of polymers. They are, however, generally classified as polymers). Proteins are made up of 21 different monomer units, called amino acids. Each protein has its own unique sequence of these amino acids, of which a plan is laid down in the genes. The most important component of the genes, DNA, is also a polymer. Nature has developed mechanisms to translate the genetic blueprint present in the DNA into protein molecules with a very low rate of errors occurring in the process. Up to 10^4 amino acid molecules have to be *polymerized* to make a protein molecule. The synthesis of such complicated polymers exactly according to a predetermined scheme is a task that lies far beyond the possibilities of conventional synthetic chemistry (although mankind has recently discovered how to let nature do this for its own benefit).

The word *polymerization* was already used by Bertholet[9] for the process in which several molecules form one large association structure. He used this word to describe the reaction of styrene, which upon heating changes from a liquid to a transparent solid, as observed in 1839 by Simon.[10] The molecular basis of this association remained in dispute. The fact that further heating of the polystyrene again leads to depolymerization supported the theory that in a polymerization reaction a physical aggregate is formed. Not until the 1920's did it become generally recognized that the units in polymers are connected by real covalent bonds.

Staudinger,[11] one of the founding fathers of polymer science, played a crucial role in the development of this idea.

Accepting the covalent nature of a polymer, the question arises what shape a linear polymer has in solution. Staudinger[12] assumed that a polymer molecule was a long rigid rod. Kuhn[13] showed that this assumption was incompatible with viscosity measurements of polymer solutions. He developed an alternative statistical theory of polymer chains as linear systems made up of independent elements (*statistical segments*, nowadays also called *Kuhn segments*). These elements can take on a large number of different conformations, resulting in a random coil shape for the overall polymer. One can say that this theory forms the basis of all subsequent theories in polymer physics. All the work presented in this thesis is based on this model of a polymer chain consisting of independent elements.

Polymers at interfaces

In many natural and technological processes the occurrence of polymers (and also oligomers) at interfaces plays a crucial role. In table 1, which is adapted from ref 14, a list is given of such processes.

Table 1

Adsorption of (or onto) polymers plays a key role in:

Adhesion	Crystallization	Soil structure
Coatings	Precipitation	Films and membranes
Lamination	Agglomeration	Biological agglutination
Reinforcements	Corrosion	Biocatalysis
Emulsions	Ageing of composites	Immune reactions
Suspensions	Crack resistance	Immunosensors
Detergent action	Drag reduction	Cell recognition
Flotation	Textile finishing	Adsorption of bacteria
Drilling and cutting	Flocculants	Drug direction
Solid lubrication	Chromatography	Genetic reproduction
Paper making	Water purification	Food stability
Magnetic discs	Polymer composites	Pesticides

In this context it is not possible to give an exhaustive overview of all these processes in which polymer adsorption phenomena are so important. We shall only mention a

few in slightly more detail. Together with the list given in table 1 (which by no means claims to be complete) this should give the reader some feeling for the diversity of applications that exist for scientific research on polymer adsorption.

We have already mentioned the ancient use of polymers to stabilize dispersions, such as ink. This same principle is also used in the production of, for example, paints, pharmaceutical products, pesticides, magnetic discs, and foods. Without adsorbed polymer a glass of refreshing milk would not look (or taste) half so nice! The opposite process of stabilization, destabilization, is also of great importance. In this case polymer molecules adsorb simultaneously onto two or more particles in a dispersion, thus causing the dispersion to flocculate. The sediment that is formed can subsequently be filtrated, which is useful in water purification. Recent research has shown that polymer chains on the cell walls of bacteria play an important role when these bacteria interact with a solid surface.[15] Proteins at interfaces are important in biotechnological applications. One can think of the adsorption of enzymes onto solid matrices in biocatalysis,[16] and of immunoglobulines in immunosensors.[17]

The study of polymer adsorption forms a discipline of its own. One cannot treat the adsorption of polymer molecules as a simple extension of the adsorption of low molecular weight species. Simplifying things just a little, one can say that the adsorption of small molecules is a "two state" process. A molecule is either adsorbed or it is not. Simple models can be used to give a statistical thermodynamic description of the adsorption. Of course, also for low molecular weight species complicating factors do occur. In certain cases the adsorption takes place on specific adsorption sites; in other cases the adsorbate can move freely over the adsorbent surface. Interactions between adsorbed molecules (which depend upon the surface coverage) may play an important role in the adsorption equilibrium. Especially in gas adsorption, sometimes multilayers can be formed. Nevertheless, with some inventivity these complications can be incorporated into fairly simple adsorption models. This is not the case for polymer adsorption.

If a polymer chain would only adsorb with all its segments in contact with the surface, then it would still be fairly easy to study polymer adsorption. But, although the situation that a polymer molecule adsorbs in a completely flat conformation is possible, it is very unlikely to occur. A polymer molecule can adsorb in very many different conformations. For example, with its first 10 segments adsorbed to the surface and with all other segments sticking out into the solution. Or with segment numbers 25, 26, 27, 98, and 110 on the surface and all others in the solution. Many other adsorbed conformations are possible. An adsorbed polymer layer consists of many molecules, each with its own conformation. In order to give a description of

5

such an adsorbed layer, one must use statistical methods. This is rather analogous to a polymer molecule in solution, whose (average) random coil shape is also the result of the many possible conformations.

Over the years different approaches have been proposed to describe polymer adsorption. The reader who wants to know more about these theories is referred to the recent overview given by Fleer et al.[18] In this introductory chapter we will pay some attention to one of the theoretical models for polymer adsorption, which has been used to compute most of the results presented in this thesis. It is the self-consistent field lattice theory of Scheutjens and Fleer.[19,20] Scheutjens and Fleer developed this theory to describe the adsorption of homopolymers. Evers et al.[21-23] extended the theory to included copolymer adsorption. Here we will only discuss the basic aspects of the theory in a qualitative manner. Elsewhere in this thesis a more quantitative description is given.

The adsorption theory of Scheutjens and Fleer is a lattice model. A lattice is used to generate the conformations of the polymer chains. Each segment is assumed to occupy a lattice site. Two connected segments must be situated on two adjacent lattice sites. Using this approximation, the number of conformations of a polymer chain is greatly reduced. When we refer to segments in the lattice model, we mean statistical segments or Kuhn segments. These cannot be identified with a single monomeric unit of the polymer chain but usually consist of several monomer units. The bonds between the segments are completely flexible. If a segment is located on a certain site, a contiguous segment can be on any of the neighbouring lattice sites. Furthermore, the excluded volume of the segments is taken into account in an average way. This means that conformations are allowed for which two or more segments are located on the same lattice site. The approximate manner in which the excluded volume is incorporated can lead to artefacts. However, it is far easier to generate the complete set of polymer conformations when one need not account for the excluded volume of the segments in an exact manner. This advantage outweighs the disadvantage of undesired artefacts.

The adsorption theory of Scheutjens and Fleer is a self-consistent field model. The phrase "self-consistent field" indicates how the polymer volume fraction profile is computed from the polymer conformations. Consider a polymer solution in contact with a smooth, flat surface. The polymer segments gain adsorption energy when they are in contact with the surface. This leads to adsorption of the polymer chains. If the volume fraction of polymer in the bulk solution is ϕ^b, then their volume fraction close to the surface will be larger than ϕ^b. We are interested in calculating the volume fraction ϕ as a function of the distance z to the surface. In the lattice model this means calculating the volume fraction $\phi(z)$ in each layer z. The volume fraction

profile $\phi(z)$ is found from a weighted average of all the polymer conformations. For each polymer conformation one knows how many of the segments are located in any layer z. But this knowledge is itself not yet enough to compute the volume fraction profile. Each conformation must also be weighted by a weighting factor. The weighting factors account for the energy of that conformation, and for the constraint that each lattice site must be filled with a polymer segment or a solvent molecule. If the segments have an adsorption energy, conformations with many adsorbed segments will have a low energy. If the polymer segments have unfavourable energetic interactions with the solvent, the energy of a conformation will depend upon the number of segment-solvent contacts. The energy of a conformation is determined by the potential energies of all its segments. In each different layer z a segment has a different potential energy $u(z)$. This potential energy is itself determined by the volume fraction profile. (For example, if the polymer segments have unfavourable energetic interactions with the solvent, the potential energy of the segments will be high if the solvent volume fraction is high and the polymer volume fraction is low). In other words, the volume fraction profile is determined by the potential energy profile, and, in turn, the potential energy profile is determined by the volume fraction profile. In equilibrium the volume fractions must be consistent with the potential field. That is why one speaks of a self-consistent field theory.

The adsorption theory of Scheutjens and Fleer is a *mean-field* model. For polymer adsorbing onto a flat surface, it is assumed that there is only a concentration gradient perpendicular to this surface (z direction). In layers parallel to the surface all interactions and volume fractions are smeared out: a mean-field approximation is applied in the x and y directions. The mean-field approximation is not really inherent to the theory, certainly not in the manner described here. In chapter 6 the mean-field approximation is implemented differently. There we are concerned with a system where it is not realistic to assume that the concentrations are a function of one coordinate only. In this chapter the volume fractions are consequently taken to be functions of two independent coordinates. The mean-field approximation is then applied in one dimension only. It would also be possible to apply the theory without any mean-field approximation, by taking the volume fractions as functions of three independent coordinates x, y, and z. However, this would mean that the number of variables increases accordingly, which very soon leads to computational difficulties. Furthermore, for adsorption onto a flat surface it is physically realistic to assume that concentration gradients only occur in the z direction.

The adsorption theory of Scheutjens and Fleer is an *equilibrium* theory. For a given system the equilibrium distribution is computed under certain constraints (for

example, a fixed chemical potential of the various species or, alternatively, a fixed amount of the components). No dynamic aspects are at all taken into account. It is only possible to calculate what the equilibrium situation is for a system, not how quickly or along what pathway that equilibrium will be reached from a given starting configuration.

Adsorption of homopolymers and copolymers

In a homopolymer chain all segments are chemically identical. If a homopolymer adsorbs, this means that all segments have an affinity for the surface. In one specific adsorbed molecule the segments will generally not all be adsorbed at the same time, but they are all able to adsorb. A very different situation can occur with copolymers. Copolymer chains consist of at least two different kinds of segments. The adsorption energies of the different segments are generally not the same. If a copolymer consists of two types of segments of which one type does adsorb and the other type does not adsorb, this can lead to a very different adsorption behaviour as compared to a homopolymer. We first consider the case that all the adsorbing segments, which we denote by the letter A, are grouped together in one block and all the nonadsorbing segments, which we denote by the letter B, are in another block. We then have an AB diblock copolymer. When such a polymer adsorbs from solution, the A blocks will cover the surface, whereas the B blocks will stick out into the solution. Especially if the B segments dissolve well in the solvent, a thick adsorption layer can be formed by these diblock copolymers.

If the A and B segments are not separated along the polymer chain but, for example, mixed in a statistical manner, the diblock copolymer will far more resemble a homopolymer. When adsorbing, the A segments will pull the B segments towards the surface. An intermediate situation occurs, when the A and B segments are not separated into two large blocks but into several smaller alternating A and B blocks (multiblock copolymers). The A blocks will adsorb, and the B blocks will form loops between the A blocks, protruding into the solution. The greatest part of this thesis is concerned with AB diblock copolymers, but in chapter 6 we also study multiblock copolymers.

As mentioned several times before, adsorbed polymer layers can impart colloidal stability to a dispersion. The ideal polymer for steric stabilization is a polymer which adsorbs in a large amount, but which also dissolves well in the solution, forming a thick protective layer around the colloidal particle. For a homopolymer these conditions are conflicting. Furthermore, homopolymers tend to form bridges between two surfaces, which can lead to an attractive force. Diblock copolymers can more effectively give colloidal stability. A diblock copolymer consists of two blocks, each

with different properties. A good stabilizer will have a strongly adsorbing A block and a nonadsorbing B block, which dissolves well in the solution. As only one end of such polymer molecules adsorbs, they will not form bridges between two surfaces. (Of course certain copolymers can form bridges. If an extra A block is added to a diblock copolymer, one gets an ABA triblock copolymer, whose two adsorbing blocks can adsorb onto different surfaces. This copolymer bridging effect is also discussed in chapter 6).

The adsorption of a polymer need not only be driven by an affinity of the segments for the surface. A dislike of the solvent can also cause adsorption. Complications can arise when in a copolymer one of the segment types (the adsorbing segments) dislike the solvent (on their own they cannot be dissolved in the solvent), while the other segment type dissolves well in the solvent. This disparity in interaction with the solvent (in such a case one speaks of a selective solvent) favours adsorption of the A segments, but it also leads to the occurrence of another phenomenon: the formation of micelles. These are aggregates of polymer molecules with the A segments in the middle, and the B segments forming a shell around them, which shields the A segments from the solvent. The formation of these micelles is analogous to the formation of micelles by surfactants, which consist of far smaller molecules. Surfactants are really very short block copolymers (one could call them block oligomers). When studying the adsorption of copolymers from a selective solvent, the equilibrium between free polymer molecules and micelles should be taken into account. This can be done using the self-consistent field lattice theory,[24] although in this thesis we will not consider the possibility of copolymers to form micelles. However, the results presented in chapter 3 can be applied to describe polymeric micelles. In chapters 3 and 4 we describe the adsorption of AB diblock copolymers onto small spherical particles. In chapter 3 we focus our attention on the distribution of the B segments around such a particle. This is a very similar situation to that which occurs for B segments in a micelle, where they are distributed around a core of A segments.

Strong-stretching approximation

For all the systems mentioned in the previous section, the adsorption can be studied using the self-consistent field lattice theory. For AB diblock copolymers we have also applied another theory to describe the adsorbed layer. Using this theory, one can calculate the distribution of the B segments. The A segments, which are strongly adsorbing, are assumed to form a thin film adjacent to the surface, so that their distribution is less interesting. If the adsorbed amount is high enough, the B blocks cannot keep their random coil conformation. If they would do so, B blocks

9

from neighbouring chains would hinder each other considerably. The excluded volume interactions lead to strongly stretched conformations.

When the B blocks are strongly stretched it is not necessary to generate all their possible conformations in order to find the equilibrium volume fraction profile. It turns out to be sufficient only to consider a set of most probable conformations. This was first realized by Semenov.[25] His approach to this problem was subsequently applied to studying (homo-)polymer chains that are end-attached to an impenetrable surface.[26,27] Such a system is often called a polymer brush, because the stretched polymer chains resemble the bristles of a brush. We have used such a polymer brush as a model for an adsorbed AB diblock copolymer. The amount of adsorbed (end-attached) polymer is then an input parameter. In a real block copolymer the B blocks are attached to a thin film of A segments, and not directly to the surface. This has only minor consequences for the profile of the B segments. Of course, in the adsorption process the adsorbed amount is determined by the adsorption equilibrium.

Although in this thesis we investigate polymer brushes as model systems for copolymers adsorbed from solution onto a solid surface, polymer brushes can also be seen as models for a variety of other interfacial systems in polymer science. First of all one can think of polymer chains that are directly grafted to a surface, either by a covalent bond with the end-segment of the chain or by a special chemical group. This situation hardly differs from an adsorbed diblock copolymer. Polymer brushes are also formed when diblock copolymers adsorb at a liquid-liquid or a liquid-air interface. (Thin liquid films, as an example of such a system, can be stabilized by diblock copolymers). In these cases we have "soft", penetrable interfaces, whose characteristics are not necessarily identical to those of a hard, impenetrable solid-liquid interface. Nevertheless, as a first approximation one can model polymer chains attached to a soft surface as a brush on a solid surface. If the brush thickness is far larger than the transition layer between the two phases, this approximation should not have many undesirable consequences. Finally, brush-like structures can be formed in melts or concentrated solutions of block copolymers. In such systems the blocks often segregate into different microdomains. These blocks can then be treated as chains grafted to the interface between two such domains. Actually, Semenov[25] first introduced the strong-stretching approximation to describe block copolymer melts. It does make a difference whether a brush is immersed in a low molecular weight solvent or in a polymer melt. The greater part of this thesis is only devoted to brushes immersed in a low molecular weight solvent. Chapter 5 is partly concerned with brushes immersed in a polymer solution. In the limit of high volume fractions of the dissolved polymer, one is dealing with a brush immersed in a

polymer melt. So, in that chapter we will briefly be concerned with brushes immersed in a polymer melt.

Outline of the thesis

This thesis divides into two parts. Chapters 1-4 deal with (co-)polymers at isolated surfaces. The equilibrium profiles are studied of unperturbed brushes and of block copolymers freely adsorbing from a solution onto an adjacent surface. Chapters 5-7 deal with the interaction between two surfaces bearing adsorbed polymer layers. In these last three chapters we use the insights obtained in the first four chapters. The results of the last three chapters are directly relevant for questions about colloidal stability.

Chapter 1 is concerned with polymer brushes on flat surfaces. Both the self-consistent field lattice theory for end-attached polymer chains and the strong-stretching approximation are introduced. Our aim is to make a rigorous comparison between both approaches. By comparing the results of the strong-stretching approximation with those of the lattice model, we explore the validity of this approximation for different chain lengths, grafting densities, and solvent qualities.

In chapter 2 an extension of the self-consistent field lattice model is introduced. This extension accounts for stiffness in the chains of the polymer brush. It also provides a better approximation for the excluded volume of the segments. These new concepts are applied to polymer brushes on isolated, flat surfaces (as in chapter 1).

Chapters 3 and 4 deal with curved surfaces. In colloidal systems polymers generally adsorb onto curved particles, so that the surface curvature is a relevant parameter when studying polymer adsorption. In chapter 3 the structure of polymer brushes on spherical and cylindrical surfaces is studied. Data for the volume fraction profiles of such brushes obtained from the lattice model are presented. We try to interpret these data using both the strong-stretching approximation and scaling arguments. We also consider the distribution of the end-segments throughout the brush. A central question is whether there is a zone near the surface from which these end segments are excluded, when the surface is strongly curved. In chapter 4 we deal with the adsorption equilibrium between free diblock copolymers and diblock copolymers adsorbed onto a spherical particle.

In chapter 5 the interaction between two flat surfaces, each with an end-attached polymer layer, is studied. This chapter can be seen as an extension of chapter 1, which dealt with a polymer brush on an isolated surface. The main aim of chapter 5 is to describe the interaction free energy of a system consisting of two such surfaces, when both surfaces are brought together. This interaction is calculated

11

both for brushes immersed in pure solvent and for brushes immersed in a solution of free polymer chains. As an introduction to the latter system, we also study the behaviour of an isolated brush immersed in a solution of free polymer.

Chapters 1-5 all deal with diblock copolymers. In these chapters we either look at freely adsorbing diblock copolymers or we use polymer brushes as a model system for adsorbed diblock copolymer layers. In chapter 6 copolymers are studied which consist of more than two blocks. The central question in this chapter is under what circumstances multiblock copolymers can be used to stabilize a dispersion, and under what circumstances such copolymers destabilize a dispersion. We first turn our attention to ABA triblock copolymers. These triblock copolymers are able to form a bridge between two surfaces, which may induce an attractive force between these two surfaces. We then move on to consider multiblock copolymers, consisting of a large number of alternatingly adsorbing and nonadsorbing blocks.

The last chapter is about the interaction between two small colloidal particles bearing adsorbed diblock copolymer layers. These layers are again modelled as terminally attached chains. The relationship between this chapter and chapter 3 is the same as that between chapters 5 and 1. In chapter 3 we deal with polymer brushes on isolated curved surfaces. In chapter 7 we study the interaction between spherical particles with polymer brushes attached to them. The central question in this chapter is how the particle curvature influences this (repulsive) interaction. This problem is of great relevance for colloidal stability, as sterically stabilized particles are always curved. If these particles are not far larger than the dimensions of the adsorbed polymer layer, then one may expect that their curvature is an important parameter in the process of steric stabilization. We try to gain more insight into this system by developing an extended version of the self-consistent field lattice theory.

All chapters can be read independent of each other.

Other scientific approaches relevant to this work

The subjects studied in this thesis can also be investigated using other theoretical or experimental approaches. We will not give an elaborate review of these, discussing the merits of all major experimental, theoretical, and simulation techniques that have been employed to investigate the behaviour of copolymers at solid-liquid interfaces. Instead, in this section we only mention some other methods that may, in principle, be compared with our model.

A great deal of our work is concerned with the equilibrium volume fraction profiles of polymer brushes. In principle these profiles can be measured using neutron scattering and neutron reflectometry. However, these techniques are not sensitive enough to investigate most of the details in the volume fraction profiles which we

calculate. It will not be easy to find direct experimental evidence for the deviations between the strong-stretching approximation and the more exact lattice predictions. It *is* possible to make a useful comparison with Monte Carlo and molecular dynamics simulations of polymer brushes. Just as the SCF lattice calculations, these simulation methods do not make any *a priori* assumption about the chain conformations. Simulations show the same sort of deviations with respect to the strong-stretching approximation as do the SCF lattice calculations.

The great disadvantage of Monte Carlo and, especially, molecular dynamics simulations is that they are computationally very demanding. The CPU times involved to simulate a (multi-chain) polymer brush of a reasonable size are orders of magnitude larger than the CPU time needed to solve the SCF equations numerically. With the present state of the art in computer technology it is certainly not possible to perform simulations for all systems presented in this study. However, in one respect Monte Carlo and molecular dynamics simulations are more reliable than our SCF calculations, as the former do not use a mean-field approximation. In a good solvent this mean-field approximation was shown to give the correct results.[28] In bad solvents there are indications that it is not correct.[29] Throughout this study we apply the mean-field approximation without questioning its validity. The large majority of the results are obtained under Θ- or better solvency conditions. In these cases one may certainly expect that the mean-field approximation for brushes has no serious shortcomings. One should, however, always bear in mind that the results are based upon this approximation.

During the past five to ten years much work has been done on polymer brushes. Chapters 1, 2, 3, and 5 clearly are part of the new discipline of "brush research". In these chapters the reader encounters many references to the major "brush publications". The three other chapters are of a more applied nature, where we try to use the theoretical framework to make predictions about interesting colloidal systems. Up to now the systems treated in these chapters have not yet received much attention, neither from a theoretical nor from an experimental point of view (although recently some work has been published on the adsorption of and (de-) stabilization by triblock copolymers;[30,31] see chapter 6). We hope, and believe, that our results on the effect of particle curvature on copolymer adsorption (chapter 4), on steric stabilization (chapter 7), and on the adsorption behaviour of multiblock copolymers (chapter 6) may inspire further theoretical and, especially, experimental investigations of such systems.

13

References

1. *Encyclopaedia Britannica* 1955, 12, 360.
2. Napper, D. H. *J. Colloid Interface Sci.* **1977**, 58, 390.
3. Napper, D. H. *Polymeric stabilization of colloidal dispersions*, Academic Press: London, 1983.
4. Faraday, M. *Phil. Trans. Roy. Soc.* **1857**, 174, 145.
5. Verwey, E. J. W.; Overbeek, J. T. G. *Theory of the Stability of Lyophobic Colloids*, Elsevier: Amsterdam, 1945.
6. Hunter, R. J. *Foundations of Colloid Science*, 1; Oxford University Press: Oxford, 1988.
7. International Union of Pure and Applied Chemistry, Macromolecular Division, Commission on Macromolecular Nomenclature, Basic Definitions of Terms Relating to Polymers 1974, *Pure Appl. Chem.* **1974**, 40, 479.
8. Alexander, A. E.; Johnson, P. *Colloid Science*, 2; Oxford University Press: Oxford, 1949.
9. Bertholet, M. *Bull. Soc. Chim. France* **1866**, 6, 294.
10. Simon, E. *Ann. Chim. Phys.* **1839**, 31, 265.
11. Staudinger, H. *Ber. Dtsch. Chem. Ges.* **1920**, 53, 1073.
12. Staudinger, H. *Naturwiss.* **1934**, 22, 84.
13. Kuhn, W. *Kolloid. Z.* **1934**, 68, 2.
14. Eirich, F. R. *J. Colloid Interface Sci.* **1977**, 58, 423.
15. Rijnaarts, H. H. M., *PhD. Thesis*, 1994, Wageningen Agricultural University.
16. Malcata, F. X.; Reyes, H. R.; Garcia, H. S.; Hill Jr, C. G.; Amundson, C. H. *J. Am. Oil Chem. Soc.* **1990**, 67, 870.
17. Karlsson, R.; Michaelsson, M.; Mattsson, L. *J. Immunol. Meth.* **1991**, 145, 229.
18. Fleer, G. J.; Cohen Stuart, M. A.; Scheutjens, J. M. H. M.; Cosgrove, B.; Vincent, B. *Polymers at Interfaces*, Chapman & Hall: London, 1993.
19. Scheutjens, J. M. H. M.; Fleer, G. J. *J. Phys. Chem.* **1979**, 83, 1619.
20. Scheutjens, J. M. H. M.; Fleer, G. J. *J. Phys. Chem.* **1980**, 84, 178.
21. Evers, O. A.; Scheutjens, J. M. H. M.; Fleer, G. J. *Macromolecules* **1990**, 23, 5221.
22. Evers, O. A.; Scheutjens, J. M. H. M.; Fleer, G. J. *J. Chem. Soc. Faraday Trans.* **1990**, 86, 1333.
23. Evers, O. A.; Scheutjens, J. M. H. M.; Fleer, G. J. *Macromolecules* **1991**, 24, 5558.
24. van Lent, B.; Scheutjens, J. M. H. M. *Macromolecules* **1989**, 22, 1931.
25. Semenov, A. N. *Sov. Phys. JETP* **1985**, 61, 773.
26. Milner, S. T.; Witten, T. A.; Cates, M. E. *Macromolecules* **1988**, 21, 2610.
27. Zhulina, E. B.; Priamitsyn, V. A.; Borisov, O. V. *Polym. Sci. USSR* **1989**, 31, 205.
28. Chakbrabarti, A.; Toral, R. *Macromolecules* **1990**, 23, 2016.
29. Binder, K.; Lai, P.-Y. *Makromol. Chem., Macromol. Symp.* **1993**, 65, 189.

30. Dai, L.; Toprakcioglu, C. *Macromolecules* **1992**, 25, 6000.
31. Johner, A.; Joanny, J.-F. *J. Chem. Phys.* **1992**, 96, 6257.

chapter 1

Self-Consistent Field Theories for Polymer Brushes.

Lattice Calculations and an Asymptotic Analytical Description

Abstract

In this chapter we compare two models for calculating the configuration of grafted polymer chains at a solid-liquid interface. The first model is the self-consistent field polymer adsorption theory of Scheutjens and Fleer as extended for end-attached chains. In this approach the equilibrium distribution of the polymer is found by averaging the statistical weights of all possible chain conformations that can be generated on a lattice. The second model is an analytical SCF theory developed independently by Zhulina, Borisov and Priamitsyn and by Milner, Witten and Cates which predicts the grafted layer structure in the case of strong chain stretching. A comparison is made between the results of both theories, and the deviations are explained from the assumptions made in the less exact analytical theory.

1.1 Introduction

Polymer chains that are grafted at one end onto an impenetrable surface form a good model for the analysis of numerous systems, such as sterically stabilized colloidal dispersions, block copolymer surfactants at solid-liquid and liquid-liquid interfaces, solutions and melts of block copolymers under the conditions in which microphases are formed, etc. Theoretical analysis of grafted chain layers was initiated by the pioneering publication of Alexander.[1] Using scaling arguments,[1-3] the main features of grafted layers were established, particularly the considerable stretching of overlapping chains perpendicular to the grafting surface. This stretching is greatest for the case of a planar grafted layer, so that the thickness of the layer H is proportional to N for solvents of various strengths. This scaling relationship between the layer thickness and the degree of polymerization suggested the picture of a mainly homogeneous layer of constant concentration and at the periphery of the layer a rapid decrease of concentration.

Further progress in the analytical theory of grafted layers was attained using the self-consistent field (SCF) approach proposed by Semenov.[4] This approach is based on assuming large stretching of the grafted chains with respect to their Gaussian dimension to allow the replacement of the set of conformations of a stretched grafted chain by their "average trajectory" (the so-called Newton or strong-stretching approximation) which significantly simplifies the description of the system. This idea was first applied by Semenov to dense grafted layers (i.e. layers without solvent) and led to a very elegant theory of super structure formation in block copolymer melts under strong segregation conditions.

This SCF approach was generalized and applied to grafted polymer layers immersed in low molecular weight solvents[5,6] and solutions or melts of mobile polymers.[7] Many effects were considered, such as the collapse of the layer due to a decrease of the solvent strength,[8] the polydispersity of grafted and mobile chains,[9] deformational[10] and dynamical[11] behaviour of grafted layers, etc.

These investigations led to a different picture of the grafted layer structure. The polymer concentration decreases monotonically on going from the surface to the outside of the layer. Furthermore, the free chain ends are distributed throughout the whole layer. The system parameters such as solvent quality, polydispersity, etc., appear to strongly influence the shapes of the volume fraction profile and the free chain end distribution.

The development of an analytical theory was accompanied by investigations of grafted layers by Monte Carlo simulations[12-15] and numerical calculations using a SCF lattice model.[12,16] In the latter method, the equilibrium concentration profile of the grafted layer is found by accounting for all the possible conformations of the

17

polymer chains that can be generated on a planar lattice. Each conformation is weighted by its Boltzmann probability factor. We emphasize that this approach gives exact results within the mean-field and lattice model approximations. No further approximations are needed to find the equilibrium distribution. Typical computation time is on the order of minutes on a desktop workstation. Parameters such as molecular weight, grafting density and solvent quality can easily be varied, thus enabling the study of the grafted layer structure under various conditions. Therefore, a detailed comparison with analytical predictions is feasible.

The aim of this chapter is the systematic comparison of results obtained by the above-mentioned analytical and numerical SCF methods for a planar layer immersed in either a pure solvent or a solution of mobile polymer. An initial comparison of both approaches for the case of only an athermal solvent[17] was very promising. In this chapter we consider a wide range of solvent strengths, including very good (better than athermal) and poor solvents.

The combination of these two different methods for the analysis of grafted layers is useful for several reasons. First, it provides a better understanding of the structural organization of grafted chain layers. Second, it enables us to check the validity of the assumptions made in the analytical theory, particularly the Newton approximation. Furthermore, the establishment of direct relationships between the analytical and the numerical results may stimulate further development of both models and their application to other systems.

In this chapter we shall consider the equilibrium characteristics of a free non-deformed planar layer, and its deformational behaviour will be considered elsewhere. In sections 2 and 3, we summarize the main ideas behind the numerical lattice model and analytical SCF theories. Section 4 is devoted to the comparison of the results obtained by both methods.

1.2 Self-Consistent Field Lattice Model

The homopolymer adsorption theory of Scheutjens and Fleer[18,19] calculates the equilibrium distribution of a polymer-solvent system at an interface by taking into account all possible conformations, each weighted by its Boltzmann probability factor. Cosgrove *et al.*[12] and Hirz[16] showed that this method can be applied to terminally attached chains by restricting the conformations to those whose first chain segment is in the layer adjacent to the surface. In this section we describe both versions for the case of nonadsorbing polymer segments, that is, where segments and solvent molecules are assumed to have the same affinity for the surface. In this case the polymer tends to avoid the surface in order to minimize the loss of conformational entropy.

Consider a lattice consisting of M layers, numbered $z/\ell = 1, 2, ..., M$, where z is the distance from the surface and ℓ the thickness of a layer. Layer 1 is the layer adjacent to the surface and layer M is in the bulk solution. We assume full occupancy of the lattice layers. Each layer consists of L lattice sites, each of which accommodates either a polymer segment or a solvent molecule. A fraction λ_0 of the surface of a lattice site is in contact with other sites in the same layer. Similarly, a fraction λ_1 is in contact with sites in a lower layer and another fraction λ_1 with sites in a higher layer. For a simple cubic lattice, which has been used to derive all the results presented in this chapter, $\lambda_0 = 2/3$ and $\lambda_1 = 1/6$. The cubic lattice gives an equal *a priory* probability to a bond between two segments in any of the four directions parallel to the surface as well as to a bond toward the surface or away from the surface.

Polymer chains in a concentration gradient

We first consider the general case of (non-grafted) polymer chains and solvent molecules distributed over the lattice. The chains are N segments long. Within each layer a mean-field approximation is applied, so we can write the volume fraction profile of segments, $\phi(z)$, and solvent molecules, $1 - \phi(z)$, as functions of z alone. In the bulk solution the polymer concentration is ϕ^b. As mentioned above, we assume that there is no net adsorption energy of the polymer segments with respect to that of the solvent. Nearest-neighbour interactions between polymer segments and solvent are accounted for by the Flory-Huggins interaction parameter χ. Because of the mean-field approximation all interactions within a layer are smeared out. This means that the potential energy $u(z)$ of a polymer segment in layer z relative to that in the bulk is given by

$$u(z)/kT = \chi\left(< 1 - 2\phi(z) > -1 + 2\phi^b\right) - \ln(1 - \phi(z)) + \ln\left(1 - \phi^b\right) \qquad (1)$$

where the angular brackets <> denote a weighted average over three layers, which accounts for the fraction of contacts that a segment or solvent molecule has with its nearest neighbours in these layers. For example, the average volume fraction of nearest-neighbour segments of a site in layer z is given by

$$<\phi(z)> = \lambda_1 \; \phi(z-\ell) + \lambda_0 \; \phi(z) + \lambda_1 \; \phi(z+\ell) \tag{2}$$

The segment potential $u(z)$, which corresponds to $-kT \ln(p_i)$ in ref 18, is the derivative of the free energy with respect to the segment concentration in layer z; i.e., it is determined by the change in free energy that takes place upon exchanging a solvent molecule in layer z with a single polymer segment in the bulk. This change is comprised of contributions from the loss of interaction energy, $-\chi<\phi(z)>$, which is due to the removal of the solvent molecule from layer z, the gain in energy from interactions of the solvent molecule with the bulk solution, $\chi\phi^b$, the gain in interaction energy due to the insertion of the segment into layer z, $\chi < 1-\phi(z)>$, its loss in interaction energy due to its removal from the bulk, $-\chi\left(1-\phi^b\right)$, and a term for the change in the translational entropy of the solvent molecule, $\ln(1-\phi(z))$ − $\ln\left(1-\phi^b\right)$. The translational entropy of the solvent is included in $u(z)$, whereas the entropy of the polymer is accounted for in the conformation statistics which are described below.

We define a segment weighting factor $G(z)$ as

$$G(z) = \exp(-u(z)/kT) \tag{3}$$

which is a Boltzmann factor of the segment potential in layer z. Detached segments (monomers) would have a distribution given by $G(z)$. The intermolecular interactions are included in $u(z)$ within the mean-field approximation, but in a chain the distribution of a segment is also affected by that of all the other segments in the same molecule and may depend on its position in the chain. The connectivity of the segments is accounted for in the end-segment weighting factor $G(z,s)$, defined as the average statistical weight of all conformations of an s-mer of which the last segment is located in layer z and the first segment may be located anywhere in the system. If segment s is in layer z, segment s − 1 must be located in one of the layers $z-\ell$, z, or $z+\ell$. This means that $G(z,s)$ is proportional to $< G(z,s-1) >$, the weighted average of statistical weights of $(s-1)$-mers of which the last segment is in one of the layers $z-\ell$, z or $z+\ell$. The angular brackets denote a similar average as defined by eq 2. Furthermore, segment s in layer z contributes a factor $G(z)$. It is now easily seen that a recurrence relation holds which enables us to calculate $G(z,s)$ for all values of s:

$$G(z,s) = < G(z,s-1) > G(z) \tag{4}$$

20

The sequence is started with $G(z,1) = G(z)$, the statistical weight of a monomer. Thus, $G(z,s)$ is calculated for all $s \leq N$, for a given set of values for $u(z)$. To arrive at our goal of finding an expression for the total segment volume fraction $\phi(s,z)$ of the sth polymer segment in layer z, we realize that the sth segment of a polymer of N segments can be viewed as being simultaneously the end-segment of an s-mer and of an $(N+1-s)$-mer. This means that the total statistical weight of the chain is given by the joint probability that both end-segments of the subchains are on the same site or, because of the mean-field approximation and apart from a factor L, in the same layer. Thus, $\phi(s,z)$ becomes

$$\phi(z,s) = C \; G(z,s)G(z,N-s+1)/G(z) \tag{5}$$

Here, the denominator accounts for the fact that segment s is counted twice (belonging to both chain parts). The normalization constant C can be obtained in two ways. In a closed system the total number n of polymer molecules is fixed and C follows from the boundary condition $n = L\sum_z \phi(z,s)$. This relation is valid for any s, since there are n segments s in the system. If we substitute $\phi(z,s)$ from eq 5 for $s = 1$ or $s = N$, we obtain:

$$C = \frac{n}{L\sum_z G(z,N)} \tag{6}$$

Alternatively, C can be expressed in the bulk concentration ϕ^b, which is especially useful for open systems. In the bulk solution $\phi(z,s)$ must equal ϕ^b/N. Moreover, according to eqs 1-3, in the bulk solution, $u(z)$ is zero and all G's are unity. Thus, from eq 5 it follows that

$$C = \phi^b/N \tag{7}$$

Finally, the total polymer volume fraction in layer z is

$$\phi(z) = \Sigma_s \phi(z,s) \tag{8}$$

This volume fraction profile, obtained for a given $u(z)$ profile, should be consistent with eq 1 for all values of z. This provides a set of M simultaneous equations in M unknown variables $u(z)$, which may be solved by the numerical method (for free as well as grafted chains) given in Appendix 1.

Grafted chains

Above, we discussed the general case of polymer chains which may adopt any possible conformation. However, if the chains have one of their ends attached to the surface, the first segment must be in the first layer. Consequently, the

21

generation of chains, using eq 4, must start with $G_g(z,1)$ (where the subscript g denotes grafting) being equal to zero for all $z \neq 1$:

$$G_g(z,1) = \begin{cases} G(z) & \text{if} \quad z = 1 \\ 0 & \text{if} \quad z \neq 1 \end{cases} \tag{9}$$

and eq 4 is replaced by

$$G_g(z,s) = \, <G_g(z,s-1)> G(z) \tag{10}$$

Generally, $G_g(z,s) \leq G(z,s)$ and $G_g(z,s)$ is zero for $z > s$. In the chain, segment s is the joint between a grafted chain of s segments and a non-grafted free chain of N–s+1 segments. Equation 4 is still valid for generating the conformations starting from the other end of the chain, i.e. the chain part from segment N down to s. Thus, for grafted chains the equivalent of eq 5 becomes:

$$\phi_g(z,s) = C_g G_g(z,s) G(z,N-s+1)/G(z) \tag{11}$$

The total number n_g of grafted polymer chains is fixed by the grafting density $\sigma = n_g/L$ and determines the value of the constant C_g according to eq 6.

Grafted chains in a solution of free polymer

If the grafted layer is immersed in a solution of free polymer chains of N_f segments, both the volume fraction profile $\phi_g(z)$ of the grafted chains and that of the free chains, $\phi_f(z)$, are calculated from the same potential energy profile u(z). In eq 1 the volume fraction of the segments $\phi(z)$ is given by $\phi_g(z) + \phi_f(z)$. To find the volume fractions of the mobile chains, $\phi_f(z)$, eqs 4 and 5 are used, and for the grafted chains eqs 9-11 are used. The normalization constant for the free polymer is determined by the bulk volume fraction ($C_f = \phi_f^b/N_f$) and that of the grafted chains by the grafting density ($C_g = \sigma / \sum_z G_g(z,N)$).

Self-consistent field

The volume fraction profiles of grafted and free polymer are now given as a function of the segment potential profile. In turn, the segment potential itself is determined by the volume fraction profile (see eq 1). The problem boils down to finding a potential profile which is consistent with the volume fraction profile that it produces. Mathematically, this is equivalent to solving an implicit set of equations for which a numerical iteration scheme is provided in Appendix 1.

1.3 Analytical Theory

The analytical SCF theory as developed by Zhulina, Priamitsyn and Borisov[20] and Milner, Witten, and Cates[6] predicts the asymptotic behaviour of grafted chains as the chain length increases. Here we summarize the main equations, emphasizing the similarities and differences with the lattice model and using the same nomenclature as in the previous section.

Consider a planar layer of long ($N_g \gg 1$) fully flexible polymer chains grafted at one end onto a solid surface with relative surface coverage $\sigma = n_g/L$, where n_g is the total number of chains and L the maximum number of chains that could be grafted onto the same surface (ℓ^2/σ is the surface area per chain, which is called σ in ref 5, and σ/ℓ^2 is the number of grafted chains per unit area, which is called σ by Milner, Witten and Cates[10]). The chain thickness ℓ (which in this chapter is assumed to be equal to the Kuhn segment length) corresponds to the lattice spacing in the model of the previous section. When the grafted chains are strongly stretched with respect to their Gaussian dimension, $R_0 = \ell\sqrt{N}$, the free energy A of the system can be written as

$$\frac{A}{LkT} = \frac{3}{2\ell^3}\int_0^H dz' \phi_g(z',N)\int_0^{z'} dz E(z \mid z',N) + \frac{1}{\ell}\int_0^H f[\phi(z)]dz \qquad (12)$$

The first term in this equation represents the contribution from the elastic chain stretching in the layer. It is determined by the function $E(z \mid z',N) = dz/ds$, which gives the local stretching of a chain at distance z from the surface when its free end is located at $z' > z$, and by the volume fraction profile of free chain ends $\phi_g(z',N)$. For a given free chain end location z', the other segments in the chain are assumed to take the most probable path from the grafting surface to z'. The chain stretching function $E(z|z',N)$ determines the position z(s) of every segment, or, equivalently, $1/E(z \mid z',N)$ gives the segment density of the chain at z when its free end is at z'. In the lattice model there are many conformations for a chain grafted with one end to the surface and with its other end at some specified location. Each segment except the first one is not specifically located in one layer but has a density distribution given by eq 5. However, the average value of $\bar{z}(s)$, which follows from the volume fraction profile $\phi(z,s)$ of segment s, is

$$\bar{z}(s) = \frac{\int_z z\phi(z,s)dz}{\int_z \phi(z,s)dz} = \sigma^{-1}\int_z z\phi(z,s)dz/\ell \qquad (13)$$

Assuming that the most probable path may be approximated by the average path, the chain stretching function $E(z|z',N)$ can now be expressed in lattice model parameters as

$$E(z \mid z',N) \approx \frac{d\bar{z}(s)}{ds} = \sigma^{-1}\sum_z z\big(\phi_g(z,s+1) - \phi_g(z,s-1)\big) \tag{14}$$

The second term in eq 12 accounts for the free energy of mixing the grafted chains with the other molecules in the system, $f[\phi(z)]$ being the free energy density of mixing and $\phi(z)$ the volume fraction of grafted polymer at height z from the surface.

Taking into account the three additional conditions below, one can derive the equilibrium volume fraction profile $\phi_g(z)$, the free chain end volume fraction profile $\phi_g(z',N)$, the local chain stretching $E(z|z',N)$, and the thickness H of the grafted layer. The first two conditions are

$$\int_0^{z'} \frac{dz}{E(z \mid z',N)} = N_g \tag{15}$$

and

$$\int_0^H \phi_g(z)dz/\ell = \sigma N_g \tag{16}$$

and the third one is the relationship between $\phi_g(z)$, $\phi_g(z',N)$, and $E(z|z',N)$ which expresses that the total volume fraction at z is the integral over z' of all contributions by chains ending at z':

$$\phi_g(z) = \int_z^H \frac{\phi_g(z',N)dz'}{E(z \mid z',N)} \tag{17}$$

In ref 20 the derivation is carried out by minimizing the free energy function A of eq 12 under these constraints, using Lagrange's method of undetermined multipliers. This results in an expression for $E(z|z',N)$ that does not depend on the character of the interactions in the layer and is given by

$$E(z \mid z',N) = \frac{\pi}{2N_g}\big(z'^2 - z^2\big)^{1/2} \qquad (\text{for} \quad 0 \le z \le H) \tag{18}$$

The chains are stretched inhomogeneously; that is, their stretching is greatest near the grafting surface and zero at the free chain end. The volume fraction profile $\phi(z)$ follows from the potential field u(z), which is given by the equation

24

$$u(z)/kT = \frac{\delta f[\phi(z)]}{\delta\phi(z)} = \begin{cases} \Lambda - \dfrac{3\pi^2 z^2}{8N_g^2 \ell^2} & \text{if } 0 \le z \le H \\ 0 & \text{if } z > H \end{cases} \tag{19}$$

where the numerical constant Λ is a Lagrange multiplier defining the reference potential of u(z). If we give Λ a value such that the potential is zero in the bulk, then eq 18 defines the potential analogously to eq 1. The shape of the potential profile u(z) is parabolic and a function only of $N\ell$, the contour length of the chain, but independent of interactions and grafting density. Milner, Witten, and Cates[6] have pointed out the equivalence between following the grafted chain from its free end toward the surface, arriving after a fixed number of segments independent of the position z' of the free end, and following a classical particle in harmonic oscillation which moves from its maximum displacement z' to the centre in a time independent of the amplitude z' and with velocity E(z|z',N). In both cases the potential energy profile is parabolic.

The shape of the volume fraction profile is not yet determined once u(z) is found, for it also depends on the exact form of $f[\phi(z)]$. The free energy of mixing can be written as a Flory type of free energy of mixing:

$$f[\phi(z)] = (1-\phi(z))\ln(1-\phi(z)) + \chi\phi(z)(1-\phi(z)) \tag{20}$$

where χ is the Flory-Huggins interaction parameter. The usual contribution of the translational entropy of the polymer chains to the free energy is absent because of the chains being grafted. Substitution of eq 20 into eq 19 gives the following relation between the potential and the volume fraction profile

$$\frac{u(z)}{kT} = -\ln(1-\phi(z)) - 2\chi\phi(z) = \begin{cases} \Lambda - \dfrac{3\pi^2 z^2}{8N_g^2 \ell^2} & \text{if } 0 \le z \le H \\ 0 & \text{if } z > H \end{cases} \tag{21}$$

The expression for u(z) also follows directly from eq 1 by putting $\phi^b = 0$ (all the polymer is grafted so there is no polymer in the bulk) and $<\phi(z)> = \phi(z)$. In the analytical approach the difference between the segment site volume fraction and the average volume fraction of nearest-neighbour segments is neglected. Thus, $<\phi(z)> = \phi(z) + \lambda_1(\phi(z+1)-\phi(z)) - \lambda_1(\phi(z)-\phi(z-1))$, the equivalence in the analytical theory is

$$< \phi(z) > = \phi(z) + \lambda_1 \partial^2\phi(z)/\partial z^2 \tag{22}$$

As we show below in Figure 4, this approximation does not lead to large discrepancies as long as the curvature of the volume fraction profile is small. The

25

value of the numerical constant Λ can be found from the boundary condition at the periphery of the layer. For a Θ-solvent or better than Θ-solvent ($\chi \leq 0.5$), $\phi(H) = 0$, while in a worse than Θ-solvent ($\chi > 0.5$), $\phi(H) = \phi^{\prime b}$, where $\phi^{\prime b}$ is the equilibrium concentration on the coexistence curve for the limit $N \to \infty$ (see also ref 21). Within the framework of the Flory approximation $\phi^{\prime b}$ is obtained from the condition

$$\Delta\mu_1/kT = \ln\left(1 - \phi^{\prime b}\right) + \phi^{\prime b} + \chi\left(\phi^{\prime b}\right)^2 = 0 \tag{23}$$

where $\Delta\mu_1$ is the chemical potential of the solvent molecules in the concentrated phase with respect to that in the dilute phase which is pure solvent. Introducing the reduced coordinate $t = z/H$ and average volume fraction $\overline{\phi}$ of polymer in the grafted layer,

$$\overline{\phi} = \int_0^1 \phi(t)dt = \frac{N_g\sigma\ell}{H} \tag{24}$$

we obtain the final equation for the profile $\phi(z)$:

$$-\ln\left(\frac{1 - \phi(t)}{1 - \phi^{\prime b}}\right) - 2\chi\left(\phi(t) - \phi^{\prime b}\right) = \frac{3\pi^2\sigma^2(1 - t^2)}{8\phi^2} \qquad \text{if} \quad 0 \leq t \leq 1 \tag{25}$$

$$\phi(t) = 0 \qquad\qquad\qquad\qquad\qquad \text{if} \quad t > 1$$

where $\phi^{\prime b} = 0$ for $\chi \leq 0.5$ and $\phi^{\prime b}$ is given by eq 23 for $\chi \geq 0.5$. The left-hand side of eq 25 is just the expression for u(z) when $\phi^b = \phi^{\prime b}$ (assuming $<\phi(z)> = \phi(z)$). When $\phi^{\prime b} = 0$, eq 25 reduces to eq 21. For worse than Θ-solvents the volume fraction profile drops from $\phi(z) = \phi^{\prime b}$ to $\phi(z) = 0$ at the periphery of the layer. This is accompanied by a discontinuity in the segment potential at this point which corresponds to the difference between the segment potential in a solution of concentration $\phi^{\prime b}$ (i.e. $\ln\left(1 - \phi^{\prime b}\right) + 2\chi\phi^{\prime b}$; see eq 21) and that in the bulk of pure solvent (i.e. zero).

In Appendix 2 a simple numerical method is given by which $\phi(t)$ can obtained from eq 25 for a given combination of χ and σ.

Finally, the free chain end volume fraction profile $\phi(z',N)$ is obtained by inversion of the integral relationship in eq 17, where the functions E(z|z',N) and $\phi_g(z)$ are given by eqs 18 and 25, respectively.

Virial expansion

For low grafting densities ($\phi(t) \ll 1$) the logarithm of eq 20 can be expanded with retention of terms of order ϕ^2 and ϕ^3 to express the free energy function $f[\phi(z)]$ in terms of the virial coefficients $v = 0.5 - \chi$ and $w = 1/6$:

$$f[\phi(z)] \approx v\phi^2(z) + w\phi^3(z) \tag{26}$$

This expression leads to less precise results, but it enables us to find relatively simple expressions for various grafted layer characteristics.[5] Expanding eqs 23 and 25 to powers of $\phi(t)$ gives the corresponding equations for the profiles $\phi(t)$ and coexistence concentration $\phi'^b = -v/2w$. For the particular cases of an athermal and a Θ-solvent the profiles are given by

$$\frac{\phi(t)}{\bar{\phi}} = \begin{cases} \dfrac{3}{2}(1-t^2) & \text{if } 0 \le t \le 1 \text{ and } \chi = 0 \\[2mm] \dfrac{4}{\pi}\left(1-t^2\right)^{1/2} & \text{if } 0 \le t \le 1 \text{ and } \chi = 0.5 \\[2mm] 0 & \text{if } t > 1 \end{cases} \tag{27}$$

The corresponding thicknesses of the layer are

$$H = \begin{cases} \left(\dfrac{8v\sigma}{\pi^2}\right)^{1/3} N_g\ell & \text{if } \chi = 0 \\[3mm] \dfrac{4}{\pi}\left(\dfrac{w\sigma^2}{2}\right)^{1/4} N_g\ell & \text{if } \chi = 0.5 \end{cases} \tag{28}$$

The inversion of the integral relationship in eq 17 gives the following expressions for the free chain end volume fraction profile $\phi_g(t,N)$:

$$\phi_g(t,N) = \begin{cases} 3\sigma t\left(1-t^2\right)^{1/2} & \text{if } 0 \le t \le 1 \text{ and } \chi = 0 \\[2mm] 2\sigma t & \text{if } 0 \le t \le 1 \text{ and } \chi = 0.5 \\[2mm] 0 & \text{if } t > 1 \end{cases} \tag{29}$$

In ref 5 it was shown that for low grafting densities the swelling coefficient α of the layer, defined as $\alpha = H(\chi = 0)/H(\chi = 0.5)$, is a universal function of the parameter

$$\beta = \frac{v}{3}\left(2w^3\sigma^2\right)^{-1/4} \tag{30}$$

27

independent of the molecular weight of the grafted chains. The parameter β depends both on the solvent quality and on the grafting density. The relationship between α and β is given by

$$\frac{\pi}{2\beta^2} = \begin{cases} -\dfrac{\alpha}{\beta} + \left(1 + \dfrac{\alpha^2}{\beta^2}\right) \arctan\left(\dfrac{\alpha}{\beta}\right) & \chi \leq 0.5 \\[3mm] -\dfrac{5\alpha}{2\beta} + \left(\dfrac{1}{4} + \dfrac{\alpha^2}{\beta^2}\right) \arctan\left(\dfrac{2\alpha}{\beta}\right) & \chi > 0.5 \end{cases} \qquad (31)$$
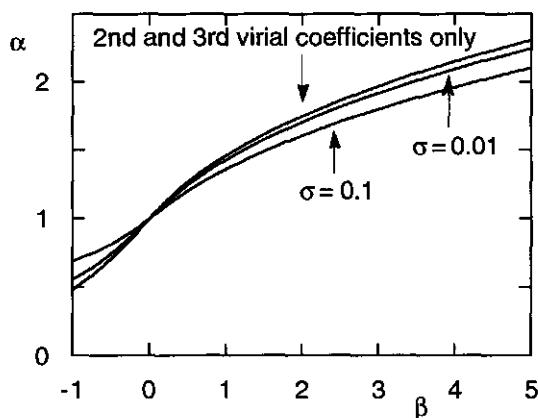

Figure 1. Swelling coefficient α versus the parameter β according to eq 31, based on a truncated virial expansion, and as calculated from the more exact eq 25 for grafting densities $\sigma = 0.1$ and 0.01.

In Figure 1 the function $\alpha(\beta)$ is plotted as given by eq 31. The curve passes through the point (0,1) at the Θ-temperature, where $\beta = 0$ (since $v = 0$) and $\alpha = 1$ by definition. As expected, in worse than Θ-solvents ($\beta < 0$) the swelling coefficient α is smaller than unity, while in good solvents ($\beta > 0$) the polymer layer is thicker than in a Θ-solvent. In most cases the swelling deviates by less than a factor of 2 from that in a Θ-solvent. For comparison, Figure 1 also shows the curves for grafting densities $\sigma = 0.01$ and $\sigma = 0.1$ that have been calculated directly from eq 25 without using the virial expansion. In the first curve only pair and ternary interactions are taken into account; in the latter two curves all higher order interactions are also accounted for. For high grafting densities these higher order interactions, which oppose the variation in swelling, become more important. For $\sigma = 0.1$ the approximation of $\alpha(\beta)$ given by eq 31 is much worse than for $\sigma = 0.01$. Clearly, eqs 26-31 lose validity for high grafting densities. In the next

section we present and compare results from the lattice model and from the analytical theory using the full expression for $f[\phi(z)]$.

Grafted chains in a polymer solution

To conclude this section, we briefly summarize the results for a grafted layer immersed in a solution of short mobile polymer chains with a degree of polymerization $N_f \ll N_g$ and a volume fraction profile denoted by $\phi_f(z)$. Now, the free energy density of mixing depends on both profiles, $\phi_g(z)$ and $\phi_f(z)$. Instead of eq 19 we have two simultaneous equations:

$$\frac{\delta f[\phi_g(t), \phi_f(t)]}{\delta \phi_g(t)} = \Lambda_g - K^2 t^2 \tag{32}$$

and

$$\frac{\delta f[\phi_g(t), \phi_f(t)]}{\delta \phi_f(t)} = \Lambda_f \tag{33}$$

with

$$K^2 = \frac{3}{8}\left(\frac{\pi H}{N_g \ell}\right)^2 \tag{34}$$

The numerical constants Λ_g and Λ_f are obtained from the boundary conditions. For the simplest case of grafted and mobile chains of the same monomer type in an athermal solvent

$$f[\phi_g(t), \phi_f(t)] = \frac{\phi_f(t)}{N_f}\ln(\phi_f(t)) + \left(1 - \phi_f(t) - \phi_g(t)\right)\ln\left(1 - \phi_f(t) - \phi_g(t)\right) \tag{35}$$

With the boundary conditions $\phi_g(H) = 0$ and $\phi_f(H) = \phi_f^b$ (where ϕ_f^b is the bulk concentration of mobile polymer) the solution of eqs 32 and 33 is

$$\phi_g(t) = \begin{cases} \begin{aligned} &(1 - \phi_f^b)\left[1 - \exp\left(-K^2\left(1 - t^2\right)\right)\right] \\ &+ \phi_f^b\left[1 - \exp\left(-K^2\left(1 - t^2\right)N_f\right)\right] \end{aligned} & \text{if } 0 \le t \le 1 \\ 0 & \text{if } t > 1 \end{cases} \tag{36}$$

$$\phi_f(t) = \begin{cases} \phi_f^b \exp\left(-K^2\left(1 - t^2\right)N_f\right) & \text{if } 0 \le t \le 1 \\ \phi_f^b & \text{if } t > 1 \end{cases} \tag{37}$$

29

No simple algebraic expression for H is available. However, the layer height is completely determined by eqs 34 and 36 and can easily be found numerically from the equation $\bar{\phi} - \int_{t=0}^{1} \phi(t)dt = 0$ for given values of ϕ_f^b, N_g, and N_f. The volume fraction profile $\phi_g(z',N)$ of free ends of the grafted chains is given by the equation

$$\phi_g(t,N) = \frac{2Kt}{N_g}\left\{\left(1 - \phi_f^b\right)D\left(\left(K^2\left(1 - t^2\right)\right)^{1/2}\right) + \phi_f^b \sqrt{N_f}\,D\left(\left(K^2\left(1 - t^2\right)N_f\right)^{1/2}\right)\right\} \qquad (38)$$

where

$$D(y) = e^{-y^2}\int_0^y e^{x^2}dx$$

is the Dawson integral.

1.4 Comparison of Results from Both Theories

In all the figures of this section the solid curves represent results obtained by the lattice model while the dashed curves show the asymptotic predictions of the analytical theory. The analytical profiles have been calculated by solving eq 25 for given values of σ and χ.
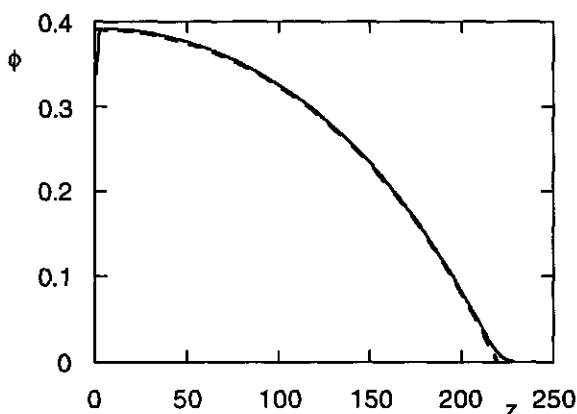

Figure 2 Volume fraction profile $\phi(z)$ according to the analytical theory (dashed curve) and the lattice model (solid curve). Parameters: $N_g = 600$, $\sigma = 0.1$, $\chi = 0$.

Figure 2 shows the volume fraction profile of a grafted polymer of 600 segments in an athermal solvent. The grafting density is 0.1; i.e., polymer chains are grafted to

10% of the surface sites. The very good agreement between the analytical predictions and the lattice calculations is striking. Only very close to the grafting surface and at the outer boundary of the grafted layer does a small difference between both curves occur. The lattice calculation shows a depletion zone at the grafting surface. Such a zone was previously seen in Monte Carlo simulations[12,13] and has also been observed by neutron scattering experiments.[22] The presence of the grafting surface restricts the conformational freedom of the polymer. This effect is neglected in the analytical theory. At the other side of the polymer layer the lattice calculation shows a "foot" protruding into the solution whereas the analytical theory predicts that the slope of the profile becomes monotonically steeper with increasing distance. This foot is an exponential decay of the segment density profile, caused by the fact that fluctuations of the average trajectory are large near the chain end where the chain stretching is weak.[23,24]
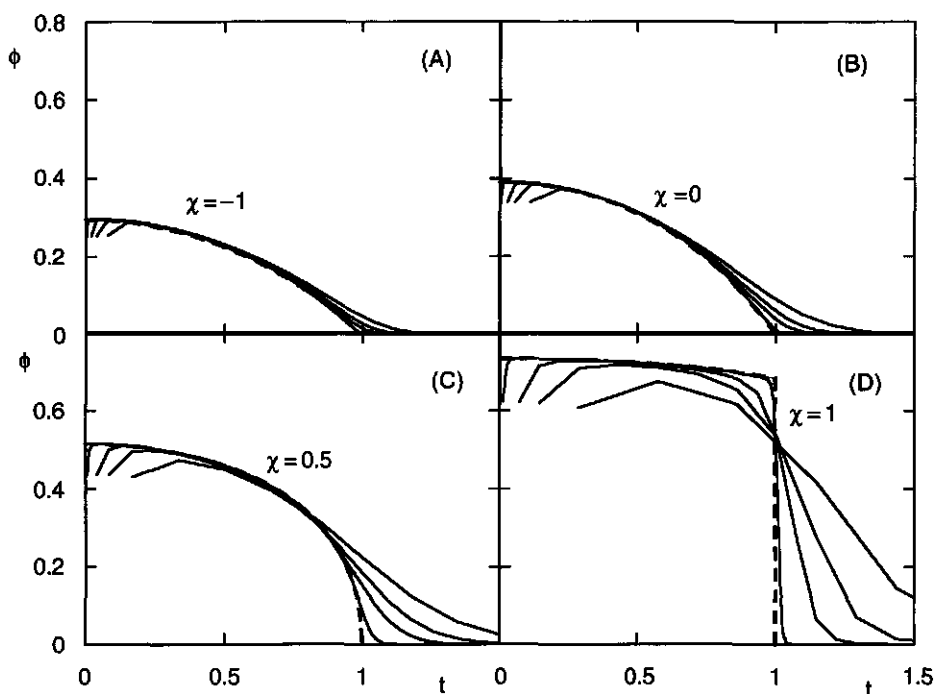

Figure 3 Volume fraction ϕ versus reduced height $t = z/H$ according to the analytical theory (dashed curve) and the lattice model for $N_g = 600$, 100, 50 and 25 (solid curves, in order of increasing deviation from the dashed curve): (A) $\chi = -1$, (B) $\chi = 0$, (C) $\chi = 0.5$, (D) $\chi = 1$. The grafting density σ is 0.1.

Figure 3 shows volume fraction profiles for different molecular weights of grafted polymer in a very good solvent ($\chi = -1$, Figure 3A), an athermal solvent (Figure 3B), a Θ-solvent (Figure 3C), and a bad solvent ($\chi = 1$, Figure 3D). In all cases the same (high) grafting density of $\sigma = 0.1$ has been used. The volume fractions are plotted as a function of the reduced height $t = z/H$, where the layer height H is taken from the analytical theory, using only eqs 24 and 25. This enables the comparison of profiles for different chain lengths N_g under the same conditions.

According to the analytical theory, $\phi(t)$ is independent of N_g. However, in agreement with Monte Carlo simulations,[13] Figure 3 shows that this is not valid for short chains. The shorter the chain length, the more the lattice model deviates from the analytical theory. Here the effect of the assumption made in the theoretical derivations that $N_g \gg 1$ is expressed. For all solvent qualities an increase in the chain length leads to a better agreement between both approaches. For a given chain length, increasing the solvent quality also leads to a better agreement. In a better solvent, the grafted layer is more strongly stretched. In a poorer solvent the layer is more dense, so that the unfavourable interactions between polymer segments and solvent molecules are reduced. In other words, the Newton approximation, which assumes strong stretching, is more valid in the case of a good solvent than for a poor solvent. Following parts A to D of Figures 3 for a fixed chain length, the breakdown of the Newton approximation becomes apparent. The deviation is largest in Figure 3D, for $\chi = 1$, where the analytical theory predicts a drop in the segment density profile at $t = 1$, whereas the lattice calculations reveal a more gradual decrease in segment density, especially for the short chains. However, in all cases the analytical theory seems to predict the asymptotic behaviour for $N \to \infty$ exactly. It is also worth noting that recent data from neutron scattering experiments on a grafted layer in a bad solvent are well described using a step function for the segment density profile.[25]

There is another effect which contributes to the deviations, especially in poor solvents. In the analytical theory it is assumed that the volume fraction $\phi(z)$ of the segments at position z is the same as $<\phi(z)>$, the average volume fraction of their nearest neighbours, whereas in the lattice model these quantities are distinguished; see eq 2. For weak curvatures of the volume fraction profile (good solvent, large N_g) the difference between $\phi(z)$ and $<\phi(z)>$ is not great, as $\phi(z - \ell) + \phi(z + \ell) \approx 2\phi(z)$, but for strong curvatures a more significant effect on the results is to be expected. This effect can be quantified by introducing the same assumption into the lattice model. This means replacing $< 1 - 2\phi(z) >$ by $1 - 2\phi(z)$ in eq 1 for the potential u(z). Parts A and B of Figure 4 give the profiles of parts C and D of Figure 3 for $N_g = 100$, together with the results for the case that $<\phi(z)>$ is set

equal to $\phi(z)$. For the Θ-solvent (Figure 4A) the two (solid) curves are virtually the same. For the bad solvent ($\chi = 1$; Figure 4B) the more approximate result is in slightly better agreement with the analytical predictions. However, a relatively large deviation still remains, which must be due to the strong-stretching approximation.
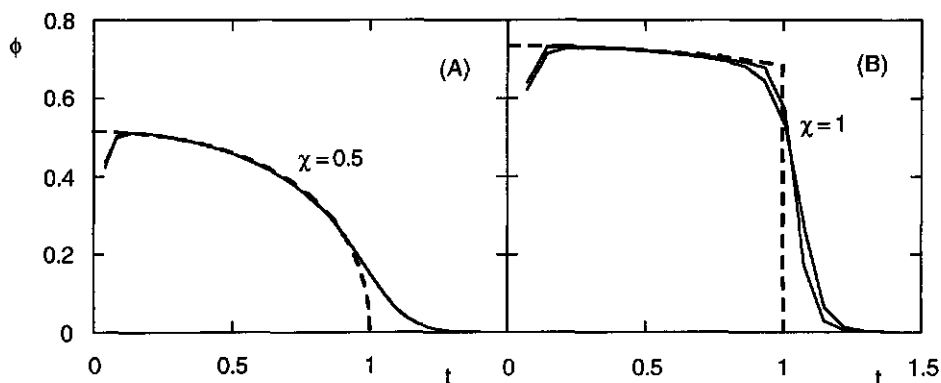

Figure 4 Effect of neglecting the curvature of the segment density profile when calculating the nearest-neighbour interactions. The segment density profiles of C ($\chi = 0.5$) and D ($\chi = 1$) of Figure 3 for $N_g = 100$ are reproduced in graphs A and B, respectively, and a second full curve in each graph represents the result when in the lattice calculations $<1 - 2\phi(z)>$ in eq 1 is replaced by $1 - 2\phi(z)$. In A the two solid curves virtually coincide. In B the latter curve is slightly more in agreement with the analytical prediction (dashed curve) where the same approximation is made.

Figure 5 shows segment potential energy profiles of a chain of 600 segments in solvents of various qualities ($\chi = 0, 0.5, 0.6, 0.75$, and 1.0). As with the volume fraction profiles, very good agreement is found between predictions from the analytical theory and lattice calculations, except at the grafting surface and at the periphery of the layer. For worse than Θ-solvents the volume fraction profile has a discontinuity at $z = H$. This discontinuity is caused by a jump in the potential profile from $u = -\ln\left(1 - \phi^{b}\right) - 2\chi\phi^{b}$ (the value of the potential at the periphery of the grafted layer; see eqs 23 and 25) to $u = 0$ (the bulk solution, in this case pure solvent, being taken as the reference state for the segment potential). As ϕ^{b} is the equilibrium volume fraction on the coexistence curve, the chemical potential of the solvent remains constant in the neighbourhood of H. The form of the curves is the same in all cases. The curves are shifted in the vertical direction only, reflecting a shift in the reference potential.
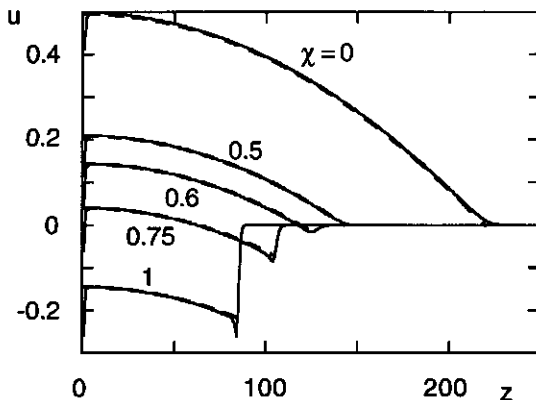
33

Figure 5 Segment potential energy profiles u(z) for grafted chains of 600 segments and grafting density 0.1 in different solvents: $\chi = 0$, 0.5, 0.6, 0.75, and 1.0 (indicated). Dashed curves: analytical predictions. Solid curves: lattice calculations.
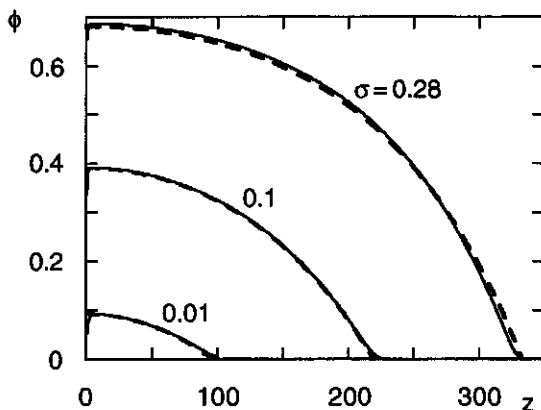

Figure 6 Effect of grafting density σ on the volume fraction profiles $\phi(z)$ according to the analytical theory (dashed curves) and the lattice model (solid curves). Parameters: $N_g = 600$, $\chi = 0$; $\sigma = 0.01$, 0.1, and 0.28 (indicated).

Decreasing the grafting density also gives less extended layers as is illustrated in Figure 6, where volume fraction profiles are given for $\sigma = 0.01$, 0.1 and 0.28. In all three cases $N_g = 600$ and $\chi = 0$. Although near the grafting surface and at the outer boundary of the grafted layer the relative deviation between the two theories

34

indeed increases with decreasing σ, the absolute differences remain roughly the same. For $\sigma = 0.28$ the lattice model predicts a volume fraction profile that is slightly stronger curved than is predicted by the analytical model. For the limiting case that the grafting density is unity the lattice model must give a step function profile ($\phi = 1$ for $z \leq N$ and $\phi = 0$ for $z > N$). We note that for these long chains a grafting density as high as even 0.1 is not easily reached in real systems. For example, adsorbed block copolymers typically give far lower densities.[26] The grafted amount in equivalent monolayers of segments, σN_g, varies from 168 for $\sigma = 0.28$ down to a more reasonable value of 6 for $\sigma = 0.01$.
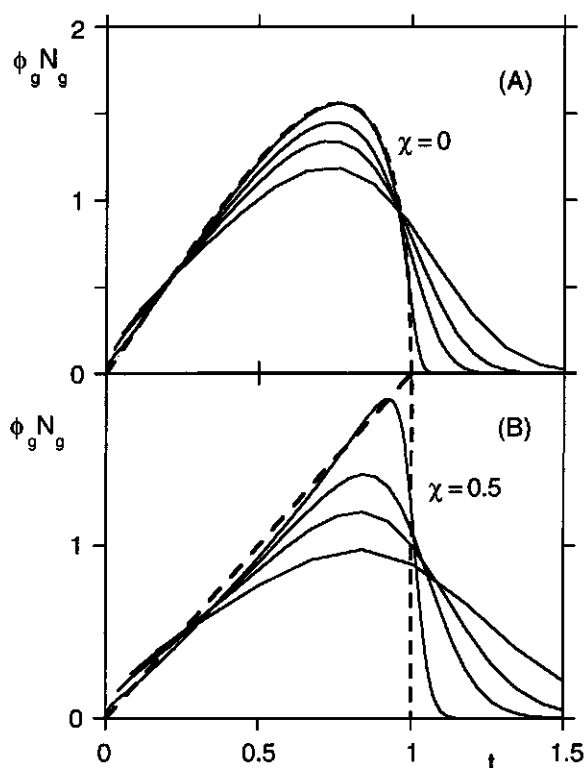

Figure 7 Distribution function of free ends, $\phi_g(t,N)N_g$, for chains of 600, 100, 50, and 25 segments and grafting density $\sigma = 0.1$, according to the analytical theory (dashed curves) and the lattice model (solid curves): (A) in an athermal solvent; (B) in a Θ-solvent.

So far, we have only compared the overall volume fraction profiles predicted by both theories. End-segment distribution profiles are plotted in Figure 7A for an athermal solvent and in Figure 7B for a Θ-solvent. Again, we use the reduced

35

height ($t = z/H$) as the abscissa in order to represent the curves for different chain lengths in one figure. Moreover, we have multiplied $\phi_g(z,N)$ by N_g, so that the areas under the curves are all the same. As was the case with the total volume fraction profile, the agreement between the analytical theory and the lattice model becomes better for longer chain lengths. The most striking feature when comparing parts A and B of Figure7 is the far better agreement for long chains in an athermal solvent compared to a Θ-solvent. However, this is mainly due to a difference in approximation. The results for the athermal solvent have been calculated using eq 38 with $\phi_f^b = 0$. This is an exact expression for $\phi_g(z,N)$ within the strong-stretching limit. Such an expression for Θ-solvents is not available. Therefore, the results for the Θ-solvent were calculated using eq 29, which was derived using the virial expansion of $f[\phi(z)]$. In spite of this approximation, it is clear that we expect a finite
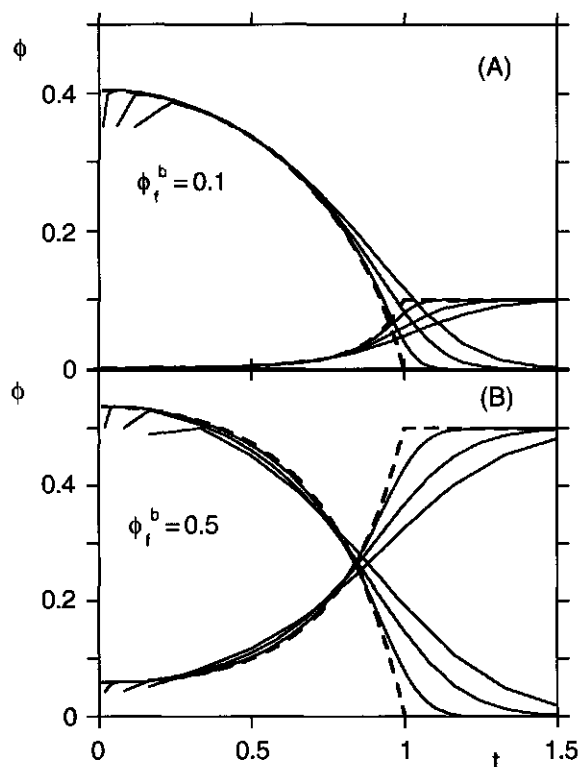

Figure 8 Volume fraction profiles of a grafted layer ($N_g = 200$, 50 and 25; $\sigma = 0.1$) immersed in an athermal solution of short mobile polymers ($N_f = 10$) of a chemically identical nature. Dashed curves: analytical theory. Solid curves: lattice model. Bulk volume fraction of mobile polymer: (A) $\phi_f^b = 0.1$; (B) $\phi_f^b = 0.5$.

end-segment volume fraction throughout the layer, also near the grafting surface, even if the grafting density is high and irrespective of the solvent quality.

We conclude by discussing the case of a grafted polymer layer immersed in an athermal solution of short mobile chains of a chemical nature identical to the grafted polymer. Parts A and B of Figure 8 show volume fraction profiles versus reduced height t for $\phi_f^b = 0.1$ and 0.5, respectively, with $N_f = 10$, $\sigma = 0.1$, and different values of N_g. Increasing the bulk volume fraction ϕ_f^b of the mobile chains compresses the grafted layer from $H = 67$ in Figure 8A to $H = 48$ in Figure 8B. Just as for grafted layers immersed in pure solvent, longer chain lengths of the grafted polymer give a better agreement between the analytical predictions and the lattice model. It is seen in Figure 8B that the mobile chains are able to penetrate throughout the grafted layer. This is due to their short length in comparison with the grafted polymer. Mobile polymer of the same chain length as the grafted polymer would only penetrate partly into the grafted layer.[27,28]

1.5 Conclusions

Very good agreement is found between the analytical theory and the lattice calculations. Only at low grafting densities of short chains in a poor solvent, considerable deviations are found between the two approaches because of the breakdown of the Newton approximation (strong chain stretching limit) in the analytical theory. The derivation of elegant expressions for the layer structure by expanding the mixing free energy in a virial series, as was done in ref 5, is only valid for relatively low grafting densities (see Figure 1).

Appendix 1

Iteration scheme for the lattice model

As we have only one type of segment and one solvent, our iteration scheme can be quite simple (Evers et al.[29] give a general scheme for systems with more than one different segment types). For a given set of values for $u(z)$, $G(z) = \exp(-u(z)/kT)$ is calculated and, from these Boltzmann factors, the volume fraction profile of grafted and free polymer is found (using eqs 3-11). The volume fraction $\phi_s(z)$ of solvent in layer z is obtained from eq A1:

$$\phi_s(z) = \left(1 - \phi^b\right)\exp\left(-u(z) + \chi(< 1 - 2\phi(z) >) - 1 + 2\phi^b\right) \qquad (A1)$$

Thus, for given values of $u(z)$, the volume fractions of grafted polymer, $\phi_g(z)$, of free polymer, $\phi_f(z)$, and of solvent, $\phi_s(z)$, can be calculated. In each layer z the sum of these volume fractions should obey the boundary constraint:

$$F(z) = \phi_g(z) + \phi_f(z) + \phi_s(z) - 1 = 0 \qquad (A2)$$

The objective functions $F(z)$ form a set of M simultaneous equations (one for each layer) in M unknown potentials $u(z)$. This set can be solved by standard numerical methods, e.g. using the Fortran program of Powell.[30]

Computational aspects for grafted chains

For long chains and high grafting densities, that is, when the chains are strongly stretched, the potentials $u(z)$ are high and $G(z) = \exp(-u(z)/kT)$ is smaller than unity. As $G(z)$ is recursively applied in eqs 4 and 10, the values of $G(z,s)$ and $G_g(z,s)$ become extremely small for large s while the normalization constant $C_g = \sigma/\sum_z G_g(z,N)$ becomes very large, easily exceeding the available numerical range on a computer. Obviously, since the volume fraction of grafted polymer, $\phi_g(z,s)$, is on the order of unity, the product of these quantities must be near unity; see eq 11. The numerical overflow and underflow can be avoided by proper scaling. First, we realize that $G(z,s)$ may be very small at small z and that it is unity for large z, i.e. in the bulk, but that we need only the initial part of the curve because in eq 11 $G(z,s)$ is multiplied by $G_g(z,s)$, which is zero for $z > s$. Consequently, the quantities $G(z, N - s + 1)$ for $z > s$ are irrelevant and may be set to zero. This eliminates the largest values and enables a substantial rescaling of the relevant section of $G(z,s)$.

Consider the extreme case of straight chains (when the grafted density $\sigma = 1$). Each segment s would be in layer $z = s$. Mathematically, $\phi_g(z,s) = 1$ if $z = s$ and

$\phi_g(z,s) = 0$ if $z \neq s$. Then, the only relevant quantities would be $G(N-s+1,s)$ and $G_g(s,s)$. In the following procedure we normalize the distribution functions so that these most important quantities are of order unity

Define scaled distribution functions $\tilde{G}(z,s)$ and $\tilde{G}_g(z,s)$ as

$$\tilde{G}(z,s) = \begin{cases} < \tilde{G}(z,s-1) > G(z)c(s) & \text{if } z \leq N-s+1 \\ 0 & \text{otherwise} \end{cases} \tag{A3}$$

$$\tilde{G}_g(z,s) = \ < \tilde{G}_g(z,s-1) > G(z)c_g(s) \tag{A4}$$

where $c(s)$ and $c_g(s)$ are introduced to compensate the low values of $G(z)$ and are chosen so that $\tilde{G}(N-s+1,s)$ and $\tilde{G}_g(s,s)$ remain on the order of unity. For example, set $c(s)$ and $c_g(s)$ equal to unity for $s = 1$ and $c(s) = 1/\tilde{G}(N-s+1,N-s+1)$ and $c_g(s) = \tilde{G}_g(s-1,s-1)$ for $s > 1$. Essentially, eqs A3 and A4 replace eqs 4 and 10, respectively. The relations between the scaled and unscaled quantities are

$$\tilde{G}(z,s) = \begin{cases} G(z,s)\prod_{s'=1}^{s} c(s') & \text{if } z \leq N-s+1 \\ 0 & \text{otherwise} \end{cases} \tag{A5}$$

and

$$\tilde{G}_g(z,s) = G_g(z,s)\prod_{s'=1}^{s} c_g(s') \tag{A6}$$

but the functions $G(z,s)$ and $G_g(z,s)$ are not used. The factors $c(s)$ and $c_g(s)$ are not too far from unity, while the multiple products in eqs A5 and A6 may be very large. The next step is to compute the scaled distribution function $\tilde{\phi}_g(z,s)$ of segment s:

$$\tilde{\phi}_g(z,s) = \tilde{G}_g(z,s)\ \tilde{G}(z,N-s+1)/G(z) \tag{A7}$$

and normalize it to obtain $\phi_g(z,s)$:

$$\phi_g(z,s) = \frac{\sigma\tilde{\phi}_g(z,s)}{\sum_z \tilde{\phi}_g(z,s)} \tag{A8}$$

This scheme applies only to grafted chains. For free chains the function $G(z,s)$ is especially relevant for large values of z and does not need to be scaled.

Appendix 2

Iteration scheme for solving equation 25

This method consists of a pair of nested loops. In the main iteration loop the variable $\bar{\phi}$ is adjusted until $\bar{\phi} - \int_{t=0}^{1} \phi(t)dt < \varepsilon$, where ε can be chosen as an arbitrarily small number. We have used $\varepsilon = 10^{-6}$. The function $\phi(t)$ is obtained in a subiteration which solves $\phi(t)$ for a series of t values, using eq 25 and the current value of $\bar{\phi}$. From the values of $\phi(t)$ the integral $\int_{t=0}^{1} \phi(t)dt$ can be approximated. For example, if $\phi(t)$ is known at $t' = \delta, 3\delta, 5\delta, ..., 1-\delta$, where δ is a sufficiently small number, the integral is approximately $2\delta\sum_{t'}\phi(t')$. Our results are obtained with $\delta = 10^{-4}$.

References

(1) Alexander, S. *J. Phys. (Paris)* **1977**, *38*, 983.
(2) de Gennes, P. G. *J. Phys. (Paris)* **1976**, *37*, 1445.
(3) de Gennes, P. G. *Macromolecules* **1980**, *13*, 1069.
(4) Semenov, A. N. *Sov. Phys. JETP* **1985**, *61*, 733.
(5) Zhulina, E. B.; Borisov, O. V.; Priamitsyn, V. A. *J. Colloid Interface Sci.* **1990**, *137*, 495.
(6) Milner, S. T.; Witten, T. A.; Cates, M. E. *Macromolecules* **1988**, *21*, 2610.
(7) Zhulina, E. B.; Borisov, O. V.; Brombacher, L. *Macromolecules* **1991**, *24*, 4679.
(8) Zhulina, E. B.; Borisov, O. V.; Priamitsyn, V. A.; Birshtein, T. M. *Macromolecules* **1991**, *24*, 140.
(9) Milner, S. T.; Witten, T. A.; Cates, M. E. *Macromolecules* **1989**, *22*, 853.
(10) Milner, S. T.; Witten, T. A.; Cates, M. E. *Europhys. Lett.* **1988**, *5*, 413.
(11) Klushin, L. I.; Skvortsov, A. M. *Macromolecules* **1991**, *24*, 1549.
(12) Cosgrove, T.; Heath, T.; Van Lent, B.; Leermakers, F.; Scheutjens, J. *Macromolecules* **1987**, *20*, 1692.
(13) Chakrabarti, A.; Toral, R. *Macromolecules* **1990**, *23*, 2016.
(14) Lai, P.-Y.; Zhulina, E. B. *J. Phys. II* **1992**, *2*, 547.
(15) Lai, P.-Y.; Binder, K. *J. Chem. Phys.* **1991**, *95*, 9288.
(16) Hirz, S. *M.S. Thesis*, University of Minnesota **1987**.
(17) Skvortsov, A. M.; Gorbunov, A. A.; Pavlushkov, I. V.; Zhulina, E. B.; Borisov, O. V.; Priamitsyn, V. A. *Polymer Science USSR* **1988**, *30*, 1706.
(18) Scheutjens, J. M. H. M.; Fleer, G. J. *J. Phys. Chem.* **1979**, *83*, 1619.
(19) Scheutjens, J. M. H. M.; Fleer, G. J. *J. Phys. Chem.* **1980**, *84*, 178.
(20) Zhulina, E. B.; Priamitsyn, V. A.; Borisov, O. V. *Polymer Science USSR* **1989**, *31*, 205.

(21) Shim, D. F. K.; Cates, M. E. *J. Phys. (Paris)* **1989**, *50*, 3535.

(22) Auroy, P.; Auvray, L.; Leger, L. *Phys. Rev. Lett.* **1991**, *66*, 719.

(23) Witten, T. A.; Leibler, L.; Pincus, P. *Macromolecules* **1990**, *23*, 824.

(24) Milner, S. T. *J. Chem. Soc. Faraday Trans.* **1990**, *86*, 1349.

(25) Auroy, P.; Auvray, L.; Leger, L. *Macromolecules* **1991**, *24*, 2523.

(26) Evers, O. A.; Scheutjens, J. M. H. M.; Fleer, G. J. *J. Chem. Soc. Faraday Trans.* **1990**, *86*, 1333.

(27) Van Lent, B.; Israels, R.; Scheutjens, J. M. H. M.; Fleer, G. J. *J. Colloid Interface Sci.* **1990**, *137*, 380.

(28) Ligoure, C.; Leibler, L. *J. Phys. (Paris)* **1990**, *51*, 1313.

(29) Evers, O. A.; Scheutjens, J. M. H. M.; Fleer, G. J. *Macromolecules* **1990**, 5221.

(30) Powell, M. J. D. In *Numerical Methods for Nonlinear Algebraic Equations*; Rabinowitz, P., Ed.; Gordon and Breach: London, 1970; p 115.

chapter 2

Chain Stiffness and Bond Correlations in Polymer Brushes

Abstract

We have incorporated chain stiffness and correlations between neighbouring bonds into a self-consistent field lattice model for end-attached polymer layers (commonly known as "brushes"). An increase in the chain stiff stiffness leads to an increasing brush height. This increase is directly related to the change of the length of a Kuhn segment in the polymer chain. Introducing correlations between neighbouring bonds gives a higher density of the brush, corresponding to a decrease of the brush height. For not too stiff chains these two effects virtually compensate each other. Hence, the volume fraction profile of "real" grafted chains is nearly identical to that of a polymer brush consisting of freely jointed chains.

2.1 Introduction

During the last several years polymer brushes, which are formed by attaching one end of each polymer chain to a surface, have been the subject of many theoretical investigations.[1] One very useful way to study such systems is to apply a self-consistent field (SCF) lattice model. For example, the polymer adsorption theory of Scheutjens and Fleer[2] has been extended to brushes.[3-5] In this model all possible conformations of polymer chains that can be generated on a lattice are weighted and averaged, using a random flight approximation for the chains (freely jointed chains). Another approach for polymer brushes has been developed by Zhulina et al.[6] and Milner et al.[7] The latter theories are based on the assumption that the total set of possible polymer conformations can be replaced by a set of most likely trajectories. They are more approximate than the lattice model but lead to more handsome mathematical expressions. For high grafting densities and long chains, this approach agrees very well with the lattice calculations.[5]

In this chapter we describe two different extensions of the lattice model. So far, the polymer molecules have been described as freely jointed chains. For example, immediate step reversals are then allowed. The polymer chain conformations are treated as step-weighted walks in a potential field. This potential field depends, in a mean-field approximation, on all the components present in the system. In contrast to the description of polymer brushes based upon scaling arguments, direct correlations are neglected: all interactions between segments enter solely through the mean potential field. The molecular architecture of the polymer chains is only reflected in the connectivity of the segments. Each bond is basically described as a Kuhn segment. In other words, the chain conformation weighting factors are calculated using a first order Markov model. The SCF theories of Zhulina et al.[6] and Milner et al.[7] are based on exactly the same physical picture. Zhulina et al. did, however, also consider the more general case that the polymer chain is stiffer than a random flight chain. They introduced a stiffness parameter p, which they defined as the ratio of the Kuhn length and the segment diameter. This stiffness can easily be incorporated into the expression for the elastic free energy of deformation (stretching) of a Gaussian coil conformation.

In this chapter we incorporate chain stiffness into the lattice model. We describe the general formalism for doing so. Basically, it means that the statistical weights of the chain conformations are calculated using a second order Markov model. We discuss two ways of implementing the general formalism for chain stiffness. One (rather trivial) way is to join each group of p consecutive segments together to form a short rigid rod. The rigid rods are then themselves freely jointed to one another. The second way is to introduce energy differences between different segment

43

orientations in a polymer chain. In the Theory section we shall first briefly review the "conventional" lattice model for freely jointed chains (f.j.c.) in a potential gradient. Then we discuss these two methods of introducing chain stiffness.

Another modification of the lattice model, which we present in section 3, is the incorporation of directional correlations between bonds in close (spatial) proximity. These bonds need not be situated close to each other along the polymer chain, nor do they even have to be on the same polymer chain. In effect, a kind of nematic ordering is taken into account. Although in this case the numerical procedure to calculate the brush profile is rather similar to that used for the freely jointed chains and that used for stiff chains, the underlying model is fundamentally different.

In the Results section a selection of data will be presented that were obtained with the various forms of the lattice model.

2.2. Theory for Markov chains

Freely jointed chains[2,5]

Consider a lattice of M layers, which are numbered $z = 1, 2, ..., M$, with layer 1 situated adjacent to the surface. The lattice spacing ℓ is equal to the polymer segment diameter. A fraction λ_0 of the contacts of a lattice site is with sites in the same layer. Similarly, a fraction λ_1 of the contacts is with sites in a lower layer and the same fraction λ_1 with sites in a higher layer. For a simple cubic lattice, which has been used to derive all the results presented in this chapter, $\lambda_0 = 2/3$ and $\lambda_1 = 1/6$. The polymer chains have a chain length of N segments, of which the first is located in the first layer. The volume fraction of these first segments is identical to the grafting density σ. The volume fraction of polymer in layer z is written as $\phi(z)$. Nearest-neighbour interactions between polymer segments and solvent are accounted for by the Flory-Huggins interaction parameter χ. Because of the mean-field approximation all interactions within a layer are smeared out. We assume throughout this chapter that the polymer segments have no adsorption energy. The potential energy $u(z)$ of a polymer segment in layer z is given by

$$u(z)/kT = -2\chi < \phi(z) > - \ln(1 - \phi(z)) \tag{1}$$

where the angular brackets <> denote a weighted average over three layers, which accounts for the fraction of contacts that a segment or solvent molecule has with its nearest neighbours in these three layers:

$$<\phi(z)> = \lambda_1 \phi(z-1) + \lambda_0 \phi(z) + \lambda_1 \phi(z+1) \tag{2}$$

We define a segment weighting factor G(z) as

$$G(z) = \exp(-u(z)/kT) \tag{3}$$

which is a Boltzmann factor of the segment potential in layer z. The connectivity of the segments in a polymer chain is accounted for by introducing the end-segment weighting factors $G(z,s|z',1)$ and $G(z,s|z',N)$. The quantity $G(z,s|z',1)$ is defined as the average statistical weight of all conformations of an s-mer of which the last segment is located in layer z and the first segment is in layer z'. As the first segment is grafted in the first layer, the quantity $G(z,s|z',1)$ is only nonzero for $z' = 1$. Moreover, for $z > s$ it automatically follows that $G(z,s|1,1) = 0$. The quantity $G(z,s|z',N)$ is defined as the average statistical weight of all conformations of an $(N-s+1)$-mer of which the first segment (s) is located in layer z and the last segment (N) is in layer z'. As this last segment may be located anywhere in the system, it is convenient to define $G(z,s|N) = \sum_{z'} G(z,s|z',N)$. For a freely jointed chain the end-segment weighting factors obey the following recurrence relations:

$$G(z,s|1,1) = \ <G(z,s-1|1,1)> G(z)$$
$$G(z,s|N) \ = \ <G(z,s+1|N)> G(z) \tag{4}$$

For $s = 1$ and $s = N$, respectively, these sequences are started as follows,

$$G(z,N|N) = G(z) \quad \forall z$$
$$\text{and} \tag{5}$$
$$G(1,1|1,1) = G(1)$$

The volume fraction $\phi(z,s)$ of polymer segment s in layer z is proportional to the product of two end-segment weighting factors:

$$\phi(z,s) = C\,G(z,s|1,1)G(z,s|N)/G(z) \tag{6}$$

Here, the denominator accounts for the fact that segment s is counted twice (belonging to both chain parts). The normalization constant C follows from the boundary condition $\sigma = \sum_z \phi(z,s)\ \forall s$. Substituting $\phi(z,s)$ from eq 6 for $s = N$ we obtain

$$C = \frac{\sigma}{\displaystyle\sum_z G(z,N|1,1)} \tag{7}$$

Finally, the total volume fraction in layer z is

$$\phi(z) = \sum_s \phi(z,s) \tag{8}$$

45

This volume fraction profile, obtained for a given u(z) profile, should be consistent with eq 1 for all values of z. This provides a set of M simultaneous equations in M unknown variables u(z), which can be solved using standard numerical procedures.

General formalism for stiff polymer chains.

We take the freely jointed chain as the starting point for our discussion. In such a chain a bond between two segments can be in six different directions on a simple cubic lattice. For a freely jointed chain the probability of any of these six directions to occur does not depend on the position of the previous bond. In this section we describe a model where this probability does depends on the previous bond. Depending on the angle the new bond makes with the previous one, we denote its conformation as "backward", "forward", or "perpendicular". This is illustrated in the Figure 1.
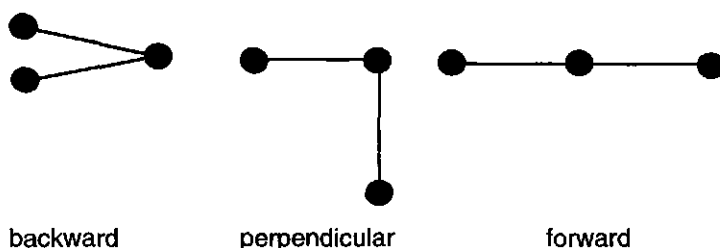

backward   perpendicular   forward

Figure 1   Three possible bond angles for a sequence of 3 connected segments on a cubic lattice.

As an example we discuss the case that segment $s-1$ of a chain is in layer $z-1$ and segment s is in layer z. Segment s+1 can be in layers $z-1$, z, or $z+1$. If it is in layer $z-1$ we have the backward conformation: the two consecutive bonds form an angle of 180° and segment $s+1$ is located on the same lattice site as segment $s-1$. If segment $s+1$ is in layer z the bond conformation is perpendicular: the bond angle is 90°. On a cubic lattice such a perpendicular conformation can be made in four directions. If segment $s+1$ is in layer $z+1$ the conformation is forward and the bond angle is 0°. We denote the a priori probability of each of these three conformations as B, P, and F, respectively, so that: $B+F+4P = 1$. For a freely jointed chain these probabilities are just given by the lattice parameters: $B = F = \lambda_1 (= 1/6)$ and $4P = \lambda_0 (= 4/6)$. It is possible to introduce a certain degree of stiffness of the chain by changing the values of the B, P, and F parameters. We discuss two approaches: (i) the freely jointed rods model; (ii) the limited bond flexibility model. First we

46

describe the general formalism to calculated the volume fraction profile of a brush consisting of stiff chains.

We consider the general case that the parameters B, P, and F are functions of the segment ranking number s. For each segment s we introduce the energies $U^B(s)$, $U^F(s)$, and $U^P(s)$ associated with backward, forward, and perpendicular conformations of its bonds, respectively. The parameters B(s), P(s), and F(s) are related to these energies as follows:

$$B(s) = C\exp\left(-U^B(s)/kT\right)$$
$$F(s) = C\exp\left(-U^F(s)/kT\right) \qquad (9)$$
$$P(s) = C\exp\left(-U^P(s)/kT\right)$$

where the normalization constant C follows from the condition that $B(s) + F(s) + 4P(s) = 1$.

When calculating the end-segment distribution functions of a polymer chain, we have to take into account whether the addition of a new bond to the chain corresponds to a backward, a forward, or a perpendicular conformation. The appropriate weighting factor for that conformation must then be included. In order to do this, we introduce the end-segment weighting factors G(z,s,d|1,1) and G(z,s,d|N) as extensions of the end-segment weighting factors G(z,s,|1,1) and G(z,s|N) as introduced for the freely jointed chain model. In the expression G(z,s,d|1,1) the letter d denotes the direction from segment s to s + 1. If segment s is located in layer z, the value of the direction d is −1 when segment s + 1 is in layer z − 1; d = 0 when segment s + 1 is also in layer z; and d = +1 when segment s + 1 is in layer z + 1. In the expression G(z,s,d|N) the letter d denotes the direction from segment s + 1 to s. The recurrence relations in eq 4 for freely jointed chains (and the starting conditions of eq 5) must now be extended to account for the contribution of the different bond conformations to the end-segment weighting factors. The resulting expressions are given in eqs A1.1 - A1.5 of Appendix 1.

In order to calculate the volume fraction of segment s (s < N) in layer z, one must realize that if the bond from segment s to segment s + 1 is in direction d, the bond from segment s + 1 to segment s must be in direction −d. Hence, we can write:

$$\phi(z,s) = \frac{\sigma}{\sum_z G(z,N \mid 1,1)} \sum_{d=-1,0,1} G(z,s,d \mid 1,1)G(z,s,-d \mid N)/G(z) \quad \text{for } s = 1, 2, \ldots, N-1$$

$$\phi(z,N) = \frac{\sigma}{\sum_z G(z,N \mid 1,1)} G(z,N \mid 1,1) \qquad (10)$$

47

This equation is a generalization of eq 6 for freely jointed chains towards stiff chains. We have made use of the fact that the end-segment ($s = N$) only has one bond. For stiff polymer chains $G(z,N|1,1)$ is defined by eq A1.2.

The model described in this section is basically a cubic lattice version of the RIS (rotational isomeric state) scheme as described by Leermakers and Scheutjens.[8]

Freely jointed stiff rods.

We now consider the case that a group of p consecutive segments is clustered into a stiff rod. These rods are freely jointed to each other. Conceptually this is the easiest model of a polymer chain with stiffness parameter p. We only discuss the situation $p = 2$ but we note that for larger values of p a straightforward generalization is possible. The bond between segments 1 and 2 can be placed in any direction. The next bond (between segments 2 and 3) must, however, be in a forward conformation. The bond between segments 3 and 4 can again be in any of the three conformations, but the bond between segments 4 and 5 must be in a forward conformation, etc.

If we have a chain of freely jointed stiff rods, each with a length of 2 segments, the segment bonds are alternatingly completely flexible and fixed in the forward conformation. The total number of segments in a chain must be an odd number in order to have an integer number of rods. In general, the chain length (expressed as number of segments) must be equal to $np + 1$, with n an integer number. In eq A1.1 we take $F(s) = 1$ and $B(s) = P(s) = 0$ for even values of s, and $B(s) = F(s) = \lambda_1$ and $P(s) = \lambda_0$ for odd values of s. In eq A1.4 we take $F(s) = 1$ and $B(s) = P(s) = 0$ for odd values of s, and $B(s) = F(s) = \lambda_1$ and $P(s) = \lambda_0$ for even values of s. In this case the polymer has to be grafted both in the first and second layer (or, more generally, in the first p layers) with a grafting density of $\sigma/2$ in both these layers. This is necessary in order to have such a set of conformations that all segments can be both in odd and even numbered layers. The easiest way to do this is to calculate the end-segment distribution functions for the chains grafted in the first layer and in those grafted in the second layer separately. The quantity $G(z,s,d|1,1)$ is replaced by $G(z,s,d|j,1)$, where the index j can take the values 1 and 2. Equation A1.3 is replaced by:

$$G(j,1,d \mid j,1) = \begin{cases} 1/6 & \text{if } d = 1 \\ 4/6 & \text{if } d = 0 \quad \text{for } j = 1, ..., p \\ 0 & \text{if } d = -1 \end{cases} \tag{11}$$

Equations A1.1, A1.2, A1.4, and A1.5 are applied both for $j = 1$ and $j = 2$. The volume fractions $\phi(z,s|j)$ are also calculated for $j = 1$ and $j = 2$:

$$\phi(z,s\,|\,j) = \frac{\sigma}{\sum_z G(z,N\,|\,j,1)} \sum_{d=-1,0,1} G(z,s,d\,|\,j,1)G(z,s,-d\,|\,N)/G(z) \quad \text{for } s = 1, 2\,...,\,N-1$$

$$\phi(z,N\,|\,j) = \frac{\sigma}{\sum_z G(z,N\,|\,j,1)} G(z,N\,|\,j,1) \tag{12}$$

The total volume fraction of polymer $\phi(z)$ in layer z is:

$$\phi(z) = \sum_{j=1,2} \sum_{s=1}^{N} \phi(z,s\,|\,j) \tag{13}$$

Limited bond flexibility.

In the limited bond flexibility model all segment bonds are treated equally. Instead of making half the bonds completely flexible and the other half completely stiff, they are all made partly stiff. We first (arbitrarily) define $B(s) = 0$ for all s, so that all conformations are excluded where bonds fold back onto the previous bond. If there were no further restrictions, $F(s) = P(s) = 1/5$ according to eq 9. However, we also introduce a "bending" energy difference $U^{ben}(s) = U^P(s)-U^F(s)$ between the forward and perpendicular conformations, which is positive if a forward conformation is preferred above a perpendicular one. In our present implementation U^{ben} is constant: $U^{ben}(s) = U^{ben}$ for all s. The chain conformation probabilities depend only upon this energy difference and not upon the absolute values of $U^F(s)$ and $U^P(s)$. Two consecutive bonds must overcome the energetic barrier U^{ben} in order to "bend" and form a 90° bond. For a cubic lattice we now can write:

$$F = 1-4P \text{ and } P = \left(4 + \exp\left(U^{ben}/kT\right)\right)^{-1} \tag{14}$$

with $F(s) = F$ and $P(s) = P$ for all s.

The two constraints that we have imposed upon the conformations (no backfolding and restricted bond flexibility) make the polymer chain stiff. For a freely jointed chain the ratio p between Kuhn length and bond length is unity. For the stiff chains p > 1. The dependence of p on P is derived in Appendix 3.

In the limited bond flexibility model U^{ben} is an input parameter. From eq 14, F and P follow directly, and B = 0 as indicated above. Then applying eqs A1.1 - A1.5 and subsequently eq 10, the volume fraction profile $\phi(z,s)$ of each segment can be calculated. Combining this with eq 8 yields the total volume fraction profile of the polymer. As for freely jointed chains, this volume fraction profile must be consistent with eq 1 for all values of z.

49

2.3 Correlations between neighbouring bonds

The freely jointed chain model, which was discussed in the first part of section 2, is an extension of the classical Flory-Huggins theory for homogeneous polymer solutions towards systems with a concentration gradient. The weighting factor of an arbitrary chain conformation follows from the end-segment weighting factors. These end-segment weighting factors are calculated using a recurrence relation where, for example, $G(z,s|1,1)$ is determined by $G(z,s-1|1,1)$, but does not directly depend on any values of $G(z,s'|1,1)$ for $s' < s-1$. That is why a freely jointed chain may be called a first order Markov chain. In the classical Flory-Huggins theory polymer chains are treated in a completely analogous manner.

The stiff chains discussed in the previous section may be considered as second order Markov chains. For these chains $G(z,s|1,1)$ depends on the position of segments $s-1$ and $s-2$. As shown above, the extension from a first order to a second order Markov chain is easy to make, both conceptually and from a computational point of view. An alternative form of the Flory-Huggins theory for homogeneous solutions can be derived using second (or higher) order Markov chains. However, this has no effect on the equations that describe the thermodynamic parameters of a polymer solution, as long as these are defined with respect to the pure amorphous phases of its constituent components. For example, the chemical potential of a monomeric solvent in a homogeneous mixture of solvent (volume fraction $1-\phi$) and polymer (volume fraction ϕ) is given by:

$$\frac{\mu - \mu^*}{kT} = \ln(1-\phi) + \phi - \phi/N + \chi\phi^2 \qquad (15)$$

The chemical potential is defined with respect to a system consisting of pure solvent, denoted by the superscript *. Equation 15 holds both for systems with freely jointed chains and for systems with second order Markov chains.

In this section we extend the lattice model for polymer brushes to incorporate correlations between neighbouring bonds. These interactions are fundamentally different from those giving rise to the chain stiffness and which were accounted for in the previous section by applying a second order Markov procedure. We now have to deal with excluded volume interactions between segments that are spatially in close proximity, but that need not at all be close to each other along the contour of the chain (in fact, the segments even need not be situated on the same chain). Below, this feature is explained in more detail.

For a Markov chain the value of $G(z,s|1,1)$ depends on $<G(z,s-1|1,1)>$ and $G(z)$ (eqs 4 or A1.1). The factor $<G(z,s-1|1,1)>$ accounts for the position of segment $s-1$, to which segment s is attached. The factor $G(z)$ is a function of the potential in

layer z. If $\phi(z) = 0$, then the second term in eq 1 contributes a factor unity to $G(z)$. All lattice sites in layer z are available for segment s. However, if $\phi(z) > 0$ and, for example, segment $s-1$ is in layer $z-1$, then there is a finite probability that the step from segment $s-1$ in layer $z-1$ to s in layer z is blocked by a polymer segment in layer z. This probability is accounted for by the nonzero value of $\phi(z)$ in the second term of eq 1, and enters through $G(z)$ into the recurrence relation (eqs 4 or A1.1). The fact that a step may be blocked is caused by the excluded volume of the segments.

At this point one must realize that the use of the term $\ln(1-\phi)$ corresponds to an approximation of fundamental importance, which is related to the mean-field character of the model. Suppose a large fraction of sites in layer z are filled with segments (s) that have a connected segment $(s-1$ or $s+1)$ in layer $z-1$. In this case the probability for a test chain to make a step from layer $z-1$ to z is higher than that predicted by eq 4. Such a step is not blocked by a segment in layer z whose preceding (or following) segment is in layer $z-1$. Parallel bonds never interfere with each other! The mean-field character of the theory discussed so far does not incorporate this aspect of the excluded volume interactions.

We can account for this effect by introducing a quantity $\phi(z|z')$ as the fraction of possible bonds between layers z and z' that is actually realized. Obviously, $\phi(z|z') = 0$ for $|z - z'| > 1$ and $\phi(z|z+1) = \phi(z+1|z)$. If segments s and $s+1$ are both in the same layer z, this means that the value of d in the end-segment weighting factors $G(z,s,d|1)$ and $G(z,s,d|N)$ is equal to zero. For $z = z'$ we may then write:

$$\phi(z \mid z) = \frac{\sigma}{\sum_z G(z,N \mid 1,1)} \sum_{s=1}^{N-1} (G(z,s,0 \mid 1,1) G(z,s,0 \mid N)) / G(z) \tag{16}$$

Similarly for $z' = z+1$ we have:

$$\phi(z \mid z+1) = \frac{\sigma}{\sum_z G(z,N \mid 1,1)} \sum_{s=1}^{N-1} \left(\begin{array}{c} G(z,s,1 \mid 1,1) G(z,s,-1 \mid N) + \\ G(z+1,s,-1 \mid 1,1) G(z+1,s,1 \mid N) \end{array} \right) \Big/ G(z) \tag{17}$$

Because of the parallel bonds, the probability of making a step from layer z to $z+1$ is increased (as compared to eq 4) by a factor

$$g(z \mid z+1) = (1 - \phi(z \mid z+1))^{-1} \tag{18}$$

On average, half of all bonds in layer z (i.e. $\phi(z|z)$) will be in the x-direction and the other half will be in the y-direction. So, the probability of making a step from layer z to z is increased by a factor

51

$$g(z \mid z) = \left(1 - \frac{1}{2}\phi(z \mid z)\right)^{-1} \tag{19}$$

These factors g(z|z') must be added to the recurrence relations (eqs A1.1 and A1.4). This leads to the new recurrence relations and starting conditions which are given in Appendix 2. In this appendix the bond correlation factors are incorporated into the general formalism for stiff polymer chains. The method is basically a cubic lattice version of the SCAF (self-consistent anisotropic field) scheme given by Leermakers and Scheutjens.[9]

Having calculated the end-segment distribution functions, the polymer volume fractions again follow from eq 10. The end-segment distribution functions are computed for a set of g(z|z) and g(z|z+1) (and u(z)) values. These values must be consistent with the volume fraction profile. This means that for a system of M layers we have to solve a set of equations with 3M variables: the potential u(z) and the factors g(z|z) and g(z|z+1) in each layer z.

The bond correlation factors can also be taken into account in the statistical thermodynamics of a homogeneous polymer solution. This leads to different results as compared to those obtained in the classical Flory-Huggins theory. As an example we again give the chemical potential of the solvent in a polymer/solvent mixture. Incorporating the bond correlations gives the following result for a cubic lattice:[9,10]

$$\frac{\mu - \mu^*}{kT} = -3\ln\left(1 - \frac{\phi}{3} + \frac{\phi}{3N}\right) + \ln(1 - \phi) + \chi\phi^2 \tag{20}$$

which reduces to eq 15 in the limit of low volume fractions.

2.4 Results

In the previous section two methods were described to incorporate chain stiffness into the lattice model. We start this section by comparing results of these two models. In Figure 2 volume fraction profiles are given for freely jointed stiff rods (with $p = 2$) and for a chain with limited bond flexibility, for a brush with a grafting density $\sigma = 0.1$ and chain length $N = 401$. In the former model the volume fraction profile is the sum of the profiles of two brushes grafted in the first and second layer, respectively. This is the reason why the data points do not all lie exactly on one smooth curve. The computations using the limited bond flexibility model were done for $U^{ben} = \ln 2$ (kT). This also corresponds to a Kuhn length $p = 2$. The brush height in Figure 2 is higher than what would be calculated for a freely jointed chain (where $p = 1$); a more detailed comparison is given in Figure 3. The overall agreement

between the results of both models is good. An advantage of the limited bond flexibility model over the freely jointed rods model is the fact that p can take any value (and not only integer values). Further computations of the effect of chain stiffness on the brush structure are shown in Figure 3, which was calculated using the limited bond flexibility model.
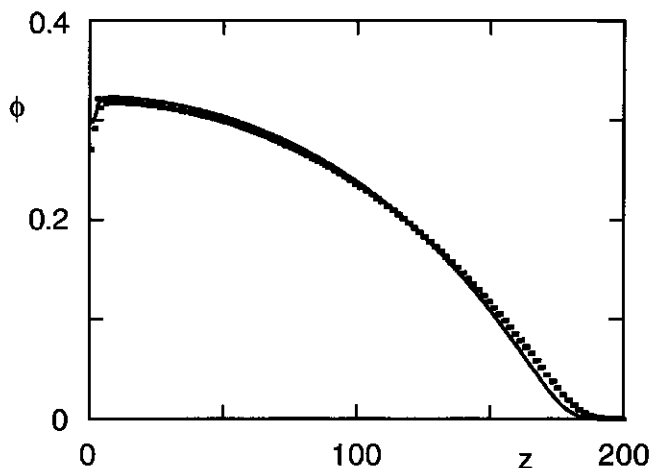

Figure 2 Volume fraction profile of a polymer brush as predicted by the model of freely jointed rods (data points) and the limited bond flexibility model (solid curve), for a stiffness $p = 2$. Grafting density $\sigma = 0.1$, athermal solvent ($\chi = 0$), chain length $N = 401$.

The solid curves in Figure 3A are the volume fractions profiles for $\sigma = 0.1$, $N = 400$, and U^{ben} varying from 0 to 5 kT. The volume fraction profile according to the freely jointed chain (f.j.c.) model is also given by a solid curve. The f.j.c. brush has a smaller height than the brush for which $U^{ben} = 0$. This is to be expected as in the latter brush direct backfolding of the chain segments is forbidden. Although U^{ben} = 0 (so that there is no energy difference between a "perpendicular" and a "forward" conformation) the prevention of direct backfolding does already lead to noticeably stiffer polymer chains. The Kuhn length for $U^{ben} = 0$ is 1.5. Increasing U^{ben} corresponds to a stiffer chain and a larger brush height. For $U^{ben} = 5$ kT ($p = 73.7$) we have reached the situation that a considerable number of chains are completely stretched (all bonds are in the "forward" conformation) and the brush height is equal to the chain length. In this case the profile approaches a step-profile.

For the f.j.c. brush and for the brush with $U^{ben} = 0$ the volume fraction profiles show a depletion zone next to the grafting surface. Previously this phenomenon has
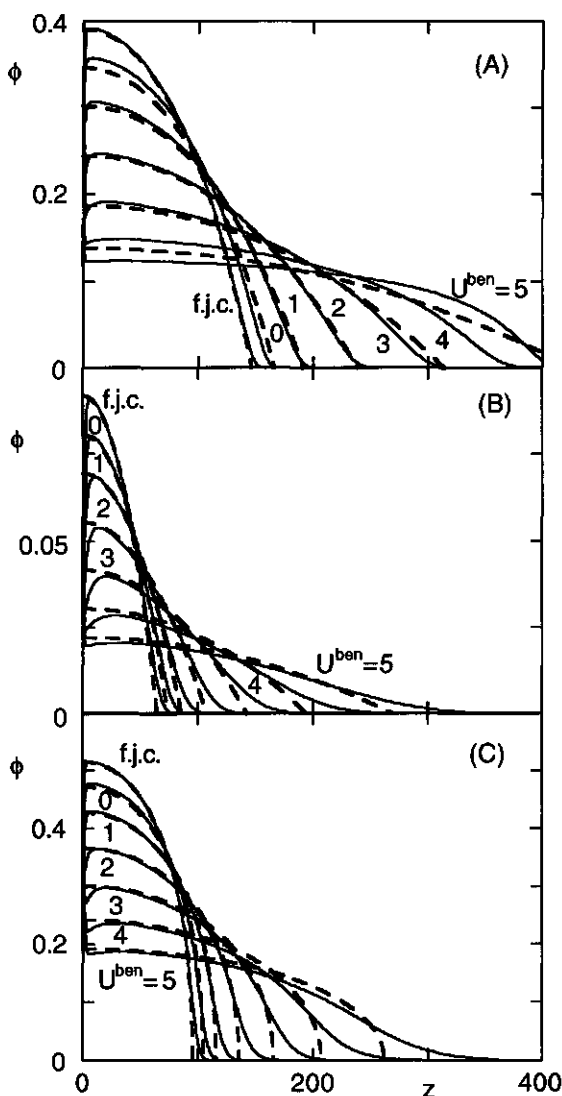
Figure 3 Volume fractions profiles predicted by the limited bond flexibility model for U^{ben} = 0, 1, 2, 3, 4, and 5 kT as indicated in the figure and for a freely jointed chain (f.j.c.), for chains of 400 segments. (A): σ = 0.1, and χ = 0; (B): σ = 0.01, and χ = 0; (C): σ = 0.1, and χ = 0.5. The dashed curves are the predictions of the theory of Zhulina et al.[6] for p = 1 (i.e. the f.j.c. model) and for stiffnesses corresponding to U^{ben} = 0, 1, 2, 3, 4 and 5 kT. In part A the dashed curve for U^{ben} = 5 kT is not shown.

been seen both in SCF calculations[5] and in Monte Carlo simulations.[11] For stiffer chains ($U^{ben} \geq 1$) the profiles are oscillatory in this zone. This behaviour is a consequence of the way in which we have defined the contribution of the first two segments towards the probability weighting function of the chain conformations (see eq A1.3). The bond between segments 1 and 2 (which goes from a site in layer 1 to either another site in layer 1 or to a site in layer 2) does not interact with a bond between segment 1 and segment 0. We could also implement the model in a slightly different way and assume that there is a polymer segment $s = 0$ in layer $z = 0$, so that the bond between segments 0 and 1 would go from layer 0 to layer 1. In that case the presence of segment 2 in layer 1 would be less favourable than it is in the present model, because the presence of segment 2 in layer 1 would mean an extra "perpendicular" conformation in the chain. In this case eq A1.3 should be replaced by:

$$G(1,1,d \mid 0,0) = \begin{cases} F & \text{if } d = 1 \\ 4P & \text{if } d = 0 \\ 0 & \text{otherwise} \end{cases} \tag{21}$$

When this modification is implemented, the oscillation disappears (this is not shown in a figure). This illustrates that the oscillation near the grafting surface is an artefact caused by the grafting procedure. Nevertheless, this has very little influence on the rest of the profile. Throughout the remainder of this chapter we will use eq A1.3, and accept the slightly irregular behaviour near the grafting surface.

The dashed curves in Figure 3A were calculated using the theory of Zhulina *et al.*[6] who incorporated chain stiffness into their expression for the entropy of stretching a polymer chain. For $p = 1$ their model agrees very well with the f.j.c. model if the full Flory-Huggins expression is used for the free energy of the system,[5] as was done to obtain the curves shown in Figure 3. For values of p up to 10 ($U^{ben} = 3$ kT) there is also a good agreement between their analytical theory and our limited bond flexibility model. For even stiffer chains the analytical model predicts a too large brush height. For $U^{ben} = 4$ kT ($p = 28$) the theory of Zhulina *et al.* has lost its physical meaning, as it predicts a brush height which exceeds the chain length.

In Figure 3B the same curves are drawn as in Figure 3A but now for a ten times lower grafting density, namely $\sigma = 0.01$. Such a grafting density is more representative for a polymer brush that is formed by adsorbing an AB-block copolymer from solution. Qualitatively the same trends are seen as in Figure 3A. The chains are less strongly stretched because of the lower densities. The theory of Zhulina *et al.* gives a reasonable description of the profiles for a value of U^{ben} as

high as 5 kT. In contrast to the situation for $\sigma = 0.1$, (virtually) no chains are yet completely stretched for $U^{ben} = 5$ kT.

Apart from the grafting density, the solvent quality is an important parameter in determining the brush structure. Figure 3C gives data for the same grafting density as Figure 3A, but now the brush is immersed in a Θ-solvent ($\chi = 0.5$). In a Θ-solvent the brush height is smaller than in an athermal solvent. As expected, this result is found for all values of the chain stiffness. The relative effect of increasing U^{ben} is roughly independent of the solvent quality (compare Figures 2A and 2C). For $U^{ben} = 4$ kT ($p = 28$) the brush height has approximately increased by a factor 2 (in comparison with a brush of freely jointed chains). In the Θ-solvent we see that for very large values of p ($U^{ben} = 5$ kT) the volume fraction profile shows a big "foot" protruding into the solution, which is not predicted by the equations of Zhulina *et al.*
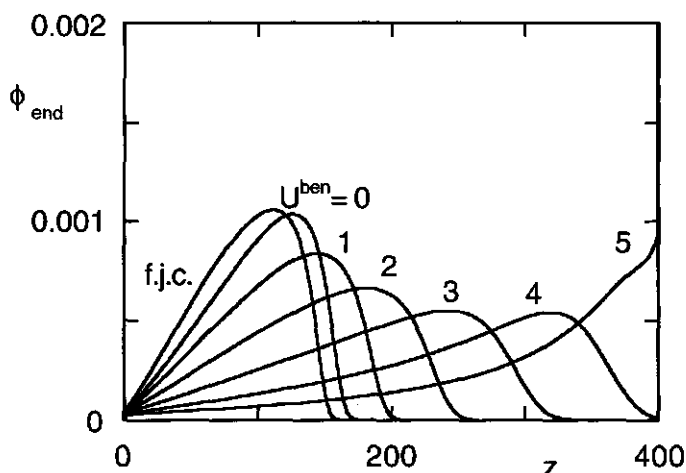

Figure 4 Volume fractions $\phi(z,N)$ of the free end-segments (s = N) of the chains for which the overall profiles are given in Figure 2.

Not only the overall volume fraction profile, but also the distribution of individual segments of the polymer chains is influenced by the chain stiffness. Figure 4 shows the distribution of the free end-segments, $\phi(z,N)$, of the chains for which the overall volume fraction profiles are plotted in Figure 3A. When U^{ben} is increased the average position of the end-segment moves to larger distances from the surface. This is consistent with the larger overall brush height as seen in Figure 3A. The end-segments are still distributed throughout the whole brush, and there is no "exclusion zone" near the surface. For $U^{ben} = 5$ kT, $\phi(z,N)$ shows a peak at z = 400. This peak is obviously due to the fact that an appreciable number of chains are fully stretched,

so that their end-segments are situated at $z = N$. Increasing U^{ben} even further leads to a growth of this peak.

Above we have clearly demonstrated that increasing the chain stiffness leads to more extended brush structures. Figures 2-4 are calculated using second order Markov models for polymer chains. Below we also present results for systems where correlations between neighbouring bonds are accounted for. As explained in the theory section, this approach is combined with a second order Markov procedure to compute the chain conformation weighting factors. The most important results are given in Figure 5.
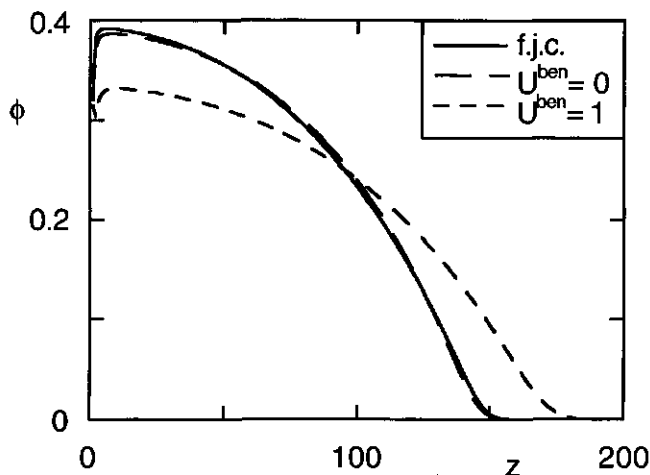

Figure 5 Volume fraction profiles taking nematic interactions (bond correlations) into account, for $U^{ben} = 0$ and 1 kT. The freely jointed chain volume fraction profile is given for comparison. Parameters: $\sigma = 0.1$, $\chi = 0$, $N = 400$.

In Figure 5 the grafting density and chain length are the same as in Figure 3A, so that the curves in Figure 5 can be directly compared with those in Figure 3A for $U^{ben} = 0$ and 1 kT. The bond correlations lead to a decrease of the brush height as compared to the limited bond flexibility model alone. For $U^{ben} = 0$ kT the bond correlation model predicts a volume fraction profile that is hardly distinguishable from the f.j.c. profile! In the limited bond flexibility model this value of U^{ben} (which corresponds to $p = 1.5$) causes a noticeable increase in the brush height. One might at first expect the bond correlations to cause a further increase in the brush height, because a stretched polymer chain would induce extra stretching of its neighbouring chains. However, the correlations between parallel bonds lead to a more efficient lateral packing of the chains, so that the density increases and the brush height

57

decreases. In order to explain this unexpected result we first investigate the bond orientations.

For the chosen parameters the polymer chains still have many bonds parallel to the grafting surface. This can be seen in Figure 6 were the factors $g(z|z+1)$ and $g(z|z)$ (defined by eqs 18 and 19) are plotted for the case $U^{ben} = 1$ kT of Figure 5. The factor $g(z|z)$ is an additional probability for a bond to remain in layer z (parallel to the surface). This probability increases as the volume fraction of bonds remaining within layer z increases. The factor $g(z|z+1)$ is an additional probability for a bond to cross from layer z to layer z+1 (so that it is oriented perpendicular to the surface). In Figure 6 one can see that throughout the whole brush $g(z|z) > g(z|z+1)$. Clearly, for a grafting density of 0.1 and a not very high chain stiffness the correlations between the more numerous parallel bonds reduce the brush height. This gives a good description of the influence of the bond correlations on the brush structure, but it does not yet provide an explanation for the fact that the packing density in the brush increases.
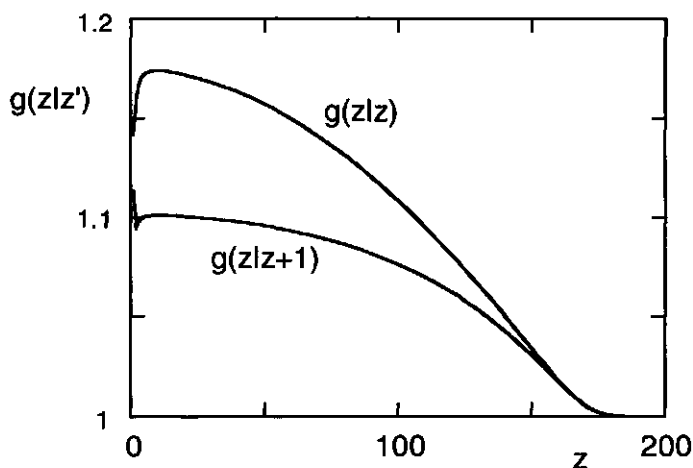
Figure 6: The nematic (bond orientation) factors $g(z|z+1)$ and $g(z|z)$ for the curve of Figure 4 with $U^{ben} = 1$ kT.

From a thermodynamic point of view the decrease of the brush height can be understood by comparing the equations for the chemical potential of the solvent in a solution of polymer chains with and without bond correlations (eqs 15 and 20). In a homogeneous solution of polymer (with volume fraction ϕ) and a monomeric solvent (volume fraction $1-\phi$) the chemical potential of the solvent is given by eq 20, when

one takes the correlations between parallel bonds into account. Expanding the logarithmic terms of this equation gives:

$$\frac{\mu - \mu^*}{kT} = -\frac{\phi}{N} + \left(\frac{(1-N)^2}{6N^2} - \frac{1}{2} + \chi \right) \phi^2 + \dots \tag{22}$$

The second virial coefficient, which for long freely jointed chains is $\frac{1}{2} - \chi$, becomes $\frac{1}{3} - \chi$ when nematic interactions are included. This means that, as long as one can neglect cubic and higher order terms in ϕ, a polymer solution with correlations between parallel bonds and a Flory-Huggins parameter χ behaves the same as a polymer solution without these correlations with an effective Flory-Huggins parameter $\chi^{eff} = \chi + \frac{1}{6}$. This hypothesis is tested in Figure 7. The solid curve is for a polymer brush without nematic interactions and $\chi = \frac{1}{6}$, the dashed curve is for a polymer with nematic interactions with $\chi = 0$. The system with nematic interactions gives a slightly larger brush height than the brush without nematic interactions. This means that when we correct the calculated profile for the shift in the effective solvency, the brush behaves as one would intuitively expect: the nematic interactions increase the brush height.

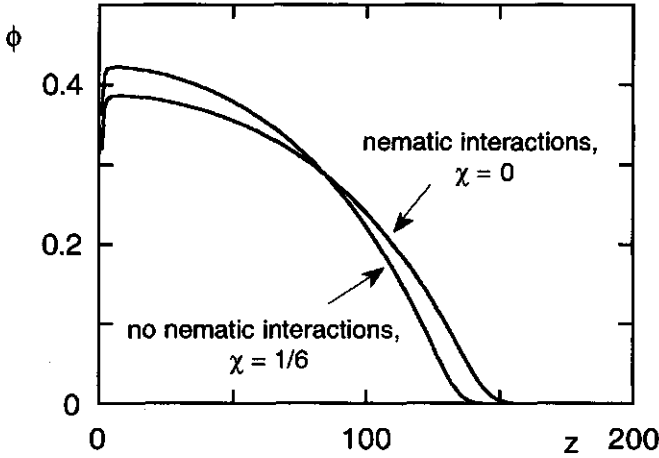**Figure 7** Comparison of the effect of bond correlations and that of solvency. The dashed curve is the same as that in Figure 4 for a brush with nematic interactions. with $U^{ben} = 0$ kT and $\chi = 0$. The solid curve is for the same chain length and grafting density, but was obtained from the limited bond flexibility model with $U^{ben} = 0$ kT (without nematic interactions) and a solvency parameter $\chi = 1/6$.

2.5 Discussion

Our main conclusion is that an increasing chain stiffness increases the height of a polymer brush, but that nematic interactions counteract this effect. One should realize that we view a polymer molecule not from an "atomistic" but from a more "coarse grained" level as we approximate it as a chain of Kuhn segments. If these segments have the same length as width it is logical to use a cubic lattice. This is the situation for which excellent agreement is found with analytical SCF models, which do not take any atomistic details into account either. When one wants to incorporate chain stiffness into the lattice model, one must make the (rather arbitrary) choice how exactly to implement this. We have done it by forbidding direct backfolding and introducing an energy difference between "forward" and "perpendicular" conformations. We could also have only introduced this bending energy and have allowed backfolding, or we could have taken interactions into account between segments that are two or more positions separated along the chain. Given the model-like character of our approach it is difficult to say which choice would best represent a "real" polymer. However, we can conclude that the effect of stiffness in our model agrees very well with the predictions of Zhulina et al., who considered the general effect of stiffness on the entropy of stretching a polymer chain (without any further assumptions as to the molecular origin of this stiffness). This strongly suggests that another way of incorporating stiffness into our lattice model would yield essentially the same volume fraction profiles for systems with the same effective chain stiffness p. Indeed, Figure 2 illustrates that two different models with the same value for p give virtually the same results.

We have shown that for not too high grafting densities the incorporation of correlations between parallel bonds in our model partly compensates the effect of chain stiffness. The easiest way to model a polymer brush is by using a freely jointed chain approach. This model can be solved analytically, as shown originally by Zhulina et al.[6] and Milner et al.[7] Their earlier work has been extended during the past few years, for example, towards polyelectrolytes,[12,13] polydisperse systems,[14] etc. All these extensions are based on freely jointed chains. In this chapter we have shown that the incorporation of both bond correlations and a moderate chain stiffness into the description of a polymer brush leads only to a small adjustment of the brush profile. This illustrates that the widely used model of freely jointed chains captures the essential trends of end-attached polymer layers.

It is also interesting to consider the implications of our findings for the comparison between SCF models and Monte Carlo simulations. In lattice Monte Carlo simulations of multi-chain systems the excluded volume of the polymer segments is usually accounted for in a rigorous manner: all system configurations are forbidden

where two or more segments overlap. The exclusion of direct backfolding and the incorporation of correlations between parallel bonds into the lattice model can be seen as a first order correction towards a more rigorous incorporation of excluded volume effects. The partly compensating effects found with excluding direct step reversals and incorporating correlations between parallel bonds explain why there is a relatively good agreement between simple SCF models and multi-chain Monte Carlo simulations.

Appendix 1: End-segment weighting factors for stiff polymer chains.

In this appendix we give the equations for the end-segment weighting factors of stiff polymer chains. These end-segment weighting factors are calculated using a second order Markov procedure on a cubic lattice.

The recurrence relation of eq 4 for $G(z,s|1,1)$ is extended to:

$$G(z,s,-1|1,1) = G(z) \times \begin{pmatrix} B(s) \times G(z-1,s-1,1|1,1) + 4P(s) \times G(z,s-1,0|1,1) + \\ F(s) \times G(z+1,s-1,-1|1,1) \end{pmatrix}$$

$$G(z,s,0|1,1) = G(z) \times \begin{pmatrix} P(s) \times G(z-1,s-1,1|1,1) + (2P(s)+F(s)+B(s)) \times G(z,s-1,0|1,1) + \\ P(s) \times G(z+1,s-1,-1|1,1) \end{pmatrix}$$

$$G(z,s,1|1,1) = G(z) \times \begin{pmatrix} F(s) \times G(z-1,s-1,1|1,1) + 4P(s) \times G(z,s-1,0|1,1) + \\ B(s) \times G(z+1,s-1,-1|1,1) \end{pmatrix}$$

$$(A1.1)$$

This equation reduces to eq 4, if $B = F = P = \lambda_1$, considering that $G(z,s|1,1) = G(z,s,-1|1,1) + G(z,s,0|1,1) + G(z,s,1|1,1)$. Eq A1.1 is valid for $s = 2, 3, ..., N-1$. For the end-segment ($s = N$) we write

$$G(z,N|1,1) = G(z) \times \left(G(z-1,N-1,1|1,1) + G(z,N-1,0|1,1) + G(z+1,N-1,-1|1,1) \right)$$

$$(A1.2)$$

For $s = 1$ we start the sequence with:

$$G(1,1,d|1,1) = \begin{cases} 1/6 & \text{if } d = 1 \\ 4/6 & \text{if } d = 0 \\ 0 & \text{otherwise} \end{cases} \tag{A1.3}$$

The first segment must be in the first layer and the first bond has complete freedom as it does not interact with a previous bond.

The quantity $G(z,s,d|N)$ is calculated from the following recurrence relations

61

$$G(z,s,1\,|\,N) = G(z) \times \left(\begin{array}{l} B(s) \times G(z-1,s+1,-1\,|\,N) + 4P(s) \times G(z-1,s+1,0\,|\,N) + \\ F(s) \times G(z-1,s+1,1\,|\,N) \end{array} \right)$$

$$G(z,s,0\,|\,N) = G(z) \times \left(\begin{array}{l} P(s) \times G(z,s+1,1\,|\,N) + (2P(s)+F(s)+B(s)) \times G(z-1,s+1,0\,|\,N) + \\ P(s) \times G(z-1,s+1,1\,|\,N) \end{array} \right)$$

$$G(z,s,-1\,|\,N) = G(z) \times \left(\begin{array}{l} F(s) \times G(z+1,s+1,-1\,|\,N) + 4P(s) \times G(z+1,s+1,0\,|\,N) + \\ B(s) \times G(z+1,s+1,1\,|\,N) \end{array} \right)$$

$$(A1.4)$$

These three equations define $G(z,s,d\,|\,N)$ for $s = 1, 2, 3, ... N-2$. For $s = N-1$ the recurrence relation is started with the expressions:

$$G(z,N-1,1\,|\,N) = G(z)\frac{1}{6}G(z-1)$$

$$G(z,N-1,0\,|\,N) = G(z)\frac{4}{6}G(z) \qquad (A1.5)$$

$$G(z,N-1,-1\,|\,N) = G(z)\frac{1}{6}G(z+1)$$

These equations contain the lattice parameters for the last bond and the segment weighting factors of the last two segments which determine this bond.

Appendix 2: Formalism for chains with bond correlations.

In this appendix the expressions for the chain-end weighting factors that were given in Appendix 1 are extended to include correlations between neighbouring bonds. As explained in the main text this means that additional weighting factors $g(z\,|\,z)$ and $g(z\,|\,z+1)$ must be taken into account for bonds within layer z (parallel to the surface), and for bonds between layers z and z+1 (perpendicular to the surface), respectively. The quantities $G(z,s,d\,|\,1,1)$ and $G(z,s,d\,|\,N)$ are then calculated from the following recurrence relations:

$$G(z,s,-1\,|\,1,1) = G(z) \times \left(\begin{array}{l} 4P(s) \times G(z,s-1,0\,|\,1,1) \times g(z\,|\,z) + \\ F(s) \times G(z+1,s-1,-1\,|\,1,1) \times g(z\,|\,z+1) \end{array} \right)$$

$$G(z,s,0\,|\,1,1) = G(z) \times \left(\begin{array}{l} P(s) \times G(z-1,s-1,1\,|\,1,1) \times g(z\,|\,z-1) + \\ (2P(s)+F(s)) \times G(z,s-1,0\,|\,1,1) \times g(z\,|\,z) + \\ P(s) \times G(z+1,s-1,-1\,|\,1,1) \times g(z\,|\,z+1) \end{array} \right) \qquad (A2.1a)$$

$$G(z,s,1\,|\,1,1) = G(z) \times \left(\begin{array}{l} F(s) \times G(z-1,s-1,1\,|\,1,1) \times g(z\,|\,z-1) + \\ 4P(s) \times G(z,s-1,0\,|\,1,1) \times g(z\,|\,z) + \end{array} \right)$$

$$\text{for } s = 2, 3, 4, ..., N-1$$

$$G(z,N\,|\,1,1) = G(z) \times \begin{pmatrix} G(z-1,N-1,1\,|\,1,1) \times g(z\,|\,z-1) + G(z,N-1,0\,|\,1,1) \times g(z\,|\,z) + \\ G(z+1,N-1,-1\,|\,1,1) \times g(z\,|\,z+1) \end{pmatrix}$$

(A2.1b)

and

$$G(z,s,1\,|\,N) = G(z) \times g(z\,|\,z+1) \times \big(4P(s) \times G(z-1,s+1,0\,|\,N) + F(s) \times G(z-1,s+1,1\,|\,N)\big)$$

$$G(z,s,0\,|\,N) = G(z) \times g(z\,|\,z) \times \begin{pmatrix} P(s) \times G(z,s+1,1\,|\,N) + (2P(s)+F(s)) \times G(z-1,s+1,0\,|\,N) + \\ P(s) \times G(z-1,s+1,1\,|\,N) \end{pmatrix}$$

$$G(z,s,-1\,|\,N) = G(z) \times g(z\,|\,z-1) \times \big(F(s) \times G(z+1,s+1,-1\,|\,N) + 4P(s) \times G(z+1,s+1,0\,|\,N)\big)$$

$$\text{for } s = 1,2,3, \ ..., \ N-2$$

(A2.2)

Eq A2.1 is started for s = 1 with:

$$G(1,1,d\,|\,1,1) = \begin{cases} 1/6 & \text{if } d=1 \\ 4/6 & \text{if } d=0 \\ 0 & \text{otherwise} \end{cases}$$

(A2.3)

and eq A2.2 is started for s = N − 1 with:

$$G(z,N-1,1\,|\,N) = G(z)\frac{1}{6}g(z\,|\,z-1)G(z-1)$$

$$G(z,N-1,0\,|\,N) = G(z)\frac{1}{6}g(z\,|\,z)G(z)$$

(A2.4)

$$G(z,N-1,-1\,|\,N) = G(z)\frac{1}{6}g(z\,|\,z+1)G(z+1)$$

Appendix 3: Kuhn parameter in the limited bond flexibility model.

For freely jointed polymer chains the Kuhn segment length is equal to the step length (or lattice spacing) ℓ. For chains with limited bond flexibility the Kuhn length increases by a factor p, which is determined by the energy U^{ben}. Consider a chain of N segments. We represent each bond i by the vector $\mathbf{l}_i$. The mean square end-to-end distance $\langle r^2 \rangle$ (in a constant potential field) can now be written as:

$$\langle r^2 \rangle = \left\langle \left(\sum_{i=1}^{N-1} \mathbf{l}_i \right) \left(\sum_{j=1}^{N-1} \mathbf{l}_j \right) \right\rangle = (N-1)\ell^2 + 2 \left\langle \sum_{i=1}^{N-1} \sum_{j=i+1}^{N-1} \mathbf{l}_i \mathbf{l}_j \right\rangle$$

(A3.1)

On a simple cubic lattice the angle between two bonds can take the values of 0, $\pi/2$, or π. It is easily seen that $\langle \mathbf{l}_i \mathbf{l}_{i+1} \rangle = F\ell^2$ and $\langle \mathbf{l}_i \mathbf{l}_{i+2} \rangle = F^2\ell^2$. In general, $\langle \mathbf{l}_i \mathbf{l}_{i+k} \rangle = F^k\ell^2$.

For N >> 1 the second summation on the right-hand side of eq A3.1 can be extended to infinity, so that:

$$\left\langle r^2 \right\rangle = (N-1)\left(1+\frac{2F}{1-F}\right)\ell^2 \tag{A3.2}$$

This corresponds to

$$p = 1+\frac{2F}{1-F} \tag{A3.3}$$

References

(1)   Milner, S. T. *Science* **1991**, *251*, 905.
(2)   Scheutjens, J. M. H. M.; Fleer, G. J. *J. Phys. Chem* **1979**, *83*, 1619.
(3)   Cosgrove, T.; Heath, T.; Van Lent, B.; Leermakers, F.; Scheutjens, J. *Macromolecules* **1987**, *20*, 1692.
(4)   Hirz, S., *M.S. Thesis*, University of Minnesota, **1987**.
(5)   Wijmans, C. M.; Scheutjens, J. M. H. M.; Zhulina, E. B. *Macromolecules* **1992**, *25*, 2657; This thesis, chapter 1.
(6)   Zhulina, E. B.; Borisov, O. V.; Priamitsyn, V. A. *J. Colloid Interface Sci.* **1990**, *137*, 495.
(7)   Milner, S. T.; Witten, T. A.; Cates, M. E. *Macromolecules* **1988**, *21*, 2610.
(8)   Leermakers, F. A. M.; Scheutjens, J. M. H. M. *J. Chem. Phys.* **1988**, *89*, 3264.
(9)   Leermakers, F. A. M.; Scheutjens, J. M. H. M. *J. Chem. Phys.* **1988**, *89*, 6912.
(10) Leermakers, F. A. M.; Lyklema, J. *Colloids Surfaces* **1992**, *67*, 239.
(11) Chakrabarti, A.; Toral, R. *Macromolecules* **1990**, *23*, 2016.
(12) Borisov, O. V.; Birshtein, T. M.; Zhulina, E. B. *J. Phys. II* **1991**, *1*, 521.
(13) Pincus, P. *Macromolecules* **1991**, *24*, 2912.
(14) Milner, S. T.; Witten, T. A.; Cates, M. E. *Macromolecules* **1989**, *22*, 583.

chapter 3

Polymer Brushes at Curved Surfaces

Abstract

In this chapter we use the polymer adsorption theory of Scheutjens and Fleer to describe polymer brushes at spherical and cylindrical surfaces that are immersed in a low molecular weight solvent. We analyse the volume fraction profiles of such brushes, focusing our attention on spherical brushes in athermal solvents. These are shown to generally consist of two parts: a power law-like part, and a part that is consistent with a parabolic potential energy profile of the polymer segments. Depending on the curvature of the surface one of these two parts is the more important, or may even dominate completely. We especially consider the distribution of the free end-segments and the possible existence of a "dead zone" for these segments. Such a dead zone is actually found and is seen to follow a scaling law in the case of large curvatures. Furthermore, the effect of diminishing the solvent quality is considered for both the total volume fraction profile and the distribution of the end-segments.

3.1 Introduction

Over the past years much effort has been put into the theoretical description of so-called polymer brushes: systems in which polymer chains are end-attached to an interface. Scaling analyses,[1,2] self-consistent field (SCF) theories,[3-6] and Monte Carlo[3,8,9] and molecular dynamics simulations[10] have been developed for and applied to these systems. Originally they were used to describe polymer brushes at flat interfaces, but recently several papers have appeared whose aim it is to describe curved interfaces.[11-13] Especially in the case of an analytical SCF theory it is a challenging, and certainly not a trivial step to extend models for flat systems to a curved geometry. The relevance of this extension is, however, self-evident. Polymer brushes can be seen as a model for adsorbed diblock copolymer layers which are able to stabilize colloidal dispersions. Generally, the surface of colloidal particles is not flat, but may easily have a radius of curvature that is comparable to the thickness of the adsorbed polymeric layer. A model based on polymers grafted to a convex interface can also be used to study solutions and melts of block copolymers under the conditions in which microphases are formed. Star-shaped polymers can be studied by using their similarity to linear chains that are grafted onto a small spherical particle.

The conceptually most simple model of a polymer brush is the scaling picture due to Alexander and de Gennes,[1,2] which assumes a step-like concentration profile with all chain ends situated on the outer side of the polymer layer. Using straightforward geometrical arguments this model was later extended by Daoud and Cotton to spherical interfaces,[14] and by Birshtein et $al.$ to cylindrical interfaces.[15,16] For such curved interfaces the volume fraction profile becomes dependent on the distance to the grafting surface:

$$\phi(z) = \sigma^{3v-1/2v} \left(\frac{R}{R+z} \right)^{(d-1)(3v-1)/2v} \tag{1}$$

where ϕ is the volume fraction, σ is the grafting density, R is the radius of curvature of the grafting surface, z is the distance to the surface (so that $r = R + z$ is the distance to the centre of the sphere or cylinder, see Figure 1), and v is the Flory exponent, which depends upon the solvent quality ($v = 3/5$ for a good solvent, $v = 1/2$ for a Θ-solvent, and $v = 1/3$ for a nonsolvent). The dimensionality d is determined by the geometry of the grafting surface: $d = 1, 2,$ and 3 for planar, cylindrical, and spherical surfaces, respectively.

A more sophisticated approach to the structure of a grafted polymer layer (at a flat surface) using self-consistent field (SCF) arguments was given in the papers of

Zhulina, Borisov, and Priamitsyn[6,17] and of Milner, Witten, and Cates.[4,5] These are all based on an idea by Semenov[18] that when a polymer chain is strongly stretched with respect to its Gaussian dimensions, it is possible to replace its set of conformations by an "average trajectory," thus significantly simplifying the description of the system. This concept was first used by Semenov to study super structure formation in block copolymer melts. Later, the SCF approach was generalized and it has been applied to grafted polymer layers immersed in both low molecular weight solvents,[5,17] as well as solutions and melts of mobile polymers.[19] Furthermore, nonequilibrium effects such as the deformational[4] and dynamical[20] behaviour of grafted layers were studied. These investigations have led to a different overall picture of the planar grafted polymer layer structure as compared to the scaling approach. The polymer concentration decreases monotonically on going away from the grafting surface and free chain ends are distributed throughout the whole layer. The precise form of the total concentration profile as well as that of the chain end distribution function depend on parameters such as solvent quality and polydispersity. In his pioneering publication Semenov[18] showed that in cylindrical and spherical convex layers the free chain ends must be excluded from the vicinity of the grafting surface. Ball et al.[11] were the first to extend this SCF approach in a rigorous manner to chains grafted to a convex interface. They derived analytical solutions for the case of densely grafted chains at a cylindrical interface immersed in a melt. With increasing curvature an exclusion zone with an increasing height appears next to the surface. Free chain ends are excluded from this zone. For the cases of spherical interfaces and brushes with solvent, equations were given that still need to be solved (numerically). Ball et al. anticipate that under these conditions the distribution of free ends will remain qualitatively the same.

Simulations of star-shaped polymers using a molecular dynamics method[21] do indeed suggest that in a spherical geometry the dead zone exists for brushes in a good solvent. However, simulations of chains grafted to a cylindrical surface in a good solvent[12] do not show this dead zone, except for $R \rightarrow 0$ (that is, when the cylinder is reduced to a single line). The M.D. simulations of ref 21 confirm the scaling prediction of eq 1 for $d = 3$.

Recently, Dan and Tirrell[13] have applied the Edwards diffusion equation approach[22] to end-attached polymer chains. They extended the numerical procedure by Dolan and Edwards[23] for grafted chains at a flat surface to cylindrical and spherical surfaces. Especially for cylindrical surfaces the scaling predictions agree badly with their results. Dan and Tirrell, who investigated brushes in a good

solvent, did find dead zones near the surface which agree fairly well with the predictions of Ball *et al.* for brushes in a melt.
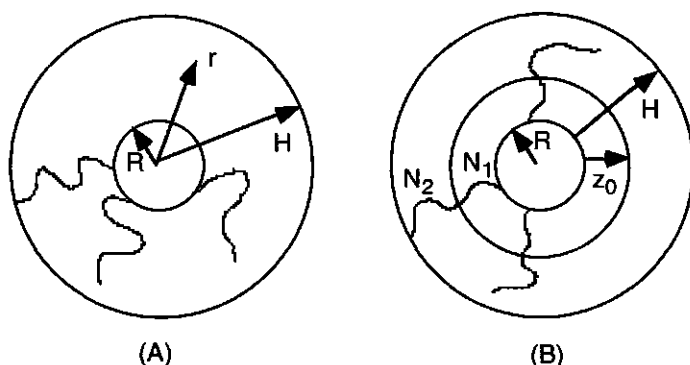

(A)   (B)

Figure 1 (A) Polymer chains that are end-attached to a curved surface with radius of curvature R form a brush of height H. The distance to the centre of the sphere or cylinder is r, and z denotes the distance to the surface. (B) For intermediate values of R the polymer brush can be divided into two parts. From $z = 0$ to $z = z_0$ all chains are stretched equally. Segment N_1 of every chain is situated at a distance z_0 from the surface. The remaining $N_2 = N - N_1$ segments are subject to a parabolic potential profile in the region $z = z_0$ to $z = H$.

In this chapter we present results from SCF lattice calculations on end-grafted chains at cylindrical and spherical surfaces in the presence of solvents of various qualities (very bad to very good). The model we use is an extension of the polymer adsorption theory of Scheutjens and Fleer[24,25] for curved geometries, which in its basic assumptions is very similar to the diffusion equation approach. However, within the approximation of using a mean-field lattice model, all properties of the system under consideration can be calculated exactly. No further approximations are needed. For example, we need not assume that the polymer segment potential is proportional to the local segment density (as was done in the numerical procedure of ref 23). Also any solvent quality can be chosen. In the next section we will go into further details concerning the lattice model. In section 5 we will show results of this model and (where possible) compare them with predictions from one of the models mentioned above. First we shall, however, introduce two analytical models in sections 3 and 4 to describe brushes in good and Θ-solvents at curved surfaces. In section 5 we will also see under what conditions these models are valid by comparing them with the lattice model calculations. In doing so, we will focus our attention on spherical brushes in athermal solvents.

3.2 Self-Consistent Field Lattice Model

In the polymer adsorption theory of Scheutjens and Fleer[24,25] the equilibrium distribution of a polymer-solvent system at an interface is calculated by taking into account all possible conformations, each weighted by its Boltzmann probability factor. Cosgrove *et al.*[3] and Hirz[26] showed that this method can be applied to terminally attached chains by restricting the allowed conformations to those whose first segment is in the layer adjacent to the surface. In a previous chapter[27] we described this modified procedure and used it to calculate characteristics of polymer brushes on flat surfaces. The basic principles of the model can also be applied in a lattice with a curved geometry, as was first demonstrated by Leermakers and Scheutjens,[28] who used such a lattice to study lipid vesicles and surfactant micelles. In this section we shall briefly review the relevant geometrical aspects of their approach.

The differences between a curved and a planar lattice are that the number of sites in a layer increases on moving away from the centre of the lattice and that the lattice transition parameters λ_-, λ_0, and λ_+ are layer dependent. A lattice site in layer r has neighbouring sites in layers $r-1$, r, and $r+1$. A fraction λ_- of these neighbouring sites are in layer $r-1$, a fraction λ_0 are in layer r, and a fraction λ_+ are in layer $r+1$. We number the layers $r = 1, 2, 3, ...$ starting from the centre of the sphere or cylinder. Applying the condition that all layers are equidistant, one finds that the volume $V(r)$, expressed in number of lattice sites, enclosed by layer r equals:

$$V_d(r) = \frac{C_d}{d} r^d \tag{2}$$

where $d = 3$ for a spherical and $d = 2$ for a cylindrical lattice (and $d = 1$ for a flat lattice). This volume is defined per surface area for $d = 1$, per length unit for $d = 2$, and per sphere for $d = 3$. The numerical constant C_d has the values $C_1 = 1$, $C_2 = 2\pi$, and $C_3 = 4\pi$. The number of lattice sites in layer r is given by $L(r) = V(r) - V(r-1)$ or

$$L_d(r) = \frac{C_d}{d} \left(r^d - (r-1)^d \right) \tag{3}$$

Differentiating $V(r)$ with respect to r gives the surface area $S(r)$ of layer r:

$$S_d(r) = C_d r^{d-1} \tag{4}$$

The transition factors $\lambda_-(r)$ and $\lambda_+(r)$ are proportional to the surface area per site in contact with the adjacent layer, so that

$$\lambda_{+d}(r) = \lambda_{+1}\frac{S_d(r)}{L_d(r)}$$

$$\lambda_{-d}(r) = \lambda_{-1}\frac{S_d(r-1)}{L_d(r)} \tag{5}$$

$$\lambda_{0d}(r) = 1 - \lambda_{+d}(r) - \lambda_{-d}(r)$$

where λ_{+1} and λ_{-1} are the values of the transition factors for the equivalent planar lattice. In all calculations presented in this chapter we have used a cubic lattice, for which $\lambda_{+1} = \lambda_{-1} = 1/6$. In a flat geometry ($d = 1$) the simple cubic lattice gives an equal a priori probability to a bond between two segments in any of the four directions parallel to the surface as well as to a bond toward the surface or away from the surface. This is in accordance with the underlying physical model of refs 4 and 6. We emphasize an important consequence of our definition of the transition probabilities. It follows from eqs 3 and 5 that

$$\lambda_{-d}(r)L_d(r) = \lambda_{+d}(r-1)L_d(r-1) \tag{6}$$

which means that the condition is satisfied that the statistical weight of a polymer conformation does not depend upon the chain end at which we start to evaluate this quantity.

When studying polymer grafted at a solid-liquid interface with a radius of curvature R, we must exclude the layers $r = 1, 2, 3, ... R$ from our system. We number our layers $z = 1, 2, 3, ...$ starting from layer $r = R + 1$ ($z = 1$), which is adjacent to the solid-liquid interface (see also Figure 1). The actual calculation of the equilibrium distribution of a polymer-solvent system now takes places completely analogously to the procedure described in ref 27. Only the transition parameters of eq 2 of this reference must be replaced by the appropriate expressions from our eq 5 and the denominator of eq 6 in ref 27 becomes $\sum_z L(z)G(z,N)$. Of course the procedure described above can not only be used to compute systems with end-grafted polymer but also for polymer adsorption from solution. In chapter 4 we present results thus found for block copolymer adsorption onto spherical colloidal particles.

As described in ref 27 a numerical iteration scheme is applied to find the self-consistent volume fraction profile of the polymer. Due to their mathematical complexity the equations cannot be solved exactly using analytical methods. In the next section we will discuss less exact SCF approaches to our system of curved brushes, which enable us to find analytical approximations for the volume fraction profile.

3.3 Analytical SCF Model

Large curvature

We will start by considering polymer chains that are end-attached to a spherical interface with a small radius of curvature (i.e. brushes with a large curvature). We make the simplifying approximation that the free ends of all chains are situated at the same distance H from the surface. The elastic chain stretching contribution to the free energy of the system for an arbitrary geometry (planar, cylindrical, or spherical) can then be written as

$$A_{el} = \frac{3f_d}{2\ell^2} \int_0^H \left(\frac{dz}{ds}\right) dz = \frac{3\ell f_d^2}{C_d} \int_0^H \frac{dz}{(z+R)^{d-1}\phi(z)} \tag{7}$$

and is defined per surface area in the planar case $(d = 1)$, per length unit in the cylindrical case $(d = 2)$, and per sphere for the spherical geometry $(d = 3)$. The local chain stretching at distance z from the surface is given by ds/dz, ℓ is the segment diameter, and $f_d = \sigma S_d(R)$ is the number of chains. In distinction to the previous section the distance z to the surface is now a continuous variable. Because of the equal stretching of all chains

$$\phi(z) = \frac{\ell^3 f_d ds}{S_d(z+R)} dz$$

The contribution to the free energy of the system due to the mixing of grafted chains and solvent molecules can be written as a virial expansion,

$$A_{mix} = \int_0^H dz \left(v\phi^2(z) + w\phi^3(z)\right) S_d(z+R) \tag{8}$$

where v and w are the second and third virial coefficients (within Flory theory $v = 0.5 - \chi$ and $w = 1/6$ The free energy functional $A_{el} + A_{mix}$ must be minimized under the constraint

$$\frac{1}{\ell^3 f_d} \int_0^H dz \, \phi(z) S_d(z+R) = N \tag{9}$$

where N is the degree of polymerization. For a given height H this leads to the equation

$$\frac{\sigma^2 R^{d-2}}{(z+R)^{2d-2}\phi^2(z)} = \frac{4}{3} v\phi(z) + 2w\phi^2(z) + \Lambda \tag{10}$$

71

where σ is the grafting density and Λ is an undetermined Lagrangian multiplier. Solving $\phi(z)$ from this equation and substituting it into eq 9 one can find Λ. Minimization of the total free energy $A_{el} + A_{mix}$ with respect to H gives the volume fraction profile for given values of R and σ. Under good solvent conditions and for large curvatures the last two terms in eq 10 may be neglected, so that[29]

$$\phi(z) = \left(\frac{3\sigma^2}{4v}\right)^{1/3}\left(\frac{R}{z+R}\right)^{\frac{2d-2}{3}} \tag{11}$$

Substituting this expression into eq 9 we find the following scaling law for the layer height:

$$H \sim \left(\sigma v N^3 R^{d-1}\right)^{\frac{1}{d+2}} \tag{12}$$

In a Θ-solvent ($v = 0$), omitting the first and last terms on the right-hand side of eq 10 leads to

$$\phi(z) = \left(\frac{\sigma^2}{2w}\right)^{1/4}\left(\frac{R}{z+R}\right)^{\frac{2d-2}{4}} \tag{13}$$

We conclude that in a spherical convex brush $\phi(z)$ scales as $(z+R)^{-4/3}$ in a good solvent, and $\phi(z) \sim (z+R)^{-1}$ in a Θ-solvent. In a cylindrical brush $\phi(z) \sim (z+R)^{-2/3}$ in a good solvent, and $\phi(z) \sim (z+R)^{-1/2}$ in a Θ-solvent. This is in agreement with eq 1. In bad solvents $\phi(z) \sim z^0$ for all three geometries. In a bad solvent ($v < 0$) the left-hand side of eq 10 can be neglected, so that

$$\phi(z) = \frac{|v|}{3w} + \left(\frac{v^2}{9w^2} - \frac{\Lambda}{2w}\right)^{1/2} = \text{const} \tag{14}$$

The value $\Lambda = v^2/6w$ obtained from the minimization of A_{mix} with respect to H under the constraint of eq 9 gives a well-known result for a collapsed globule,

$$\phi(z) = \frac{|v|}{2w} \tag{15}$$

Small curvature

We will now discuss the opposite case of small curvature (R is large). We limit ourselves to good solvents and spherical surfaces. Other geometries and solvent qualities can be described along similar lines. Of course, for infinitely large radii of

72

curvature the polymer brush is described by a parabolic potential profile, which in a good solvent leads to a brush height H_0 given by the equation,

$$H_0 = \left(\frac{8}{\pi^2}\right)^{1/3} \ell N v^{1/3} \left(\ell^2 \sigma\right)^{1/3} \tag{16}$$

Following Liatskaya et al.[30] and Milner et al.[31] we assume that for low curvatures it is still a good approximation to describe the polymer brush by a parabolic potential profile. The brush height H will then depend upon the relative curvature ω^{-1}, which we define as the ratio of the flat brush height and the radius of curvature of the surface, $\omega = R/H_0$. In a good solvent this height H at a spherical surface is given by the equation

$$\left(\frac{H}{H_0}\right)^3 \left(1 + \frac{3H}{4\omega H_0} + \frac{1}{5}\left(\frac{H}{\omega H_0}\right)^2\right) = 1 \tag{17}$$

The corresponding volume fraction profile is

$$\phi(z) = \frac{3\sigma N \ell^3}{H_0} \left(\frac{H}{H_0}\right)^2 \left(1 - \left(\frac{z}{H}\right)^2\right) \tag{18}$$

and the distribution function of free ends:

$$g(z) = \frac{3zH^2}{H_0{}^3} \left\{ \left[2 + \frac{3H}{\omega H_0} - \frac{2}{3}\left(\frac{H}{\omega H_0}\right)^2 + \frac{8}{3}\left(\frac{H}{\omega H_0}\right)^2 \left(\frac{z}{H}\right)^2\right]\left(1 - \left(\frac{z}{H}\right)^2\right)^{\frac{1}{2}} - \frac{H}{\omega H_0}\left(2 - 3\left(\frac{z}{H}\right)^2\right) \text{Ln}\left(\frac{1 + \left(1 - \left(\frac{z}{H}\right)^2\right)^{\frac{1}{2}}}{\frac{z}{H}}\right) \right\} \tag{19}$$

This result was previously derived by Liatskaya et al.[30]

The approximations made in this model turn up when one examines the function g(z). For low values of z it becomes negative. Of course a probability smaller than zero has no physical meaning. It is possible to interpret the zone where $g(z) \leq 0$ as an area where no end-segments are located. We define Δ_p as the size of this "dead zone", so that $g(\Delta_p) = 0$. The value of Δ_p (where the subscript p stands for parabolic) depends on the curvature of the surface. Figure 2A shows the relative thickness of the dead zone, Δ_p/H, as a function of R/H. The

73

maximum relative value for the dead zone is reached in the limit $R/H \rightarrow 0$, when $\Delta_p = H/2$. When $R/H \ll 1$ the layer height scales as $R^{2/5}N^{3/5}\sigma^{1/5}$, so that the absolute value of the dead zone $(\Delta_p \sim H \sim R^{2/5})$ increases with R and passes through a maximum at $R/H \approx 1$, as can be seen in Figure 2B. For small curvatures $(R/H \gg 1)$ Δ_p decays exponentially with R.
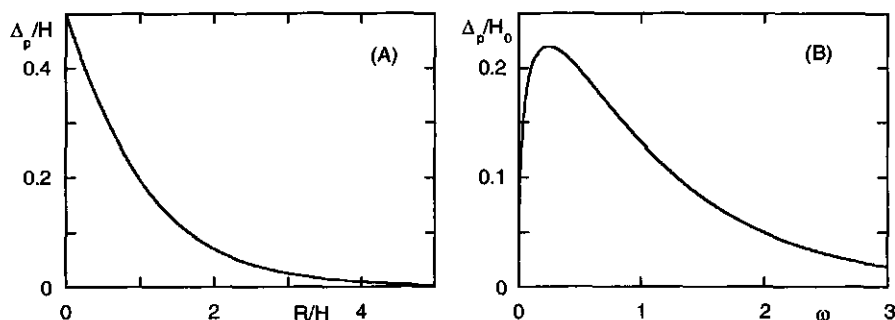

Figure 2 (A) The behaviour of the dead zone for free ends in the parabolic potential approximation; Δ/H is given as a function of R/H (Δ: dead zone size, H: layer height, R: radius). Note that H itself depends on R for a given chain length. (B) The ratio of dead zone length Δ and flat brush height H_0 is given as a function of the relative radius of curvature ω.

Intermediate curvatures

For intermediate radii of curvature we make the approximation that the volume fraction profile is a combination of the two previously discussed profiles. Up to a distance z_0 from the surface (see Figure 1B) all chains are stretched equally. Per chain there are N_1 segments in this part of the brush. The other N_2 segments are situated in a parabolic potential profile and can be thought of as being grafted to an imaginary radial surface with radius $R + z_0$. For a spherical layer in a good solvent this leads to the following overall profile:

$$\phi(z) = \begin{cases} \left(\dfrac{3}{64\pi^2}\right)^{1/3} \dfrac{f^{2/3}v^{-1/3}\ell^{4/3}}{(R+z)^{4/3}} & \text{for } 0 \leq z \leq z_0 \\[3mm] \dfrac{3\pi^2}{16\ell^2 N_2^2 v}\left(H^2 - (z-z_0)^2\right) & \text{for } z_0 \leq z \leq H+z_0 \end{cases} \tag{20}$$

where $f = f_3$ is the number of chains per sphere ($f = 4\sigma\pi R^2$). The values of N_1, N_2, H, and z_0 follow from the three conditions:

1) continuity of the profile at $z = z_0$:

74

$$\left(\frac{3}{64\pi^2}\right)^{1/3}\frac{f^{2/3}v^{-1/3}\ell^{4/3}}{(R+z)^{4/3}} = \frac{3\pi^2}{16v\ell^2N_2^2}H^2 \Rightarrow$$

$$H = \frac{2v^{1/3}f^{1/3}\ell^{5/3}N_2}{3^{1/3}\pi^{4/3}(R+z_0)^{2/3}} \tag{21}$$

2) conservation of segments in the inner layer:

$$f\ell^3N_1 = \int_0^{z_0}\phi_1 4\pi(R+z)^2 dz \Rightarrow$$

$$N_1 = \frac{3(3\pi)^{1/3}v^{-1/3}f^{-1/3}}{5\ell^{5/3}}\left((R+z_0)^{5/3} - R^{5/3}\right) \tag{22}$$

3) conservation of segments in the outer layer:

$$f\ell^3N_2 = \int_{z_0}^{z_0+H}\phi(z)4\pi(R+z)^2 dz \Rightarrow$$

$$\frac{\pi^3(R+z_0)^2H^3}{2vf\ell^5N_2^3}\left(1+\frac{3H}{4(R+z_0)}+\frac{H^2}{5(R+z_0)^2}\right) = 1 \tag{23}$$

Rearranging these equations and introducing $u = z_0/R$, one can write,

$$u = \left(\frac{1+\dfrac{5}{3}\left(\dfrac{\pi^2}{6}\right)^{1/3}\omega^{-1}}{1+\dfrac{5}{6}\pi c}\right)^{3/5} - 1 \tag{24}$$

where the constant c is defined by

$$c = -\frac{15}{8}+\left(\frac{225}{64}+5\left(\frac{3\pi}{4}-1\right)\right)^{\frac{1}{2}} \approx 1.334 \tag{25}$$

We now define a critical relative curvature ω_{cr}, so that for $\omega > \omega_{cr}$ the potential profile is parabolic, whereas for $\omega < \omega_{cr}$ the volume fraction profile is a combination of both models. For $\omega < \omega_{cr}$ there is a zone $\Delta = z_0 + \Delta_p$ where no end-segments are located. For a spherical brush $\omega_{cr} \approx 0.563$.

For a cylindrical layer in a good solvent the similar procedure gives $\omega_{cr} = (4/3\pi)^{1/3}(2\pi-8/3)^{-1} \approx 0.207$. For a cylindrical brush a parabolic potential profile may be assumed over a wider range of curvatures than for a spherical brush. The

combined profiles for Θ-solvents and bad solvents in spherical and cylindrical geometries can be found in the same manner.
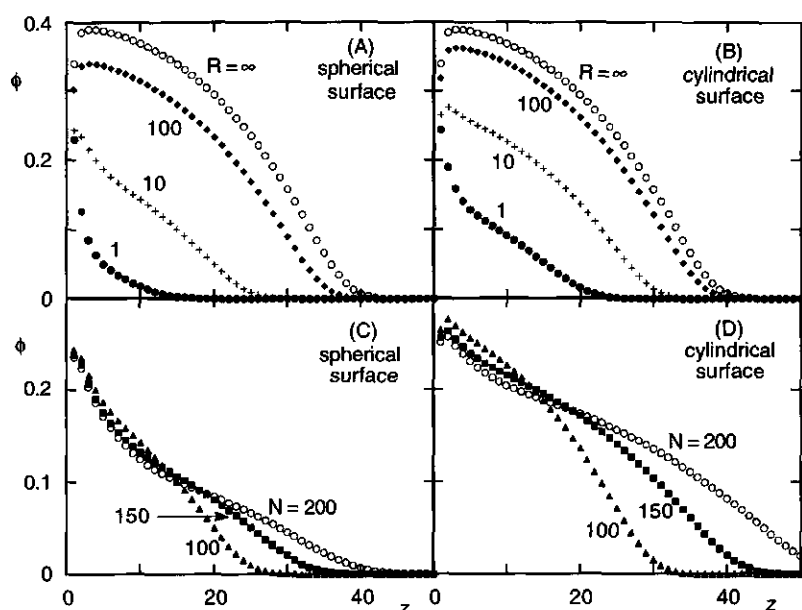

Figure 3 Effect of radius of curvature and chain length on the segment distribution in spherical and cylindrical geometries. (A) and (B) chain length N = 100; (●) R = 1, (+) R = 10, (◆) R = 100, (O) R=∞. (C) and (D) R = 10; (▲) N = 100, (■) N = 150, (O) N = 200. (A) and (C) spherical geometry; (B) and (D) cylindrical geometry. In all cases $\chi = -0.5$.

3.5 Results

The effects of surface curvature and chain length on the volume fraction profiles of brushes at spherical and cylindrical surfaces is shown in Figure 3. Here a very good solvent has been used ($\chi = -0.5$), which gives slightly more extended brushes than an athermal solvent. Parts A and B are drawn for a (relatively) short chain length of 100 segments. For low curvatures the profile has a large resemblance with the profile of a brush on a flat surface (R = ∞), which is also drawn for comparison. Upon increasing the curvature, the shape of a growing part of the profile becomes convex. The same trend can be seen in parts C and D, where curves are drawn for different chain lengths but with the same radius of curvature. Increasing the chain length has a similar effect on the shape of the

76

profiles as decreasing the radius of curvature. The parameters in Figure 3 are the same as those in Figures 2 and 3 of Dan and Tirrell's paper,[13] which were calculated with an excluded volume parameter v = 1. The shape of our profiles is very similar to theirs. However, Dan and Tirrell consistently predict layers that are slightly more strongly stretched, and consequently slightly less dense. For example, for a spherical interface with R = 100 and N = 100 they calculate a brush height that is approximately 10% larger than ours. Probably this is due to the way solvent-segment interactions are taken account of by the excluded volume parameter. As stated above, all our calculations were done using a cubic lattice. For a flat interface this lattice gives exact correspondence with the SCF theory of Zhulina *et al.* and Milner *et al.* in the limit of infinite chain length.[27]
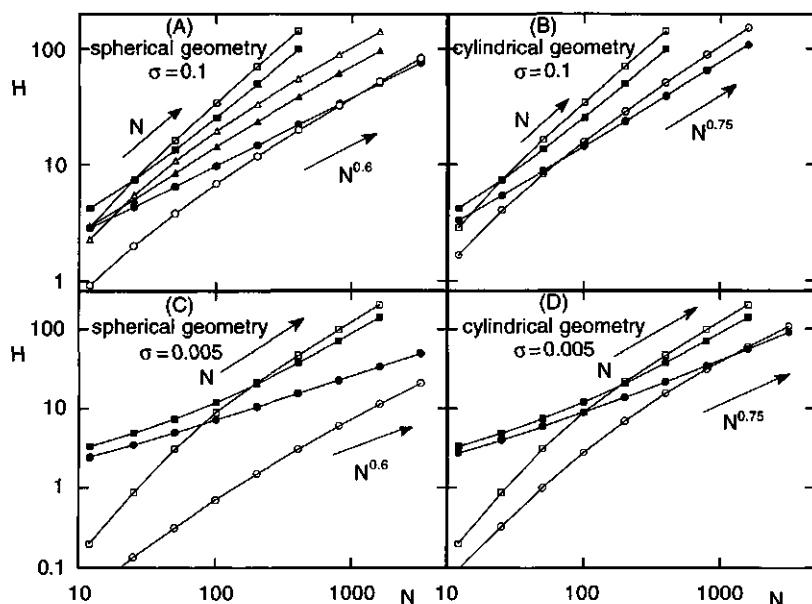

Figure 4 Brush thickness as a function of chain length in an athermal solvent. The brush thickness has both been expressed as the average segment height and as the hydrodynamic thickness (see text). Parameters: (A and C) spherical geometry; (B and D) cylindrical geometry; (A and B) $\sigma = 0.1$; (C and D) $\sigma = 0.005$. Symbols: ($\bullet$) R = 1; ($\blacktriangle$) R = 10; ($\blacksquare$) R = ∞; Open symbols are hydrodynamic heights; filled-in symbols are average heights.

Figure 4 gives the brush thickness as a function of polymer chain length under various conditions. This thickness has been calculated in two different ways. First, we have defined an average brush height H_{av} in a similar fashion as in ref 13,
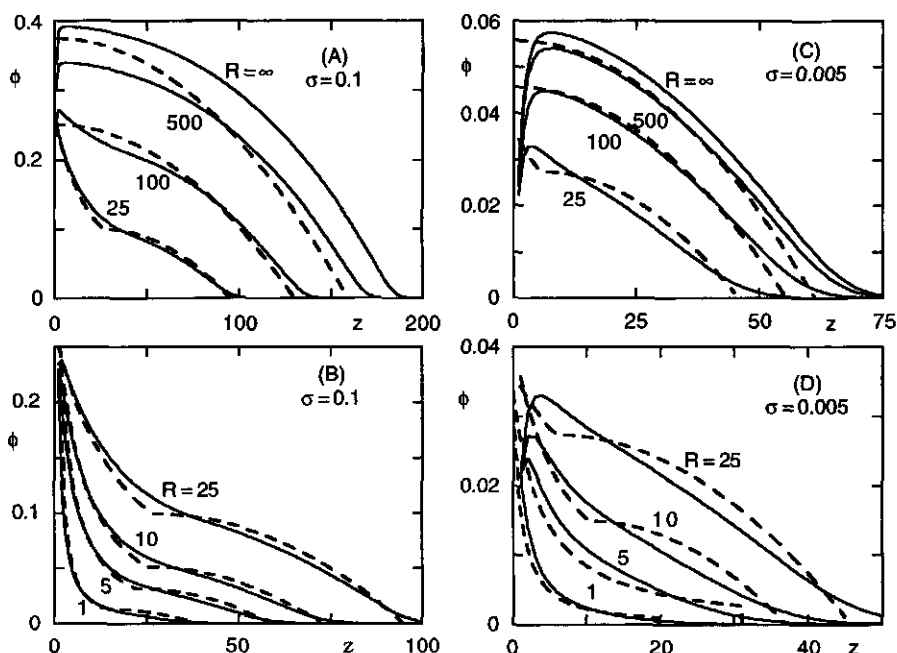
Figure 5 Volume fraction profiles for a spherical surface; $N = 500$; (A) $\sigma = 0.1$, $R = \infty$, $R = 500$, $R = 100$, and $R = 25$; (B) $\sigma = 0.1$, $R = 25$, $R = 10$, $R = 5$, and $R = 1$; (C) $\sigma = 0.005$, $R = \infty$, $R = 500$, $R = 100$, and $R = 25$; (D) $\sigma = 0.005$, $R = 25$, $R = 10$, $R = 5$, and $R = 1$. In all cases $\chi = 0$. The solid curves are lattice calculations. For $R = 500$ and $R = 100$ the dashed curves are the "parabolic potential profile" approximation. In (D) the dashed curves for $R = 1$ and $R = 5$ follow from the "fixed chain ends" model. All other dashed curves were calculated according to the combined model.

$$H_{av} = \left(\frac{\sum_z z^2 (z+R)^2 \phi(z)}{\sum_z (z+R)^2 \phi(z)} \right)^{\frac{1}{2}} \tag{26}$$

which is basically a second moment of the volume fraction profile. Secondly, we have calculated the hydrodynamic layer thickness H_{hy}, using the theory of Cohen Stuart *et al.*,[32] taking the hydrodynamic constant $C_H = 1$. To apply this theory to curved surfaces we assume that all solvent flow takes place concentrically with respect to the surface (the flow has no component in a direction perpendicular to the surface). For low Reynolds numbers this seems a reasonable approximation for many practical systems. (Both H_{av} and H_{hy} give smaller values than the brush height H as defined in e.g. ref 17). When the grafting density is high ($\sigma = 0.1$) we

78

find very good agreement with the scaling law $H_{av} \sim N$ for a flat surface, and for a spherical surface with $R = 1$ (star-shaped polymer) we find equally good agreement with the scaling law $H_{av} \sim N^{0.6}$. For cylindrical surfaces the expected scaling behaviour $H_{av} \sim N^{0.75}$ is found for $R = 1$. When $\sigma = 0.005$ increasing deviations occur from these power laws, which for flat surfaces are caused by the "foot of the parabolic profile".[27,33] The hydrodynamic thicknesses agree less well with the predicted power law. Experimentally the hydrodynamic thickness may, however, be the most easily accessible parameter for defining brush thicknesses in these systems.
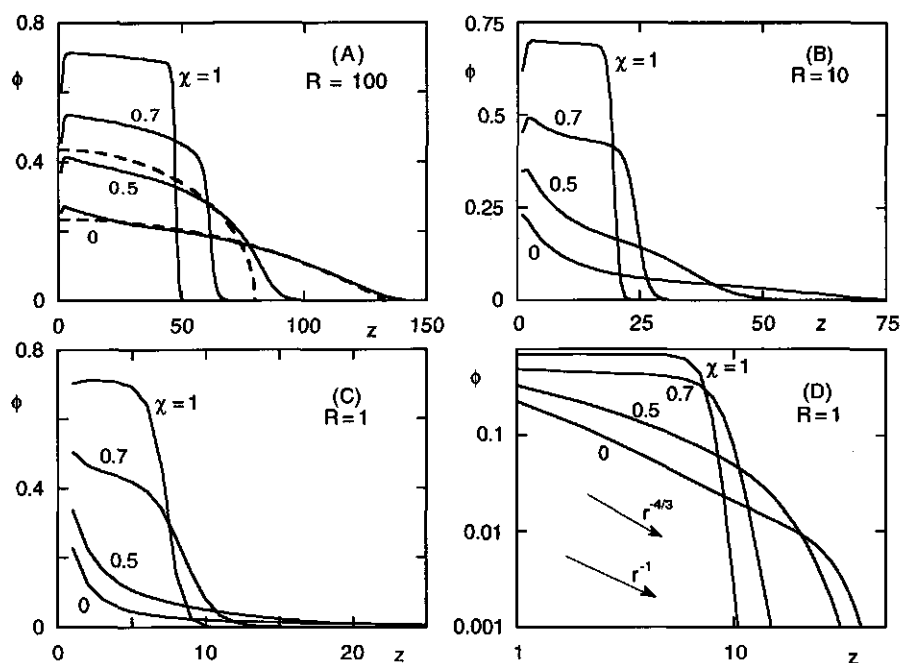

Figure 6 Volume fraction profiles in a spherical geometry for different solvent qualities: a decrease of the solvent quality leads to a collapse of the grafted layer. In (A) the dashed curves are the parabolic potential model predictions. For $R = 1$ the profiles are also given on a logarithmic scale to be able to check for a power law dependency between ϕ and z. Parameters: $\sigma = 0.1$; $N = 500$; $\chi = 0$, 0.5, 0.7, 1; (A) $R = 100$; (B) $R = 10$; (C and D) $R = 1$.

In Figure 5 lattice volume fraction profiles (full curves) are given for $N = 500$ in a spherical geometry with $\sigma = 0.1$ and $\sigma = 0.005$ ($\sigma = 0.1$ is a very high grafting density, which won't easily be reached by adsorbing block copolymers, but which may be a good value for modelling a star polymer (when $R = 1$); $\sigma = 0.005$ is a

more reasonable value for the grafting density on sterically stabilized colloidal particles). The dashed curves have been calculated with the equations of section 3. The curves for R = 500 and R = 100 (when $\omega > \omega_{cr}$) are given by the parabolic potential profile approximation. For smaller values of R (when $\omega < \omega_{cr}$) the "combined model" gives a reasonably good fit with the lattice calculations. The dashed curves for $\sigma = 0.005$ and R = 5, and R = 1 follow directly from eq. 11. For these small values of R the "fixed chain ends" model agrees best with the lattice calculations.

Figure 6 shows how the solvent quality influences the polymer brushes. As is the case with flat brushes, a worse solvent gives a more compact grafted layer. For $\chi \approx 1$ the volume fraction profile is well approximated by a step-profile, irrespective of the interface curvature, in agreement with eq 14 (of course, the height of the brush does depend on the curvature). When the curvature is not too large (R = 100 in Figure 6A) a brush can still be reasonably well described by the parabolic potential profile approximation applied in a Θ-solvent. For R = 1 the exponent of the initial decay of the profile gradually changes from 4/3 to 1 when the solvency changes from $\chi = 0$ to $\chi = 0.5$.
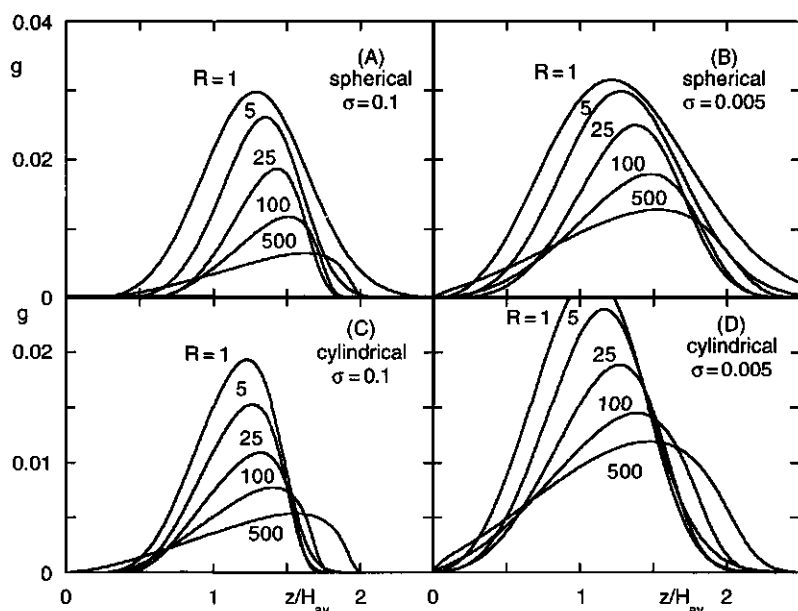

Figure 7 Free chain end distribution functions g, as a function of the reduced distance to the surface z/H_{av}, for various radii of curvature as indicated; (A and B) spherical geometry; (C and D) cylindrical geometry; (A and C) $\sigma = 0.1$; (B and D) $\sigma = 0.005$. Further parameters: N = 1000; $\chi = 0$.

Figure 7 gives the exact distribution functions of free chain ends of the polymer chains. The function $g(z/H_{av})$ is drawn, where H_{av} is given by eq 26 and $g(z) = \phi(z,N)L^d(z)/\sigma L^d(1)$ with $\phi(z,N)$ the volume fraction profile of the end-segments. Figure 7 illustrates the existence of a dead zone in both the spherical and cylindrical geometries. Of course, the probability that an end-segment is located in this zone is not absolutely zero, but very small. As long as $\sigma < 1$ a polymer chain conformation with an end-segment bending back to the surface will have a finite probability. This makes it difficult to speak about the absolute size of the dead zone within our lattice SCF model. One can only use an arbitrary definition for the dead zone, for example the area where $g(z)$ is smaller than 5% of its maximum value.[13] Some conclusions concerning the behaviour of this zone can be drawn from Figure 7. When the radius of curvature is small, an increase in R leads to a larger dead zone, both in absolute terms (which is partly caused by an increase in the layer height) and in relative terms (as a fraction of the layer height, which can, for example, be expressed by H_{av}). Increasing R even further at a certain point leads to a decrease of the dead zone size and eventually results in its total disappearance. These trends are clearly seen in parts A and C of Figure 7, where the grafting density is high ($\sigma = 0.1$). For the far lower grafting density of 0.005, which in many practical systems may still be a very realistic value, the dead zone is significantly smaller.

The behaviour of the dead zone size as a function of surface curvature is at least qualitatively in agreement with eq 19 (parabolic potential profile) and with the combined model. In Figure 8 the chain end distribution g is given as a function of z as calculated from the lattice model (solid curves), and the parabolic potential model and the combined model (dashed curves) for grafting densities of 0.1 and 0.005. There is a fair correspondence between the lattice calculations and the predictions of section 3. In the parabolic potential model the negative values of g for small z must be compensated by too large values of g elsewhere. This is the main reason for the differences found round the maximum of $g(z)$. Nevertheless for all sets of parameters the analytical equations correctly predict the location of this maximum. The lattice calculations do consistently show a smaller dead zone and an appreciably wider distribution of free end-segments at the tip of the brush. These segments are located in the "foot" of the parabolic profile. Especially for smaller values of R, the differences between the two curves become significant. For very small R the end-segments certainly do not all tend to be concentrated in a narrow zone (although the overall volume fraction profile, as seen above, does tend to the −4/3 power law of the "fixed chain ends" model). Overall, the approxi-

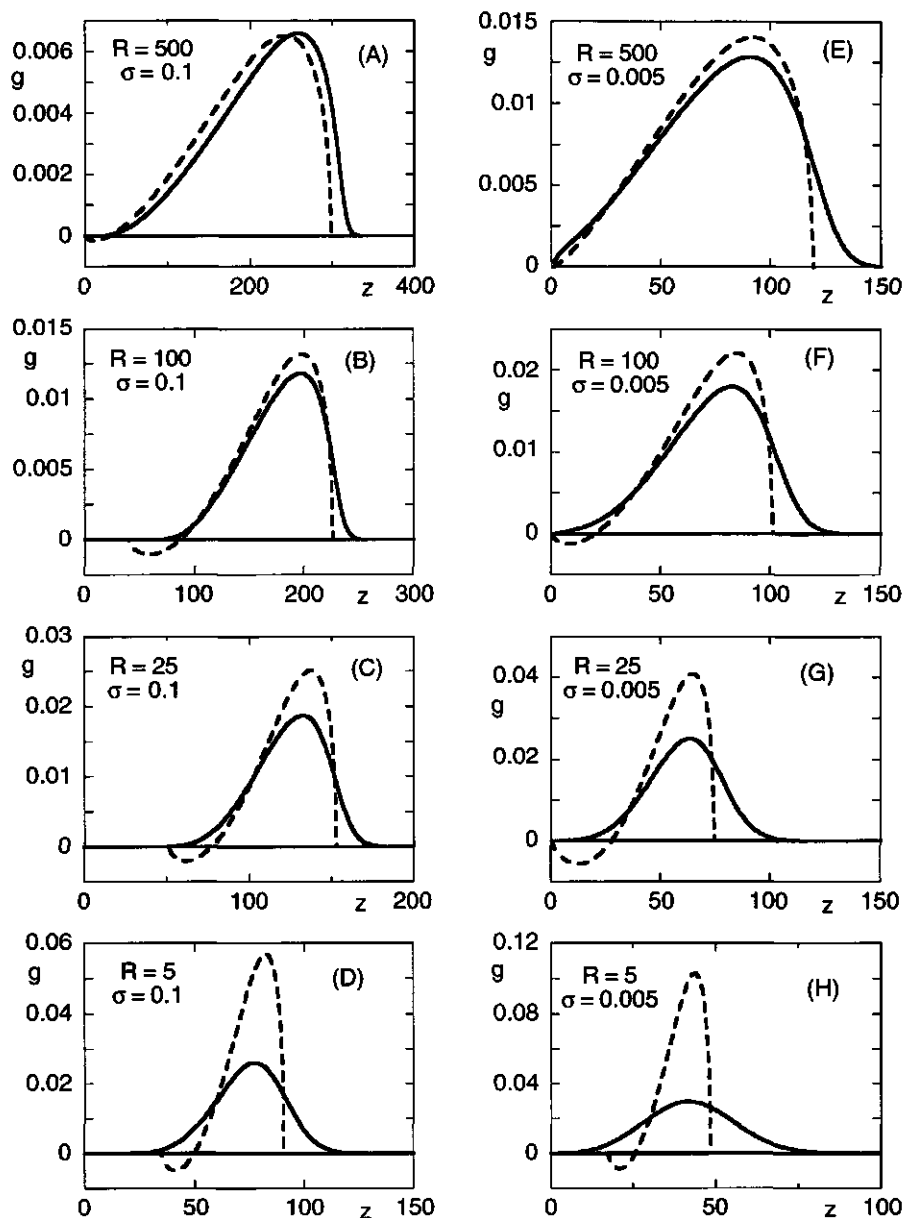**Figure 8** Free chain end distribution functions g, as a function of z in a spherical geometry for σ = 0.1 (A-D) and σ = 0.005 (E-H). The solid curves are lattice calculations, the dashed curves are the analytical equations (the parabolic potential profile model was used for A,E,F, and G, and the combined model was used for B,C,D, and H). Further parameters: N = 1000; χ = 0.

82

mate analytical equations give a reasonable prediction of the dead zone size.

Figure 9 explores a possible scaling behaviour of the free-end distribution. Both in the limit of small particle radius and for brushes under parabolic potential conditions the brush height scales as

$$H \sim \left(\sigma N^3 R^{d-1}\right)^{\frac{1}{d+2}}$$

This suggests that the free end-segments and the dead zone size may have a similar scaling dependence. Parts A-C of Figure 9 show the end-segment distribution function g in a spherical geometry as a function of $z/\left(N^{3/5}R^{2/5}\sigma^{1/5}\right)$. If the scaling law $\Delta \sim N^{3/5}R^{2/5}\sigma^{1/5}$ were correct all curves should become zero at the same value of $z/\left(N^{3/5}R^{2/5}\sigma^{1/5}\right)$. This is not the case. A better approximation would be to assume that the dead zone is equal to the first part z_0 of the combined model. From eqs 21-23 one can then derive that

$$\frac{\Delta}{\left(\sigma N^3 R^{d-1}\right)^{\frac{1}{d+2}}} = v^{\frac{1}{d+2}}\left(\frac{\left(\frac{8}{\pi^2}\right)^{\frac{1}{3}}\omega + \frac{d+2}{3}\left(\frac{4}{3}\right)^{\frac{1}{3}}}{1+\frac{d+2}{6}\pi c}\right)^{\frac{3}{d+2}} - v^{\frac{1}{d+2}}\left(\left(\frac{8}{\pi^2}\right)^{\frac{1}{3}}\omega\right)^{\frac{3}{d+2}}$$

$$\approx 0.509 \text{ for } \omega \to 0 \quad \text{if } d=3 \qquad\qquad (27)$$
$$\approx 0.224 \text{ for } \omega \to 0 \quad \text{if } d=2$$

where the constant c is given by eq 25. In the legends of Figure 9 the values of $\Delta/\left(N^3R^{d-1}\sigma\right)^{1/(d+2)}$ are also given as calculated from this equation. For short chain lengths (e.g. R = 5, N = 200, σ = 0.1; see Figure 9C) and for very low grafting densities (e.g. R = 5, N = 1000, σ = 0.005; see Figure 9B) deviations start to occur from eq 27 which are caused by the fact that the chains are not strongly stretched for these parameters. We do indeed see that for small values of ω (e.g. for R = 5, N = 1000, and σ = 0.1 we have ω = 0.015) the dead zone size approaches the value given by eq 27 for $\omega \to 0$. Of course one must realize that the exact lattice calculations also take "fluctuations" into account which allow a finite number of conformations to have their end-segments bend back to the power-law part of the volume fraction profile. This is analogous to the "foot" that occurs in the volume fraction profile at the tip of the brush and explains why the curves do not show a sharply defined border of the dead zone. On the other hand eq 27 of course neglects the existence of a dead zone Δ_p in the parabolic potential part of the profile. For (R = 100, N = 1000, σ = 0.1; Fig 9A) one sees that the dead zone is

significantly larger than the value predicted by eq 27. In this case the contribution of Δ_p to the total dead zone Δ becomes apparent. Figure 9 also shows that when N
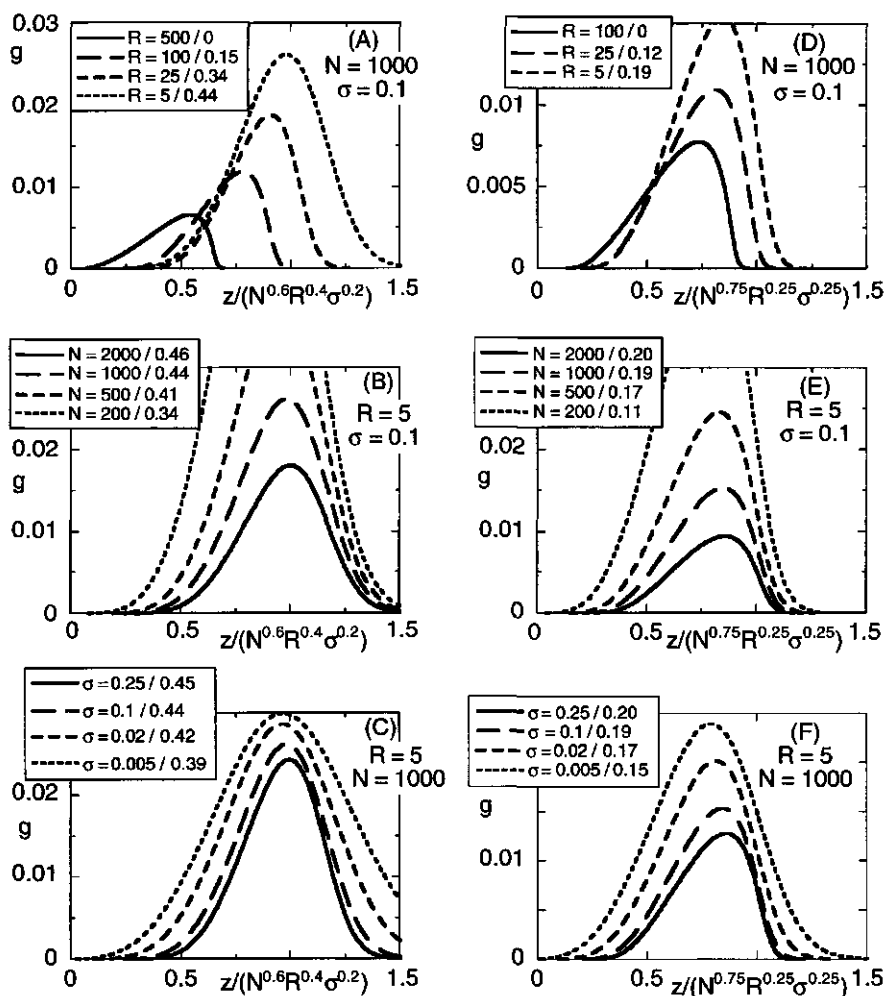
Figure 9 The distribution function g as a function of the normalized distance to the surface in a spherical geometry (A-C) and in a cylindrical geometry (D-F). This distance has been normalized to check the expected scaling behaviour of the dead zone: $\Delta \sim N^{3/5}R^{4/5}\sigma^{1/5}$ for a spherical surface, and $\Delta \sim N^{3/4}R^{1/4}\sigma^{1/4}$ for a cylindrical surface. Parameters: R, N, and σ as indicated in the figure; $\chi = 0$. In the legends the numerical values of eq 27 are also given for the indicated set of parameters.

and σ are changed, the location of the maximum of the function $g(z/(\sigma N^3 R^{d-1})^{1/(d+2)}$ hardly changes. The area under the curves does change but

this is because we have defined $\int g(z)dz = 1$. If the curves in parts B and C of Figure 9 are normalized so that

$$\int g\left(z \Big/ \left(\sigma N^3 R^{d-1}\right)^{1/(d+2)}\right) d\left(z \Big/ \left(\sigma N^3 R^{d-1}\right)^{1/(d+2)}\right) = 1$$

all curves virtually collapse onto a master curve. This is, however, not the case for the curves in Figure 9A. Increasing the particle radius shifts the maximum in g to lower values of $z \Big/ \left(\sigma N^3 R^{d-1}\right)^{1/(d+2)}$.

Parts D-E of Figure 9 show the same curves as parts A-C for a cylindrical surface. Most dead zones are slightly larger than predicted by eq 27. This is caused by the contribution of Δ_p to the total dead zone Δ. The general shape of the curves shows the same behaviour as in the spherical geometry. The values of Δ are smaller than those for the spherical surfaces, but the dependence of Δ upon N, R, and σ is very similar to that found in parts A-C of Figure 9.
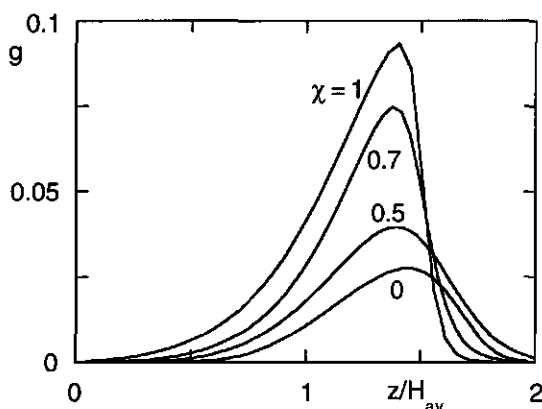
Figure 10 The influence of solvent quality on the chain end distribution. Parameters: R = 25, N = 500, σ = 0.1, spherical geometry, χ = 0, 0.5, 0.7, 1.

The effect of solvent quality on the free chain end distribution is demonstrated in Figure 10. For solvents varying from good (athermal) to very bad ($\chi = 1$) $g(z/H_{av})$ has been drawn for a brush on a spherical surface with a high grafting density ($\sigma = 0.1$). Decreasing the solvent quality leads to a collapse of the polymer layer as was seen in Figure 7. However, the distribution of chain ends changes relatively little. Of course the area in which the end-segments are located becomes smaller, as the layer height itself becomes smaller, and so the size of the dead zone decreases. The relative size of the dead zone also decreases slightly (as seen from

85

the curve of g versus the reduced distance to the surface, z/H_{av}), but this turns out to be a minor effect.

3.6 Discussion and Conclusions

In this chapter we have shown that the lattice model of the Scheutjens and Fleer theory can be usefully extended to study polymer brushes at spherical and cylindrical interfaces. The efficient method this theory uses to generate chain conformations makes it possible to study the characteristics of polymer brushes over a wide range of chain lengths (e.g. for far longer chain lengths than is at present possible using simulation techniques). We again emphasize that this theory gives exact solutions within the mean-field theory, in which only nearest-neighbour interactions are accounted for. This makes it an obvious reference point with which to compare approximate analytical SCF descriptions of polymer brushes. We first compared volume fraction profiles with those calculated by Dan and Tirrell.[13] We found good agreement between both models. This is not surprising as both our approaches are based on a very similar physical model.

We have concentrated ourselves on analysing the volume fraction profiles of brushes at spherical surfaces immersed in an athermal, low molecular weight solvent. For small curvatures the parabolic potential profile model agrees very well with the more accurate lattice calculations. The differences between both descriptions can be largely explained by the fact that the analytical model only takes into account pair interactions between segments. For flat surfaces differences of the same order of magnitude appear in the volume fraction profile when higher terms are neglected in the mixing free energy of polymer and solvent. Similarly, the distribution of free end-segments is roughly the same in both models.

For decreasing radii of curvature the spurious effect of negative values of g(z) for low z becomes more prominent. As $\int g(z)dz = 1$ this leads to too high values of g(z) outside the dead zone. Furthermore, the lattice calculations predict a finite volume fraction of free chain ends beyond the "classical" chain height. This "foot" of the volume fraction profile can be explained completely analogously to that at the flat interface.[27,33] Increasing the curvature leads to the appearance of a power law-like part in the volume fraction profile.

The "combined model" that we introduced gives a reasonable description of the volume fraction profile by dividing it into two parts. The distribution of free ends in this model is too narrow, but the position of the maximum of this distribution is the same as in the lattice model. For very small particles the lattice model certainly does not indicate that all chain ends are situated at the same height above the

surface. The total volume fraction profile for such particles does, however, tend to the scaling law $\phi \sim z^{-4/3}$.

Our lattice calculations show very clear indications of the presence of a dead zone both near spherical and cylindrical interfaces. This is in contradiction with the molecular dynamics results of Murat and Grest,[12] who found no evidence for the existence of a dead zone near a cylindrical surface for any finite radius of curvature. A quantitative comparison of our results with those of Ball et al.[11] is not possible, as they solved their SCF equations for a system that we have not considered in this chapter, namely a cylindrical brush under melt conditions. Our calculations do, however, suggest that the dead zone size is not a simple monotonic function of the radius. We have tried to explain the radius dependency of the dead zone size in terms of the "combined model" for the volume fraction profile. We hope that our data and this tentative interpretation will encourage further work aimed at better understanding of this dead zone behaviour.

In conclusion, we have showed that upon decreasing the solvent quality the grafted layer collapses and forms a step-like profile, irrespective of the curvature. A decrease in solvent quality also leads to a decrease in the dead zone size, but, even for a (far) worse than Θ-solvent, a dead zone can still exist.

3.7 References

1. Alexander, S. *J. Phys. (Paris)* **1977**, 38, 983.
2. de Gennes, P. G. *Macromolecules* **1980**, 13, 1069.
3. Cosgrove, T.; Heath, T.; Van Lent, B.; Leermakers, F.; Scheutjens, J. *Macromolecules* **1987**, 20, 1692.
4. Milner, S. T.; Witten, T. A.; Cates, M. E. *Europhys. Lett.* **1988**, 5, 413.
5. Milner, S. T.; Witten, T. A.; Cates, M. E. *Macromolecules* **1988**, 22, 583.
6. Zhulina, E. B.; Priamitsyn, V. A.; Borisov, O. V. *Polymer Science USSR* **1989**, 31, 205.
7. Chakrabarti, A.; Toral, R. *Macromolecules* **1990**, 23, 2016.
8. Lai, P. Y.; Binder, K. *J. Chem. Phys.* **1991**, 95, 9288.
9. Lai, P. Y.; Zhulina, E. B. *J. de Phys. II* **1992**, 3, 547.
10. Murat, M.; Grest, G. S. *Macromolecules* **1989**, 22, 4054.
11. Ball, R. C.; Marko, J. F.; Milner, S. T.; Witten, T. A. *Macromolecules* **1991**, 24, 693.
12. Murat, M.; Grest, G. S. *Macromolecules* **1991**, 24, 704.
13. Dan, N.; Tirrell, M. *Macromolecules* **1992**, 25, 2890.
14. Daoud, M.; Cotton, J. P. *J. Phys. (Paris)* **1982**, 43, 531.
15. Birshtein, T. M.; Zhulina, E. B. *Polymer* **1984**, 25, 25.

16. Birshtein, T. M.; Borisov, O. V.; Zhulina, E. B.; Khokhlov, A. R.; Yurasova, T. *Polym. Sci. USSR* **1987**, 29, 1293.
17. Zhulina, E. B.; Borisov, O. V.; Priamitsyn, V. A. *J. Colloid Interface Sci.* **1990**, 137, 495.
18. Semenov, A. N. *Sov. Phys. JETP* **1985**, 61, 733.
19. Zhulina, E. B.; Borisov, O. V.; Brombacher, L. *Macromolecules* **1991**, 24, 4679.
20. Klushin, L. I.; Skvortsov, A. M. *Macromolecules* **1991**, 24, 1549.
21. Grest, G. S.; Kremer, K.; Witten, T. A. *Macromolecules* **1987**, 20, 1376.
22. Dolan, A. K.; Edwards, S. F. *Proc. R. Soc. London Ser. A* **1974**, 337, 509.
23. Dolan, A. K.; Edwards, S. F. *Proc. R. Soc. London Ser. A* **1975**, 323, 427.
24. Scheutjens, J. M. H. M.; Fleer, G. J. *J. Phys. Chem* **1979**, 83, 1619.
25. Scheutjens, J. M. H. M.; Fleer, G. J. *J. Phys. Chem.* **1980**, 84, 178.
26. Hirz, S. *M.S. Thesis*, University of Minnesota **1987**.
27. Wijmans, C. M.; Scheutjens, J. M. H. M.; Zhulina, E. B. *Macromolecules* **1992**, 25, 2657; This thesis, chapter 1.
28. Leermakers, F. A. M.; Scheutjens, J. M. H. M. *J. Phys. Chem.* **1989**, 93, 7417.
29. Zhulina, E. B.; Borisov, O. V.; Priamitsyn, V. A.; Birshtein, T. M. *Macromolecules* **1991**, 24, 140.
30. Liatskaya, Y. V.; Zhulina, E. B.; Birshtein, T. M. *unpublished results*
31. Milner, S. T.; Witten, T. A. *J. Phys. France* **1988**, 49, 1951.
32. Cohen Stuart, M. A.; Waajen, F. H. W. H.; Cosgrove, T.; Vincent, B.; Crowley, T. L. *Macromolecules* **1984**, 17, 1825.
33. Milner, S. T. *J. Chem. Soc. Faraday Trans.* **1990**, 86, 1349.

chapter 4

Copolymer Adsorption on Small Particles

Abstract

In this chapter we use self-consistent field theory to study the adsorption of diblock copolymers onto small colloidal particles. The particles are modelled as spheres and the assumption is made that the adsorption parameter of the adsorbing segments is independent of the particle curvature. We find that the adsorbed amount per unit of surface area increases with increasing curvature. The hydrodynamic layer thickness decreases greatly with increasing curvature. The root-mean-square layer thickness does not vary much when the curvature changes.

4.1 Introduction

Recently Evers *et al*.[1-3] published a statistical thermodynamic model to describe the adsorption of copolymers. This work is an extension of the self-consistent field theory of Scheutjens and coworkers,[4-6] which was developed to describe polymers at interfaces. In one of their papers Evers *et al*.[2] studied the effect of the molecular composition of a diblock copolymer on its adsorbed amount. They showed that when the total length of the diblock copolymer is kept constant, a maximum is found in the adsorbed amount as a function of the fraction of adsorbing segments. This result is of great practical importance for the stabilization of colloidal dispersions, as a larger adsorbed amount generally corresponds to a larger thickness and, hence, to better stabilizing properties. Wu *et al*.[7] have recently presented the results of an experimental study of the effect of the composition of a diblock copolymer on its adsorbed amount. They adsorbed a block copolymer consisting of a (dimethylamino)ethyl methacrylate block and a *n*-butyl methacrylate block from 2-propanol onto silica and found a maximum adsorbed amount for a certain ratio of both block lengths, as predicted by Evers *et al*. Marquez and Joanny[8] developed a different approach to the problem. They proposed a scaling model for diblock copolymer adsorption from a nonselective solvent. This model also predicts a maximum in the adsorbed amount as a function of the fraction of adsorbing segments.[9-10] Hence, the maximum in the adsorbed amount of a diblock copolymer as a function of its composition seems to be a well established fact.

The self-consistent field approach of Evers *et al*.[1] is a lattice model for incompressible systems. It is based on the following fundamental approximations:

(i) The polymer molecules are described as Markov chains (i.e. they are freely jointed) on a lattice.

(ii) The many-chain problem is reduced to considering a test chain in an "external" field made up by the surrounding chains.

(iii) Only short-range (nearest-neighbour) interactions are taken into account.

The papers of Evers *et al*.[1-3] consider adsorption at infinitely large, flat interfaces. In colloidal dispersions polymers adsorb onto curved particles. As long as the radius of curvature of these particles is far larger than the dimensions of the adsorbed layer, one can model the adsorbent as a flat surface. However, when the radius of curvature is of the same order of magnitude as the adsorbed layer thickness, one should explicitly account for this curvature. In this chapter we discuss the effect of particle curvature on the adsorbed amount and layer thickness of a diblock copolymer. We apply the theory of Evers *et al*. in a spherical lattice as described by Leermakers and Scheutjens.[6] In such a lattice the layers form equidistant, concentric shells. The differences between a planar lattice and a spherical lattice are: (i) the

number of sites L(z) in layer z increases on moving away from centre of the lattice; (ii) the lattice transition parameters are layer-dependent. These parameters, denoted as $\lambda_-(z)$, $\lambda_0(z)$, and $\lambda_+(z)$, are defined as the fraction of neighbours a site in layer z has in layers $z-1$, z, and $z+1$, respectively. The layers are numbered $z = 1, 2, 3, \ldots$ starting at the centre of the lattice and moving outwards. Leermakers and Scheutjens have given expressions for the number L(z) of sites in a layer and for the lattice transition parameters as a function of z. Wijmans and Zhulina[11] used such a lattice to describe a polymer brush on a spherical particle. In this case the central R layers of the lattice are occupied by the particle. We use the same approach to study the adsorption of polymer molecules from solution onto a spherical particle. In this case the polymer layer is in equilibrium with the bulk solution.

4.2 Results

All calculations were performed using a hexagonal lattice, i.e. $\lambda_+(\infty) = \lambda_-(\infty) = 3/12$. The copolymers consist of an adsorbing block of A segments (anchor) and a block of nonadsorbing B segments (buoy). We denote the length of the A block as N_A and the length of the B block as N_B. Nearest-neighbour interactions between segments are accounted for by the Flory-Huggins parameter χ. The solvent is taken to be a poor solvent for the A block and a good solvent for the B block ($\chi_{AO} = 0.5$ and $\chi_{BO} = 0$, where O denotes the solvent, and $\chi_{AB} = 0.5$).

Following Silberberg,[12] we introduce an adsorption energy parameter χ_{sAO} for segment A, which is defined as the dimensionless difference $\left(u_O^a - u_A^a\right)/kT$, where u_A^a is the adsorption energy of segment A, and u_O^a is the adsorption energy of a solvent molecule. If χ_{AS} is the conventional Flory-Huggins parameter between A segments and adsorbent molecules (S), then $\chi_{sAO} = -\lambda_-(R+1)\{\chi_{AS} - \chi_{OS}\}$ because a fraction $\lambda_-(R+1)$ of an adsorbed segment (situated in layer R+1) is in contact with adsorbent sites. For a given value of χ_{AS} the lattice model implies that the adsorption energy parameter χ_{sAO} is an (increasing) function of the radius of curvature R. In the calculations we have kept χ_{sAO} constant and we have used $\chi_{sAO} = 2$. This corresponds to $\chi_{AS} = -8$ for a flat surface if $\chi_{OS} = 0$, and to higher values of χ_{AS} if R is small. The assumption of a constant χ_{sAO} seems reasonable when the adsorption is caused by a specific interaction, such as the formation of a hydrogen bond. In the case of non-specific interactions (e.g. van der Waals forces) this assumption might be less justifiable. In an experimental system with (very) small particles one should always bear this complicating factor in mind. In contrast to the A segments the B segments are taken as nonadsorbing: $\chi_{sBO} = 0$.
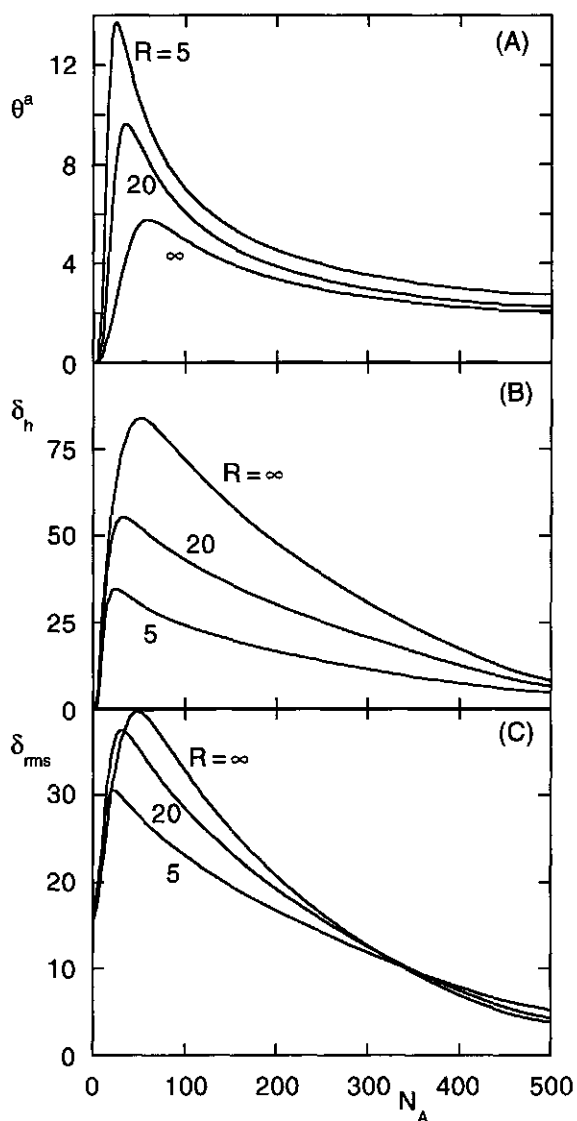
Figure 1 (A) adsorbed amount θ^a per unit of surface area; (B) hydrodynamic layer thickness δ_h; (C) root-mean-square layer thickness δ_{rms} as a function of the number of adsorbing segments N_A in an AB diblock copolymer. The radius R of the adsorbent particle is indicated. Parameters: $\chi_{AO} = 0.5$; $\chi_{BO} = 0$; $\chi_{AB} = 0.5$; $\chi_{sAO} = 2$; $\chi_{sBO} = 0$; $\phi^b = 10^{-4}$.

Figure 1 shows results for the adsorption of diblock copolymers onto spherical particles. The bulk solution volume fraction ϕ^b of polymer is kept constant at

$\phi^b = 10^{-4}$. Figure 1 was calculated for (monodisperse) polymer chains with a total chain length (i.e. number N_A of A segments plus number N_B of B segments) of 500. The values of the particle radius are indicated in the Figure. In part A the adsorbed amount θ^a (expressed as the total number of segments in adsorbed chains per unit of surface area) is given as a function of N_A. The parameters have been chosen such that for $R = \infty$ the system is the same as in Figure 3 of ref 2.

For all values of R, θ^a is a non-monotonic function of N_A, exhibiting a maximum for $N_A < 100$. Evers et al. explained this maximum as follows. When the fraction of A segments is smaller than corresponding to this maximum, the anchoring is weak: the adsorbed amount is low because the total adsorption energy per chain is small. Beyond this maximum the adsorbed amount decreases with increasing N_A because the surface region is overcrowded by adsorbing A segments, and the freely dangling B blocks become shorter.

When the surface is curved the adsorbed amount per unit area is larger than for a flat surface. A decrease in R leads to an increase in the adsorbed amount for all possible compositions of the polymer. The curved geometry allows the B blocks, which are protruding into the solution, more lateral freedom, which makes the adsorption process entropically more favourable. The curvature dependence is most pronounced for chain compositions with a relatively long buoy block (small N_A). For $R = 5$ up to twice as much polymer can be adsorbed per unit of surface area as compared to a flat surface. When the length of the A block is significantly increased beyond its optimal value the curvature effect is strongly reduced. In the limiting case of an adsorbing homopolymer (no B segments, only A segments) the adsorbed amount is only slightly larger for $R = 5$ than for $R = \infty$. Furthermore, Figure 1A shows that the maximum in the adsorbed amount curve shifts to slightly lower A segment fractions when the curvature is increased: a smaller sticking energy is required if the B blocks hinder each other to a lesser extent.

An important parameter to characterize an adsorbed polymer layer is its thickness. The effect of the particle curvature on the layer thickness has also been studied, as is shown in parts B and C of Figure 1. It turns out that, even qualitatively, the effect depends strongly on the way in which one defines the adsorbed layer thickness.

We first consider the hydrodynamic layer thickness δ_h, plotted in Figure 1B. The hydrodynamic layer thickness of polymer adsorbed onto colloidal particles can be determined from techniques such as photon correlation spectroscopy, that measure diffusion times. The hydrodynamic layer thickness was calculated under the assumption that all flow of the solvent takes place concentrically to the surface. This assumption enables us to apply the theory of Cohen Stuart et al.[13] to calculate the

93

hydrodynamic layer thickness from the volume fraction profile. We take the hydrodynamic constant C_h equal to unity.[2,13] Clearly, the assumption of concentric flow is not correct. For small particles one expects that this assumption overestimates the layer thickness. However, that would only enhance the curvature effect we find for the hydrodynamic layer thickness dependency. The main conclusion from Figure 1B is that, upon decreasing R, the hydrodynamic layer thickness also decreases. At first sight this might seem a little puzzling, as the adsorbed amount increases with increasing curvature. However, a decrease in R implies that the volume fraction profile of the B segments falls off more quickly (see also Figure 2). The hydrodynamic layer thickness is a measure for the spatial extension of the volume fraction profile.

In Figure 1C the root-mean-square (rms) layer thickness δ_{rms} is given for the same systems. The rms layer thickness can be determined from a static light scattering experiment. This measure of the layer thickness is defined as:

$$\delta_{rms} = \left(\frac{\sum_z z^2 \phi(z) L(z)}{\sum_z \phi(z) L(z)} \right)^{\frac{1}{2}}$$

Here, L(z) is the number of lattice sites in layer z. For $N_A < 300$, δ_{rms} turns out to be an increasing function of R, just as δ_h. The relative differences between the layer thicknesses found for different values of R are far smaller than those found for the hydrodynamic layer thickness, and follow more closely the adsorbed amount θ^a. For large values of N_A ($N_A > 400$) one even finds that δ_{rms} is a decreasing function of R. The different results as compared to the hydrodynamic layer thickness can be explained by the definition of the rms layer thickness. The latter thickness does not measure the extension of the volume fraction profile $\phi(z)$ but is a measure for $L(z)\phi(z)$. Although the volume fraction profile falls of far more quickly when the curvature is increased, L(z) times the volume fraction profile does so less strongly. The quantity $L(z)\phi(z)$ is proportional to the fraction of segments at a given distance z from the surface.

In Figure 2 volume fraction profiles of the B blocks are plotted. These data apply to chains consisting of 40 A and 460 B segments. The decrease of the hydrodynamic layer thickness with increasing curvature can easily be understood from these volume fraction profiles. If in this Figure ϕ were multiplied by L(z), the profiles for small R would increase more than those for large R. This explains the different R-dependency of δ_h and δ_{rms}. The shape of the curves in Figure 2 is the same as what one would expect for nonadsorbing polymer chains terminally attached to a spherical surface. For large R the volume fraction profile corresponds

to a parabolic potential profile. For small R it changes to a power law. This behaviour was studied more extensively in ref 11.
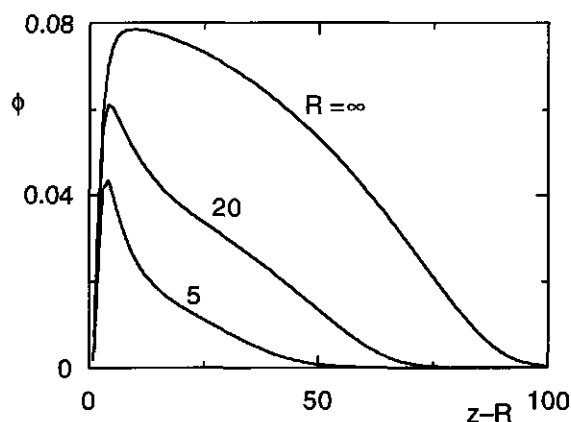

Figure 2 Volume fraction profiles for the B segments of $A_{40}B_{460}$ copolymers adsorbing onto spherical particles with radius R (indicated). All parameters are the same as in Figure 1.

4.3 References

1. Evers, O. A.; Scheutjens, J. M. H. M.; Fleer, G. J. *Macromolecules* **1990**, 23, 5221.
2. Evers, O. A.; Scheutjens, J. M. H. M.; Fleer, G. J. *J. Chem. Soc. Faraday Trans.* **1990**, 86, 1333.
3. Evers, O. A.; Scheutjens, J. M. H. M.; Fleer, G. J. *Macromolecules* **1991**, 24, 5558.
4. Scheutjens, J. M. H. M.; Fleer, G. J. *J. Phys. Chem.* **1979**, 83, 1619.
5. Scheutjens, J. M. H. M.; Fleer, G. J. *J. Phys. Chem.* **1980**, 84, 178.
6. Leermakers, F. A. M.; Scheutjens, J. M. H. M. *J. Phys. Chem.* **1989**, 93, 7417.
7. Wu, D. T.; Yokoyama, A.; Setterquist, R. L. *Polymer J.* **1991**, 23, 711.
8. Marques, C. M.; Joanny, J. F. *Macromolecules* **1989**, 1451.
9. Guzonas, D.; Hair, M. L.; Cosgrove, T. *Macromolecules* **1992**, 25, 2777.
10. Fleer, G. J.; Cohen Stuart, M. A.; Scheutjens, J. M. H. M.; Cosgrove, T.; Vincent, B. *Polymers at Interfaces,* Chapman & Hall: London, 1993.
11. Wijmans, C. M.; Zhulina, E. B. *Macromolecules* **1993**, 26, 7214; This thesis, chapter 3.
12. Silberberg, A. *J. Phys. Chem.* **1968**, 48, 2835.
13. Cohen Stuart, M. A.; Waajen, F. H. W. H.; Cosgrove, T.; Vincent, B.; Crowley, T. L. *Macromolecules* **1984**, 17, 1825.

chapter 5

Effect of Free Polymer on the Structure of a Polymer Brush

and Interaction Between Two Polymer Brushes

Abstract

Self-consistent field (SCF) calculations are presented of a planar grafted polymer layer that interacts with either free polymer chains or with another grafted layer. Three different systems are studied. The first is a grafted polymer layer immersed in a polymer solution. The interaction between grafted and free polymer can significantly influence the grafted polymer volume fraction profile. For grafted chains that are strongly stretched the lattice calculations are compared with the theory of Zhulina, Borisov and Brombacher (*Macromolecules 1991, 24, 4679*). Good agreement is found when the free chain length is far smaller than the grafted chain length. The scaling behaviour of the penetration of free polymer into the grafted layer is also studied for this system. In the second type of system the interaction between two grafted layers in the absence of free polymer is considered. The lattice calculations agree well with the theory of Zhulina *et al.* In the third system free polymer is present between the interacting grafted layers. If this free polymer has a small chain length, its main effect on the interaction free energy is the compression of the free grafted layers, and only repulsion is found. However, for larger chain lengths an attraction between the grafted layers appears.

5.1 Introduction

In a previous paper[1] the self-consistent field (SCF) description of non-compressed polymer brushes was discussed. Assuming that the chains in such a brush are strongly stretched with respect to their free Gaussian dimension, one can elegantly describe the structure of such a system by following a suggestion first introduced by Semenov.[2] In this approach all possible conformations of the polymer chains are replaced by a set of most probable conformations. For a given system this assumption can be rigorously checked using a SCF theory that involves the generation of all possible chain conformations on a lattice. The assumption of strong chain stretching is valid for a polymer brush immersed in a low molecular weight solvent under a very wide range of solvent qualities, but this assumption breaks down under extreme conditions, notably for very short chain lengths. The same holds for a polymer brush that is immersed in a solution of short mobile chains which are chemically identical to the grafted chains.

In this paper we shall discuss interactions between grafted layers in the absence and in the presence of free polymer. First, we discuss an isolated brush immersed in a solution of free polymer with the same chemical composition (but not necessarily the same degree of polymerization) as the grafted polymer. Here, the interesting issue is to what extent the free polymer penetrates into the grafted layer. Scaling dependencies will be derived for the degree of interpenetration as a function of grafting density, free and grafted chain lengths, and free polymer concentration. Second, the interaction between two planar grafted polymer layers immersed in a solvent will be considered. Zhulina *et al.*[3] and Milner *et al.*[4] showed how the strong chain stretching description of a single polymer brush can be extended to describe the interaction between two grafted layers if the interpenetration of these two layers is neglected. By comparing the predictions of this theory with the results of lattice calculations we hope to gain more insight into the behaviour of compressed polymer layers. In particular the effects of weak chain stretching, and the interpenetration of opposite layers will be studied. The third system discussed in this paper is a combination of the two previous ones: the interaction of two grafted layers in a solution of free polymer. In section 2 the theoretical methods are described, in section 3 numerical and analytical results are given, and in section 4 we discuss these results.

5.2 Theory

Lattice Model

Grafted polymer, solvent, and free mobile polymer is distributed on a planar lattice, consisting of M layers of L sites each, between two parallel plates. The diameter, ℓ, of the segments defines the lattice spacing. We restrict ourselves to the case of grafted and free polymer molecules of identical segment types in an athermal solvent. For large interplate distances $M\ell$ this system reduces to that of two isolated polymer brushes immersed in a polymer solution. If $M\ell$ is smaller than twice the brush thickness, we have two brushes in interaction. We consider polymer chains that are grafted at one end onto one of the two plates with a relative surface coverage $\sigma = n_g/L$, where n_g is the total number of chains grafted to that plate. In general, we want to compute the equilibrium distribution of all three components on the lattice for given values of M, σ ($0 \le \sigma \le 1$), grafted chain length N_g, free chain length N_f, and bulk volume fraction ϕ_f^b of the mobile polymer ($0 \le \phi_f^b \le 1$). This is done by weighting all possible conformations of the polymer chains by their Boltzmann probability factor. In a previous paper[1] we showed how the Scheutjens-Fleer formalism for polymer adsorption can be used to find the volume fraction profiles of such systems with grafted chains in the presence or absence of free polymer. In that paper we also discussed the computational problems that arise when long polymer chains are considered with a high grafting density.

For two interacting brushes the free energy A(M) of the system can be calculated as:[5]

$$\frac{A(M)}{LkT} = \sigma \ln\left(\sigma N_g \left(\sum_{z=1}^{M} G_g(z,N_g)\right)^{-1}\right) + \frac{\theta_f}{N_f}\ln\phi_f^b + \theta_s \ln(1-\phi_f^b) - \sum_{z=1}^{M}\frac{u(z)}{kT} \qquad (1)$$

Here θ_f and θ_s are the amount of free polymer and the amount of solvent molecules in the system, respectively, expressed in equivalent monolayers. The quantity $G_g(z,N_g)$ is the average weight of all conformations of a grafted chain of which the end segment is in layer z and u(z) is the potential energy profile of the polymer segments. When describing the interaction between two layers, it is convenient to define the excess surface free energy A^s as

$$\frac{A^s(M)}{L} = \frac{A(M)}{L} - \left(\mu_s - \mu_s^*\right)\theta_s - \left(\mu_f - \mu_f^*\right)\frac{\theta_f}{N_f} \qquad (2)$$

98

Here, $\mu_s - \mu_s^*$ and $\mu_f - \mu_f^*$ are the chemical potentials of the solvent and free polymer, respectively, defined with respect to their pure amorphous phases (denoted by *). They are equal to:[6]

$$\frac{\mu_s - \mu_s^*}{kT} = \ln\left(1 - \phi_f^b\right) + \phi_f^b\left(1 - 1/N_f\right)$$

$$\frac{\mu_f - \mu_f^*}{kT} = \ln\phi_f^b + \left(1 - N_f\right)\left(1 - \phi_f^b\right)$$

(3)

The interaction free energy $A^{int}(M)$ between two layers can now be written as the difference between the excess surface free energy at the given plate separation M and the excess surface free energy at infinite plate separation:

$$A^{int}(M) = A^S(M) - A^S(\infty)$$

(4)

Analytical theory for a polymer brush immersed in a solution of free polymer

In this section we briefly review the results of Zhulina et al.,[7] who made an elaborate SCF analysis of polymer brushes immersed in a solution of mobile polymer. Assuming that $N_f \ll N_g$, so that the size of a mobile chain is much smaller than the characteristic length over which the volume fraction profile of the grafted chains decays, one can write the free energy density functional of mixing grafted polymer, free polymer and solvent as:

$$\ell^{-3}f(z) = \left(1 - \phi_f(z) - \phi_g(z)\right)\ln\left(1 - \phi_f(z) - \phi_g(z)\right) + \frac{\phi_f(z)}{N_f}\ln\phi_f(z)$$

(5)

In the bulk solution ($z > H$, where H is the brush thickness) $\phi_g(z) = 0$, so that one can write

$$\ell^{-3}f^b = \left(1 - \phi_f^b\right)\ln\left(1 - \phi_f^b\right) + \frac{\phi_f^b}{N_f}\ln\phi_f^b$$

(5a)

By combining f(z) with the elastic term in the free energy of the polymer brush, one can derive an expression for the total free energy of the brush (see ref 7 for details). One can also derive equations for the grafted and free polymer volume fraction profiles $\phi_g(z)$ and $\phi_f(z)$. In the next section we will discuss the interaction between two polymer brushes, which can be analysed by studying how their free energy changes upon compression. First we discuss the shape of an isolated brush immersed in a solution of free polymer.

99

The volume fraction profiles of the grafted and free chains are given by the equations[7]

$$\phi_g(z) = (1 - \phi_f^b)\left[1 - \exp\left\{-K^2\left(H^2 - z^2\right)\right\}\right] + \phi_f^b\left[1 - \exp\left\{-K^2\left(H^2 - z^2\right)N_f\right\}\right]$$

$$\phi_f(z) = \phi_f^b \exp\left\{-K^2\left(H^2 - z^2\right)N_f\right\} \tag{6}$$

where z is the distance from the surface and K is given by

$$K^2 = 3\pi^2/8\ell^2 N_g^2$$

The layer thickness H can be obtained from the normalization condition

$$\int_0^H \phi_g(z)dz = \sigma N_g \ell^3$$

to give the equation

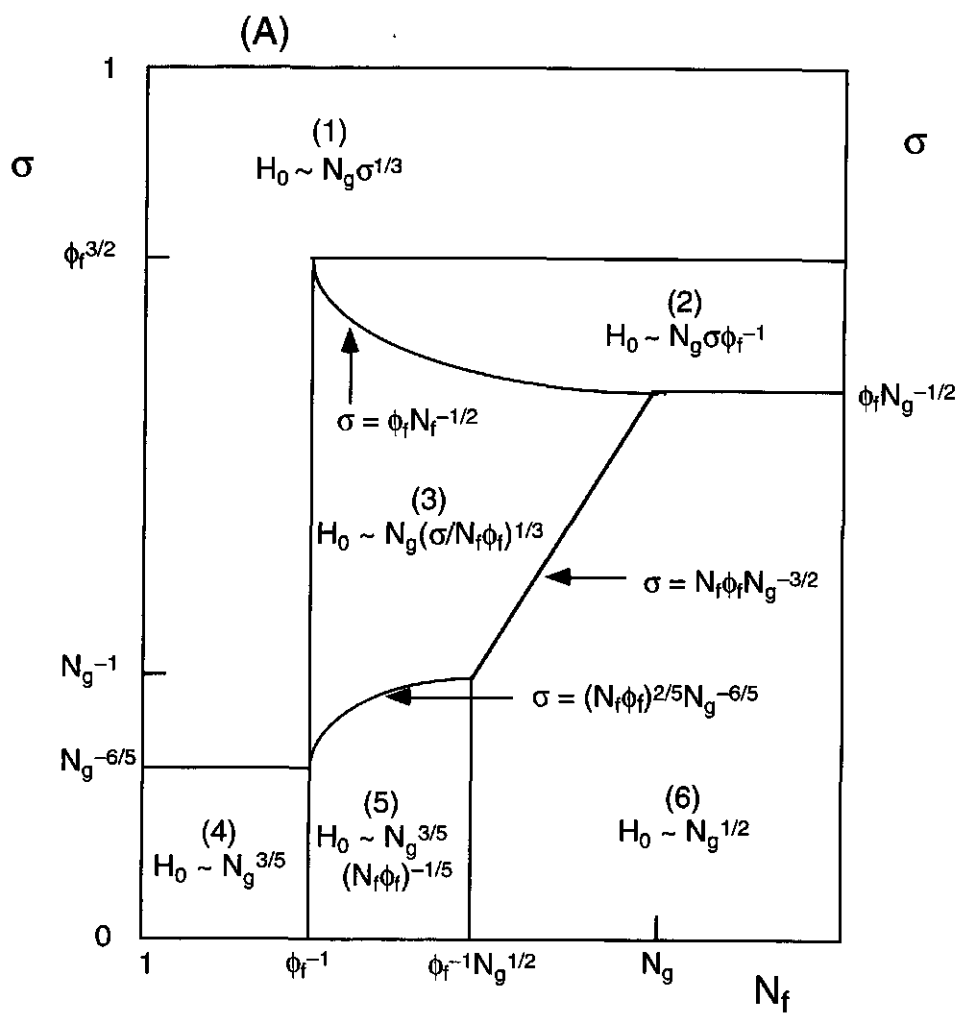$$KH = N_g \sigma K\ell + (1 - \phi_f^b)D(KH) + \phi_f^b N_f^{-1/2}D(KN_f^{1/2}H) \tag{7}$$

where

$$D(x) = e^{-x^2}\int_0^x e^{t^2}dt$$

is the Dawson integral. Equations 6 and 7 give the volume fraction profiles $\phi_g(z)$ and $\phi_f(z)$, and the brush thickness H as functions of N_g, N_f, and σ. However, these equations are only valid provided $N_f \ll N_g$ and under the condition that the grafted chains are strongly stretched ($H \gg N_g^{1/2}$).

In order to extend our consideration to low grafting densities and arbitrary lengths of the free polymer chains, we have to use scaling arguments.[8] Although scaling arguments do not provide structural details of the system (volume fraction profiles, distribution of free ends, etc.), the combination of scaling and SCF results gives a general picture of a brush immersed in a polymer solution. Below, we analyse the power-law dependencies of the brush thickness and we also consider the degree of penetration of the free polymer into the polymer brush. These characteristics are studied as functions of N_f and σ. Of course, for $N_f \ll N_g$ and $H \gg N_g^{1/2}$, the explicit expressions for H, $\phi_g(z)$, and $\phi_f(z)$ are available.

Figure 1A presents a diagram of state of a polymer brush immersed in a solution of free polymer. This figure shows the different power-laws that exist for the dependence of H on σ and N_f. The boundaries between the regimes where these laws are valid are also indicated.

100

(A)

σ (left axis), σ (right axis)

1

$\phi_f^{3/2}$

N_g^{-1}

$N_g^{-6/5}$

0

(1)
$H_0 \sim N_g \sigma^{1/3}$

(2)
$H_0 \sim N_g \sigma \phi_f^{-1}$

$\phi_f N_g^{-1/2}$

$\sigma = \phi_f N_f^{-1/2}$

(3)
$H_0 \sim N_g (\sigma / N_f \phi_f)^{1/3}$

$\sigma = N_f \phi_f N_g^{-3/2}$

$\sigma = (N_f \phi_f)^{2/5} N_g^{-6/5}$

(4)
$H_0 \sim N_g^{3/5}$

(5)
$H_0 \sim N_g^{3/5} (N_f \phi_f)^{-1/5}$

(6)
$H_0 \sim N_g^{1/2}$

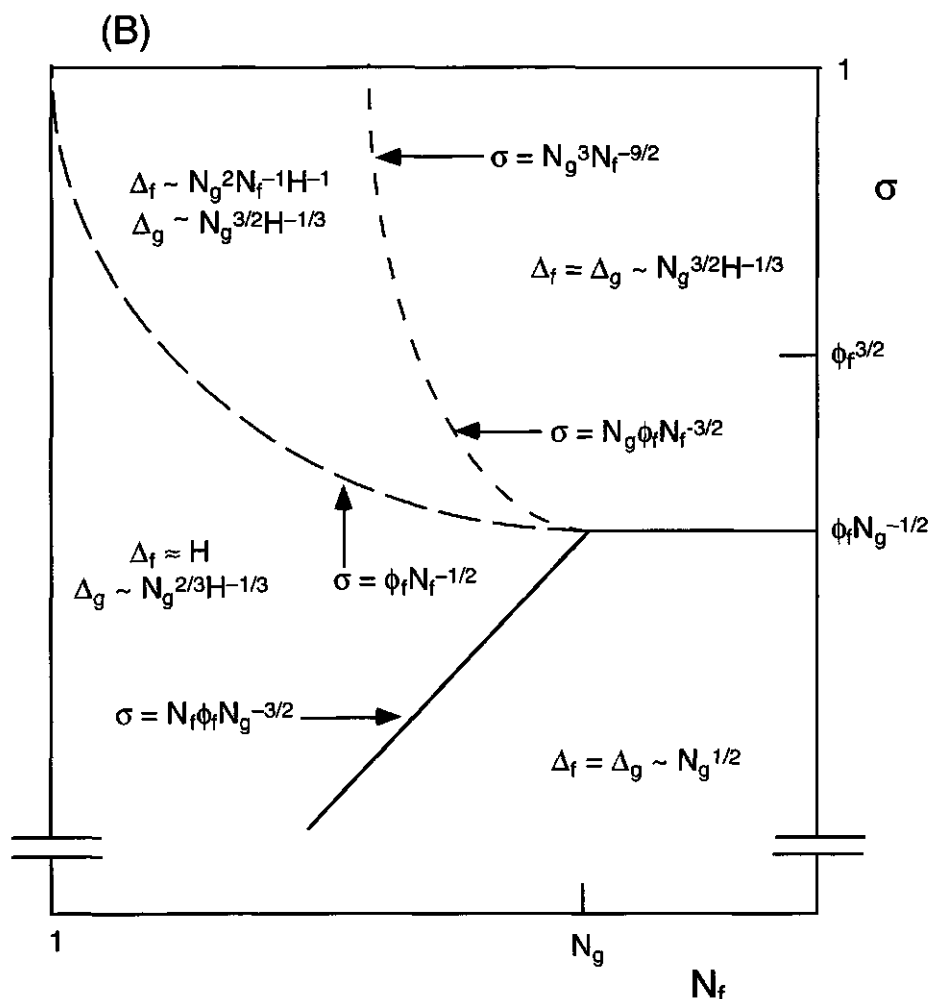1 ϕ_f^{-1} $\phi_f^{-1} N_g^{1/2}$ N_g

N_f

(B)

Figure 1 Diagram of state showing the various regimes for a single grafted polymer layer immersed in a polymeric solution. The grafted polymer has a chain length N_g and is grafted at a density σ. The free polymer is chemically identical to the grafted polymer, has a chain length N_f and its volume fraction in the bulk is ϕ_f (in the text this quantity is indicated as ϕ_f^b). In Figure 1A the regions with different scaling laws for the thickness H of the grafted layer are shown. In Figure 1B the boundaries are given between regions with different scaling laws for Δ_f (the penetration length of free polymer penetrating into the grafted layer) and Δ_g (the penetration length of grafted polymer penetrating into the bulk solution).

For high grafting densities as well as for low degrees of polymerization of the free polymer we are in region 1, which may be called the regime of "brush

dominance".[8] The brush thickness scales exactly the same as in a pure low-molecular weight solvent:

$$H \sim N_g \sigma^{1/3} \tag{8}$$

Regions 2 and 3 may be called the regimes of "solution dominance". In region 2 the free polymer is excluded from the brush, which is compressed by the osmotic pressure of the surrounding solution, leading to the following scaling behaviour of the brush height:

$$H \sim N_g \sigma / \phi_f^b \tag{9}$$

In region 3 free polymer penetrates into the brush and screens interactions between grafted polymer segments. This screening can be described by introducing an effective virial coefficient for pair interactions between these segments, $v_{eff} = \left(N_f \phi_f^b\right)^{-1} < 1$, so that the brush thickness scales as

$$H \sim v_{eff}^{1/3} N_g \sigma^{1/3} = N_g \sigma^{1/3} \left(N_f \phi_f^b\right)^{-1/3} \tag{10}$$

Equations 8-10 can be derived by expanding the expression for H given in eq 7.

In regions 4, 5, and 6 the grafting density is so low that the grafted chains are either nonoverlapping, or only slightly overlapping (for $\sigma > N_g^{-1}$ in region 6). For small values of N_f (region 4, where $N_f \phi_f^b < 1$) the free polymer has a negligible effect and the grafted chains essentially behave as isolated coils:

$$H \sim N_g^{3/5} \tag{11}$$

For larger values of N_f ($N_f \phi_f^b > 1$) the effect of the free polymer chains can again be accounted for by introducing an effective virial coefficient, $v_{eff} = \left(N_f \phi_f^b\right)^{-1}$, so that

$$H \sim v_{eff}^{1/5} N_g^{3/5} = N_g^{3/5} \left(N_f \phi_f^b\right)^{-1/5} \tag{12}$$

For $N_f > N_g^{1/2} / \phi_f^b$ (region 6) the grafted chains can be described as Gaussian coils:

$$H \sim N_g^{1/2} \tag{13}$$

It is interesting to note that for grafting densities $N_g^{-1} < \sigma < \phi_f^b N_g^{-1/2}$ addition of free polymer to a polymer brush immersed in pure solvent can change the scaling dependence of the brush height from that of a strongly stretched polymer ($H \sim N_g$) to that of a Gaussian coil ($H \sim N_g^{1/2}$). The boundaries of the regions shown in

Figure 1A can be directly found by equating the scaling dependencies on both sides of these boundaries.

Up to now we have only considered the overall brush height. A further important parameter is the degree in which the free and grafted layers interpenetrate. Let Δ_f be the penetration length of the free polymer into the brush and Δ_g the penetration length of the grafted polymer into the solution. It has previously been shown[9,10] that for grafted polymer chains that are strongly stretched, the latter interpenetration length scales as

$$\Delta_g \sim N_g^{2/3} H^{-1/3} \tag{14}$$

This scaling relationship has a wide applicability. It is valid both for compressed and non-compressed brushes, for good and bad solvents, as well as for brushes immersed in a melt. One expects this scaling law to describe the degree of penetration Δ_g of the grafted chains into the polymer solution in all three regions of Figure 1A (regions 1, 2, and 3) where the grafted chains are strongly stretched.

The behaviour of the free polymer chains is more complicated. When N_f is large only a fraction of the segments of a free chain penetrate into the brush. These segments experience the parabolic potential profile $u(z)$ of the brush,

$$u(z) = K^2 \left(H^2 - z^2 \right) \tag{15}$$

with K defined below eq 6. If n segments of the free polymer chain penetrate into the brush up to a distance Δ_f from the outer boundary of the brush, then the free energy increases with an amount:

$$\frac{\Delta F}{kT} \cong \int_{H-\Delta_f}^{H} u(z) \left(\frac{dn}{dz} \right) dz \cong \frac{n}{\Delta_f} \int_{H-\Delta_f}^{H} u(z) dz \cong nK^2 H \Delta_f \cong \frac{H \Delta_f^3}{\ell^4 N_g^2} \tag{16}$$

The last equality in eq 16 takes into account that the free polymer chains are not stretched, so that $\Delta_f^2 \cong n\ell^2$. Balancing ΔF with the thermal energy (~kT), one obtains

$$\Delta_f \sim N_g^{2/3} H^{-1/3} \tag{17}$$

This scaling dependence holds when $n \approx \Delta_f^2 / \ell^2 < N_f$, or $H > \ell N_g^2 N_f^{-3/2}$. For smaller values of N_f whole molecules of the free polymer penetrate into the brush. The increase in free energy due to the presence of a free polymer in the brush at a distance z' from the grafting surface is:

104

$$\frac{\Delta F}{kT} \cong \frac{N_f^{1/2}}{\ell} \int_{z'-\ell N_f^{1/2}}^{z'} K^2\left(H^2 - z^2\right)dz \cong K^2 N_f\left(H^2 - z'^2\right) \cong \frac{N_f H \Delta_f}{N_g^2} \tag{18}$$

where $\Delta_f = H - z'$ and the free chains are again assumed to be Gaussian. Balancing this expression with the thermal energy leads to another scaling law for Δ_f:

$$\Delta_f \sim N_g^2 N_f^{-1} H^{-1} \tag{19}$$

This dependence should hold for $\ell N_g^2 N_f^{-3/2} > H > \ell N_g N_f^{-1/2}$. When $H < \ell N_g N_f^{-1/2}$ the free polymer penetrates throughout the whole brush ($\Delta_f \approx H$).

In Figure 1B the two dashed curves give the boundaries between the areas where Δ_f follows the various scaling laws derived above. To the right of the curve with the short dashes Δ_f equals Δ_g and scales as $N_g^{2/3} H^{-1/3}$. For $\sigma > \phi_f^{b3/2}$ (i.e. for systems in region 1 of the diagram of Figure 1A) this means that the penetration lengths scale as $N_g^{1/3} \sigma^{-1/9}$. The volume fraction profiles of the grafted and free chains are symmetrical around their intersection point. The free chains only partly penetrate into the brush. Between both dashed curves whole molecules of the free polymer penetrate into the brush, but $\Delta_f < H$. The free chains penetrate farther into the brush than the grafted chains do into the solution, so that the volume fraction profiles become asymmetrical. This asymmetry is even more pronounced left of the curve with the long dashes, where the free chains penetrate throughout the whole grafted layer: $\Delta_f \approx H$, while Δ_g is still given by eq 14. In region 6, where the grafted chains are no longer strongly stretched, $\Delta_f \approx \Delta_g \approx H \approx \ell N_g^{1/2}$.

Analytical theory for the interaction between two brushes

We now consider the case of two interacting brushes in a solution of mobile polymer with a bulk volume fraction ϕ_f^b. Analytical expressions for the volume fraction profiles and conformational free energy of a compressed brush were obtained earlier.[7] Here we extend the results of ref 7 in order to calculate the free energy of interaction of two brushes which are compressed against each other. We take into account the redistribution of the free polymer during the compression. As before, the interpenetration of the two opposite brushes is neglected. The interacting brushes are considered as being compressed against an impermeable surface which is situated in the middle of the two grafted layers.

The equilibrium amount of free polymer as a function of the degree of compression was given in eqs 23 and 25 of ref 7. When the two brushes just do not yet overlap (so that the interplate distance $M\ell = 2H$) the amount of free polymer, $\theta_f(2H)$, in the system equals:

$$\theta_f(2H) = \frac{2\phi_f^b}{\sigma} \frac{D\left(KN_f^{1/2}H\right)}{KN_f^{1/2}} \tag{20}$$

where H is given by eq 7. When the brushes are compressed we define a compression ratio q as $M\ell/2H$, which is smaller than unity for compressed brushes. The amount of free polymer decreases when q decreases. Introducing the ratio $y = \theta_f(M)/\theta_f(2H)$, we can write the following implicit equation for the amount of free polymer:

$$y = \frac{D(x)}{D(qx)} \times \left(\frac{KHq - \sigma' - N_f^{1/2}\phi_f^b D(x)y}{\left(1 - \phi_f^b\right)D(x)}\right)^{N_f} \tag{21}$$

where D(x) is again the Dawson integral, the normalized grafting density σ' is defined as $\sigma' = \pi(3/8)^{1/2}\sigma$, and $x = N_f^{1/2}KM\ell/2$. The conformational free energy A(M) of a brush compressed to a distance $M\ell$ ($< 2H$) is given by eq 18 of ref 7:

$$\frac{A(M)}{LkT} = \frac{M}{2\sigma}\left\{ \frac{M^2K^2}{12} + \frac{2\theta_f(M)\ell^3\sigma}{N_fM}\ln\left(\theta_f(M)\sigma\left(\int_0^{M/2}\exp\left(\ell^2K^2N_fx^2\right)dx\right)^{-1}\right) + $$
$$\left(1 - \frac{2N_g\sigma}{M} - \frac{2\theta_f(M)\sigma}{M}\ln\left((M/2 - N_g\sigma)\left(\int_0^{M/2}\exp\left(\ell^2K^2x^2\right)dx\right)^{-1}\right)\right) \right\} \tag{22}$$

The interaction free energy as defined by eqs 2 and 4 is:

$$A^{int}(M) = A(M) - A(2H) + \frac{\left(\mu_f - \mu_f^*\right)}{N_f}\left(\theta_f(2H) - \theta_f(M)\right) + \left(\mu_s - \mu_s^*\right)\left(\theta_s(2H) - \theta_s(M)\right) \tag{23}$$

After some rearrangements the final result becomes

$$\frac{A^{int}(M)}{LkT} = \frac{2}{\sigma K\ell^2}\left\{ \frac{2}{3}(KH)^3\left(1 - q^3\right) - (KH)^2\sigma'\left(1 - q^2\right) + \right.$$
$$\frac{\phi_f^b D(x)}{N_f^{3/2}}\left[y\ln\left(y\phi_f^b D(x)(D(qx))^{-1}\right) - \ln\phi_f^b\right] + \left(KHq - \sigma' - y\phi_f^b D(x)N_f^{-1/2}\right) \times \tag{24}$$
$$\left.\ln\left[\left(KHq - \sigma' - y\phi_f^b D(x)N_f^{-1/2}\right)(D(KHq))^{-1}\right] - \left(1 - \phi_f^b\right)D(KH)\ln\left(1 - \phi_f^b\right) \right\} +$$
$$\frac{2H}{\sigma\ell}\left\{ (1 - q)\left(\ln\left(1 - \phi_f^b\right) + \phi_f^b(1 - 1/N_f)\right) + (1 - y)x^{-1}D(x)\left(N_f^{-1}\ln\phi_f^b - \ln\left(1 - \phi_f^b\right) + N_f^{-1} - 1\right) \right\}$$

This equation is only valid for relatively short mobile chains, since it does not take into account the loss in conformational free energy of the chains in the gap

between the two brushes. For long mobile chains this should explicitly be taken into account.

5.3 Results

Grafted chains in a polymer solution

All lattice model results that are presented in this section were computed using a cubic lattice. Figure 2 shows volume fraction profiles of polymer brushes that are immersed in a polymer solution, calculated both with the analytical theory (eqs 6 and 7) and the lattice model. The chain length N_f of the mobile polymer is 10 segments and the lattice calculations (solid curves) have been made for grafted polymer chain lengths N_g of 50, 200, and 600. According to eq 7 $H \sim N_g$, so that the volume fraction profiles given by eq 6 (dashed curves) are independent of N_g if they are plotted as a function of the reduced distance z/H. The longer the grafted chain length, the better the agreement with the analytical equations. For shorter grafted chain lengths the profile of the grafted component shows a clear "foot" protruding into the solution. The shorter chains also show a clear depletion zone near the surface, which is absent in the analytical model. These features are completely analogous to the situation where the brush is immersed in a one-component low molecular weight solvent. The system of Figure 2 belongs to region 1 of the phase diagram of Figure 1A. The volume fraction profiles of the free and grafted chains are asymmetric around their intersection point. This is especially clear for high N_g. Whole molecules of the free component (which are only 10 segments long) move into the brush, but they do not penetrate farther than approximately 50% of the brush height.

In Figure 3 the analytical model is compared with the lattice calculations for systems in regions 1 $(\sigma = 0.1)$, 2 $(\sigma = 0.02)$, and 3 $(\sigma = 0.004)$ of the phase diagram. The bulk volume fraction of free polymer has a value of 0.1 in all cases. In each case the results are shown for a small free polymer ($N_f = 30$, which is 5% of the chain length of the grafted polymer), and for a larger free polymer ($N_f = 300$, which is half the grafted chain length). In the derivation of eq 6 it was assumed that $N_f \ll N_g$. Indeed, for all three grafting densities shown in Figure 3 the curves for $N_f = 30$ show better agreement between the lattice calculations and eq 6 than do the curves for $N_f = 300$. For $N_f = 30$ the brush thickness H is described well by eq 7. The penetration length Δ_g decreases with increasing H and is approximately given by eq 14. The free polymer penetrates the brush over a length Δ_f which exceeds Δ_g and becomes equal to H for low grafting densities; these trends agree well with the scaling relations given in Figure 1B.
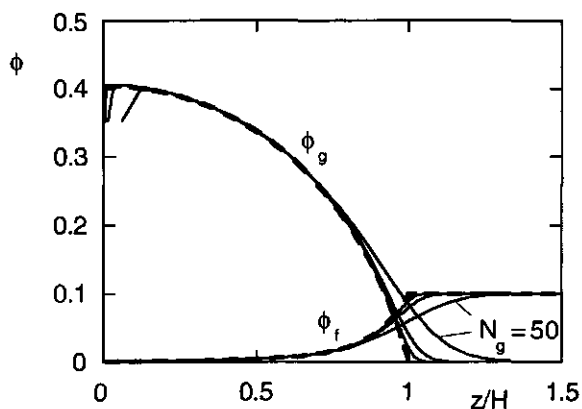
Figure 2 Volume fraction profiles of brushes immersed in a solution of short mobile polymers with chain length $N_f = 10$. The volume fractions of both grafted and free chains are given as a function of the reduced distance z/H to the grafting surface. The layer height H has been calculated using eq 7. The dashed curves give ϕ_g and ϕ_f as predicted by eq 6 (these curves do not depend upon N_g as $H \sim N_g$). The solid curves follow from lattice model calculations. Further parameters: $N_g = 50$, 200, and 600; $\sigma=0.1$; $\phi_f^b = 0.1$.

The analytical volume fraction profiles of the grafted component deviate slightly from the lattice calculations at the surface and at the periphery of the layer. These are well known effects that are also seen with brushes immersed in a one-component low molecular weight solvent. The presence of the surface leads to a narrow depletion layer for the grafted polymer, and because of their finite chain length some chains stretch farther away from the surface than they should according to eq 6. For $N_f = 300$ eq 7 still gives a good estimate of the brush height, but it predicts a far too sharp boundary of the grafted and free polymer layers. Especially for the higher grafting densities this effect is very pronounced. It is caused by the very approximate way in which the translational entropy of the mobile chains is accounted for in the derivation of eq 6.

If a full description is wanted of the system consisting of grafted polymer immersed in a solution of relatively long free polymer chains, one must combine eq 7 with the scaling dependencies of the penetration lengths Δ_f and Δ_g. These were given in the previous section (eqs 14-19). In Figure 3 the lattice curves for $N_f = 30$ are asymmetric around the intersection point of the two profiles. This is in agreement with the prediction for the region left of the curve with the short dashes in Figure 1B. For $N_f = 300$ one moves into the symmetrical region, so that $\Delta_f = \Delta_g$. The scaling dependence of Δ_f on N_f, N_g, and H is shown in Figures 4 and

5. In all cases the penetration length has (arbitrarily) been defined as the distance over which $\phi_f(z)$ falls from $\phi_g(z)$ (i.e. the volume fraction at the intersection point of both profiles) to half this value. The systems which correspond to the data points of Figure 4 are described in table 1A. They all belong the symmetric area of the phase diagram. The penetration length Δ_f indeed scales as $N_g^{2/3}H^{-1/3}$, as predicted by eq 17. Table 1B gives the systems that are shown in Figure 5. These belong to the asymmetric area of the phase diagram. In this case the penetration length Δ_f scales as $N_g^2(N_fH)^{-1}$, as expected from eq 19.
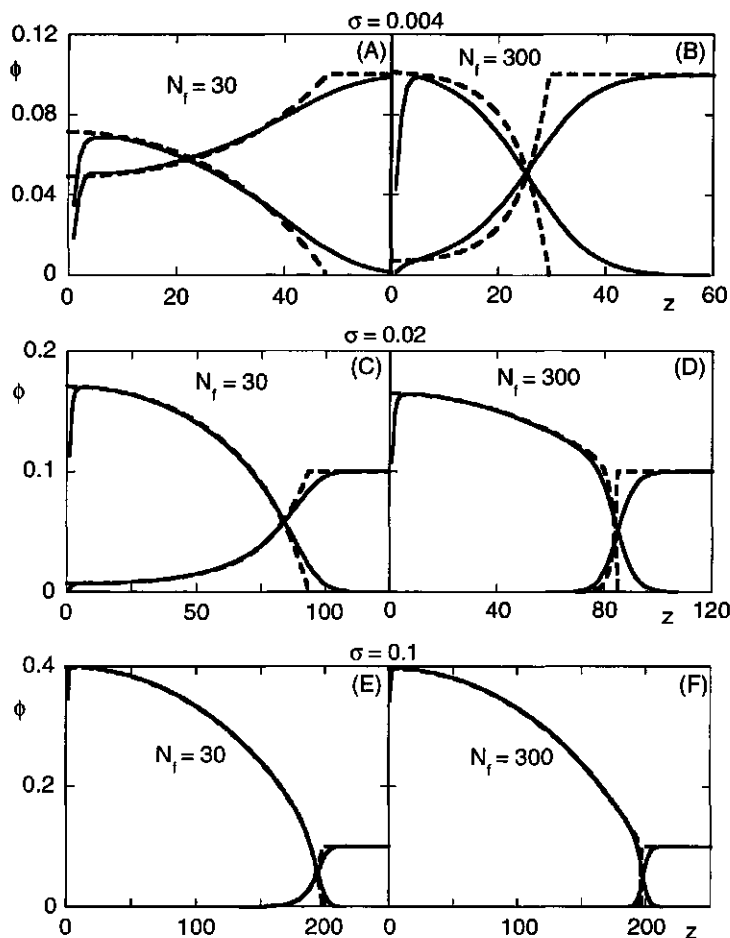

Figure 3 Volume fraction profiles of brushes immersed in solutions of relatively short ($N_f = 30$) and relatively long ($N_f = 300$) mobile polymers. The dashed curves follow from eq 5 and the solid curves are lattice calculations. In all cases $N_g = 600$ and $\phi_f^b = 0.1$. The grafting density and free chain length are indicated in the graphs.
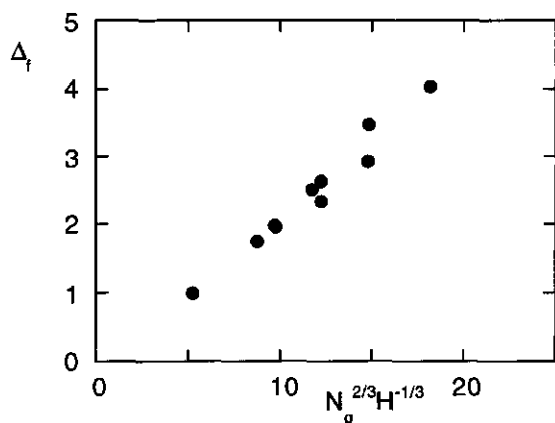
Figure 4 The penetration length Δ_f of free polymer into the brush as a function of grafted chain length N_g, and brush height H. The systems presented in this Figure belong to the "symmetric area" of Figure 1B. The data of these systems are given in table 1.
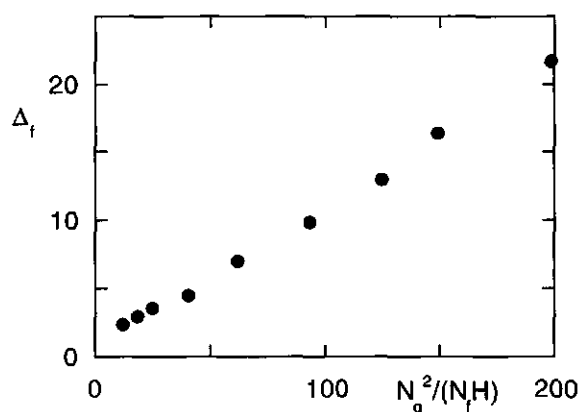

Figure 5 The same as Figure 4 for systems that are in the "asymmetric area" of Figure 1B. The data of these systems are given in table 2.

So far, we have considered grafted polymer chains that are strongly stretched ($H \sim N_g$, regions 1, 2, and 3 of the phase diagram). When $\sigma < \phi_f^b N_g^{-1/2}$, an increase of the chain length of the mobile polymer leads to a transition of the grafted chains from a strongly stretched ($H \sim N_g$) to a Gaussian coil conformation ($H \sim N_g^{1/2}$). Equation 6, whose derivation was based upon the grafted chains being strongly stretched, is then no longer valid. In Figure 6 lattice calculations are shown for systems that are expected to show this Gaussian coil behaviour. Only the volume fractions of the grafted component are shown. Reduced coordinates have been

110

used to clearly demonstrate the scaling behaviour of the grafted polymer chains. One can conclude from Figure 6 that H indeed scales as $N_g^{1/2}$. However, the volume fraction profiles themselves do not precisely obey this scaling relationship: the scaled profiles do not exactly collapse onto one master curve.

Table 1A

N_g	σ	N_f	ϕ_f^b	$N_g^{2/3}H^{-1/3}$	Δ_f
100	0.5	200	0.1	5.2029	0.99538
300	0.1	200	0.1	8.7143	1.7501
300	0.5	200	0.5	9.7201	1.9633
300	0.1	200	0.1	9.6549	1.9923
300	0.5	200	0.5	11.713	2.5159
600	0.1	6000	0.1	12.205	2.3393
600	0.1	200	0.1	12.226	2.6399
600	0.1	600	0.5	14.758	2.9248
600	0.1	200	0.5	14.802	3.4746
600	0.01	600	0.1	18.171	4.0375

Table 1B

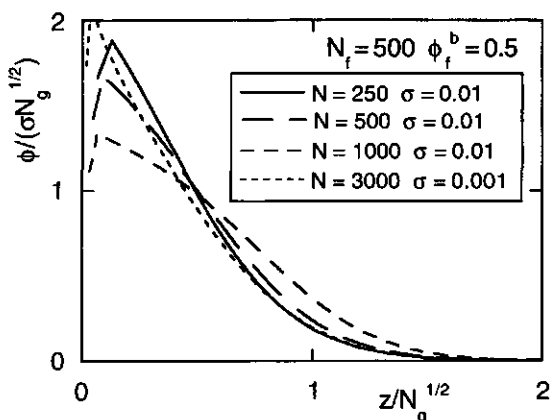| N_g	σ	N_f	ϕ_f^b	N_g^2/N_fH	Δ_f
200	0.1	50	0.1	12.054	2.3500
200	0.1	50	0.1	18.250	2.9801
400	0.1	50	0.1	24.446	3.5590
200	0.25	10	0.1	40.374	4.4948
200	0.1	10	0.1	61.696	6.9966
300	0.1	10	0.1	93.175	9.8712
400	0.1	10	0.1	124.64	12.986
300	0.1	10	0.5	149.00	16.394
400	0.1	10	0.5	198.61	21.709

Figure 6 Volume fraction profiles of systems in region 6 of Figure 1. Only the grafted chains are shown. All curves are lattice calculations. The reduced distance to the grafting surface $zN_g^{-1/2}$ is used as the abscissa to check the relationship $H \sim N_g^{1/2}$. The reduced volume fraction $\phi/(\sigma N_g^{1/2})$ is used as the ordinate, so that the areas under all curves are equal. In all cases $\phi_f^b = 0.5$ and $N_f = 500$. The values of σ and N_g are shown in the Figure.

Interaction between two brushes in pure solvent

Figure 7 shows interaction curves for the compression of two polymer brushes in a pure solvent (no free polymer present). The solid curve is the analytical prediction of eq 24, where in this case all terms containing ϕ_f^b and y vanish. The other curves were obtained from the lattice model for $N_g = 50$, 200, and 600. The insets show the interaction on a semi-logarithmic scale. Equation 24 predicts that $A^{int}(q) \sim N_g$. For long chains the lattice calculations approach the prediction of eq 24. The agreement also becomes better for larger grafting densities (see Figure 7B). These trends are the same as those found when comparing volume fraction profiles of non-compressed brushes. For small compressions $(q \approx 1)$ relatively large deviations remain between the lattice calculations and the strong-stretching model, even for long chain lengths. This is most clearly seen from the curves drawn on a semi-logarithmic scale. Here only the outer most part of the brush is being compressed. In this case the exponential decay ("foot") of the profile, predicted by the lattice model, has a relatively strong effect on the interaction curve. This causes the interaction free energy to have a finite positive value for values of q larger than unity.

In Figure 8 volume fraction profiles calculated from the lattice model are given for $N_g = 600$ and $\sigma = 0.01$. The profiles of the brushes on both surfaces are drawn individually for three interplate distances: M = 200 (q = 1.03), M = 50

(q = 0.26), and M = 20 (q = 0.10). In Figure 8A (q = 1.03) the brushes just start to interact with each other. Although q > 1, so that according to the "classical" prediction of eq 24 there should not yet be any interaction, the tips of both profiles do already slightly overlap, giving rise to a finite free energy of interaction, which is neglected in the analytical theory.
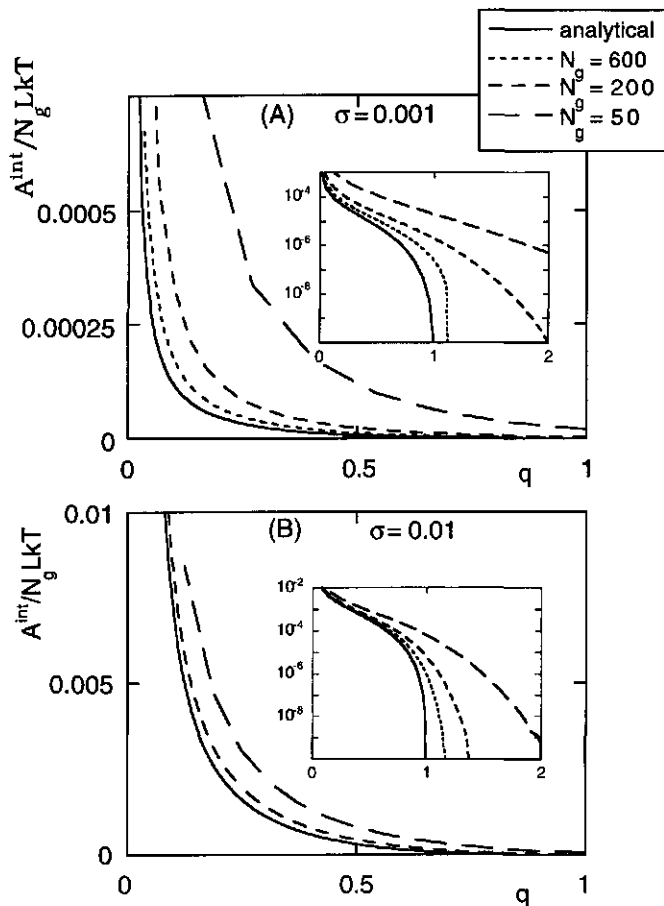

Figure 7 Interaction curves between two brushes in the absence of free polymer. The lattice calculations for $N_g = 600$, 200, and 50 are compared with eq 24 (solid curve). Grafting density: $\sigma = 0.001$ (A), 0.01 (B). The insets show the interaction free energies on a semi-logarithmic scale.

The analytical theory further neglects the fact that when two brushes are compressed against each other, the chains attached to both surfaces will to a certain extent interpenetrate. This can be clearly seen in parts B and C of Figure 8. Decreasing the plate separation eventually leads to a complete overlap of both

layers. Taking into account this interpenetration should lead to a slightly less repulsive interaction.
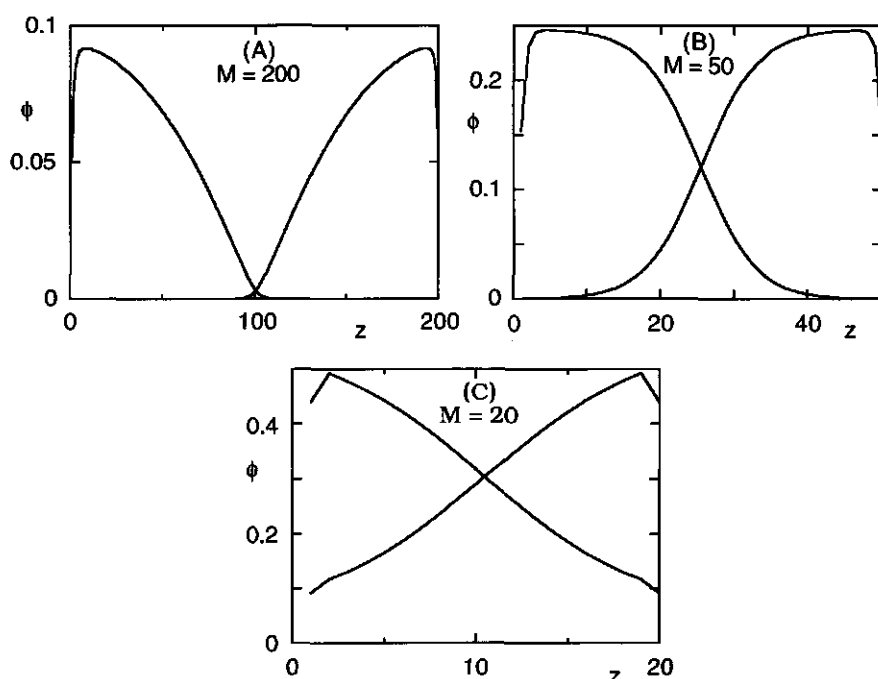

Figure 8 Volume fraction profiles of two brushes that are compressed against each other. $N_g = 600$; $\sigma \approx 0.01$. The degrees of overlap are as follows: for $M = 200$ $q = 1.03$; for $M = 50$ $q = 0.26$; for $M = 20$ $q = 0.10$.

In Figure 9 the effect of this interpenetration on the free energy of interaction is quantified for a brush with a chain length of 200 segments and a grafting density of 0.01. The results of the lattice model are given for three different cases. The first is the compression of two brushes on opposite surfaces (which is denoted in the figure legend as "two brushes"). This is exactly the same system as shown in the previous figures. In the second case a single brush (denoted as "one brush") is compressed by a bare surface (i.e. a surface bearing no grafted polymer); q is now defined as $M\ell/H$. In this case there is no interpenetration, as the chains cannot move through the surface by which they are compressed. Therefore one would expect a better agreement with eq 24. However, the agreement is worse. Below we explain the reason of this discrepancy. The curves denoted by "adsorbing chains" in Figure 9 have been calculated for the same system as that denoted by "one brush", but now the segments of the polymer have a small attractive interaction with

the bare surface. The value of this attraction can be described by the adsorption energy χ_s as defined by Silberberg.[11] We have chosen $\chi_s = -\ln(5/6)$, which is the critical adsorption energy of an infinitely long polymer chain on a cubic lattice.
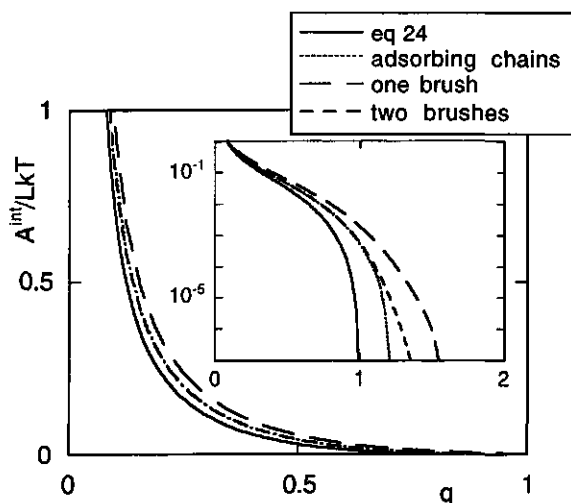

Figure 9 Interaction curves between two brushes and between a brush and a wall. Parameters: $N_g = 200$; $\sigma = 0.01$. The solid curve is calculated using eq 24. The curve "two brushes" is the free energy of interaction when two similar brushes are compressed against each other; in this case the chains in both brushes can interpenetrate. The "one brush" curve gives the free energy of interaction of a single brush which is compressed by a hard impenetrable surface. The "adsorbing chains" curve is calculated for the same system, but in this case the grafted polymer chains have a small adsorption energy for the surface which compresses them.

For all three cases of Figure 9 the lattice calculations give a more repulsive interaction than that predicted by the analytical theory. At any separation the compression of a brush by a bare surface is more repulsive than the similar compression by another brush. The difference between these two systems is not, however, solely due to the interpenetration that occurs between the two brushes. The bare surface also imposes entropical restrictions on the conformations of the grafted polymer chains. This unfavourable entropical interaction is compensated when there is an attractive interaction of the segments with the surface, as is the case for the curves denoted by "adsorbing chains". The "adsorbing chain" curve and the curve for "two brushes" virtually coincide, except for very small compressions ($q > 1$). When the outermost parts of two brushes start to overlap, the interpenetration of the chains leads to a decrease in the repulsive interaction. For $q < 1$ this effect has become negligible.

At high compressions the two layers very strongly overlap. Nevertheless, for small values of q the analytical equations for the free energy of interaction (where this overlap is neglected) agree very well with the lattice calculations. In this region the osmotic pressure forms the major contribution to the free energy, so that the exact shape of the volume fraction profile becomes less important.
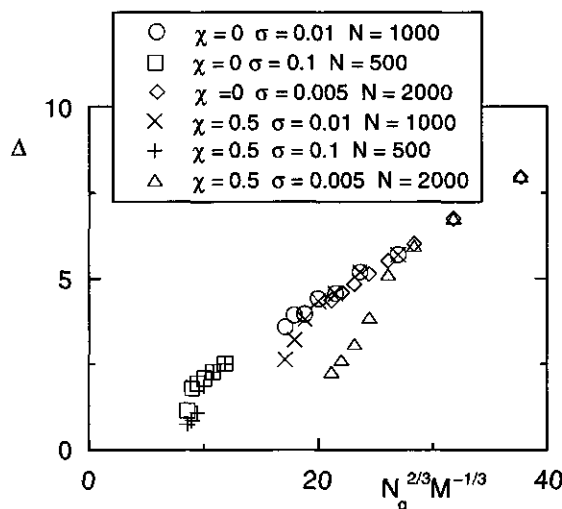

Figure 10 Distance of interpenetration Δ, when two equal brushes are compressed against each other. M is the distance between both grafting surfaces, expressed in number of lattice layers. This figure checks the scaling dependence predicted by eq 14. The solvent qualities, grafting densities, and chain lengths for the various sets of data points are given in the legend.

In Figure 10 the amount of interpenetration is plotted for six different systems. The interpenetration length Δ has been defined as the distance from the mid-plane to the plane where the penetrating chains have a volume fraction equal to half their volume fraction in the middle. The parameter Δ is expected to scale as $N_g^{2/3}M^{-1/3}$, analogous to the scaling relation given in eq 14 for the interpenetration distance Δ_g of a brush into a polymer solution.[3] We may indeed conclude from Figure 10 that $\Delta \sim N_g^{2/3}M^{-1/3}$, irrespective of chain length, grafting density and solvency ($\chi = 0$: good solvent; $\chi = 0.5$: Θ-solvent). For small values of M the data of all six systems obey this scaling relationship rather accurately. Of course, it is to be expected that for larger values of M deviations occur. In these cases the calculated points do not lie on the master curve. When M becomes twice the brush height there cannot be any interpenetration at all.
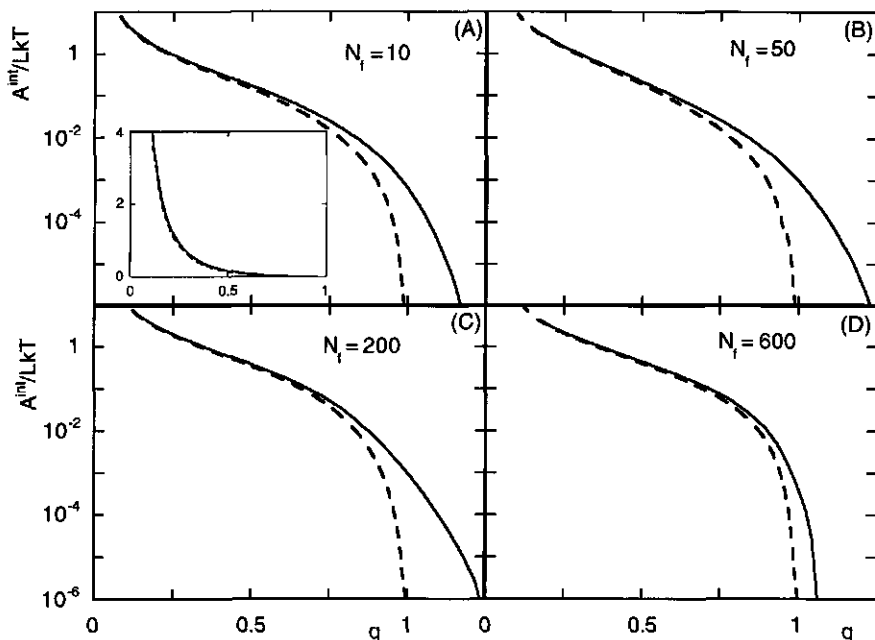
Figure 11 Interaction curves of two brushes in a polymer solution for various chain lengths of free polymer: $N_f = 10$ (A), 50 (B), 200 (C), and 600 (D). Other parameters: $N_g = 600$; $\sigma = 0.01$; $\phi_f^b = 0.1$. The inset shows the data for $N_f = 10$ on a linear scale. All other graphs are on semi-logarithmic scale.

Figure 11 shows interaction curves of brushes in a polymer solution. An important parameter in the calculation of $A^{int}(q)$ is the amount of mobile polymer, $\theta_f(M)$, between the plates when they are at an arbitrary separation M. Figure 12 shows the relative amount of free polymer in the system, $y = \theta_f(q)/\theta_f(q=1)$, for $N_g = 600$, $\sigma = 0.01$, and $N_f = 10$ and 50. There is excellent agreement between the lattice model and the prediction of eq 21 for the amount of free polymer expelled from the gap between the brushes.

In all cases of Figure 11, for large compressions ($q < 0.5$) the analytical equations agree very well with the lattice calculations. The inset for $N_f = 10$ shows the interaction curve on a linear scale. Plotted on this scale the figure shows that over the whole range of q eq 24 predicts the interaction very well when free polymer chains are present in the system. For the other values of N_f (50, 200, and 600) a linear plot (not shown) displays the same agreement between the two models. To study the interaction at $q \approx 1$ it is more convenient to plot the free

117

energy of interaction on a logarithmic scale, as is done in Figure 11 for all four values of N_f. The lattice calculations predict a more repulsive interaction for small compressions, which is due to the "foot" in the volume fraction profile. This is similar to the case for a polymer brush in a pure solvent. The contribution of the foot turns out to depend on the free chain length. For $N_f = 50$ or 200 it shows up for slightly larger values of q than it does for $N_f = 10$, but for $N_f = 600$ the contribution of the foot seems to become less important.
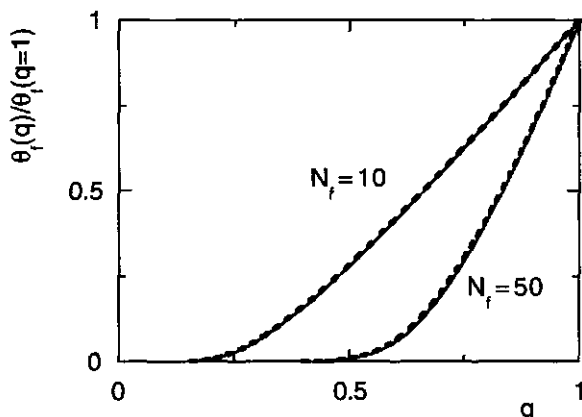

Figure 12 The fraction of free polymer remaining between two brushes when these are compressed for two values of N_f. Other parameters: $N_g = 600$; $\sigma = 0.01$; $\phi_f^b = 0.1$. The dashed curves are calculated using eq 21, and the solid curves are the lattice model predictions.

However, for high N_f the situation is more complicated, as is shown in Figure 13. Increasing the chain length of the mobile polymer leads to an attractive minimum in the interaction curve for $q > 1$. For $N_f = 600$ ($= N_g$) this starts to have an important effect on the total interaction free energy for small compressions. Van Lent et al.[12] extensively studied this attraction between polymer brushes in a polymeric solution. It is an effect that has also been found experimentally and can be easily understood for the limiting case when there is no grafted polymer (i.e. $\sigma = 0$). Due to the depletion of free polymer in the vicinity of the surfaces an attractive osmotic force appears. Some experimental results indicate that this attraction can also exist when the surfaces are covered by a grafted layer (see, for example, ref 13 and the references given therein). Van Lent et al. showed that such an attraction is predicted by the SCF lattice theory. However, they only considered systems for which $N_f \geq N_g$. For all values of ϕ_f^b an increase of N_f then leads to a deeper attractive minimum in the interaction curve. In contrast with the situation that no grafted polymer is present, this attraction was shown to be an entropic effect

caused by the grafted chains themselves and not directly by the free polymer. The grafted chains mix more easily with chains from the other grafted layer than with the free polymer coils.
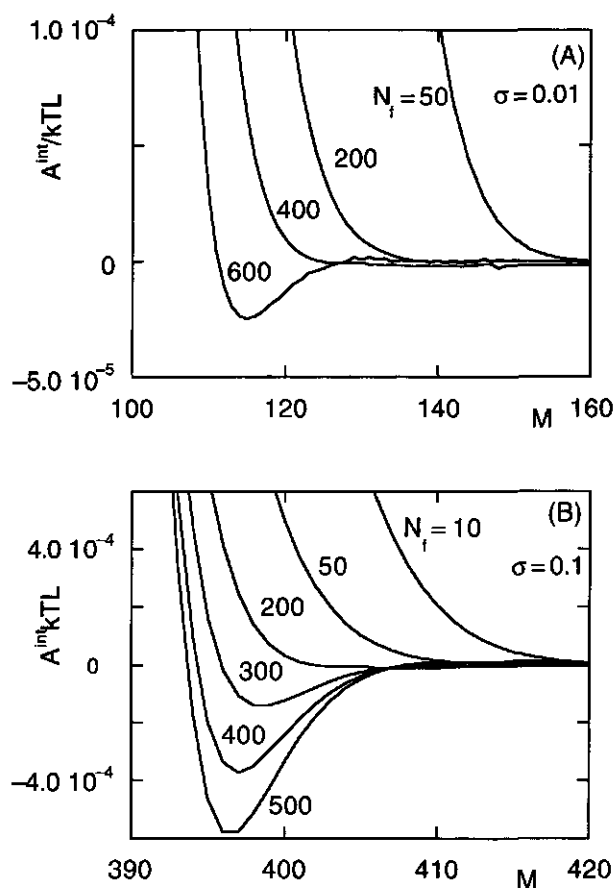

Figure 13 Effect of the chain length of the mobile polymer on the interaction curves near the onset of interaction (q around 1). For large values of N_f an attractive minimum appears. Grafting density: $\sigma = 0.01$ (A), and $\sigma = 0.1$ (B). Other parameters: $N_g = 600$; $\phi_f^b = 0.1$.

Figure 13 shows that in order to find an attractive minimum the free polymer must exceed a certain minimum chain length. Increasing the grafting density decreases this minimum value of N_f. For example, when $N_f = 400$ there is no attractive minimum if $\sigma = 0.01$ (Figure 13A) but for the higher grafting density $\sigma = 0.1$ such a minimum does occur (Figure 13B). In Figure 13 for any q the repulsion is larger for shorter N_f. Furthermore, the minimum shifts to a smaller plate

separation when N_f is increased. In Figure 11 this trend was not found for the dependency of the repulsion on N_f. This can be explained by the fact that in Figure 11 the free energy of interaction is given as a function of the relative compression q, whereas in Figure 13 it is given as a function of the plate separation M. The brush height itself depends on N_f, which explains the apparent non-monotonic dependency of the repulsion on N_f found in Figure 11.
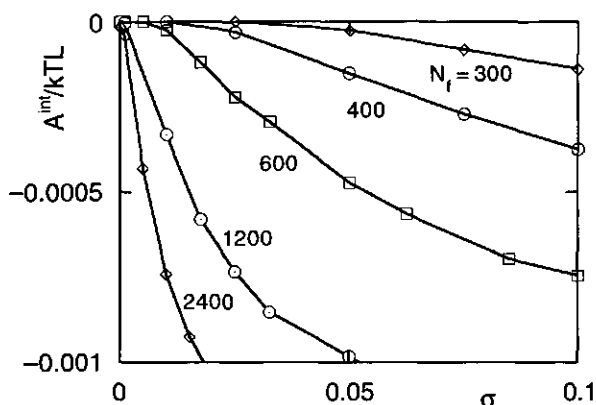

Figure 14 Depth of the minimum in the interaction curve as a function of the grafting density. Parameters: $N_g = 600$; $\phi_f^b = 0.1$; the values of N_f are indicated in the Figure.

It would be useful to interpret these results using the diagram of state of Figure 1. We find that for strongly stretched chains the attraction only occurs when the grafted and free polymer profiles are symmetric around their intersection point (region 1 for high N_f). However, this symmetry condition is not sufficient for attraction to occur. If it were, then in Figure 13 there should be an attraction for $N_f > N_g^{2/3}\sigma^{-2/9}$ when $\sigma > \phi_f^{b^{3/2}}$ (i.e. $N_f > 119$ when $\sigma = 0.1$). The minimum value of N_f turns out to be larger than this. For a system in which there is an attractive minimum, the depth of this minimum depends on the grafting density. This is shown in Figure 14, where the value of the attractive minimum is given as a function of σ. This is done for a constant grafted chain length ($N_g = 600$) and five different free chain lengths. For small N_f the attraction disappears completely below a certain grafting density. Only at extremely low densities does it then reappear again. This is difficult to see in the figure because the curves practically coincide with the left ordinate axis. That the attraction must reappear at low coverages is obvious, as for $\sigma = 0$ one recovers the depletion attraction of two surfaces without grafted layers. However, Figure 14 shows that increasing the grafting density from zero to just a

very low value ($\sigma < N_g^{-1}$) already makes the attraction disappear. The grafted chains then still have unstretched conformations. This corresponds with the bottom part of Figure 1A.

4 Discussion and Conclusions

In this paper we have explored the applicability of the strong chain stretching approach to give an SCF description of end-grafted polymer layers that either interact with each other or with free polymer in solution. This approach has previously been shown to agree very well with more exact lattice calculations in describing isolated (i.e. noninteracting) grafted layers. In this case significant deviations occur only very close to the surface (depletion effect) and at the periphery of the grafted layer (exponential decay of the volume fraction profile). For long enough polymer chains these deviations are negligible but for short chain lengths they may become important.

Our lattice calculations indeed show that the onset of interaction between two brushes is situated at a larger distance than twice the "strong-stretching brush height" (for which we defined the reduced surface separation q to be unity). For $N_g = 50$ and $\sigma = 0.01$, representative for the adsorption of a short block copolymer, there is already a free energy of interaction of the order of 10^{-3} kT per lattice site for q = 1.25. Assuming a lattice spacing ℓ of the order of 1 nm, this is an interaction that should be just within the detection limit of the surface force apparatus. In this context it is interesting to note that Milner[14] made a quantitative comparison between experimental force-distance data and strong chain stretching SCF equations. Only at large separations did he find the theoretical repulsion to be significantly lower than the experimental data. Although he prefered to explain this discrepancy by a polydispersity argument, our calculations suggest that it may also be explained by the approximate character of the strong-stretching theory, and would even occur for completely monodisperse brushes. In Figure 7 one can also see that even for long chain lengths ($N_g = 600$) and large compressions (q < 0.25) there is still a small difference between the lattice calculations and eq 24. This may be caused by the depletion zone next to the surface, which is still present for small values of M (see Figure 8).

When two polymer brushes are compressed against each other the distance Δ over which chains penetrate into the opposite layer scales as $N_g^{2/3} M^{-1/3}$ (Figure 10). This interdigitation has, however, hardly any effect on the normal force between both layers. But that does not necessarily mean that the overlap of both grafted layers is of no consequence whatsoever. When the polymer brushes are

compressed and subsequently a lateral (shearing) force is applied, the overlap of both layers will probably significantly influence the interaction. In principle, this can be investigated using the apparatus of Klein *et al.*,[15] which measures both normal and lateral forces.

When polymer is added to the solution in which a polymer brush is immersed, the grafted layer is compressed. The resulting volume fraction profiles of the grafted and free components are given by eq 6. For short free chain lengths this equation gives as good a description of the profiles as the strong-stretching theory does for brushes immersed in a one-component low molecular weight solvent. For longer free chain lengths the overlap area of the grafted and free components is described poorly. However, as far as only the brush height is concerned, eq 7 still agrees very well with the lattice calculations.

A new feature we have added to the system of grafted plus free polymer is the penetration lengths of both components into the opposite phase. Using simple thermodynamic arguments we derived scaling laws for the two penetration lengths in different parts of the diagram of states. These scaling laws were corroborated by the lattice calculations. In principle, it is possible to determine the volume fraction profiles of the grafted and free chains individually in a neutron reflectivity experiment. By contrast-matching one of the two components with the solvent, only the other component is detected. Thus the interpenetration of both layers might be checked experimentally. As far as we know this has not yet been done.

When free polymer is present in the solution, eq 24 can be used for the free energy of interaction between two brushes (this equation predicts a purely repulsive interaction). Only when the free polymer chain length exceeds a critical value (which depends upon the grafting density and grafted polymer chain length) does the interaction profile which is obtained from the lattice model acquire a qualitatively new feature: for $q \geq 1$ an attractive minimum appears. It is not possible to explain this in terms of the diagram of state in Figure 1. The minimum is deepest when $\sigma = 0$ (i.e. for hard surfaces). For relatively short chain lengths ($N_f < N_g$) even a very small amount of grafted polymer already causes the attraction to disappear. It should be possible to verify this prediction experimentally. Practical applications are perhaps possible in systems where depletion attraction undesirably leads to flocculation.

References

1. Wijmans, C. M.; Scheutjens, J. M. H. M.; Zhulina, E. B. *Macromolecules* **1992**, 25, 2657; This thesis, chapter 1.
2. Semenov, A. N. *Sov. Phys. JETP* **1985**, 61, 733.
3. Zhulina, E. B.; Borisov, O. V.; Priamitsyn, V. A. *J. Colloid Interface Sci.* **1990**, 137, 495.
4. Milner, S. T.; Witten, T. A.; Cates, M. E. *Macromolecules* **1988**, 21, 2610.
5. Evers, O. A.; Scheutjens, J. M. H. M.; Fleer, G. J. *Macromolecules* **1991**, 24, 5558.
6. Flory, P. J. *Principles of Polymer Chemistry* ; Cornell University Press: Ithaca, NY, 1953.
7. Zhulina, E. B.; Borisov, O. V.; Brombacher, L. *Macromolecules* **1991**, 24, 4679.
8. de Gennes, P. G. *Macromolecules* **1980**, 13, 1069.
9. Zhulina, E. B.; Semenov, A. N. *Polymer Science USSR* **1989**, 31, 196.
10. Witten, T. A.; Leibler, L.; Pincus, P. A. *Macromolecules* **1990**, 23, 824.
11. Silberberg, A. *J. Chem. Phys.* **1968**, 48, 2835.
12. Van Lent, B.; Israels, R.; Scheutjens, J. M. H. M.; Fleer, G. J. *J. Colloid Interface Sci.* **1990**, 137, 380.
13. Vincent, B.; Edwards, J.; Emmet, S.; Jones, A. *Colloids and Surfaces* **1986**, 18, 261.
14. Milner, S. T. *Europhys. Lett.* **1988**, 7, 695.
15. Klein, J.; Perahia, D.; Warburg, S. *Nature* **1991**, 352, 143.

chapter 6

Multiblock Copolymers and Colloidal Stability

Abstract

Block copolymers that have both adsorbing and nonadsorbing blocks can be used to stabilize colloidal dispersions. However, they can also induce an attraction between two particles by forming bridges between the surfaces. In this chapter we investigate when such an attraction occurs and how its magnitude depends on the relevant system parameters. Most attention is paid to end-adsorbed triblock (A-B-A) copolymers and a few calculations are presented for polymers consisting of a larger number of blocks ((A-B)$_n$-A with n > 1). Adsorbed layers of triblock copolymers with identical adsorbing groups always cause an attractive part in the two particle interaction curves. Adsorbed layers of multiblock (n > 1) copolymers with long blocks behave similar to triblock copolymers. When their blocks become very short, these multiblock copolymers resemble homopolymers whose interaction parameters have some average value of those for both types of blocks.

6.1 Introduction

Colloidal dispersions can be sterically stabilized by diblock copolymers. These polymers must contain an adsorbing block (anchor, A) and a block that dissolves in the solution (buoy, B), forming a protective layer. The interaction between two such adsorbed diblock copolymer layers has been studied extensively, both from an experimental and a theoretical point of view, over the past few years (see, for example, refs 1-4).

Adsorbed diblock copolymer layers give a purely repulsive interaction when the solvent is a good solvent for the B block. This interaction can be modelled by considering two terminally grafted polymer layers (polymer brushes), which can be fully described using the "classical" parabolic potential profile approximation.[2,5] Calculated interaction free energies have been fitted[6] to match experimental data. In this approach the grafting density (adsorbed amount of polymer) is an input parameter. In this respect the block copolymer adsorption theory of Evers et al.[4] is more advanced as the chemical potential of individual chains is explicitly accounted for, so that one can consider the equilibrium between the polymer layer and the bulk solution. Evers et al. predicted that the adsorbed amount of a diblock copolymer depends strongly on its composition (ratio between the A and B block lengths). As long as the solvent is a good solvent for the B block, the free energy of interaction between two adsorbed polymer layers is purely repulsive. At the theta point of the B block an attraction starts to appear in the free energy of interaction.

In this chapter we study the interaction between two adsorbed multiblock copolymer layers. The emphasis will be on triblock copolymers, although in section 5 we will pay some attention to polymers consisting of a larger number of blocks. The triblock copolymers have a central buoy block (B) and two anchoring blocks (A). When both these end blocks are adsorbed to the same surface, so that the polymer chain forms a large loop with the buoy block protruding into the solution, one intuitively expects the two adsorbed layers to repel each other in much the same way as two diblock copolymer layers. Such repulsive interaction has in fact been determined experimentally.[7] However, one can also envisage the situation that the triblock copolymer forms a bridge between both surfaces, with the two A blocks of one polymer chain adsorbed to different surfaces. This bridge formation will influence the interaction force and may lead to an attraction between the surfaces.

In this chapter we investigate the interaction between two adsorbed A-B-A polymer layers in a nonselective athermal solvent, using the statistical thermodynamic lattice theory of Evers et al.[4,8] This is a self-consistent mean-field model which involves the generation of all possible conformations of the polymer chains on a lattice between two flat surfaces. Each conformation is weighted by its

Boltzmann factor to find the contribution of this conformation to the overall equilibrium distribution. The lattice layers are numbered $z = 1, 2, 3, ..., M$ from one surface to the other, and each lattice layer consists of L lattice sites. A lattice site accommodates either a polymer segment or a solvent molecule. Nearest-neighbour interactions between two species p and q are accounted for by the Flory-Huggins parameter χ_{pq}. The symbols p and q denote either a polymer segment (A or B), a solvent molecule (O), or a molecule of the adsorbent (S). All results were computed using a simple cubic lattice, where every lattice site has six neighbours, of which a fraction $\lambda_1 = 1/6$ is in each of the adjacent layers. More information on the theory, which is taken from ref 4, is given in the appendix.

The central question in this chapter is how relevant parameters, such as the relative blocks lengths and the adsorption energy parameter χ_{AS} of the A segments influence the free energy of interaction. This problem can be divided into two parts. First, one needs to know how these parameters influence the adsorption at an isolated surface. Second, one must determine the interaction between two adsorbed layers. Adsorbed diblock copolymers form adsorbed layers which can be well described by an end-grafted B-layer (polymer brush). The density of such a brush is given by the adsorbed amount, which depends strongly on the composition of the polymer chain. An adsorbed triblock copolymer layer can be seen as a modified polymer brush with adsorbing "stickers" at the free ends of the polymer chains. Milner and Witten[9] have developed a theory for the interaction between two such grafted telechelic polymer layers. In section 3 we compare our lattice computations for grafted telechelic polymer layers with their predictions. We combine these computations with an investigation of the adsorbed amount (grafting density) as a function of chain composition and segmental adsorption energy. Thus we provide a full picture of the behaviour of adsorbed triblock copolymer layers under good solvency conditions for the buoy block.

In section 4 we consider triblock copolymers whose buoy and anchor blocks have an equal affinity for the surface but a different interaction with the solvent (which leads to homopolymer-like behaviour). This kind of polymers is important in many practical systems. The interaction curves of such molecules depend critically on the difference between the interactions of both blocks with the solvent. In section 5 we pay some attention to the interaction curves of copolymers consisting of a larger (> 3) number of blocks. In industrial and technological applications copolymers nearly always consist of a large number of (polydisperse and ill-defined) blocks. Our calculations are a first step towards a better understanding of the interfacial physics of such complicated systems. Many (bio-)macromolecules, for example proteins, may be considered as multiblock copolymers.

126

6.2 Polymer brushes with stickers

We consider the interaction between two polymeric brushes, formed by attaching (grafting) one end of a polymer to a surface. The other end of the polymer has an adsorbing A group. Milner and Witten[9] have also studied this system. They argue that when the surfaces are far apart the grafted chains form loops. When the surfaces are brought together the polymer chains can exist in two distinct classes of conformations. Either the sticker group adsorbs onto the grafting surface (so that the chain still forms a large loop), or it adsorbs onto the opposite surface (leading to a bridging conformation). As the affinity of the A group for both surfaces is taken to be equal, the adsorption energy of the A block should not have any effect on the interaction free energy. An attractive and purely entropical contribution to the interaction free energy arises because of the possibility of a chain to form a bridging conformation. This bridging effect is important when the surface separation is of the order of twice the brush height h or less.
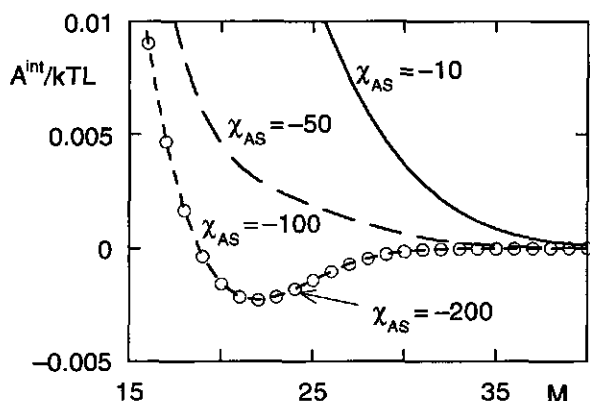

Figure 1   Free energy of interaction of a grafted $B_{100}A_1$ layer with grafting density $\sigma = 0.01$. The location of the first B segment is fixed in the first layer (adjacent to the surface). The various curves are for different values of χ_{AS} as indicated in the figure. All other χ parameters (between A and B segments, between A and solvent, between B and solvent, between B and the surface, and between solvent and the surface) are taken to be zero. The free energy is expressed in units of kT per surface site. The number of lattice layers M gives the distance between both surfaces.

Figure 1 shows the free energy of interaction for grafted layers of $B_{100}A_1$, where the first B segment is grafted to the surface with a grafting density $\sigma = 0.01$. The grafting density is defined as the number of chains per surface site. The Flory-Huggins χ_{AS} parameter between segment A and the surface, which determines the

adsorption energy of an A segment, has a large influence on the interaction between the grafted layers. For $\chi_{AS} = 0$ (not shown in Figure 1) one has the familiar, purely repulsive interaction between two homopolymer brushes. When χ_{AS} becomes more negative this interaction becomes less repulsive and even shows an attractive minimum for highly negative values of χ_{AS}. Above a certain critical value the interaction does no longer depend on χ_{AS}.
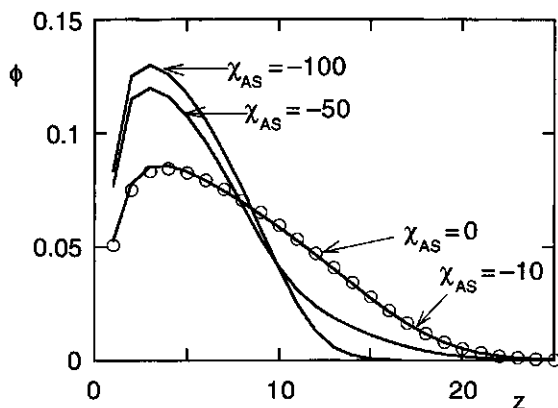

Figure 2 Volume fraction profiles of the B segments of the grafted $B_{100}A_1$ layers of Figure 1. These are profiles of the isolated layer, that is, when the surfaces are far apart (noninteracting). The adsorption strengths of the A segments (χ_{AS}) are indicated.

In Figure 2 volume fractions of the isolated layer are shown for different values of χ_{AS}. The curve for $\chi_{AS} = -10$ still virtually coincides with the curve for $\chi_{AS} = 0$. But for $\chi_{AS} = -50$ one sees that the layer is far less extended. A significant fraction of the A segments are now adsorbed to the grafting surface.

Figure 3 shows how the interplate distance affects the distribution of the A segments between the two surfaces. An A segment can either be adsorbed to the grafting surface (loop conformation), to the opposite surface (bridging conformation), or it may dangle somewhere in between (as a free, i.e. nonadsorbed, segment). The figure shows the fraction of A segments in loops, bridges, and free ends. When the adsorption energy is small (Figure 3A) and the surface separation is large, most chains have their ends freely dangling in solution. Only a small fraction form loops. This fraction is not high enough to have a considerable effect on the volume fraction profile (compare the curves for $\chi_{AS} = 0$ and -10 in Figure 2). When the surfaces approach one another, the number of loop conformations increases and some chains start to form bridges. This leads to an attractive energetic contribution to the

free energy of interaction. For higher adsorption energies (Figure 3B) a larger portion of chains form loops in the isolated layer. This gives a less extended polymer layer (see Figure 2). Upon approach of the surfaces, bridges are formed at the expense of both loop and "free chain end" conformations. The formation of bridges has both an energetic and an entropic effect on the interaction free energy.
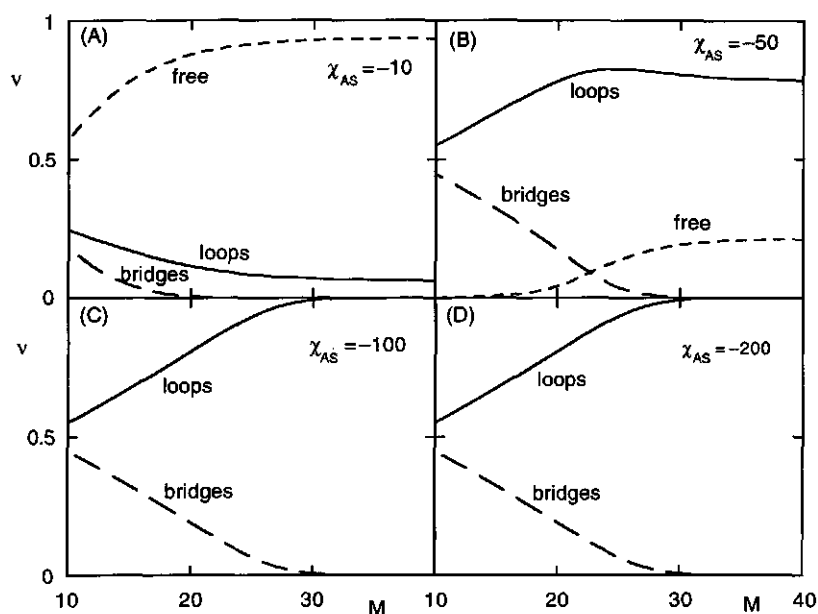

Figure 3 The fraction v of A segments in loops, bridges, and free ends, as a function of the distance M between the surfaces, for the system of Figure 1. The four curves are for different adsorption strengths, as indicated.

Comparing Figures 1 and 3 one sees that, once the segmental adsorption energy of the stickers is large enough to force all chains in the isolated layer to adopt a loop conformation, the free energy of interaction becomes independent of the actual value of the adsorption energy. For $\chi_{AS} = -100$ the interaction curve is the same as that for $\chi_{AS} = -200$. When the surfaces are relatively far apart all chains form loops. At this surface separation the B segments have a volume fraction profile comparable to that of a grafted brush with chain length $N = 50$ and $\sigma = 0.02$ (i.e. a chain length that is twice as small and a grafting density that is twice as large). The difference in free energy per surface site between such a brush and one with $N = 100$ and $\sigma = 0.01$ is 0.033 kT. Because this is significantly smaller than the total adsorption energy of a grafted $B_{100}A_1$ chain (which is $\lambda_1 \sigma \chi_{AS} kT$) the chain is completely in a loop conformation.

129

When the surfaces approach one another an increasing number of loop conformations change to bridging conformations. This has no effect on the total energy of the system but it does change the entropy. This is the regime which Milner and Witten consider in their paper.[9] We will subsequently refer to it as the MW regime. One can also reach this regime by increasing the length of the A block rather than the adsorption energy of the A segment. The total available adsorption energy of a chain is just the product of the A block length N_A (number of segments in an A block) and their segmental adsorption energy.
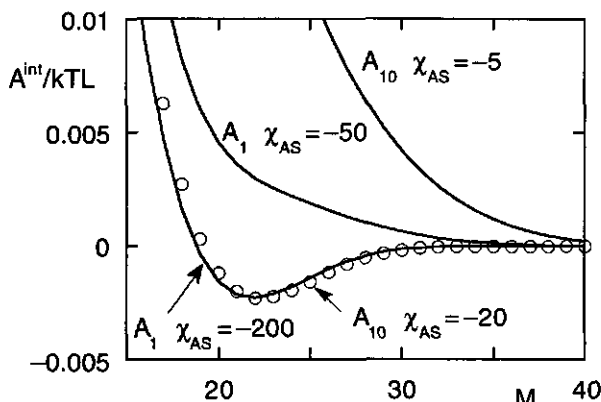

Figure 4 Free energy of interaction of grafted $B_{100}A_1$ and $B_{100}A_{10}$ layers. The adsorption strengths of the A segments (χ_{AS}) are indicated in the figure.

In an experiment it will probably be easier to increase the A block length than to change the adsorption energy of the individual monomers. However, increasing the block length by a certain factor does not always have exactly the same effect as increasing the segmental adsorption energy by the same factor. This can be seen in Figure 4. In this figure interaction curves are shown for two $B_{100}A_1$ and for two $B_{100}A_{10}$ layers. The grafted $B_{100}A_1$ layer with $\chi_{AS} = -50$ has a total potential binding energy per chain that is equal to that of a $B_{100}A_{10}$ brush with $\chi_{AS} = -5$ (so that $N_A\chi_{AS} = -50$). Similarly, the grafted $B_{100}A_1$ layer with $\chi_{AS} = -200$ has a total potential binding energy per chain that is equal to that of a $B_{100}A_{10}$ brush with $\chi_{AS} = -20$. The $B_{100}A_{10}$ chains must, however, have all their A segments in the first layer to actually benefit from this total adsorption energy. As this is entropically less favourable, the free energy of interaction is more repulsive for the $B_{100}A_{10}$ brush with $\chi_{AS} = -5$ than for the $B_{100}A_1$ brush with $\chi_{AS} = -50$. Only when $N_A\chi_{AS}$ is strongly negative (e.g. -200) does the interaction free energy curve of the $B_{100}A_{10}$

brush approach that of the $B_{100}A_1$ brush with the same adsorption energy per chain. This situation corresponds again to the MW regime.
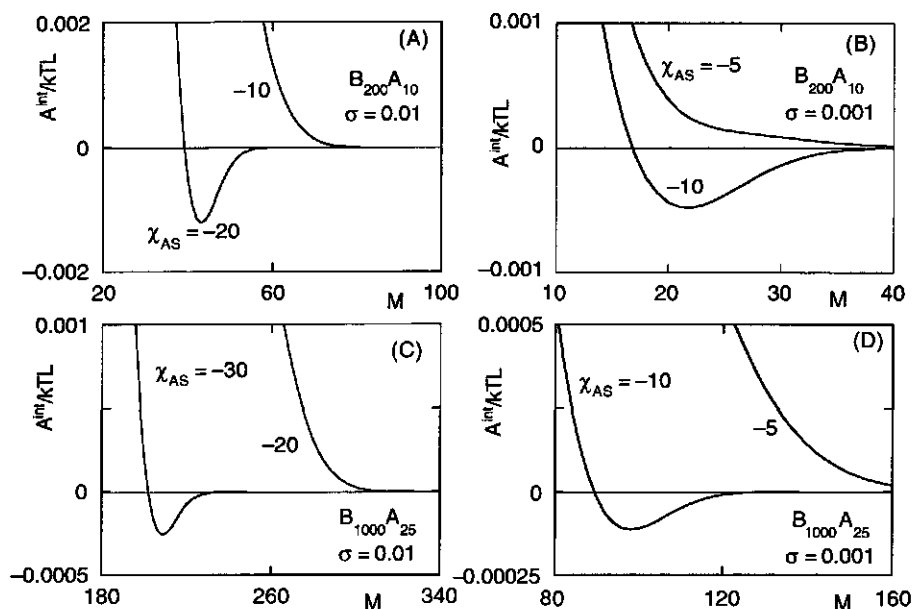

Figure 5 Free energy of interaction for various telechelic polymer layers. Diagrams A and B are for $B_{200}A_{10}$ chains, C and D for $B_{1000}A_{25}$ chains. Grafting densities and adsorption strengths of the A segments are indicated in the figure.

In Figure 5 interaction curves are shown for two chain lengths (with $N_B = 200$ and 1000, respectively) and two grafting densities (0.01 and 0.001). Again there is an attractive region in the free energy of interaction when χ_{AS} is sufficiently negative. At $\sigma = 0.001$ and $N_B = 200$ (Figure 5A) an attraction occurs for $N_A\chi_{AS} = -200$, whereas at the same grafting density and $N_B = 1000$ (Figure 5C) a value of -250 is not enough for attraction. Longer chains require stronger sticking energies for bridging attraction to occur. The same trend is present at $\sigma = 0.001$ (parts B and D in Figure 5). Similarly, increasing the grafting density at constant N_B also requires stronger sticking: $N_A\chi_{AS} = -100$ at $N_B = 200$ is sufficient for attraction when $\sigma = 0.001$ (Figure 5B) but not when $\sigma = 0.01$ (Figure 5A). The interaction curves in Figure 5 that have a minimum are all in the MW regime.

Figure 6 shows values for the depth and location of the minimum in the interaction free energy curve as a function of N (= N_B) and σ. The minimum in the interaction curve scales as $\sigma^{1/3}N^{-1}$ (Figure 6A) as predicted by Milner and Witten. Only for low grafting densities and very short chain lengths do significant deviations

occur from this scaling law. Under these circumstances the brush profiles differ considerably from their "classical" parabolic form. The minimum always occurs at a surface separation d that is larger than the separation 2h at which both (parabolic) brushes would just touch. The value of h has been calculated using the procedure described in ref 10. Figure 6B suggests that the difference $d - 2h$ is proportional to the isolated brush height $h \sim N\sigma^{1/3}$. This is not in agreement with the argument of Milner and Witten that $d - 2h \approx \xi$, where ξ is a penetration length defined as $\xi \equiv h(R/h)^{4/3}$, and $R \sim N^{1/2}$ is the radius of the (mean-field) chains in solution. This should lead to the scaling dependency $d - 2h \sim N^{1/3}\sigma^{-1/9}$.
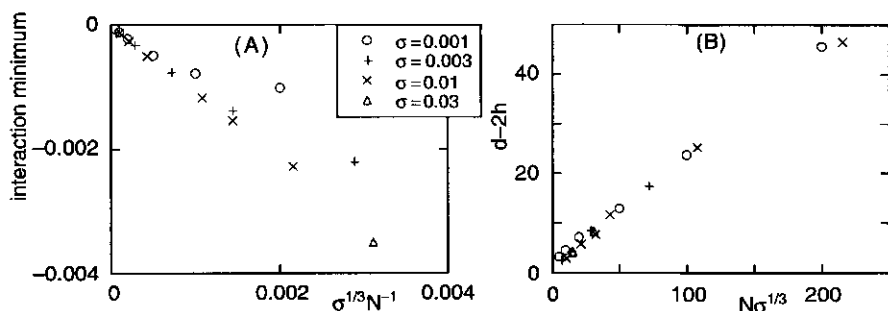

Figure 6 The depth and location of the minimum in the interaction free energy for systems in the MW regime. Diagram A gives these minima as a function of $\sigma^{1/3}/N$. Diagram B shows the position of the minimum as a function of $N\sigma^{1/3}$; $d - 2h$ is the distance between the outer edges of two parabolic brushes.

6.3 Adsorbing triblock copolymers

The equilibrium adsorbed amount (θ^a) of a triblock copolymer depends on its composition and the adsorption strength of the adsorbing segments in a similar manner as that of a diblock copolymer.[11] An illustration is given in Figure 7. This figure shows the surface density $\sigma = \theta^a/N$, where $N = 500+2x$, of adsorbing $A_xB_{500}A_x$ chains for two different segmental adsorption energies of the A segments. The surface density σ is the adsorbed amount θ^a (in equivalent monolayers) divided by the chain length N. This definition is completely analogous to the grafting density of a polymer brush. However, for a grafted layer σ is an input parameter, whereas here it follows from the equilibrium calculation. When the A block is very short the adsorbed amount is small as the chains cannot gain enough adsorption energy. Increasing the A block length leads to an increase in the adsorbed amount. Beyond

a certain value of x, a further increase of the A-block size leads to a decrease of the adsorbed amount: the long A-blocks then lie relatively flat on the surface, and leave less space for other adsorbed chains.
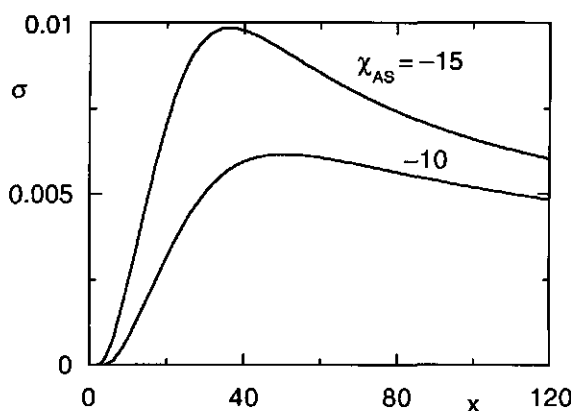

Figure 7 The normalized adsorbed amount σ of $A_xB_{500}A_x$ copolymers as a function of the adsorbing A block length x. The surface density σ is the adsorbed amount θ^a (in equivalent monolayers) divided by the chain length N. Parameters: bulk volume fraction $\phi^b = 10^{-4}$; $\chi_{AS} = -15$ and $\chi_{AS} = -10$; all other χ parameters are zero.

At the given segmental adsorption energies, the chains adsorb with both end groups onto the surface for all values of x. This means that practically all chains (> 99%) are in a "loop conformation". On approach of two surfaces bearing such adsorbed layers, the chains will be able to change from their loop conformation to a bridging conformation (MW regime). One expects that this should lead to an attractive minimum in the free energy of interaction. This is indeed the case, as can be seen in Figure 8.

In this figure the free energy of interaction is given as a function of surface separation for $\chi_{AS} = -10$ and an A block length of 10, 20, and 40 segments. For x = 10 and x = 20 the adsorbed amount is well below its maximum. For x = 40 the adsorbed amount is roughly at its maximum value (see Figure 7). The solid curves were calculated for chains that are in restricted equilibrium and the dashed curves correspond to full equilibrium with the bulk solution (see appendix). The inset of Figure 8 shows the same data on a different scale, so that the behaviour at high compressions (small plate separation M) can be seen.

In all cases there is an attractive part in the interaction curves of Figure 8. For x = 40 the minimum is deepest and is also situated at the largest surface separation.

This is in full agreement with the dependence of this minimum on the grafting (adsorption) density σ that we found for telechelic brushes (see Figure 6). For $x > 40$ the depth of the minimum will again decrease because σ becomes smaller. For all values of x the attraction has a purely entropical origin, and is caused by the possibility of chains in a loop conformation to form bridges. A grafted polymer layer with a grafting density equal to the adsorption density of the $A_xB_{500}A_x$ chains would give the same attractive minimum if the grafted chains had a strongly adsorbing sticker group (not shown in the figure).
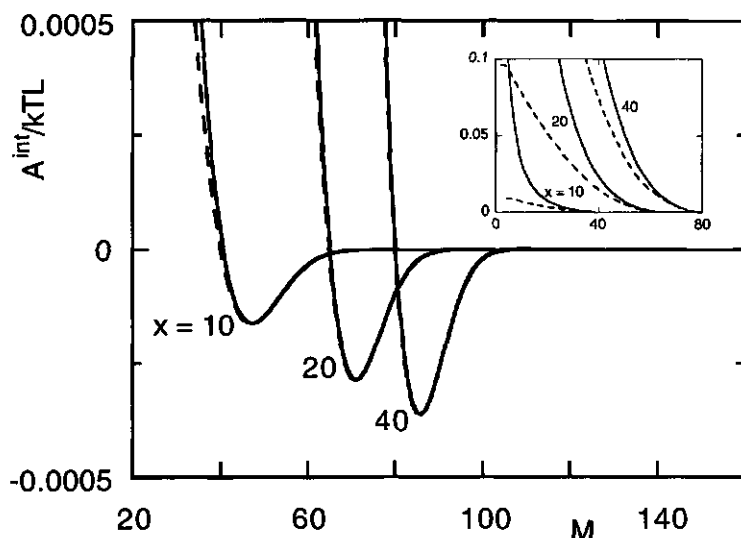

Figure 8   Interaction curves for adsorbed $A_xB_{500}A_x$ layers for $x = 10$, 20, and 40 and $\chi_{AS} = -10$. The solid curves are for a constant amount of polymer in the system (restricted equilibrium). This amount corresponds to the equilibrium adsorbed amount at large surface separation for $\phi^b = 10^{-4}$. The dashed curves were calculated for a constant chemical potential of the polymer chains (full equilibrium). The inset shows the same data on a larger scale.

The main conclusion of the calculations presented in Figure 8 is that under full and restricted equilibrium circumstances end-adsorbing triblock copolymers induce an attraction between two surfaces. This has as a practical implication that such polymers should be able to cause flocculation of a dispersion. However, experimental data with the surface force apparatus do not support this hypothesis. Dai and Toprakcioglu[7] used PEO-PS-PEO triblock copolymers adsorbed from toluene onto mica, and only found attraction between the mica surfaces when a bare mica surface was compressed against a surface with an adsorbed polymer layer.

After repeating a large number of compression and decompression cycles the attraction disappeared, which they explained by assuming that the polymer was now symmetrically divided over both surfaces with the PS blocks protruding into the solution and causing the repulsion. The discrepancy between the experimental data and the theoretical predictions might be caused by a small asymmetry in the polymer molecule. If one of the adsorbing groups is larger than the other the attraction will be decreased. This effect is discussed in more detail below. Furthermore, it is unlikely that in the surface force experiment thermodynamic equilibrium is reached. However, this does not necessarily mean that equilibrium can never be reached in an experiment. A triblock copolymer stabilized colloidal dispersion left to equilibrate might well show aggregation.

The solid curves in Figure 8 were calculated for chains that are in restricted equilibrium (the amount of polymer is held constant). In this figure the dashed curves show results of calculations in which the chemical potential of the polymer chains is held constant (so that the amount of polymer in the system decreases as the surfaces approach one another). Up to the minimum in the free energy curve there is very little difference between the full equilibrium and the restricted equilibrium interactions. Beyond this point, the repulsion is far less when the chemical potential is kept constant (this is most clearly seen in the inset, which shows the free energy of interaction on a much larger scale). In full equilibrium the system does, however, remain repulsive. This has also been found for diblock copolymers[4] but not for homopolymers.[12]
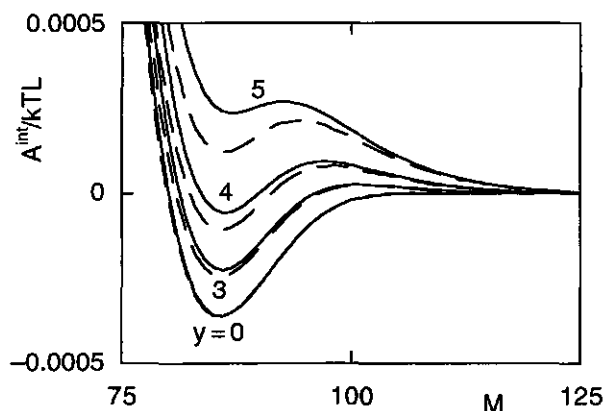

Figure 9   Interaction curves for $A_{40+y}B_{500}A_{40-y}$ polymers. Solid curves: restricted equilibrium; dashed curves: full equilibrium. All further parameters as in Figure 8.

Up to now we have only considered triblock copolymers which have equally sized adsorbing groups. Using an asymmetric polymer with different size anchoring groups one should be able to construct purely repulsive telechelic polymer systems. The larger A block will adsorb preferentially to the surface, leaving the smaller block dangling in solution. The behaviour of such asymmetric telechelic polymers is explored in Figure 9. Here the free energy of interaction is shown for $A_{40+y}B_{500}A_{40-y}$ chains. For $y = 0$ the curve of Figure 8 for $x = 40$ is recovered. Increasing y means that the asymmetry of the chains is increased while their overall composition is kept constant. When the chains become more asymmetric the interaction becomes less attractive. For $y = 5$ (corresponding to a rather modest asymmetry) the interaction is repulsive at all separations, although it still has a local minimum. These calculations indicate that an experimental verification of the telechelic attraction would require a very carefully designed model system. An attraction will only be found for polymers with virtually equally sized monodisperse adsorbing blocks.

6.4 Triblock copolymers with blocks of different solvency

In many systems of practical interest involving adsorbing triblock copolymers both types of blocks have an affinity for the surface. In this section we assume that this affinity is exactly the same for both segment types. Preferential adsorption of one of them can still occur if the interactions of the A and B blocks with the solvent are different. The exact characteristics of such an adsorbed layer depend critically on the interaction between the solvent and the segments. This is illustrated in Figure 10 for $A_{20}B_{100}A_{20}$ chains in full equilibrium between two surfaces. Both the A and B blocks have energetically favourable interactions with the surfaces ($\chi_{AS} = \chi_{BS} = -5$). The solvent O is a good solvent for the B block ($\chi_{BO} = 0$), whereas it is a poor solvent for the A block ($\chi_{AO} > 0.5$). We neglect the possibility of these molecules to form micelles and only consider the equilibrium between free polymer chains in solution and adsorbed chains. The molecules adsorb because of the bad solvency of the A blocks.

If χ_{AO} were zero, we would be considering an adsorbing homopolymer, giving an attractive interaction. For a relatively low positive value of χ_{AS} the interaction curve still strongly resembles that of a simple homopolymer. Even for $\chi_{AO} = 0.75$ the general shape of the interaction curve is that of a homopolymer, with attraction at any plate distance. At low separations this attraction becomes rather strong. For $\chi_{AO} = 1$ the interaction at large separations is similar to that of the triblock copolymers discussed in the previous section. However, for small M an attractive

region is found which is absent in Figure 8. For $\chi_{AO} = 2$ there is an attraction at large surface separation (M > 30) followed by a strong repulsion at lower separation; in this case the attractive part at small M does not show up. It is interesting to note that the curve for $\chi_{AO} = 1$ has the same features as found in the well known DLVO theory for colloid stability[13] under the combined action of electrostatic repulsion and van der Waals attraction, with a secondary minimum, a repulsive maximum, and a primary minimum. In restricted equilibrium the attraction at low separation is not present because the polymer cannot be squeezed out of the system (not shown).
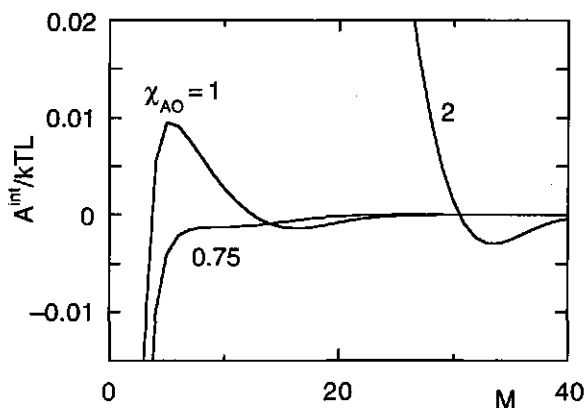

Figure 10 Interaction curves for $A_{20}B_{100}A_{20}$ molecules in full equilibrium. In this figure the adsorption energy of the A and B segments is the same but their solvencies are different: $\chi_{BO} = 0$, χ_{AO} is positive as indicated. Other parameters: $\chi_{AS} = \chi_{BS} = -5$, $\chi_{BO} = 0$, $\phi^b = 10^{-4}$.

6.5 Multiblock copolymers

We conclude with a discussion of copolymers consisting of more than three blocks. Their behaviour can be best understood by applying the concepts developed in section 3 for triblock (ABA) copolymers. We again limit ourselves to good (athermal) solvent conditions for both types of blocks, with the A segments having a strong affinity for the surface whereas the B blocks do not adsorb. The interaction between adsorbed $(A_xB_y)_nA_x$ layers can again be compared with the interactions between terminally attached $(A_xB_y)_n$ layers with a fixed grafting density σ. In Figure 11A interaction profiles are given for grafted $(A_xB_y)_n$ layers with $n = 1$, $n = 2$, $n = 4$, and $n = 8$. In all cases $\chi_{AS} = -27$ and $\sigma = 0.005$. The first segment of the first B block is always the grafted segment. The total chain length is kept constant at 1100 and on

average there is one A segment for every ten B segments, so that $x = 100/n$ and $y = 1000/n$. For $n = 8$ this does not lead to an integer value for the length of the A blocks. In this case the A blocks have alternating lengths of 12 and 13 segments. Starting with $n = 1$ and increasing the number of blocks, the attractive minimum shifts to smaller separations, and the depth of the attractive well increases. However, for $n = 8$ this trend completely breaks down. Below, we interpret these findings.
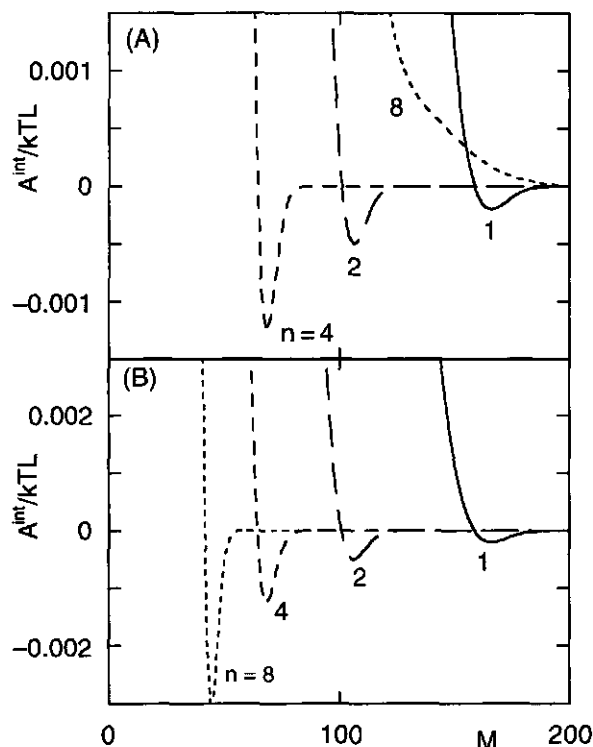
Figure 11 Interactions curves for grafted multiblocks $(A_xB_y)_n$ (A) and diblocks A_xB_y (B). The grafting density is 0.005 in (A) and 0.005n in (B), so that the amount of polymer in the system is the same for all curves. The adsorption energy of A segments is $\chi_{AS} = -27$, all other χ parameters are zero.

In the B part of Figure 11 interaction curves are shown for grafted A_xB_y diblock chains with a grafting density of 0.005n. The values chosen for n and for the block lengths x and y are the same as in Figure 11A. Hence, the grafted chains are shorter and the grafting density is higher than in Figure 11A, but the amount of polymer is the same in both diagrams. Figure 11B was calculated to test the hypothesis that these A_xB_y diblock layers should give approximately the same interaction profiles as

138

the multiblock layers. In an isolated grafted copolymer layer the adsorbing blocks all tend to adsorb onto the surface, thus forming a structure that is very similar to a grafted diblock layer with an n times higher grafting density. When the surfaces approach each other, the difference is that the multiblock copolymers have the opportunity to form larger bridges (comprising several consecutive blocks). The diblock copolymers can only form bridges consisting of one B and one A block. So, the interaction profiles for both systems need not necessarily be exactly the same. Only for n = 1 the curves in diagrams A and B are identical.
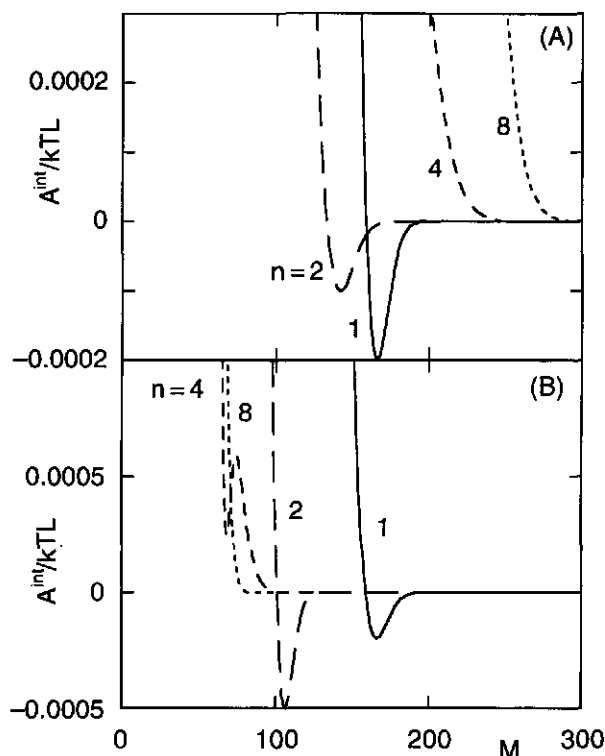
Figure 12 The same as Figure 11 but now for $\chi_{AS} = -15$.

The shape of the curves in Figure 11B is qualitatively the same as those in Figures 1 and 5 for large negative values of χ_{AS}. The attractive part in this type of curve is due to bridging, as discussed extensively in section 2. Increasing the value of n leads to stronger attractive wells which occur at lower values of the surface separation M. This is a consequence of the simultaneous decrease of the chain length and increase of the grafting density. For n = 2 and n = 4 the location and the

139

depth of the minimum are roughly the same as for the corresponding curves in Figure 11A. Clearly, the interaction between these grafted multiblock layers can be understood by treating a multiblock copolymer as a set of diblock copolymer chains. For n = 8 the diblock copolymer still shows the same type of behaviour as the other diblock copolymer systems, but the multiblock system does not show any attraction at all. This is because χ_{AS} is not sufficiently negative to anchor all the short A blocks firmly to the surface. If the A segments would have a higher adsorption affinity, the multiblock would also show an attractive minimum which is comparable to that found for the diblock copolymer. This point is illustrated in Figure 12.

Figure 12 shows data for the same systems as Figure 11, but now for a weaker adsorption: $\chi_{AS} = -15$. Again, in diagram A the interaction is shown for the multiblock and in diagram B for the diblock copolymer chains. We start the discussion by considering Figure 12B. For n = 1 and n = 2 the same interaction is found as for $\chi_{AS} = -27$. In these cases the total surface affinity is large enough to ensure complete adsorption of the A blocks, and the MW regime applies. For larger n (n = 4 and n = 8) no attraction is left. Here, we have moved out of the MW regime. In section 2 it was shown that for higher grafting densities a higher adsorption energy of the A segments is needed to give an attraction. In Figure 12B this effect is partly compensated by the fact that an increase of n leads to a decrease of the chain length. At given grafting density a decrease in the chain length leads to a lower adsorption energy needed to reach the MW regime. Apparently, the increase of the grafting density has a larger effect than the decrease of the chain length. For n = 4 the interaction profile still shows a local minimum (with a positive value), for n = 8 the repulsion increases monotonically when the surfaces are brought together, as for homopolymer brushes

The differences between Figures 11B and 12B are also present between Figures 11A and 12A. The attraction between the multiblock layers for n = 4 and $\chi_{AS} = -27$ disappears when χ_{AS} is changed to −15. The attractive well for n = 2 still exists if $\chi_{AS} = -15$ but is shallower and has shifted to a larger separation than in Figure 11A. Clearly, the value of χ_{AS} determines whether there is an attraction between the grafted multiblock layers. Similar trends are found for the diblock copolymer layers. However, for a given value of n a more negative value of χ_{AS} is required for an attraction to occur between the multiblock layers as compared to the diblock layers.

In Figure 13 the effect of χ_{AS} is shown in more detail. Interaction curves are shown for grafted $(B_{500}A_{50})_2$ chains (i.e. n = 2) and different values of χ_{AS}. For $\chi_{AS} = -11$ the interaction is still purely repulsive. For $\chi_{AS} = -14$ there is a clear attractive minimum but when χ_{AS} is further decreased this minimum moves to smaller surface separations and becomes deeper. For $\chi_{AS} = -21$ the maximum

attraction is reached, coinciding with the attraction in the $B_{500}A_{50}$ diblock system. In this case the distribution of A segments in both blocks is virtually identical. For $\chi_{AS} = -14$ the outer A block forms slightly more bridging conformations than the middle A block. This explains the different attractive components. Note that it is possible to find interaction curves with two minima (e.g. for $\chi_{AS} = -16$).
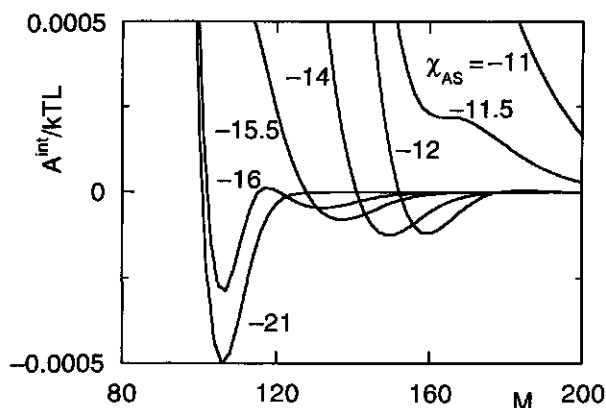

Figure 13 Interaction curves for grafted $(B_{500}A_{50})_2$ chains. Parameters: $\sigma = 0.005$, $\chi_{AS} = -11, -11.5, -12, -14, -15.5, -16, -21$; all other χ parameters are zero.

So far we have only considered grafted multiblock copolymers. Figure 14 shows interaction curves that were calculated taking into account the adsorption equilibrium. The molecular formula of the polymers is $(A_xB_y)_nA_x$ with n equal to 1, 4, 10 (diagram A) and 10, 20, 50, and 100 (diagram B). The total number of A segments per chain is 200 and the total number of B segments per chain is 1000. Thus, for n = 4 we have $(A_{40}B_{250})_4A_{40}$ chains. For larger values of n the A blocks cannot all be made of exactly the same number of segments. However, the difference between two block lengths within one chain is never larger than one segment. For example, for n = 10 the computations were done for chains with the following composition: $A_{19}(B_{100}A_{18})_9B_{100}A_{19}$.

When comparing the curves for different n, the first observation is that increasing n leads to interactions that start at smaller separations. This is because the adsorbed amount decreases when the polymer chains are divided into smaller blocks (while keeping the overall composition the same). This implies that the adsorbed layer thickness also decreases, so that the interactions start at lower surface separations. When n = 1 we have a triblock copolymer; this system was discussed in section 3. The curves for n = 1 show the same type of behaviour as shown in Figure 8. At M ≈ 150 there is an attraction that is caused by the possibility

141
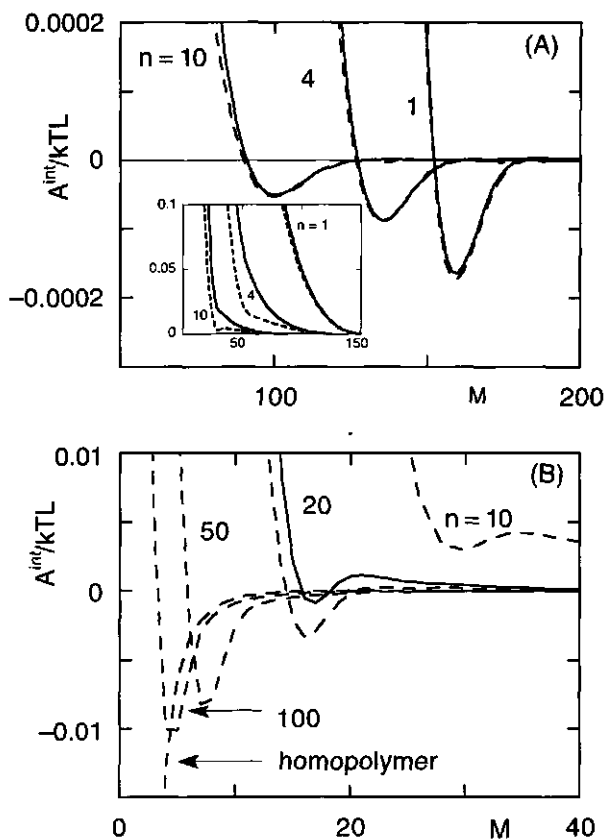
Figure 14 Interaction curves for adsorbing $(A_x B_y)_n A_x$ chains in full equilibrium (dashed curves) and restricted equilibrium (solid curves). The total number of A segments per chain, $(n+1)x$, equals 200 and the total number of B segments, ny, equals 1000. Parameters: $\phi^b = 10^{-4}$, $\chi_{AS} = -15$, all other χ parameters zero; $n = 1$, 4, 10, 20, 50, and 100. The interaction curve of a homopolymer (1200 segments) with $\chi_{AS} = -6.3$ is also shown.

of the chains to form bridging conformations. When the layers are further compressed a strong repulsion is found (see the inset of Figure 14A). The depth of the attractive well decreases when the chains are divided into smaller blocks, and the minimum moves to smaller surface separations. For relatively small n (Figure 14A) the trends are qualitatively the same under restricted and full equilibrium conditions. For n = 1 the attraction is simply due to the formation of bridges by one B block with an adsorbing block at both its ends. For larger n values (n = 4, 10) multiblock bridges are formed. For n = 10 the minimum appears at a surface

142

separation M ≈ 100, which is equal to the length of one B block. A single-block bridge would have to be virtually completely stretched, which is of course not very likely because of the large entropy penalty; hence the bridges consist of several B blocks. Further compression of the system leads to a strong osmotic repulsion. However, for n = 10 a local minimum appears in the interaction curve around M ≈ 30, see diagram B.

For even smaller block lengths (i.e. large n) this minimum becomes more pronounced, increases in magnitude and leads to a strong attraction. One should bear in mind that the free energy scale in part B of Figure 14 is two orders of magnitude larger than that in part A of Figure 14. Such a strong attraction is to be expected, considering the fact that for large values of n the multiblock copolymer starts to resemble a homopolymer whose characteristics are a weighted average of those of both types of blocks. The interaction free energy of such a homopolymer is also shown in Figure 14B for comparison. Indeed for large n (n = 100) the interaction curve is rather similar to that of such a homopolymer. Individual B blocks can now form bridges between the surfaces. Only when the separation becomes very small (3 layers for n = 100) does the interaction become repulsive again. However, at this distance the total inter-particle interaction in a dispersion may already be dominated by Van der Waals forces between the particles onto which the polymer chains adsorb. When using multiblock copolymers to impart steric stability, it is therefore advisable to use polymers with long blocks.

6.6 Concluding remarks

We have shown that polymer brushes with an adsorbing end-group can have an attractive part in their free energy of interaction. For a given grafting density σ and chain length N the end-group must have a certain minimum adsorption strength for this attraction to occur. The depth of the attractive minimum scales as $\sigma^{1/3}N^{-1}$, as predicted previously by Milner and Witten.[9] Polymer brushes with an adsorbing end-group can be seen as a model system to describe end-adsorbing triblock copolymers (telechelic polymers). We have also performed calculations on such triblock copolymers, taking the adsorption equilibrium with the bulk solution into account. In this case we also find an attractive part in the interaction curve. The magnitude of the attraction is, however, relatively small. Direct experimental evidence for this attraction is not available as yet, as far as we know. The attraction disappears when the two adsorbing blocks have different sizes. In this case triblock copolymers become good stabilizers.

The behaviour of multiblock copolymers consisting of a small number of blocks is qualitatively similar to the behaviour of triblock copolymers. Multiblock copolymers consisting of a large number of small blocks start to resemble homopolymers. A relatively strong attraction at low surface separations is characteristic for such systems.

We have further shown that adsorbing copolymers for which the solvency of the two blocks is different can give a rather complicated free energy of interaction. The details of these curves depend strongly on the precise values of the interaction parameters.

Appendix: The self-consistent field theory

An arbitrary segment p (for example, $p = A$ (anchor), $p = B$ (buoy), or $p = O$ (solvent)) has a potential energy in layer z that is defined with respect to the bulk solution (indicated by the index b) as

$$u_p(z) = u'(z) + kT \sum_q \chi_{pq} \left(< \phi_q(z) > - \phi_q^b \right) \tag{A.1}$$

The term $u'(z)$ is a Lagrange parameter which has the physical meaning of a hard-core repulsion, and ensures that the lattice layers are completely filled. The summation takes place over all different segment types present in the system, including the adsorbent S, which is treated as a component with a volume fraction equal to unity for $z = 0$ and $z = M+1$, and a volume fraction equal to zero for all intermediate values of z. The angular brackets in eq A.1 denote a weighted average over the layers $z-1$, z, and $z+1$:

$$<\phi(z)> = \lambda_1\phi(z-1) + \lambda_0\phi(z) + \lambda_1\phi(z+1) \tag{A.2}$$

where λ_0 and λ_1 are the a priori probabilities to move from a lattice site to a neighbouring site in the same layer, or to a site in a neighbouring layer, respectively. In a cubic lattice $\lambda_0 = 4/6$ and $\lambda_1 = 1/6$. Monomers are distributed over the lattice according to their monomer distribution function, $G_p(z)$, which is a Boltzmann factor of $u_p(z)$,

$$G_p(z) = \exp\left(-u_p(z)/kT\right) \tag{A.3}$$

The volume fraction of a free monomer p in layer z is simply given by

$$\phi_p(z) = \phi_p^b \exp\left(-u_p(z)/kT\right) \tag{A.4}$$

The computation of the volume fraction $\phi_i(z,s)$ in layer z due to segment s of a chain molecule i is more involved. The segments of this molecule are numbered $s = 1, 2, ..., s-1, s, s+1, ..., N_i-1, N_i$. We first define the end-segment weighting factor $G_i(z,s\,|\,1)$ of a subchain consisting of the first s segments of molecule i. The end segment of this s-mer must be located in layer z but the first segment may be located anywhere in the system. If segment s in layer z, segment $s-1$ must be located in one of the layers $z-1$, z, or $z+1$. This means that $G_i(z,s\,|\,1)$ is proportional to $<G_i(z,s-1\,|\,1)>$, where the angular brackets denote a similar average as defined by eq A.2. Furthermore, segment s in layer z contributes a factor $G_i(z,s)$, which is identical to $G_p(z)$ if s is of type p. It is now easily seen that a recurrence relation holds which enables us to calculate $G_i(z,s\,|\,1)$ for all values of s

$$G_i(z,s\,|\,1) = <G_i(z,s-1\,|\,1)> G_i(z,s) \tag{A.5}$$

This recurrence relation is started for s = 1 with $G_i(z,1\,|\,1) = G_i(z,s) = G_p(z)$ if the first segment is a segment of type p. If molecule i is grafted to the surface (as polymer chains in a brush) only those conformations must be taken into account whose first segment is located directly adjacent to the surface. This is done by starting the recurrence relation as follows:

$$G_i(z,1\,|\,1) = \begin{cases} G_i(z,1) & \text{if } z = 1 \text{ or } z = M \\ 0 & \text{otherwise} \end{cases} \tag{A.6}$$

In a completely analogous way we may define the end-segment weighting factor $G_i(z,s\,|\,N_i)$ of the subchain consisting of the segments s, s+1, ..., N_i, of which segment N_i may be anywhere in the system but segment s must again be located in layer z. The total statistical weight of all conformations of molecule i with segment s in layer z is given by the joint probability that both subchains have their end-segment in layer z. Thus, $\phi_i(z,s)$ becomes

$$\phi_i(z,s) = C_i \frac{G_i(z,s\,|\,1)G_i(z,s\,|\,N_i)}{G_i(z,s)} \tag{A.7}$$

The denominator in this equation accounts for the fact that in the two end-segment weighting factors segment s is counted twice (s belongs to both subchains). The normalization constant C_i can be obtained in two different ways. In a closed system the total amount θ_i of molecules i, which is expressed in equivalent monolayers, is fixed (this is the case in restricted equilibrium) and C_i follows from the condition $\theta_i = N_i \sum_z \phi_i(z,s)$, which holds for all segments s. For chains that are end-grafted to a surface with grafting density σ the amount of polymer is given by $\theta_i = N_i\sigma$. Substituting $s = N_i$, one finds

145

$$C_i = \frac{\theta_i}{N_i \sum_z G_i(z, N_i \mid 1)} \tag{A.8}$$

Alternatively, C_i can be expressed in the bulk concentration ϕ_i^b of molecule i. As in the bulk $\phi_i(z,s)$ equals ϕ_i^b/N_i and the potentials $u_p(z)$ of all segments p are, by definition, zero, it follows that

$$C_i = \frac{\phi_i^b}{N_i} \tag{A.9}$$

For a given $u(z)$ profile for all segment types that are present in the system, the volume fraction profiles of all molecules can be calculated from eqs A.3 - A.9. These volume fraction profiles must obey the constraint that all lattice sites are filled:

$$\sum_{i,s} \phi_i(z,s) = 1 \;\; \forall z \tag{A.10}$$

Also, the volume fraction profiles must be consistent with eq A.1. An initial guess is made of the $u(z)$ profiles and in an iteration procedure this profile is adjusted until both these conditions are met. Numerical details of this iteration procedure have been published elsewhere.[8]

Free energy

Once the volume fraction profiles are known all thermodynamic functions can in principle be calculated. We are especially interested in the interaction free energy. Evers et al.[7] showed by deriving the canonical partition function that the free energy A of the system is given by

$$\frac{A(M)}{kTL} = \sum_i \frac{\theta_i}{N_i} \ln(N_i C_i) - \sum_{z,p} \phi_p(z) u_p(z) + \frac{1}{2} \sum_{z,p,q} \phi_p(z) \chi_{pq} \langle \phi_q(z) \rangle - \frac{1}{2} \sum_i \left(\theta_i \sum_{p,q} \phi_{pi}^* \chi_{pq} \phi_{qi}^* \right) \tag{A.11}$$

The quantity ϕ_{pi}^* denotes the fraction of segments in molecule i that are of type p. The free energy given by eq A.11 is defined with respect to a reference state in which all molecules are separated into their pure amorphous phases. The surface excess free energy A^σ of a system with respect to its bulk solution is found by subtracting the contribution to the free energy due to molecules that are in full equilibrium with the bulk solution:

$$\frac{A^\sigma(M)}{kTL} = \frac{A(M)}{kTL} - \sum_j \frac{\theta_j \mu_j}{N_j} \tag{A.12}$$

146

The summation over j does not include the molecules that cannot move out of the system (for example, for the solid curves of Figure 9 only the solvent, and not the triblock copolymer, is included in the summation). The interaction free energy at a surface separation equal to M is the difference between the surface excess free energy at this separation and its value at very large separation, where the adsorbed layers do not yet interact:

$$\frac{A^{int}(M)}{kTL} = \frac{A^{\sigma}(M)}{kTL} - \frac{A^{\sigma}(\infty)}{kTL} \tag{A.13}$$

References

1. De Gennes, P. G. *Comptes Rendus Acad. Sc. Paris, Serie 2* **1985**, 300, 17.
2. Milner, S. T.; Witten, T. A.; Cates, M. E. *Macromolecules* **1988**, 8, 2610.
3. Taunton, H. J.; Toprakcioglu, C.; Fetters, L. J.; Klein, J. *Macomolecules* **1990**, 23, 571.
4. Evers, O. A.; Scheutjens, J. M. H. M.; Fleer, G. J. *Macromolecules* **1991**, 24, 5558.
5. Zhulina, E. B.; Priamitsyn, V. A.; Borisov, O. V. *Polym. Sci. USSR* **1989**, 31, 205.
6. Milner, S. T. *Europhys. Lett.* **1988**, 7, 695.
7. Dai, L.; Toprakcioglu, C. *Macromolecules* **1992**, 25, 6000.
8. Evers, O. A.; Scheutjens, J. M. H. M.; Fleer, G. J. *Macromolecules* **1990**, 23, 5221.
9. Milner, S. T.; Witten, T. A. *Macomolecules* **1992**, 25, 5495.
10. Wijmans, C. M.; Scheutjens, J. M. H. M.; Zhulina, E. B. *Macromolecules* **1992**, 25, 2657; This thesis, chapter 1.
11. Evers, O. A.; Scheutjens, J. M. H. M.; Fleer, G. J. *J. Chem. Soc. Faraday Trans.* **1990**, 86, 1333.
12. Scheutjens, J. M. H. M.; Fleer, G. J. *Macromolecules* **1985**, 18, 1882.
13. Hunter, R. J. *Foundations of colloid science*; Oxford University Press: Oxford, 1987.

chapter 7

On the Colloidal Stability of Small Polymer-Coated Particles

Abstract

A self-consistent field model is developed which enables the calculation of the interaction between two spherical particles bearing adsorbed polymer layers. We use cylindrical coordinates, so that the potential field can vary in both the radial and axial direction. Data are presented for the free energy of interaction for two particles with end-attached polymer chains in a good (athermal) solvent. The repulsion is less strong than the repulsion predicted by applying Derjaguin's approximation to a system with two similar interacting flat surfaces with end-attached polymer. This is explained by the greater freedom of the polymer chains to move laterally out of the gap between the particles as compared to polymer chains between flat surfaces.

7.1 Introduction

It is well known that polymers can greatly influence the surface properties of colloidal dispersions and thus determine the stability of these dispersions. Adsorbing homopolymers can impart steric stability, but may also cause bridging flocculation between different surfaces. The latter property can be utilized to flocculate and sediment impurities. This is, for example, relevant in the process of water purification. Polymeric stabilization of colloidal dispersions has many useful industrial and technological applications in the preparation of paints, inks, lubricants, etc. With block copolymers even better stabilizing properties can be achieved than with homopolymers. Diblock copolymers with one adsorbing and one nonadsorbing block give larger adsorbed amounts than homopolymers consisting only of adsorbing segments. Ideally, the nonadsorbing block dissolves well in the solvent, and forms an extended layer around the particle surface. Formation of bridges is prevented by steric hindrance between these nonadsorbing blocks.

The adsorption of polymers at isolated interfaces and the interaction between two flat surfaces bearing an adsorbed polymer layer have been studied extensively. Self-consistent field theories have been developed for the adsorption of homopolymers[1-3] and block copolymers,[4-6] as well as for grafted polymer layers.[7-11] All these theories assume that the surface is an infinitely large flat plane. Many experiments have been performed with the surface force apparatus to measure the force between two adsorbed polymer layers (for an overview see, for example, Luckham[12]). In such experiments the polymer is adsorbed onto cylindrically curved surfaces with a radius of curvature on the order of 1 cm, which is many orders of magnitude larger than the radius of gyration of a free polymer coil or of the thickness of an adsorbed polymer layer. In this case forces are indeed measured that agree well with theoretical predictions based on the assumption of a flat surface.[13]

Colloidal dispersions generally consist of particles with a radius roughly between 10 nm and 10 μm. Polymer adsorption often plays an important role in such systems. As long as the particle radius is far larger than the radius of gyration of the polymer, such systems can be described using the theories for flat surfaces mentioned above. However, when both radii have the same order of magnitude, one expects these models to loose their validity. As far as we know, no theory exists that predicts the interaction between such particles in the presence of adsorbing polymer. The aim of this chapter is to study the interaction between two small spherical particles bearing adsorbed polymer layers. For this purpose we

have developed a lattice model which is an extension of the Scheutjens-Fleer theory.

The statistical mechanical theory for homopolymer adsorption developed by Scheutjens and Fleer[1-3] uses a planar lattice on which concentration gradients in one dimension may occur. This model can be used to describe adsorption phenomena both at a single planar surface and between two interacting flat surfaces. Leermakers and Scheutjens[14] generalized the lattice theory of Scheutjens and Fleer to non-planar geometries. Especially the spherical lattice, which is made up out of concentric equidistant layers, is interesting for our purpose. For the case of a single sphere it is sufficient to consider only concentration gradients in one dimension; within one layer R the concentrations of all species may be taken to be constant. The spherical lattice, with gradients in one dimension, has been used to describe the aggregation of surfactant and block copolymer molecules into micelles. However, it can also be used to model polymer adsorption onto a single spherical surface. If the particle onto which adsorption occurs has a radius of ℓR_p (ℓ being the lattice spacing), this simply means that the inner R_p layers of the lattice are inaccessible to all molecules in the system. The volume fractions in the layers beyond R_p are assumed to be a function of the distance to the surface only, that is, of the layer number. Within each concentric layer a mean-field is applied.

Unfortunately, it is not possible to model two interacting spherical surfaces using this approach. In this case one cannot assume that the volume fraction profile is simply a function of the distance to one point. In order to model two interacting particles we have used a lattice with cylindrical coordinates. In the next section we will describe this cylindrical lattice in more detail. In the subsequent sections we will show how this lattice can be used to model a polymer solution between two spherical particles. We shall mainly direct our attention toward terminally attached polymer chains. These can be seen as a model for adsorbed diblock copolymers. In the *results* section we present data for the free energy of interaction between two spheres with terminally attached chains.

No results are given for adsorbing polymers in equilibrium with a bulk solution. However, in Appendix 2 we do describe a method that can be used to model the interaction in the presence of polymers which adsorb from solution onto the particles.

7.2 Theory

The Lattice

We start by briefly describing the spherical lattice.[14] Here the layers form concentric, equidistant shells. The differences between a planar lattice and a spherical lattice are: (i) the number of sites per layer increases on moving away from the centre of the lattice and (ii) the lattice transition parameters (λ) are layer-dependent. The lattice transition parameters $\lambda_-(R)$, $\lambda_0(R)$, and $\lambda_+(R)$ are defined as the fraction of neighbouring sites in layer $R-1$, layer R, and layer $R+1$, respectively, of a lattice site in layer R. If all layers are equidistant the volume enclosed by layer R equals:

$$V(R) = \ell^3 (4/3)\pi R^3 \tag{1}$$

The number L(R) of lattice sites in layer R is then

$$L(R) = \ell^{-3}(V(R) - V(R-1)) = (4/3)\pi(3R(R-1)+1) \tag{2}$$

The first layer (R = 1) of a spherical lattice, situated in the centre, contains $(4/3)\pi$ lattice sites. The surface area of the Rth layer equals

$$S(R) = 4\pi\ell^2 R^2 \tag{3}$$

and determines the transition factors, which are proportional to the surface area per site in contact with the adjacent layer:

$$\lambda_+^s(R) = \lambda_+^p \frac{S(R)}{\ell^2 L(R} = \lambda_+^p \frac{3R^2}{3R(R-1)+1}$$
$$\lambda_-^s(R) = \lambda_+^p \frac{S(R-1)}{\ell^2 L(R} = \lambda_+^p \frac{3(R-1)^2}{3R(R-1)+1} \tag{4}$$

where the superscript s denotes the spherical lattice and p denotes planar. This lattice can be used to compute the volume fraction profile of polymer around a single isolated particle. If that particle has a radius of ℓR_p the layers R = 1, 2, 3, ..., R_p are not accessible for the molecules in solution. The volume fractions are calculated as functions of R only. We call this the one-dimensional model: the mean-field approximation is applied within each concentric shell, that is, over two dimensions, so that there is a concentration gradient in one dimension only (the radial direction).

The cylindrical lattice can be seen as a planar lattice where each lattice layer is divided into concentric equidistant rings. One could also say that a circular lattice is placed into each layer z of the planar lattice. Now concentration gradients in two

dimensions can be accounted for: in the normal (z) and in the radial (R) direction. We refer to this as the two-dimensional model. So we write the volume fractions as a function of z and R: $\phi(z,R)$. An arbitrary lattice site (z,R) has neighbouring sites in the same layer: (z,R), $(z,R+1)$ and $(z,R-1)$ and in adjacent layers: $(z+1,R)$, and $(z-1,R)$. We define lattice parameters $\lambda_{\Delta z,\Delta R}(z,R)$ where Δz and ΔR can take the values $-$, 0, or $+$ for "downward", "lateral", or "upward" steps in directions z and R, respectively. Either Δz or ΔR should be zero: "diagonal" sites (e.g. $(z+1,R+1)$ and $(z-1,R-1)$) are not considered to be nearest neighbours, so that $\lambda_{+,+} = \lambda_{+,-} = \lambda_{-,+} = \lambda_{-,-} = 0$. Hence, for transitions to a lower or a higher layer $\Delta z = -$ or $+$, and $\Delta R = 0$; and similarly $\Delta R = -$ or $+$ and $\Delta z = 0$ in the cases of transitions to an inner ring or an outer ring within the same layer. Finally, $\Delta z = \Delta R = 0$ for steps within the same layer z and the same ring R. For transitions to a lower or a higher layer one simply has the same lattice parameters as for a planar lattice, so that (in a cubic lattice):

$$\lambda_{+,0}(z,R) = \lambda_1^p = 1/6$$
$$\lambda_{-,0}(z,R) = \lambda_1^p = 1/6$$

(5)

For transitions within the same layer z one must calculate the corresponding circular lattice parameters $\lambda_{\Delta R}^c$. It is easily seen that the number of sites in a circular ring of the cylindrical lattice is just

$$L^c(R) = \pi\left(R^2 - (R-1)^2\right) = \pi(2R-1)$$

(6)

and that the circular lattice parameters are

$$\lambda_+^c(R) = \lambda_1^p \, 2R/(2R-1)$$
$$\lambda_-^c(R) = \lambda_1^p \, 2(R-1)/(2R-1)$$

(7)

This means that we have the following transition parameters within the same layer z for a cubic cylindrical lattice:

$$\lambda_{0,-}(R) = \frac{R}{6R-3}$$

(8a)

$$\lambda_{0,0}(R) = \frac{1}{3}$$

(8b)

$$\lambda_{0,+}(R) = \frac{R-1}{6R-3}$$

(8c)

Analogous to the case of the planar lattice we define $<\phi(z,R)>$ as:

152

$$< \phi(z,R) > \; = \; \sum_{\Delta z=-,0,+} \; \sum_{\Delta R=-,0,+} \Big(\lambda_{\Delta z,\Delta R} \times \phi(z+\Delta z, R+\Delta R) \Big) \tag{9}$$
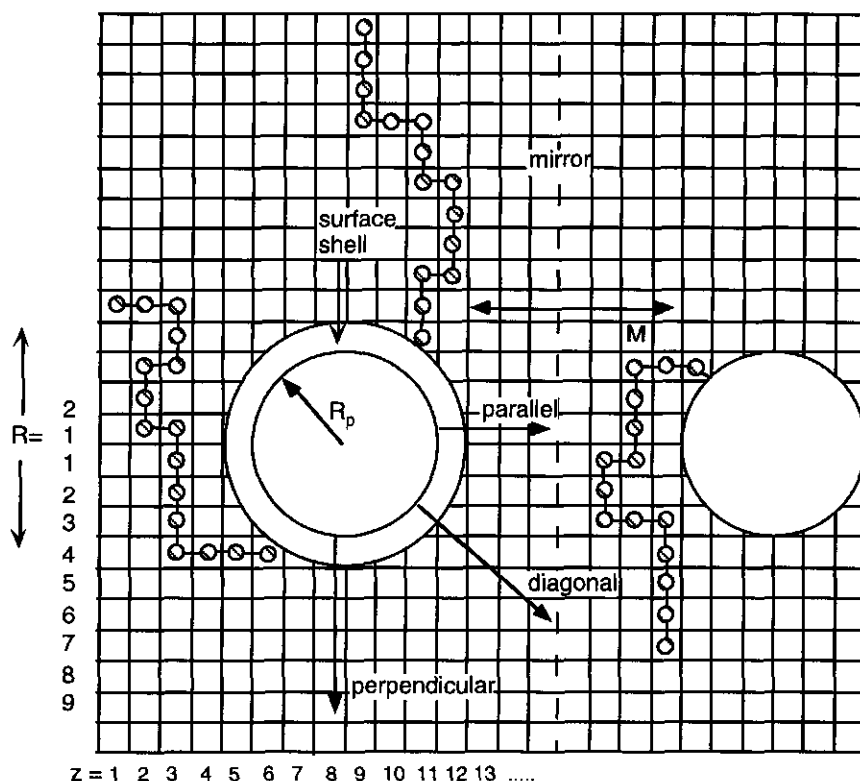

Figure 1 Cross section through the lattice. Two spherical particles, both with a radius of R_p lattice sites, are separated by M layers of lattice sites. The layers z are flat but the lattice has a cylindrical symmetry around the central axis connecting the particles. Hence, the parameter R refers to cylindrical shells around this axis, and the intersection of these shells with the planar layers defines rings with a given combination of z and R. Examples of possible polymer chain configurations are given. Three directions are shown in this cross section, denoted as "parallel", "diagonal", and "perpendicular".

To model interfacial phenomena a particle with radius R_p is placed in the middle of the lattice. This means that certain lattice sites are inaccessible to the molecules in the system. Figure 1 shows a cross-section through the lattice. A second particle has been drawn in this picture, as we are interested in modelling the interaction between two particles. However, for symmetry reasons the part of the lattice to the right of the line marked "mirror" need not actually be taken into

153

account in the computations. The size of the system, i.e. the number of layers between the particles and the mirror, determines the interparticle distance. Obviously, the number of layers and rings between the particle and the other boundaries of the system have to be chosen large enough not to introduce any spurious boundary effects. For example, if the number of rings is too small the polymer chains are compressed "sideways".

A minor problem is posed by the fact that a spherical particle does not naturally fit into the cylindrical lattice. The surface of the particle does not coincide with the boundaries between lattice layers. This problem can be solved by treating the particle as an extra component which has a fixed volume fraction ϕ_P in every lattice site; the value of ϕ_P varies from 0 for sites that completely belong to the solution to 1 for sites that are completely within the particle. A site that lies on the interface between particle and solution has a particle volume fraction $\phi_P(z,R)$ equal to the volume fraction of that site on the particle side of the interface. In the example of Figure 1, $0 < \phi_P(z,R) < 1$ for $R = 3$ and $z = 7$, 8, ..., 12, and for $R = 1$ and $z = 7$ or 12, i.e. those sites through which the particle surface cuts. The sum over $\phi_P(z,R)L(R)$ must give the total particle volume:

$$\sum_{z,R} \phi_P(z,R)L(R) = \frac{4}{3}\pi R_p^3 \tag{10}$$

Algebraic expressions for $\phi_P(z,R)$ can be derived (see Appendix 1). This procedure leads to a smoothening out of the particle surface. However, we want the total surface area of the particle to be the same as in the spherical lattice. When energetical interactions between solution species and the surface are taken into account (which is necessary to describe the adsorption equilibrium of adsorbing molecules) the particle surface area is an important parameter. When polymer chains are studied that are grafted to the surface at a given density σ the total surface area is also important, as it determines the total amount of polymer in the system. To solve this problem, we consider the surface shell as the concentric shell between a distance R_p and a distance $R_p + 1$ from the particle centre. This shell cuts through several lattice sites. Some of these (at the inside) contain a nonzero particle volume fraction $\phi_P(z,R)$, for example sites (z,R) with $z = 7$ and $R = 2$ or 3 in Figure 1. Other sites (at the outside) belong partly to the solution, and this part falls outside the surface shell. Examples of this type are $z = 6$ and $R = 2$ or 3 in Figure 1.

We define a quantity $v(z,R)$ as the part (by volume) of each site (or ring) which is within a distance $R_p + 1$ of the surface. For sites entirely outside the surface shell $v(z,R) = 0$, for those completely inside this shell $v(z,R) = 1$; only for sites partly in

154

this shell $v(z,R)$ is in between 0 and 1. The quantity $v(z,R)$ may be calculated with the equations given in Appendix 1, after replacing R_p by $R_p + 1$. Analogous to eq 10 we have:

$$\sum_{z,R} v(z,R)L(R) = \frac{4}{3}\pi(R_p + 1)^3 \tag{11}$$

The difference $v(z,R) - \phi_P(z,R)$ characterizes the accessible part of lattice sites overlapping with the surface shell; only for these sites the difference is nonzero. For sites entirely inside or entirely outside the surface shell $v(z,R) - \phi_P(z,R)$ is zero. The accessible volume of the entire surface shell is obtained by subtracting eq 10 from eq 11. Only segments in this surface shell have energetical interactions with the surface. For grafted polymer the grafting density σ may be identified with the volume fraction of grafting segments in the surface shell.

Terminally attached polymer chains

Consider two spherical particles at a distance M from each other; the distance between the particle centres is $M + 2R_p$. Both particles carry end-grafted polymer chains with a density σ. The polymer chain length is N. Nearest-neighbour interactions between solvent and polymer segments are accounted for by the Flory-Huggins parameter χ. The segments do not adsorb onto the grafting surface. The total number of polymer segments in the system is denoted by θ, so that the number of polymer chains per particle is θ/N. This number equals the number of grafting segments, which is σ times the volume of the surface shell:

$$\frac{\theta}{N} = \frac{4}{3}\pi\sigma\left((R_p + 1)^3 - R_p^3\right) \tag{12}$$

For large R_p this equation reduces to the well known form $\theta/N = 4\pi\sigma R^2$.

We need to calculate the (two-dimensional) volume fraction profile $\phi(z,R)$ of the polymer segments as a function of M. This enables us to find the free energy of the system as a function M. The calculation of $\phi(z,R)$ is completely analogous to that of $\phi(z)$ for a polymer layer grafted to a flat surface,[1,15] but some modifications are necessary to account for the two-dimensional nature of the present problem.

We define the potential energy $u(z,R)$ of a polymer segment in ring (z,R) as

$$u(z,R)/kT = -2\chi < \phi(z,R) > -\ln(1 - \phi_P(z,R) - \phi(z,R)) \tag{13}$$

The corresponding segment weighting factor $G(z)$ is given by

$$G(z,R) = \exp(-u(z,R)/kT) \tag{14}$$

155

We define the end-segment weighting factor $G(z,R;s|1)$ as the average statistical weight of all conformations of an s-mer of which the last segment is located in the ring (z,R) given that the first segment is grafted to the particle surface. We further define $G(z,R;s|N)$ as the average statistical weight of all conformations of an $(N-s+1)$-mer of which the last segment (segment s of the grafted polymer chain) is located in the ring (z,R) and the first segment (segment N of the grafted chain) may be anywhere in the system (except, of course, on sites where $\phi_P(z,R) = 1$). The quantities $G(z,R;s|1)$ and $G(z,R;s|N)$ can be calculated from the recurrence relations:

$$G(z,R;s|1) = G(z,R) < G(z,R;s-1|1) > \tag{15a}$$
$$G(z,R;s|N) = G(z,R) < G(z,R;s+1|N) > \tag{15b}$$

where the values of $G(z,R;1|1)$ and $G(z,R;N|N)$ are given below (eqs 18-21).

Consider polymer chains of length N that are grafted to the surface with a grafting density given by eq 12. We assume that the chains are grafted homogeneously onto the surface. When the two particles interact, two different situations may be envisaged. Either the grafting segments are allowed to move over the surface, thus being able to find a more favourable conformation for the chains, or they are kept fixed in the same position. We first consider the latter case. This condition implies that the volume fraction of the first (grafting) segment of this polymer on a site (z,R) must be:

$$\phi(z,R;1) = \frac{\theta(v(z,R)-\phi_P(z,R))}{\frac{4}{3}\pi N\left((R_p+1)^3 - R_p^3\right)} \tag{16}$$

The volume fraction of a segment s on a site (z,R) is in general given by the connectivity law,

$$\phi(z,R;s) = C\frac{G(z,R;s|1)G(z,R;s|N)}{G(z,R)} \tag{17}$$

where C is a normalization constant. Eq 16 is a solution of eq 17 for all values of z, R and $G(z,R)$ if we define $G(z,R;1|1)$ and C as follows,

$$G(z,R;1|1) = \frac{G(z,R)(v(z,R)-\phi_P(z,R))}{G(z,R;1|N)} \tag{18}$$

and

$$C = \frac{\theta}{\frac{4}{3}\pi N\left((R_p+1)^3 - R_p^3\right)} \tag{19}$$

156

Equation 18 gives the starting value for the recurrence relation of eq 15a. The calculation of the recurrence relation of eq 15b is started with:

$$G(z,R;N \mid N) = G(z,R) \tag{20}$$

Applying eqs 17 and 19 then gives the polymer volume fraction profile. This profile, obtained for a given set of values for $u(z,R)$, should be consistent with eq 13 for all values of z and R.

Instead of using the procedure described above for a fixed distribution of the grafting segments, we can also assume that the chains have an average grafting density σ but that, when the two particles approach each other, the grafting segments may redistribute themselves over the surface to find the equilibrium distribution. We then replace eq 18 by:

$$G(z,R;1 \mid 1) = \begin{cases} G(z,R) & \text{if} \quad v(z,R) - \phi_P(z,R) \neq 0 \\ 0 & \text{otherwise} \end{cases} \tag{21}$$

The first segment of a polymer chain may be located on any site that is at least partly within the sphere with radius $R_p + 1$. Eq 21 is used for the recurrence relation of 15a, eq 20 is still used for the recurrence relation of 15b. The volume fraction profile is calculated using eq 17 with the normalization constant C given by:

$$C = \frac{\theta}{N \displaystyle\sum_{z,R} G(z,R;N \mid 1)L(R)} \tag{22}$$

Free Energy

The free energy of the system can be written as a straightforward extension of the one-dimensional analogue:[4]

$$\frac{A - A^*}{kT} = \sigma \ln NC - \sum_{z,R} L(R)u(z,R)/kT +$$
$$\sum_{z,R} L(R)\chi \big(-2 < \phi(z,R) > + \, \phi(z,R) < \phi(z,R) > + \, \phi(z,R) \big) \tag{23}$$

This expression holds for a two component system with grafted polymer (chain length N, and grafting density σ) and a monomeric solvent.

When the polymer is grafted to the surface, and the grafting segments are all kept at a fixed position during the calculations, it is necessary to slightly modify the first term in this equation. Chains that are grafted in different rings (z,R) can be all treated as separate components. The amount of polymer grafted to ring (z,R)

equals $L(R)N\sigma\big(\nu(z,R)-\phi_P(z,R)\big)$. The expression $\sigma\ln NC$ from the first term of eq 23 can now be written as a summation over all rings in which chains are grafted:

$$\sum_{z,R}\left(L(R)\sigma\big(\nu(z,R)-\phi_P(z,R)\big)\ln\left(\frac{L(R)N\sigma\big(\nu(z,R)-\phi_P(z,R)\big)}{G(N\,|\,z,R;1)}\right)\right) \tag{24}$$

where $G(N\,|\,z,R;1)$ is defined as $\sum_{z',R'}L(R')G(z',R';N\,|\,z,R;1)$, with

$$G(z',R';s\,|\,z,R;1)=G(z',R')<G(z',R';s-1\,|\,z,R;1)>$$

$$\text{and}\quad G(z',R';1\,|\,z,R;1)=\begin{cases}G(z,R) & \text{if } z=z' \text{ and } R=R' \\ 0 & \text{otherwise}\end{cases} \tag{25}$$

7.3 Results and Discussion

In this section we present results of calculations for the interaction between two particles with end-grafted nonadsorbing polymer. We limit ourselves to good solvency conditions ($\chi = 0$). Our aim is to study the influence of the particle radius on the free energy of interaction between the two particles. For large values of R_p ($R_p \gg M$) this interaction free energy can be directly related to the interaction between two flat surfaces. Derjaguin[16] showed that the interaction force $F_s^{int}(M)$ between such spherical particles is proportional to the interaction free energy $A_p^{int}(M)$ per unit area between two equivalent planar surfaces:

$$F_s^{int}(M)=2\pi R_p A_p^{int}(M) \tag{26}$$

The free energy of interaction between two planar surfaces can be calculated using the "classical" one-dimensional model on a flat (cubic) lattice. For large R_p we can thus write the interaction free energy between two spheres $A_s^{int}(M)$ as an integral over $F_s^{int}(M)$:

$$A_s^{int}(M)=2\pi R_p \int_{M'=\infty}^{M'=M} A_p^{int}(M')dM' \tag{27}$$

Ideally, we would like to calculate the function $A_s^{int}(M)/R_p$ using the two-dimensional lattice model for a large range of values of R_p. For large R_p this function should become independent of R_p and approach the values given by eq 27. However, due to computational limitations we have only been able to perform calculations for particles that are so small that large deviations from the results predicted by eq 27 should be expected. In Figures 2 and 3 we show the results for

158

a system with $R_p = 5$, $N = 50$, and $\sigma = 0.1$. The model with "fixed" grafting segments has been used for both these figures. Before we discuss the free energy of interaction for this system, we must prove that the volume fraction profiles as calculated with the two-dimensional model are consistent with those obtained from a one-dimensional model.
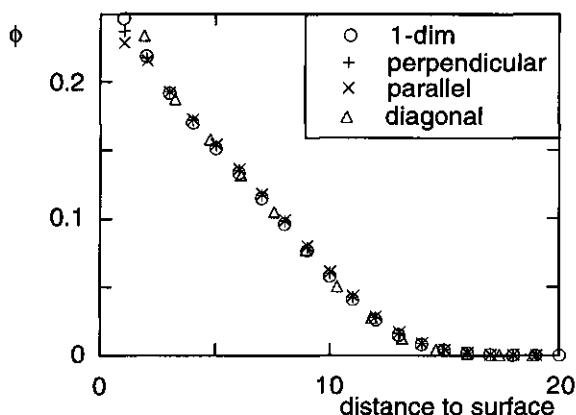

Figure 2 Polymer volume fractions in three directions (perpendicular, parallel, diagonal; see Figure 1) around a spherical particle calculated with the two-dimensional model with fixed grafting points. The volume fractions as predicted by the one-dimensional model are also shown. Parameters: $R_p = 5$; $N = 50$; $\sigma = 0.1$; $\chi = 0$.

This comparison is shown in Figure 2, where the volume fraction profile around one particle is plotted for large M (so that the two particles do not yet interact). In this case the profile should correspond with the profile that is calculated using the one-dimensional spherical lattice. Moreover, the volume fractions should be isotropic around the particle. In Figure 2 the polymer volume fractions are shown in three directions denoted as parallel, diagonal, and perpendicular. The "parallel" direction is along the axis that joins the centres of both particles. The "perpendicular" and "diagonal" directions make an angle of 90° and 45° with this axis, respectively (see Figure 1). The volume fraction profile of end-attached polymer chains on an isolated spherical particle has been extensively studied in ref 17. Here we only note that there is a satisfactory correspondence between the profiles in these three directions and the profile that follows from the one-dimensional calculations. This is a proof of the consistency of our model. Very close to the particle surface the agreement is not perfect. This artefact is caused by the way in which we model the surface. We expect that the polymer volume

159

fractions close to the surface only significantly influence the free energy of interaction when both particles are brought very close together.
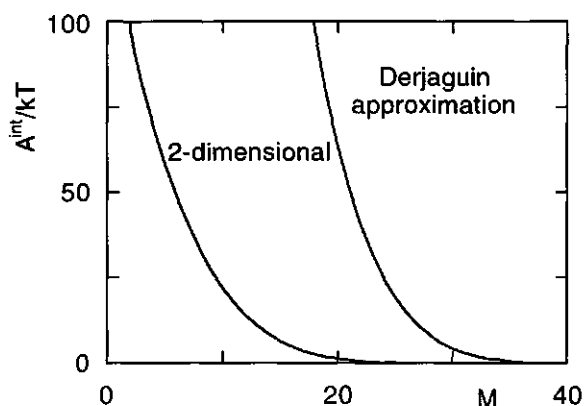

Figure 3 Free energy of interaction between two spherical particles as a function of their separation ("interaction profile"), for the two-dimensional model with fixed grafting points, and according to the Derjaguin approximation (eq 27). Parameters as in Figure 2.

The free energy of interaction for two interacting particles is shown in Figure 3. The same quantity is also shown as predicted by Derjaguin's approximation (eq 27). The free energy calculated in this way is far more repulsive than when it is computed using the two-dimensional model. Of course we are dealing with a situation where the assumption $R_p \gg M$ is not valid. For small particles the repulsion is far less because the polymer chains can move sideways. This movement is not accounted for in the Derjaguin approximation. In Figure 4 it is demonstrated how the polymer chains use this freedom to move out of the gap between the particles when M becomes small. In this Figure the volume fraction profile is shown in the perpendicular direction. For large M this profile is the same as that in any other direction. For smaller M the volume fractions increase in the perpendicular direction. This is due to the redistribution of the polymer tails sticking out into the solution.

Figures 2-4 were all computed for a fixed homogeneous grafting density. The grafting points of the polymer chains are then not able to move laterally over the surface. If they were able to do so, this would provide an additional mechanism to decrease the free energy of the system. However, this effect turns out to be of relatively minor importance. Figure 5 shows the free energy of interaction both for

160

fixed grafting points (i.e. using eq 18) and mobile grafting points (i.e. using eq 21). Both curves do not start to deviate significantly until relatively large compressions.
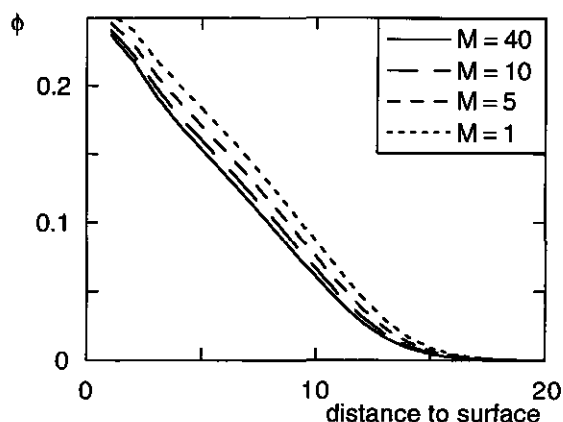
Figure 4 Volume fractions in the perpendicular direction for the system of Figure 3. The profiles are shown for various particle separations M, and illustrate the movement of the chains out of the region between the particles.
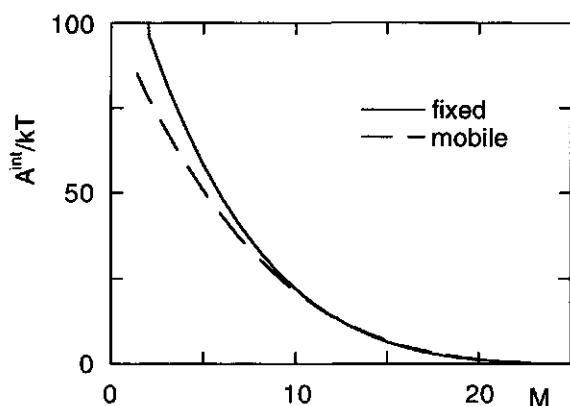
Figure 5 The free energy of interaction between two spherical particles as calculated with the "fixed grafting ends" model and the "mobile grafting ends" model. The system is the same as that of Figure 2.

Figure 6 shows the volume fraction profile in the various directions for the model with mobile grafting points for isolated particles. For $z > 5$ the volume fractions are isotropic around the particle surface and coincide with the volume fractions that are predicted by the one-dimensional model. Near the particle surface one can see that in the parallel and perpendicular directions lower volume fractions are found

161

than in the diagonal direction; the deviations are stronger than in Figure 2. This is caused by the way that the grafting is accounted for in eq 21. The first segment of a polymer has a roughly equal probability to be situated on any lattice site for which $v(z,R) > 0$. This includes sites for which $v(z,R)$ is far smaller than unity, so that the greater part of such sites is outside the sphere with radius $R_p + 1$ around the centre of the particle. Some of the grafting segments are then not in contact with the surface. It would be possible to improve on this model in such a way that the polymer chains are all really grafted within the first layer from the particle surface. However, our model already gives a very good profile for slightly larger distances from the surface. The volume fractions at these larger distances are most important for the interaction profile.
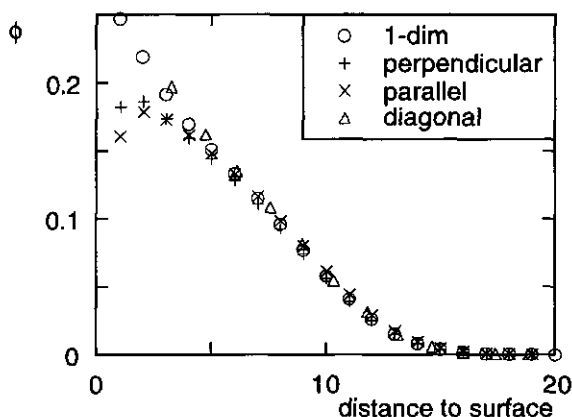
Figure 6 The polymer volume fractions around the particle in the "mobile ends" model. All parameters are the same as in Figure 2.

Figure 7 shows interaction curves for different values of R_p. The free energy of interaction is divided by the particle radius in order to compare the data for the different curves. For large values of R_p one would expect that the curves coincide with the one-dimensional calculation ("Derjaguin approximation"). When R_p is increased the repulsive interaction does indeed increase. However, due to computational limitations no results can be shown for $R_p > 10$. Figure 7 is calculated using the "fixed ends" model. This means that the closest approach between the two particles is $M = 2$. At this separation enough room is left between the particles for a grafting segment on both surfaces. This is why the curve for $R_p = 2$ stops at $A^{int}/R_p kT \approx 30$. In the one-dimensional model (two flat plates) the smallest distance of approach is $M = 2\sigma N$, because then the whole volume between both surfaces is filled with polymer.

Figure 7 The free energy of interaction between spheres with various radii of curvature. The free energy A^{int} divided by the particle radius R_p is given 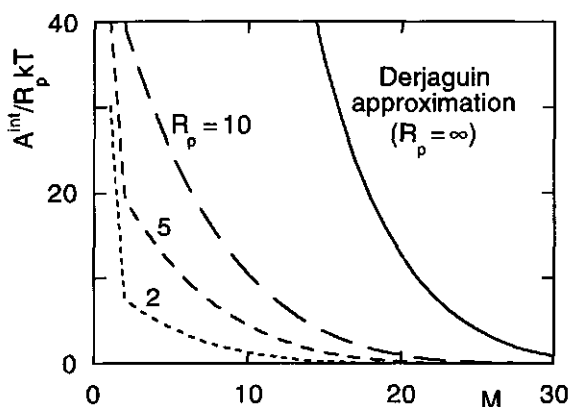as a function of the particle separation M for $R_p = 2$, 5, and 10. The other parameters are the same as in Figure 2. The solid curve gives the Derjaguin approximation for the free energy of interaction.

7.4 Concluding Remarks

We have shown that the interaction between two small spherical particles bearing adsorbed polymer layers is far less repulsive than would be expected from the interaction between two equivalent flat surfaces. We have described a self-consistent field model to quantify this "small particle effect". The question remains whether one can also experimentally detect this effect.

It is not possible to directly measure the force between two colloidal particles, as one can do between two macroscopic surfaces. Neither is it easy to extract detailed information of this force from bulk measurements on colloidal systems, although, in principle, this is possible. Force/interparticle separation plots can be calculated from osmotic pressure measurements of colloidal dispersions.[18,19] Alternatively, the high shear limit of the shear modulus of monodisperse spherical particles can also be written as a function of the particle interaction potential.[20] Costello et al.[21] measured forces between layers of adsorbed comb copolymers with the surface force apparatus, and compared them to osmotic force and rheological data on similar colloidal systems. They found a reasonable agreement with the directly measured force/distance profiles between macroscopic surfaces. However, they were considering colloidal particles with a radius which was an order of magnitude larger than the adsorbed layer thickness. It would be very interesting to repeat their

163

analysis with carefully chosen model systems in which the colloidal particle radius has the same order of magnitude as, or is even smaller than, the adsorbed layer thickness.

Another way to experimentally tackle this problem would be using an atomic force microscope. One would have to attach a single colloidal particle to the tip of the microscope. Then the interaction could be measured between this tip (onto which a polymer layer would first have to be adsorbed) and a flat surface with an adsorbed polymer layer. The interaction between a sphere and a plane should be in between the interaction between two planes and the interaction between two spheres. Our lattice model can easily be extended to model the interaction between a sphere and an (infinitely large) plane: the mirror in Figure 1 has only to be replaced by an impenetrable wall.

We hope that this chapter may direct the attention of experimentalists towards studying the effect of adsorbed polymer on the interaction between small particles.

Appendix 1

From geometrical arguments one can derive what fraction $\phi_P(z,R)$ of a ring (z,R) lies within a sphere with radius R_p that has its centre in the middle of the lattice (i.e. between layers 1 and 0). See Figure 8 for the definition of the layer numbers z used in this appendix. Below we give the equations for $\phi_P(z,R)$. Their derivation is straightforward. In order to simplify our notation we introduce the variables $\tilde{R}$ and $\tilde{\tilde{R}}$, defined as: $\tilde{R}^2 = R_p{}^2 - (R-1)^2$ and $\tilde{\tilde{R}}^2 = R_p{}^2 - R^2$. One can distinguish six different cases. In Figure 8 it is indicated which lattice sites correspond to these six cases. Below we only consider rings in the layers $z > 0$. From symmetry arguments if follows that $\phi_P(-|z|,R) = \phi_P(|z|+1,R)$.

1) $R_p{}^2 \geq z^2 + R^2$

The whole ring (z,R) is situated within the particle, i.e. $\phi_P(z,R) = 1$.

2) $R_p{}^2 \leq (z-1)^2 + (R-1)^2$

The whole ring (z,R) is situated outside the particle, i.e. $\phi_P(z,R) = 0$.

For the next 4 cases we can write:

$$\phi_P(z,R) = X + \int_a^b dz' \frac{\pi\tilde{R}}{\pi\left(R^2(R-1)^2\right)}$$

164

2	2	2	2	2	2	2	2	2	2
2	2	2	2	2	2	2	2	2	2
2	2	4	3	5	5	3	4	2	2
2	2	6	1	1	1	1	6	2	2
2	2	5	1	1	1	1	5	2	2
2	2	5	1	1	1	1	5	2	2
2	2	6	1	1	1	1	6	2	2
2	2	4	3	5	5	3	4	2	2
2	2	2	2	2	2	2	2	2	2

$$z = -4 \quad -3 \quad -2 \quad -1 \quad 0 \quad 1 \quad 2 \quad 3 \quad 4 \quad 5$$
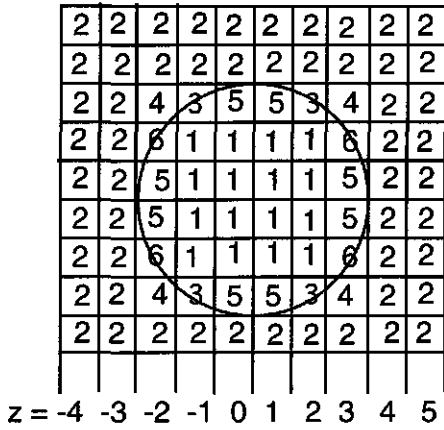
Figure 8 Definition of the layer numbers z used in Appendix 1. The six different types of lattice sites mentioned in this appendix are illustrated.

We distinguish the following situations:

3) $z^2 + R^2 > R_p{}^2 \geq z^2 + (R-1)^2$ and $(z-1)^2 + R^2 > R_p{}^2 \geq (z-1)^2 + (R-1)^2$

In this case $X = 0$, $a = z-1$, $b = z$, so that the volume fraction is:

$$\phi_P(z,R) = \frac{\tilde{R}^2 - z^2 + z - 1\!/3}{\tilde{R}^2 - \tilde{\tilde{R}}^2}$$

4) $R_p{}^2 < z^2 + (R-1)^2$ and $(z-1)^2 + R^2 \geq (z-1)^2 + (R-1)^2$

In this case $X = 0$, $a = z-1$, $b = \tilde{R}$, so that the volume fraction is:

$$\phi_P(z,R) = \frac{\dfrac{2}{3}\tilde{R}^3 - (z-1)\left(\tilde{R}^2 - \dfrac{1}{3}(z-1)^2\right)}{\tilde{R}^2 - \tilde{\tilde{R}}^2}$$

5) $z^2 + R^2 > R_p{}^2 \geq z^2 + (R-1)^2$ and $R_p{}^2 \geq (z-1)^2 + R^2$

In this case $X = \tilde{\tilde{R}} - z + 1$, $a = \tilde{\tilde{R}}$, $b = z$, so that the volume fraction is:

$$\phi_P(z,R) = \tilde{\tilde{R}} - z + 1 + \frac{\tilde{R}^2\left(z - \tilde{\tilde{R}}\right) - z^3/3 + \dfrac{1}{3}\tilde{\tilde{R}}^3}{\tilde{R}^2 - \tilde{\tilde{R}}^2}$$

6) $R_p{}^2 < z^2 + (R-1)^2$ and $R_p{}^2 \geq (z-1)^2 + R^2$

In this case $X = \tilde{\tilde{R}} - z + 1$, $a = \tilde{\tilde{R}}$, $b = \tilde{R}$, so that the volume fraction is:

$$\phi_P(z,R) = 1 - z + \tilde{\tilde{R}} + \frac{\dfrac{2}{3}\tilde{R}^3 - \tilde{\tilde{R}}\left(\tilde{R}^2 - \dfrac{1}{3}\tilde{\tilde{R}}^2\right)}{\tilde{R}^2 - \tilde{\tilde{R}}^2}$$

165

Appendix 2

In this appendix we show how the adsorption of a polymer which is in equilibrium with a bulk solution can be incorporated into our model for two interacting spheres. An adsorbing polymer is supposed to gain (adsorption) energy whenever one of its segments is adjacent to the surface, i.e. in the surface shell that is situated between the spherical particle with radius R_p and an imaginary sphere with radius R_p+1. However, in our model the surface shell does not consist of discrete lattice sites. So we introduce the probability $v'(z,R)$ that an adsorbing segment in a site (z,R) interacts with the surface as

$$v'(z,R) = \left(v(z,R) - \phi_P(z,R)\right)/\left(1 - \phi_P(z,R)\right)$$

This probability is only defined for sites where $\phi_p(z,R) < 1$. For sites outside the surface shell $v'(z,R) = 0$. The weighting factor of a monomer A on a site adjacent to the particle can now be written as

$$G_A(z,R) = v'(z,R)G_A^{ads}(z,R) + (1 - v'(z,R))G_A^{non}(z,R) \tag{A2.1}$$

where $G_A^{ads}(z,R)$ is the weighting factor of an adsorbed monomer on this site and $G_A^{non}(z,R)$ is the weighting factor of a nonadsorbed monomer on the same site. Equation A2.1 is a special case of the two-state lattice model used by previous authors.[22,23] The monomer factors are the Boltzmann factors of the potentials $u_A^{non}(z,R)$ and $u_A^{ads}(z,R)$ for nonadsorbed and adsorbed segments A on site (z,R), respectively:

$$G_A^{ads}(z,R) = \exp\left(-u_A^{ads}(z,R)/kT\right) \tag{A2.2a}$$

$$G_A^{non}(z,R) = \exp\left(-u_A^{non}(z,R)/kT\right) \tag{A2.2b}$$

For lattice sites that are completely surrounded by solution sites (i.e. $<\phi_P(z,R)> = 0$), the monomer weighting factors are equal to the nonadsorbing monomer weighting factors. In this case the splitting up of the segment weighting factors into an adsorbed and a nonadsorbed term becomes trivial. In general the adsorbed and nonadsorbed segment potentials can be written as:

$$\frac{u_A^{ads}(z,R)}{kT} = -\chi_{sA} + \sum_B \chi_{AB} < \phi_B(z,R) > + u'^{ads}(z,R) \tag{A2.3a}$$

$$\frac{u_A^{non}(z,R)}{kT} = \sum_B \chi_{AB} < \phi_B(z,R) > + u'^{non}(z,R) \tag{A2.3b}$$

The terms $\chi_{sA}\left(=-\lambda_{-1}^{s}(z')\chi_{AP}\right)$, where $z'=R_p+1$, and $\sum_B \chi_{AB} < \phi_B(z,R) >$ account for the energetical contributions to the potential, and $u'^{ads}(z,R)$ and $u'^{non}(z,R)$ are the (segment-independent) hard core potentials that ensure that both the adsorbing and the nonadsorbing parts of every site (z,R) are completely filled with segments. We define $\chi_{sO} = 0$. Defining $\Delta u' = u'^{ads}-u'^{non}$ and combining eqs. A2.1-A2.3 gives:

$$G_A(z,R) = G_A^{ads}(z,R) \times \left(v'(z,R) + (1-v'(z,R))\exp\left(-\chi_{sA} + \Delta u'(z,R)\right)\right) \qquad (A2.4)$$

Monomers.

The easiest case to consider is that of a system consisting of only monomers. For the volume fraction of a segment A in site (z,R) we can write:

$$\begin{aligned}
\phi_A(z,R) &= G_A(z,R)\phi_A^b \\
&= v'(z,R)G_A^{ads}(z,R)\phi_A^b + (1-v'(z,R))G_A^{non}(z,R)\phi_A^b \qquad (A2.5) \\
&= v'(z,R)\phi_A^{ads} + (1-v'(z,R))\phi_A^{non}
\end{aligned}$$

The following condition must be satisfied:

$$\sum_A \phi_A^{ads}(z,R) = \sum_A \phi_A^{non}(z,R) = 1-\phi_P(z,R) \qquad (A2.6)$$

This equation gives a relationship between $u'^{ads}(z,R)$ and $u'^{non}(z,R)$ which can be derived by substituting A2.4 into A2.6:

$$\sum_A \phi_A^b G_A^{ads}(z,R) = 1-\phi_P(z,R)$$

so that

$$\sum_A \phi_A^b \frac{G_A(z,R)}{v'(z,R)+(1-v'(z,R))\exp\left(-\chi_{sA}+\Delta u'(z,R)\right)} = 1-\phi_P(z,R) \qquad (A2.7)$$

This equation must be solved numerically.

Polymers

For polymers the recurrence relations (eq 15) must be used to find the volume fractions of segments. The total volume fraction of segment s of a polymer i on site (z,R) is again the sum of an adsorbed and a nonadsorbed fraction:

167

$$\phi_i(z,R;s) = v'(z,R)\phi_i^{ads}(z,R;s) + (1-v'(z,R))\phi_i^{non}(z,R;s) =$$

$$C_i < G(z,R;s-1|1) > \left(v'(z,R)G^{ads}(z,R) + (1-v')G^{non}(z,R)\right) < G(z,R;s+1|r) > \quad \text{(A2.8)}$$

Applying condition (A2.6) we can write the general form of (A2.7) for polymers by substituting A2.4 and A2.8 into A2.6:

$$\sum_i \sum_s \phi_i^{ads}(z,R;s) = 1 - \phi_P(z,R)$$

so that

$$\sum_i \sum_s \frac{\phi_i(z,R,s)}{v'(z,R) + (1-v'(z,R))\exp(\chi_{sA} - \Delta u'(z,R))} = 1 - \phi_P(z,R)$$

which can be rewritten as

$$\sum_A \frac{\phi_A(z,R)}{v'(z,R) + (1-v'(z,R))\exp(\chi_{sA} - \Delta u'(z,R))} = 1 - \phi_P(z,R) \quad \text{(A2.9)}$$

Numerical method

The (total) segment potentials are used as iteration variables. From the segment potential profile $\{G_A(z,R)\}$ the (total) segment volume fraction profile $\{\phi_A(z,R)\}$ is calculated. Applying (A2.9) for every site the hard core potential difference $\Delta u'(z,R)$ is found (this involves solving an equation with one variable, which must, however, generally be done numerically). Rewriting eqs. A2.1 - A2.3 gives $G_A^{non}(z,R)$ as an explicit function of $\Delta u'(z,R)$:

$$G_A^{non}(z,R) = \frac{G_A(z,R)}{(1-v'(z,R)) + v'(z,R)\exp(\chi_{sA} - \Delta u'(z,R))} \quad \text{(A2.10)}$$

so that $\phi_A^{non}(z,R)$ can be calculated. For every segment type A we now define a function $f_A(z,R)$ for every site (z,R) which must be 0 if the field is self-consistent:

if $\quad v'(z,R) = 1 \quad$ or $\quad v'(z,R) = 0$:

$$f_A(z,R) = \frac{1}{1-\phi_P(z,R)} - \frac{1}{\displaystyle\sum_A \phi_A(z,R)} - \alpha_A(z,R) + \alpha(z,R)$$

if $\quad 0 < v'(z,R) < 1$:

$$f_A(z,R) = \frac{2}{1-\phi_P(z,R)} - \frac{1}{\displaystyle\sum_A \phi_A^{non}(z,R)} - \frac{1}{\displaystyle\sum_A \phi_A^{ads}(z,R)} - \alpha_A(z,R) + \alpha(z,R)$$

where

$$\alpha_A(z,R) = \begin{cases} \dfrac{u_A^{non}(z,R)}{kT} - \displaystyle\sum_B \chi_{AB}\left(\dfrac{<\phi_B(z,R)>}{\displaystyle\sum_C \phi_C(z,R)} - \phi_B^b \right) & \text{if} \quad v'(z,R) < 1 \\[3em] \dfrac{u_A(z,R)}{kT} - \displaystyle\sum_B \chi_{AB}\left(\dfrac{<\phi_B(z,R)>}{\displaystyle\sum_C \phi_C(z,R)} - \phi_B^b \right) + \chi_{sA} & \text{if} \quad v'(z,R) = 1 \end{cases}$$

$$\alpha(z,R) = \frac{\displaystyle\sum_A \alpha_A(z,R)}{\displaystyle\sum_A 1}$$

(A2.11)

References

1. Scheutjens, J. M. H. M.; Fleer, G. J. *J. Phys. Chem.* **1979**, *83*, 1619.
2. Scheutjens, J. M. H. M.; Fleer, G. J. *J. Phys. Chem.* **1980**, *84*, 178.
3. Scheutjens, J. M. H. M.; Fleer, G. J. *Macromolecules* **1985**, *18*, 1882.
4. Evers, O. A.; Scheutjens, J. M. H. M.; Fleer, G. J. *Macromolecules* **1990**, *23*, 5221.
5. Evers, O. A.; Scheutjens, J. M. H. M.; Fleer, G. J. *J. Chem. Soc. Faraday Trans.* **1990**, *86*, 1333.
6. Evers, O. A.; Scheutjens, J. M. H. M.; Fleer, G. J. *Macromolecules* **1991**, *24*, 5558.
7. Cosgrove, T.; Heath, T.; Van Lent, B.; Leermakers, F.; Scheutjens, J. *Macromolecules* **1987**, *20*, 1692.
8. Milner, S. T.; Witten, T. A.; Cates, M. E. *Europhys. Lett.* **1988**, *5*, 413.
9. Milner, S. T.; Witten, T. A.; Cates, M. E. *Macromolecules* **1989**, *22*, 853.
10. Zhulina, E. B.; Priamitsyn, V. A.; Borisov, O. V. *Polym. Sci. USSR* **1989**, *31*, 205.
11. Zhulina, E. B.; Priamitsyn, V. A.; Borisov, O. V. *J. Colloid Interface Sci.* **1990**, *137*, 495.
12. Luckham, P. F. *Adv. Colloid Interface Sci.* **1991**, *34*, 191.
13. Milner, S. T. *Europhys. Lett.* **1988**, *7*, 695.
14. Leermakers, F. A. M.; Scheutjens, J. M. H. M. *J. Phys. Chem.* **1989**, *84*, 178.
15. Wijmans, C. M.; Scheutjens, J. M. H. M.; Zhulina, E. B. *Macromolecules* **1992**, *25*, 2657; This thesis, chapter 1.
16. Derjaguin, B. V. *Kolloid-Z.* **1934**, *69*, 155.
17. Wijmans, C. M.; Zhulina, E. B. *Macromolecules* **1993**, 26, 7214; This thesis, chapter 3.
18. Evans, R.; Napper, D. H. *J. Colloid Interface Sci.* **1978**, *63*, 43.

19. Rorhsetzer, S.; Kovacs, P.; Nagy, M. *Colloid Polym. Sci.* **1986**, *264*, 812.
20. Zwanzig, R.; Mountain, R. D. *J. Chem. Phys.* **1965**, *43*, 4464.
21. de L. Costello, B. A.; Luckham, P. F.; Tadros, T. F. *Langmuir* **1992**, *8*, 464.
22. Björling, M.; Linse, P.; Karlström, G. *J. Phys. Chem.* **1990**, *94*, 471.
23. Israëls, R.; Scheutjens, J. M. H. M.; Fleer, G. J. *Macromolecules* **1993**, *26*, 5405.

SUMMARY

Copolymers consisting of both adsorbing and nonadsorbing segments can show an adsorption behaviour which is very different from that of homopolymers. We have mainly investigated the adsorption of AB diblock copolymers, which have one adsorbing block (anchor) and one nonadsorbing block (buoy). The anchors adsorb from solution onto a surface and the buoys protrude into the solution. Thus, a *polymer brush* is formed. This name is derived from the resemblance between the protruding chains of B segments and the bristles of a brush. The presence of the adsorbing segments can be neglected when studying the characteristics of such a polymer brush, which is then modelled as (B-) homopolymer molecules which are terminally attached to the surface of a solid interface.

In **chapter 1** two self-consistent field (SCF) theories are introduced which give a description of such a polymer brush. The first of these theories is a lattice model. It takes into account all possible conformations that can be generated on a lattice; the molecules are treated as freely jointed chains. The overall volume fraction profile (that is, the polymer volume fraction ϕ as a function of the distance z to the surface) is then found by weighting each conformation with an appropriate Boltzmann factor. This theory can both be applied for systems with end-attached polymer molecules and for systems with freely adsorbing chains. The volume fraction profiles for any given system must be found using a complicated numerical procedure.

The second theory explicitly assumes that the polymer molecules are strongly stretched. Under this assumption only a fraction of all possible molecular conformations need be taken into account to find the volume fraction profile. Although this approach is less exact than the lattice model, it has as a major advantage that an analytical expression can be derived for the shape of the volume fraction profile. A simple algebraic expressions is also available for the brush height, if only the second and third order terms of a virial expansion of the free energy of mixing polymer and solvent are taken into account. If this free energy is accounted for in a more exact manner, one must (numerically) calculate the brush height from a (simple) integral equation.

In the first chapter we make a detailed comparison of the predictions of both theories for a polymer brush at a flat surface in a low molecular weight solvent. In general an excellent agreement is found between the results of both theories. Significant deviations only occur very close to the surface and at the periphery of the grafted layer. In the lattice model there is a small depletion zone near the grafting

surface, which is caused by the entropical restrictions imposed upon many polymer conformations by this impenetrable surface. The lattice calculations further show a "foot" of the volume fraction profile, which extends further away than the brush height as calculated from the strong-stretching approximation. The relative importance of these deviations increases with decreasing chain length, decreasing grafting density, and decreasing solvent quality. In order to find good quantitative agreement between the lattice calculations and the strong-stretching theory, one must incorporate the full Flory-Huggins expression for the mixing free energy of polymer and solvent into the latter theory. The derivation of elegant, analytical expressions for the layer structure by expanding this free energy in a virial series is only valid for low grafting densities.

In all chapters except the second, the polymer chains are treated as freely jointed chains in a potential gradient. In **chapter 2** more elaborate models are introduced for the polymer chains. Chain stiffness is incorporated by reducing the flexibility of the segment bonds. Stiffer chains give larger brush heights. Over a large range of chain stiffnesses the volume fraction profiles agree well with analytical expressions based on the incorporation of chain stiffness into the Gaussian approximation for the local stretching of a polymer chain. A further modification is a first order correction to the excluded volume interactions in the generation of the chain conformations. This correction slightly reduces the brush height. The opposing effects of this correction on the one hand, and chain stiffness on the other, suggest that the freely jointed chain is a good model for "real" polymers.

Chapter 3 considers polymer brushes on cylindrical and spherical surfaces with a radius of curvature R. On such surfaces the dependence of the brush height H on the chain length N differs from that of a flat brush. SCF lattice calculations are presented to investigate this dependency as a function of R. For large values of R the scaling law $H \sim N$ is recovered for both spherical and cylindrical surfaces. For $R = 1$ good agreement is found with the scaling laws $H \sim N^{0.6}$ (spherical surface) and $H \sim N^{0.75}$ (cylindrical surface). Polymer brushes on spherical surfaces can be seen as a model for AB diblock copolymers adsorbed onto small colloidal particles. For $R = 1$ a star-branched polymer molecule in solution is modelled.

The volume fraction profile of the brush is also studied as a function of R. For this purpose we focus our attention on spherical brushes immersed in athermal solvents. For large radii of curvature we make the assumption that the potential energy profile of the segments can be approximated by a parabolic function, as for flat surfaces. Applying this approximation, we derived an analytical expression for the volume fraction profile which agrees reasonably well with the lattice calculations. For very small radii of curvature the lattice calculations predict volume fraction profiles which

follow the scaling prediction ($\phi \sim z^{-4/3}$ for spherical brushes in athermal solvents). For intermediate curvatures we propose an analytical expression for the volume fraction profile which is a combination of the parabolic potential near the surface, and the scaling form farther away from the surface. Thus, over the whole range of radii of curvature, analytical expressions for the volume fraction profiles are available which give reasonably good correspondence with the lattice calculations.

We also studied the "dead zone" from which the free ends are excluded near the grafting surface. The lattice calculations show such a dead zone under all solvency conditions, both for spherical and cylindrical surfaces. The extension of this zone is a non-monotonic function of the surface curvature. The relative size of this zone (with respect to the brush height) is a decreasing function of R. No easy analytical expression is available for the size of the dead zone.

In **chapter 4** the adsorption equilibrium of AB diblock copolymers is considered for adsorption from solution onto small spherical particles. For adsorption onto flat surfaces it is known that the adsorbed amount shows a maximum as a function of the size of the adsorbing block, if the total chain length is kept constant. The thickness of the adsorbed layer shows a similar behaviour. Assuming that the adsorption energy is independent of surface curvature, we showed that the maximum in the adsorbed amount increases when the surface curvature increases. The hydrodynamic layer thickness of the adsorbed layer decreases strongly with increasing surface curvature. This increase occurs for all ratios of anchor to buoy sizes. On the other hand, the root-mean-square layer thickness changes much less as a function of the surface curvature. Depending on the anchor to buoy size ratio, it may either increase or decrease when the surface becomes more strongly curved.

Chapter 5 treats the interaction between two polymer brushes, both in the presence and absence of free polymer in the solution. In this chapter we first study the effect of free polymer chains in solution on the height and volume fraction profile of an isolated polymer brush. Using self-consistent field and scaling arguments, diagrams of state are constructed, which indicate different regimes with different scaling laws for the brush height and for the interpenetration of free and grafted polymer chains, as a function of grafting density, free and grafted chain length, and bulk volume fraction of the free polymer. These scaling laws are again corroborated by SCF lattice calculations. Predictions are also given for the volume fraction profiles of free and grafted chains based on the strong-stretching approximation. In the derivation of these expressions it is explicitly assumed that the free chain length is far smaller than the brush height. When this condition is satisfied, the volume fraction profiles from the lattice calculations agree excellently with those predicted by the strong-stretching theory. When this condition is not satisfied, both approaches

still predict the same height, but the strong-stretching theory gives a far too sharp interface between the grafted layer and the free polymer.

The repulsive interaction between two compressed brushes starts at slightly larger separations according to the lattice calculations than one would expect from the strong-stretching approximation. This is caused by the "foot" of the volume fraction profile. This phenomenon occurs both in the absence and in the presence of free polymer in the solution. When free polymer is present the free energy of interaction can have an attractive part, caused by the depletion of the free chains.

Chapter 6 deals with the interaction between two surfaces bearing adsorbed multiblock copolymer layers. We first study ABA triblock copolymers. Grafted layers of B chains with an end A block ("brushes with stickers") are used to model an adsorbed layer of such polymers. When the A adsorption energy of such a grafted layer is small, the free energy of interaction between two surfaces is purely repulsive. When this adsorption energy increases, a minimum appears, which reaches a limiting value at a certain adsorption energy. The minimum adsorption energy needed to find an attraction increases with increasing grafting density σ, and chain length N. The absolute value of this minimum also depends on N and σ. It scales as $\sigma^{1/3}N^{-1}$. The minimum always occurs at a separation d that is larger than the separation 2h at which the brushes are just in contact if the "feet" in the profiles are neglected. The difference $d - 2h$ scales as $N\sigma^{1/3}$. The attraction has an entropic origin. When the surfaces are far apart, the grafted chains form loops, with the A blocks adsorbed to the grafting surface. When the surfaces are brought together, the A block of a grafted chain can either adsorb onto the surface to which this chain is grafted, or it can adsorb onto the other surface. This freedom to choose between two surfaces leads to an entropically driven attraction.

The interaction between adsorbed layers of ABA triblock copolymers (where the adsorbed amount is determined by the equilibrium between free and adsorbed chains) has an attractive part if the copolymer chains are symmetric. The interaction curve is the same as that of a grafted layer ("brush with stickers") with a grafting density corresponding to the adsorbed amount of the triblock copolymers. If one of the adsorbing blocks is larger than the other block, the attraction decreases. For a relatively low asymmetry (one block roughly 20% larger than the other) the attraction disappears completely.

Multiblock copolymers consisting of more than three blocks can form bridges between two surfaces comprising several blocks. We studied the interaction between two surfaces bearing adsorbed multiblock copolymer layers. The overall composition of the polymer chains was kept constant, but the chains were divided into different numbers of A and B blocks (so that the blocks become shorter when

174

there are more blocks per chain). Chains with smaller blocks give smaller adsorbed layer thicknesses, so that the interaction starts at smaller separations. In all cases an attractive part is found in the interaction curve. Copolymer chains consisting of alternating small blocks of A and B segments very much resemble homopolymers (with properties that are some average of the A and B segments). These copolymers show a strong attraction at small separations (<10 layers), and repulsion at very small surface separations (around 2 layers).

So far, we have only considered situations were the solvent is a good solvent for both blocks. The A blocks adsorb preferentially with respect to the B blocks, because the former have a stronger intrinsic affinity for the surface. We also consider the adsorption of an ABA triblock copolymer were both blocks have the same intrinsic affinity for the surface, but where the solvent is poorer for the A block. Now the A blocks adsorb preferentially, because of the selectivity of the solvent. We also pay attention to the interaction between two surfaces bearing adsorbed layers of such copolymers. When the interactions between the A and B segments and the solvent differ only slightly, the interaction curve resembles that of an adsorbing homopolymer, with an attraction at small separations. When these interactions differ a great deal, the interaction resembles that of a "conventional" triblock copolymer, with an attractive part at a large separation and repulsion at smaller surface separations. In the intermediate situation a more complicated interaction curve is found.

The subject of **chapter 7** is the interaction between two small particles bearing adsorbed polymer layers. An extended version of the lattice SCF theory was introduced, which takes account of gradients in two directions. In this version a cylindrical coordinate system is used, so that the volume fractions can vary both parallel to the axis connecting the centres of both particles, and in planes perpendicular to this axis. Results are presented for terminally attached polymer layers. It is first shown that this cylindrical model gives an isotropic profile around one isolated particle. This profile agrees well with the profile calculated from the "conventional" SCF lattice model, where a concentration gradient can exist in one direction only. Various free energy of interaction curves are presented for two spherical particles with terminally attached chains.

If two spherically curved surfaces bearing adsorbed polymer layers interact, then the Derjaguin approximation relates this interaction to that between two similar flat surfaces, as long as the radius of curvature is far larger than the adsorbed layer. In chapter 7 we deal with systems where this condition does not hold. That is why we find interactions that are far less repulsive than the interaction according to Derjaguin's approximation. For increasing radii of curvature R, the interaction does

move in the direction of the interaction predicted for very large R by the Derjaguin approximation. On a molecular level the decreased repulsion can be explained by the freedom of the grafted chains to mover laterally out of the gap between the two particles. Whether or not the grafting segments themselves can also move over the surface plays only a minor role.

Copolymeren aan het vast-vloeistof grensvlak

SAMENVATTING

Copolymeren die zijn opgebouwd uit adsorberende en niet-adsorberende segmenten kunnen een adsorptiegedrag vertonen dat sterk afwijkt van het adsorptiegedrag van homopolymeren. In dit proefschrift hebben we de meeste aandacht besteed aan de adsorptie van AB diblok-copolymeren, bestaande uit een adsorberend blok van A segmenten (het "anker") en een niet-adsorberend blok van B segmenten (de "boei"). De ankers adsorberen uit een oplossing op een oppervlak, terwijl de boeien in de oplossing blijven uitsteken. Op deze manier wordt een zogenaamde *polymeerborstel* gevormd. Deze naam brengt de overeenkomst tot uitdrukking tussen de in de oplossing uitstekende staarten van B segmenten en de haren van een borstel. Wannneer de structuur van zo'n polymeerborstel bestudeerd wordt, kan de aanwezigheid van de adsorberende segmenten verwaarloosd worden. De borstel wordt dan voorgesteld als moleculen van een (B) homopolymeer die eindstandig aan een vast oppervlak verankerd zijn.

In **hoofdstuk 1** worden twee zelf-consistente veld (ZCV) theorieën besproken die gebruikt kunnen worden om polymeerborstels te beschrijven. Het doel van deze theorieën is om de volumefractie ϕ van het polymeer uit te rekenen als functie van de afstand z tot het oppervlak. Eén van deze theorieën is een roostermodel. Het volumefractieprofiel in de borstel wordt berekend door alle mogelijke conformaties van de polymeerketens in rekening te brengen. Hierbij wordt ervan uitgegaan dat de bindingen tussen de segmenten volkomen flexibel zijn (binnen de beperkingen die door het rooster worden opgelegd). Bovendien wordt het uitgesloten volume van de segmenten slechts in een gemiddelde-veld benadering meegenomen. Aan conformaties waarbij meer dan één segment zich in het zelfde roosterhokje bevinden, wordt een eindige waarschijnlijkheid toegekend. We noemen dit het "ideale spookketen" model voor een polymermolecuul. Het volumefractieprofiel wordt gevonden door alle conformaties met een bijbehorende Boltzmannfactor te wegen. Deze theorie kan zowel toegepast worden op systemen met eindstandig verankerde polymeerketens, als op systemen waarbij geadsorbeerde polymeermoleculen in evenwicht zijn met vrije moleculen in de bulkoplossing. In alle gevallen moet een ingewikkelde numerieke procedure worden toegepast om het volumefractieprofiel uit te rekenen.

De tweede theorie is op meer benaderingen gebaseerd dan het roostermodel. Er wordt vanuit gegaan dat de polymeerketens in een borstel sterk gestrekt zijn (in verhouding tot de afmetingen van een statistische kluwen in oplossing). Deze aanname maakt het mogelijk het volumefractieprofiel te berekenen uitgaande van slechts een fractie van alle mogelijke conformaties van de polymeerketens. Het grote voordeel van deze aanpak is dat een analytische uitdrukking kan worden afgeleid voor de vorm van het volumefractieprofiel. Indien de verandering van de vrije energie die optreedt bij menging van polymeer en oplosmiddel geschreven wordt als een viriaalreeks (met de polymeervolumefractie als variabele), kan ook voor de dikte van de borstel een eenvoudige algebraïsche vergelijking worden afgeleid. Hiertoe is het wel noodzakelijk vierde en hogere orde termen van de polymeervolumefractie te verwaarlozen. Indien ook deze hogere termen in rekening worden gebracht, moet de borsteldikte numeriek berekend worden uit een (eenvoudige) integraalvergelijking.

In dit eerste hoofdstuk wordt een uitgebreide vergelijking gemaakt tussen de voorspellingen die deze beide theorieën geven voor de structuur van een polymeerborstel op een vlak oppervlak in een laagmoleculair oplosmiddel. In het algemeen bestaat er een uitstekende overeenstemming tussen de voorspellingen van beide theorieën. Er treden alleen vlak bij het oppervlak en aan de buitenkant van de verankerde laag significante afwijkingen op. In het roostermodel wordt een kleine depletielaag gevonden naast het oppervlak waaraan de ketens verankerd zijn. Deze laag wordt veroorzaakt door het feit dat dit ondoordringbare oppervlak een groot aantal ketenconformaties onmogelijk maakt. Bovendien voorspelt het roostermodel een "voet" in het volumefractieprofiel, met eindige waarden voor de volumefractie op een afstand tot het oppervlak die groter is dan de borsteldikte voorspeld door de "sterke-strekkingstheorie". De relatieve grootte van deze afwijkingen neemt toe wanneer ketenlengte, verankeringsdichtheid en kwaliteit van het oplosmiddel afnemen. De volledige Flory-Huggins uitdrukking voor de verandering in de vrije energie bij menging van polymeer en oplosmiddel moet in rekening worden gebracht om een goede (kwantitatieve) overeenstemming tussen de sterke-strekkingstheorie en het roostermodel te vinden. Alleen voor lage volumefracties kan de eerder genoemde viriaalontwikkeling gebruikt worden om handzame, analytische uitdrukkingen voor de structuur van de verankerde laag af te leiden.

In het grootste deel van dit proefschrift worden polymeermoleculen benaderd als ideale spookketens in een potentiaalgradient. Echter, in **hoofdstuk 2** worden ingewikkeldere modellen gebruikt om, uitgaande van de boven genoemde roostertheorie, de ketens in een polymeerborstel te beschrijven. Er wordt ten eerste rekening gehouden met ketenstijfheid door de flexibiliteit van segmentbindingen te

beperken. Stijvere ketens leiden tot dikkere borstels. Dit effect kan ook goed beschreven worden in de analytische theorie door stijfheid mee te nemen in de Gaussische benadering voor de locale strekking van een ketenmolecuul. Daarnaast wordt een eerste orde correctie toegepast op de gemiddelde-veld benadering voor het uitgesloten volume van segmenten in het roostermodel. Deze correctie leidt tot iets minder dikke borstels. Het feit dat deze correctie een tegengesteld effect heeft dan de invoering van ketenstijfheid, suggereert dat de ideale spookketen een redelijk model is voor "echte" polymeren.

In **hoofdstuk 3** worden polymeerborstels op bolvormig en cylindrisch gekromde oppervlakken bestudeerd. De borsteldikte H op zulke oppervlakken hangt anders af van de ketenlengte N dan op een vlak oppervlak. ZCV roosterberekeningen zijn uitgevoerd om te onderzoeken hoe het verband tussen H en N beïnvloed wordt door de kromtestraal R van het oppervlak. In de limiet van zeer hoge R wordt zowel voor bolvormige als voor cylindervormige oppervlakken een rechtevenredig verband tussen H en N gevonden, zoals ook op vlakke oppervlakken het geval is. Voor zeer kleine waarden van R ($R = 1$) worden de volgende evenredigheidsrelaties gevonden: $H \sim N^{0.6}$ (bolvormig oppervlak) en $H \sim N^{0.75}$ (cylindervormig oppervlak). Polymeerborstels op bolvormige oppervlakken zijn een goed model voor geadsorbeerde AB diblok-copolymeermoleculen op een klein kolloïdaal deeltje. Voor $R = 1$ is de borstel een model voor een stervormig polymeer in oplossing.

Er is ook onderzocht hoe de volumefractieprofielen afhangen van de kromtestraal. Hiertoe hebben we onze aandacht gericht op bolvormige borstels in atherme oplosmiddelen. Voor hoge waarden van R kan bij benadering gesteld worden dat de potentiële energie van de segmenten in een borstel een parabolisch functie is van de afstand z tot het oppervlak (voor vlakke borstels is dit een zeer goede benadering). Deze benadering leidt tot een analytische uitdrukking voor het volumefractieprofiel die inderdaad redelijk overeen komt met de uitkomsten van het roostermodel voor grote waarden van R. Voor zeer kleine waarden van R leveren de roosterberekeningen profielen op die overeenstemmen met reeds eerder afgeleide evenredigheidsrelaties ($\phi \sim z^{-4/3}$ voor bolvormige borstels in een atherm oplosmiddel). Voor tussenliggende waarden van R kan het profiel worden opgevat als een combinatie van het parabolische profiel dicht bij het oppervlak en de evenredigheidsrelatie verder weg van het oppervlak. Door deze drie verschillende gevallen te onderscheiden zijn we erin geslaagd om voor alle kromtestralen (benaderende) analytische uitdrukkingen af te leiden voor het volumefractieprofiel van de polymeerborstels.

Een laatste onderwerp dat in hoodstuk 3 aan de orde komt is de aanwezigheid van een zone naast het oppervlak waar geen vrije uiteinden van verankerde

polymeerketens voorkomen. De roosterberekeningen tonen aan dat zo'n "dode zone" in alle oplosmiddelen kan bestaan, zowel in bolvormige als cylindrische borstels. De absolute grootte van deze zone is geen monotoon dalende of stijgende functie van de kromtestraal. De relatieve grootte (in verhouding tot de borsteldikte) is een monotoon dalende functie van R. Het is niet gelukt om een analytische uitdrukking te geven voor de grootte van de dode zone, zelfs niet bij benadering.

Het onderwerp van **hoofdstuk 4** is het adsorptieëvenwicht voor de adsorptie van AB diblok-copolymeren uit een oplossing op kleine, bolvormige, kolloïdale deeltjes. Het is bekend dat wanneer zulke polymeren op een vlak oppervlak adsorberen, de geadsorbeerde hoeveelheid als functie van de grootte van het adsorberende blok door een maximum gaat. Ook de dikte van de geadsorbeerde laag vertoont in dat geval een maximum. Ervan uitgaande dat de adsorptieënergie onafhankelijk is van de oppervlaktekromming, hebben we laten zien dat het maximum in de geadsorbeerde hoeveelheid toeneemt als het oppervlak sterker gekromd is. De hydrodynamische laagdikte neemt af bij toenemende kromming. Deze toename vindt plaats voor alle verhoudingen van de ankergrootte ten opzichte van de boeigrootte. Daarentegen verandert de middelbare laagdikte slechts weinig, wanneer het oppervlak sterker gekromd wordt. Afhankelijk van de verhouding van de ankergrootte ten opzichte van de boeigrootte kan de hydrodynamische laagdikte zowel (enigszins) toenemen als afnemen.

In **hoofdstuk 5** wordt gepoogd meer inzicht te krijgen in de interactie tussen twee polymeerborstels, zowel in aanwezigheid als in afwezigheid van vrij polymeer in de oplossing. Eerst wordt in dit hoofdstuk de invloed onderzocht van vrij polymeer op de dikte en het profiel van een geïsoleerde borstel. Evenredigheidsrelaties zijn afgeleid die het verband weergeven tussen de laagdikte en de penetratiediktes van vrije polymeerketens in de borstel en verankerde ketens in de oplossing enerzijds, en de verankeringsdichtheid, de lengte van de verankerde ketens, de lengte van de vrije ketens en de bulkvolumefractie van de vrije ketens anderzijds. Deze relaties worden bevestigd door ZCV roosterberekeningen. Ook worden de volumefractieprofielen van de verankerde en de vrije ketens afgeleid. Deze afleiding is wederom gebaseerd op de theorie voor sterk gestrekte ketens in een polymeerborstel. Er wordt hierbij verondersteld dat de lengte van de vrije ketens veel kleiner is dan de borsteldikte. Wanneer aan deze voorwaarde voldaan is, komen de volumefractieprofielen inderdaad zeer goed overeen met de roosterberekeningen. Wanneer dat niet meer het geval is, voorspellen beide theorieën nog steeds dezelfde borsteldikte. De sterke-strekkingstheorie voorspelt dan echter een veel te scherp grensvlak tussen de verankerde laag en het vrije polymeer.

Beide theorieën zijn ook met elkaar vergeleken voor de interactie tussen twee tegen elkaar samengedrukte borstels. Het roostermodel voorspelt al bij een grotere afstand tussen de twee borstels een repulsieve interactie dan de sterke-strekkingstheorie. Deze interactie op grote afstand wordt veroorzaakt door de reeds eerder genoemde "voet" in het volumefractieprofiel, waardoor de verankerde laag iets verder in de oplossing uitsteekt dan volgens de sterke-strekkingstheorie het geval is. Wanneer er ook nog vrij polymer in de oplossing aanwezig is, kan er een depletie-attractie tussen de borstels plaatsvinden.

Hoofdstuk 6 gaat over de interactie tussen vlakke platen waarop multiblok-copolymeren zijn geadsorbeerd. Eerst wordt de aandacht gericht op ABA triblok-copolymeren. Deze kunnen gemodelleerd worden als eindstandig verankerde B ketens met aan hun niet verankerde uiteinde een adsorberend A blok ("borstels met plakkertjes"). Wanneer de adsorptieënergie van de A segmenten klein is, geven twee oppervlakken met zulke verankerde lagen slechts een repulsieve interactie te zien. Wannneer deze adsorptieënergie toeneemt, onstaat er ook een attractief minimum in de interactie vrije energie. Met verder toenemende adsorptieënergie bereikt de absolute waarde van dit minimum een limietwaarde. De minimale adsorptieënergie die nodig is voor deze attractie neemt toe als de verankeringsdichtheid σ toeneemt en ook wanneer de ketenlengte N toeneemt. De absolute waarde van het minimum is evenredig met $\sigma^{1/3}N^{-1}$. Het minimum treedt altijd op bij plaatafstanden d die groter zijn dan de afstand 2h waarbij de verankerde lagen elkaar net zouden raken, indien de "voeten" van de profielen niet in rekening worden gebracht. Het verschil $d-2h$ is evenredig met $N\sigma^{1/3}$. De aantrekking heeft een entropische oorsprong. Wanneer de plaatafstand groot is, is het A blok van een verankerde keten geadsorbeerd op het oppervlak waar deze keten op verankerd is. De keten vormt op deze manier één grote lus. Wanneer de plaatafstand kleiner wordt, kan dit A blok kiezen op welk oppervlak het wil adsorberen. Door deze toename van vrijheidsgraden neemt ook de entropie van het systeem toe. Dit is de oorzaak van de attractie tussen de twee platen.

De interactie tussen twee geadsorbeerde lagen van ABA triblok-copolymeren (waarbij de geadsorbeerde hoeveelheid bepaald wordt door het evenwicht tussen vrije en geadsorbeerde ketens) heeft altijd een attractieve component indien de copolymeerketens symmetrisch zijn. De interactiecurve is gelijk aan die van twee verankerde lagen (borstels met plakkertjes) met een verankeringsdichtheid die overeenkomt met de geadsorbeerde hoeveelheid. Indien één van de adsorberende blokken groter is dan de andere, neemt de aantrekking sterk af. Reeds bij een relatief lage asymmetrie (het ene blok ca. 20% groter dan het andere) is de interactie geheel repulsief.

181

Multiblok-copolymeren die uit meer dan drie blokken bestaan kunnen bruggen vormen die uit meerdere blokken zijn opgebouwd. De interactie tussen twee oppervlakken waarop copolymeren met alternerende A en B blokken zijn geadsorbeerd, is ook onderzocht. Hierbij werd het totale aantal segmenten van een bepaald type in een copolymeerketen steeds constant gehouden. Het aantal blokken per keten werd echter gevarieerd (zodat de blokken korter worden wanneer het aantal blokken per keten toeneemt). Wanneer de bloklengte verkleind wordt, wordt de geadsorbeerde laag dunner. In dit geval begint de interactie tussen de twee geadsorbeerde lagen dan ook pas op relatief kleinere afstanden. Copolymeer-moleculen die uit zeer kleine, elkaar afwisselende A en B blokken bestaan, lijken erg op homopolymeren die zijn opgebouwd uit segmenten waarvan de eigenschappen een gemiddelde zijn van de A en de B segmenten. Net als homopolymeren vertonen deze copolymeren een sterke attractie voor kleine plaatafstanden (<10 lagen), die slechts op zeer korte afstanden (ca. 2 lagen) gevolgd wordt door een sterke repulsie.

Tot nu toe hebben we alleen situaties beschouwd waarbij het oplosmiddel een goed oplosmiddel is voor beide blokken. De A segmenten adsorberen en de B segmenten adsorberen niet, omdat de eerste wel een affiniteit hebben voor het oppervlak en de tweede niet. Adsorptie van de A segmenten kan echter ook plaats vinden vanwege de selectiviteit van het oplosmiddel. We beschouwen de situatie dat zowel de A als de B segmenten een intrinsieke affiniteit bezitten voor het oppervlak. De B segmenten lossen goed op (atherm oplosmiddel), maar de A segmenten niet. Het A blok van een copolymeer zal nu preferent adsorberen, omdat het zich niet graag in de oplossing bevindt. In het geval van ABA triblok-copolymeren kan de interactie tussen twee zulke geadsorbeerde lagen interessante verschijnselen opleveren. Als de interacties van de A en de B segmenten slechts weinig van elkaar verschillen, lijkt de interactie op die van een homopolymeer. Op korte afstanden is er een attractie. Als deze interacties zeer sterk verschillen, lijkt de interactie op die van een "normaal" copolymeer, met een attractie op grote afstand, gevolgd door een sterke repulsie op kortere afstanden. In de tussen liggende gevallen worden ingewikkeldere interactiecurves gevonden.

Het onderwerp van **hoofdstuk 7** is de interactie tussen twee kleine, bolvormige deeltjes met een geadsorbeerde polymeerlaag. De ZCV roostertheorie wordt hier toegepast op systemen met concentratiegradienten in twee onafhankelijke richtingen. Er wordt daartoe gebruikt gemaakt van een cylindrisch coördinatenstelsel. De volumefracties kunnen nu zowel in de axiale richting (evenwijdig aan de verbindingsas tussen de middelpunten van de twee deeltjes) als in de radiële richting (loodrecht hierop staand) variëren. In dit laatste hoofdstuk worden resultaten gepresenteerd voor deeltjes die zijn bedekt met eindstandig

verankerde ketens. Als de twee deeltjes ver van elkaar verwijderd zijn, is het volumefractieprofiel rondom één zo'n deeltje isotroop. Dit profiel is bovendien nagenoeg gelijk aan het profiel dat berekend wordt met het "conventionele" ZCV model, waarbij er slechts sprake kan zijn van een concentratiegradiënt in één richting. Dit is een bewijs voor de correctheid van het tweedimensionale model.

De interactie tussen twee zulke bolvormige deeltjes kan met behulp van de Derjaguin benadering gerelateerd worden aan de interactie tussen twee overeenkomstige vlakke platen. Deze benadering gaat echter alleen op wanneer de kromtestraal van de deeltjes veel groter is dan de polymeerlaagdikte. Dat is niet het geval voor de systemen in dit hoofdstuk. Daarom worden er interacties gevonden die veel minder repulsief zijn dan volgens de Derjaguin benadering. Voor toenemende kromtestralen verschuift de interactie wel in de richting van de Derjaguin benadering. Op moleculair niveau kan de verminderde repulsie verklaard worden uit de vrijheid die de verankerde ketens hebben om de ruimte tussen de deeltjes te verlaten, wanneer deze deeltjes naar elkaar toe komen. Of de verankerde segmenten van de ketens hierbij wel of niet vrij over dit oppervlak kunnen bewegen, speelt daarbij een ondergeschikte rol.

Curriculum Vitae

Christopher Michael Wijmans werd op 4 juli 1966 geboren te Amsterdam, alwaar hij aan het Hervormd Lyceum West het O.V.W.O. diploma behaalde. In 1983 begon hij de studie Moleculaire Wetenschappen aan de toenmalige Landbouwhogeschool Wageningen. De doctoraalstudie omvatte de afstudeervakken Fysische Chemie en Moleculaire Fysica, alsmede een praktijktijd die aan het Cavendish Laboratory te Cambridge werd doorgebracht. Na zijn afstuderen in 1989 was hij vier jaar lang als toegevoegd onderzoeker bij de vakgroep Fysische en Kolloïdchemie in dienst van de Landbouwuniversiteit. Gedurende deze periode is het onderzoek uitgevoerd dat in dit proefschrift beschreven wordt.